University of Sussex

A University of Sussex DPhil thesis

Available online via Sussex Research Online:

http://eprints.sussex.ac.uk/

This thesis is protected by copyright which belongs to the author.

This thesis cannot be reproduced or quoted extensively from without first obtaining permission in writing from the Author

The content must not be changed in any way or sold commercially in any format or medium without the formal permission of the Author

When referring to this work, full bibliographic details including the author, title, awarding institution and date of the thesis must be given

Please visit Sussex Research Online for more information and further details

The hair cell antigen/Ptprq: Lipid phosphatase activity,

intracellular domain interactors, Apical targeting and

Evidence that it is a Proteoglycan

A thesis submitted towards fulfilment of the requirement for the

degree of Doctor of Philosophy

by

Gowri Dinesh Nayak

to

The University of Sussex

School of Life Sciences

January 2010

ACKNOWLEDGEMENTS

UNIVERSITY OF SUSSEX

GOWRI DINESH NAYAK

SUBMITTED FOR THE DEGREE OF DOCTOR OF PHILOSOPHY

The hair cell antigen/Ptprq: Lipid phosphatase activity, intracellular domain interactors, Apical targeting and Evidence that it is a Proteoglycan

SUMMARY

Ptprq, a receptor-like phosphatase known to be associated with the shaft connectors of stereocilia, is a protein required for the maintenance of the hair-bundle structure. The extracellular domain of Ptprq has numerous potential sites for N-glycosylation and the cytoplasmic domain has phosphatidyl inositol phosphatase activity *in vitro*. The current project was aimed at determining whether Ptprq regulates inositol phosphate levels in the hair bundle, identifying the intracellular binding partners of Ptprq, understanding what targets Ptprq to the apical membrane, and finally, elucidating whether Ptprq is a proteoglycan. The results show that EHD3, a protein involved in endocytosis, interacts with the intracellular domain of Ptprq and that a major part of the apical targeting signal in Ptprq lies in the N-glycosylated moieties of the extracellular domain. Also, evidence was found indicating that Ptprq is a chondroitin sulphate proteoglycan and that there may be a developmentally-regulated isoform carrying the DSD-1 epitope. Glycosylation variants of Ptprq may be responsible for the regional variation in the appearance of the shaft connectors.

LIST OF ABBREVIATIONS

AEE	apical early endosome
ALA	ankle link antigen
ANTH	AP180 N-terminal homology
AP-1	adaptor protein 1
AP-2	adaptor protein 2
ARE	apical recycling endosomes
BAPTA	1,2-bis (o-aminophenoxy) ethane-N,N.N',N'-tetraacetic acid
BCIP	bromo-4chloro-3-indolyl phosphate
BCK	brain creatine kinase
BEE	basolateral early endosomes
Btk	bruton's tyrosine kinase
Cdh23	cadherin 23
CE	common endosomes
CFTR	cystic fibrosis transmembrane conductance regulator
CL4 cells	LLC-PK1 cells
CSPG	chondroitin sulphate proteoglycan
DAG	diacylglycerol
dH_2O	distilled water
DMSO	dimethylsulphoxide
DSD-1	dermatan sulphate dependent-1

DTT	dithiothreitol
E	embryonic
Ecto	ectodomain
EEA1	early endosome autoantigen1
EGFP	enhanced green fluorescent protein
EH	Eps15 homology
ENTH	epsin n-terminal homology
ER	endoplasmic reticulum
ERC	endocytic recycling complex
ERM	ezrin-radixin-moesin
FAPP	four-phosphatase-adaptor proteins 1 and 2
FERM	4.1-ezrin-radixin-moesin
FNIII	fibronectin type III repeats
FYVE	Fab1p,YOTB,Vac1p and EEA1
GAG	glycosaminoglycan
GFP	green fluorescent protein
GPI	glycosylphosphatidylinositol
GRP	general receptor for phosphoinositides-1
GST	glutathione S-transferase
HBHBSS	HEPES buffered Hank's balanced salt solution
HCA	hair cell antigen

HEK293	human embryonic kidney 293 cells
HRP	horse radish peroxidase
Ic	intracellular
IHC	inner hair cell
IMS	industrial methylated spirit
LB	lysogeny broth
LE	late endosomes
LYS	lysosomes
mAb	monoclonal antibody
MDCK	Madin-Darby canine kidney
MVB	multivesicular bodies
NBT	nitro-blue tetrazolium chloride
OHC	outer hair cell
P	postnatal
PBS	phosphate buffered saline
Pcdh15	protocadherin 15
PCR	polymerase chain reaction
PDZ	postsynaptic density, discs large and zone-occludens
PEPP1	PI3P-binding PH-domain protein-1
PH	pleckstrin homology
PI	phosphoinositides

PIPase   phosphatidyl inositol phosphatase

PKB   protein kinase B

PLCδ1   phospholipase C δ1

PMCA   plasma-membrane Ca_{2+}-ATPase

PMSF   phenylmethylsulphonyl fluoride

PtdIns   phosphatidylinositol

PTEN   phosphatase and tensin homolog deleted on chromosome ten

PTPase   protein tyrosine phosphatase

Ptprq   protein tyrosine phosphatase receptor type Q

PTPβ   protein tyrosine phosphatase β

PTPζ/RPTPβ protein tyrosine phosphatase ζ/receptor protein tyrosine phosphatase β

PVP   polyvinylpyrrolidone

PX   phagocyte oxidase

RME-1   receptor mediated endocytosis-1

RT-PCR   reverse transcriptase polymerase chain reaction

SDF3   stromal derived factor 3

SDS-PAGE   sodium dodecyl sulphate polyacrylamide gel electrophoresis

SOC   medium super optimal broth with catabolite repression medium

SP   signal peptide

TAFF1   tandem FYVE fingers-1

TAPP   tandem pleckstrin homology domain containing protein

TBE   tris borate EDTA

TBS   tris buffered saline

TE   tris EDTA

TGN   trans Golgi network

TJ   tight junction

TLA   tip link antigen

TM   transmembrane

U   units

UV   ultraviolet

VLGR1   very large G-protein coupled receptor 1

WASP   wiskott-aldrich syndrome protein

TABLE OF FIGURES

TABLE OF TABLES

CHAPTER 1

Introduction

1.1 The inner ear

The inner ear is composed of mechanosensory organs that enable the detection of sound and provide the sensations of balance and motion. It is divided into two functional parts, the auditory organ or cochlea and the vestibular system, with the latter comprising the three semicircular canal organs as well as the two otoconial organs, the utricle and saccule. These are all enclosed within the bony labyrinth (see figure 1.1). In mammals, the organ of Corti is located inside the coiled cochlea and is specialized to serve as a microphone, a device in which the sound pressure waves that are transmitted from the outer ear are converted into electrical impulses that the auditory nerve then carries to the brain. The semicircular canals are placed orthogonal to each other and contain mechanosensory structures called cristae that are maximally sensitive to rotation in the 3 cardinal planes, whilst the utricle and saccule have maculae that are stimulated by linear acceleration in the horizontal and vertical planes respectively. In addition to these organs, the avian inner ear has two extra maculae, the macula neglecta and the lagena macula. The hearing organ of the bird is a slightly curved structure and is called the basilar papilla. Common to these various inner ear organs is a specialized mechanosensory epithelium that is sensitive to the mechanical disturbances caused by the various external stimuli (Slepecky, 1996).
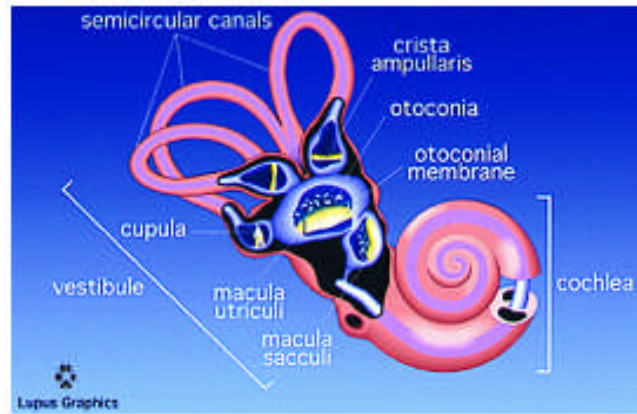
Figure 1.1: General organization of the mature mammalian inner ear. This picture is from Cohen-Salmon et al., (1997).

1.2 Hair cells, hair bundles and hair bundle links

The mechanosensory epithelia in the auditory and vestibular organs of the inner ear are composed of sensory hair cells and non-sensory supporting cells (Slepecky, 1996; Lim, 2005). Mechanosensory hair cells are also found in the neuromasts of the lateral line systems of fish and amphibia. The hair cells detect mechanical stimuli and transmit information about these stimuli as electrical signals to the brain via the afferent nerve fibres. Though the various types of hair cells are sensitive to different types of stimuli, and although they are morphologically distinguishable from each other, they all bear at their apical surface a mechanosensitive hair bundle that is anchored to a cuticular plate. Deflections of the hair bundle along its axis of sensitivity opens mechanically gated cation channels resulting in a current, largely carried by K^+ ions, flowing through the hair cell. This generates an intracellular receptor potential. Whilst being equipped with mechanosensory cells, the vestibular and the auditory organs also possess various accessory structures that assist in producing hair bundle deflections as appropriate responses to external stimuli. A common feature employed by the cochlear and vestibular organs in the inner ear is an extracellular matrix that overlies the mechanosensitive epithelia. An otoconial membrane lies over the surface of the macula

of the utricle and saccule, while the ampullae of the semi-circular canals have a cupula sitting on top of each crista. In the cochlea, a gel-like acellular structure known as the tectorial membrane lies over the surface of the organ of Corti (see figure 1.2).

1.2.1 Hair cells and supporting cells

The morphology of the hair cells depends on their location within the inner ear organs. The mammalian cochlea contains inner and outer hair cells, while the vestibular organs contain type I and type II hair cells, and all of these types of hair cell are morphologically distinct from each other (Slepeckly, 1996). The inner hair cells (IHCs) are flask shaped and contacted by afferent neurons (see figure 1.2). The outer hair cells (OHCs) are cylindrical and receive mainly efferent innervation (see figure 1.2). The IHCs and OHCs also perform different roles; the IHCs are truly sensory in nature and are involved in detecting the mechanical disturbances caused by incoming sound vibrations and in transmitting information to the brain, while the OHCs respond to incoming sound vibrations and regulate basilar membrane motion thereby enhancing the performance of the cochlea (Slepeckly, 1996). The type I hair cells in the vestibular epithelia of birds, mammals and reptiles are chalice-shaped and enclosed in the calyx endings of afferent neurons while the cylindrical type II hair cells are found in all vertebrate vestibular epithelia and are contacted by afferent synaptic boutons (see figure 1.3; Slepeckly, 1996). In addition, efferent fibres form synapses with both types of hair cells or their afferents.
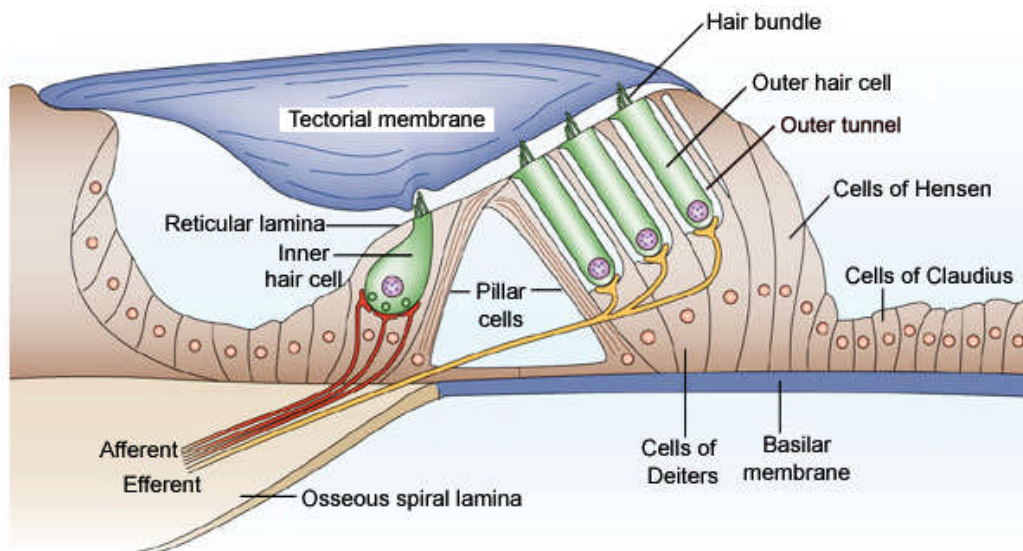
Figure 1.2: Structure of the organ of Corti. The two types of hair cells, IHCs and OHCs, and all the supporting cells are also shown. The tectorial membrane lies on top of the organ of Corti and contacts the outer hair cell bundles. This picture is adapted from Fettiplace and Hackney, 2006.
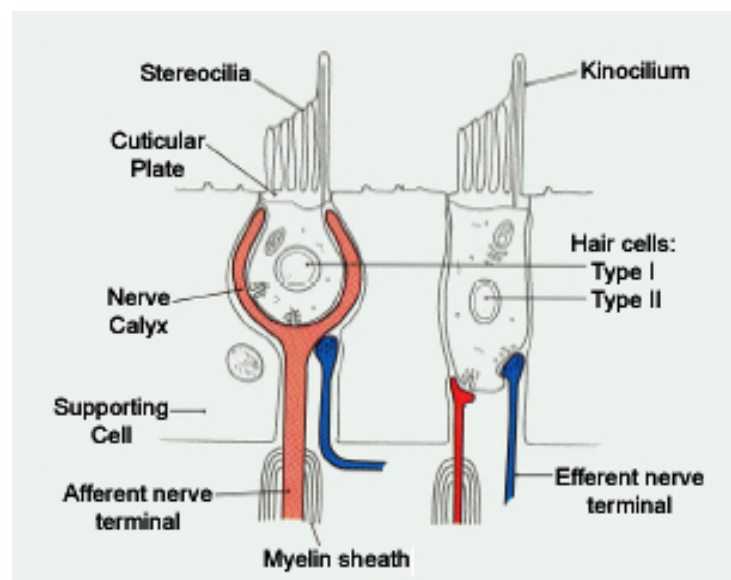
Figure 1.3: The two types of vestibular hair cells, type I and type II, and the nerve endings that innervate them are shown. The picture is adapted from the Dickman lab website of the School of Medicine, Washington University, St Louis.

The hair cells are surrounded by supporting cells that extend from the basement membrane to the apical surface of the mechanosensitive epithelia (see figure 1.2; Slepeckly, 1996; Lim, 2005). Neighbouring hair cells are therefore prevented from contacting each other by the supporting cells and the hair cells form tight junctions and

desmosomes with the contacting supporting cells. In the organ of Corti, specialised supporting cells are present known as pillar cells, Deiter's cells and Hensen's cells (see figure 1.2). The pillar and Deiter's cells that surround the OHCs form a rigid scaffolding around these hair cells and are specialised to withstand mechanical stress and transmit stimulus-induced motion of the basilar membrane to the reticular lamina (see figure 1.2). The columnar Hensen's cells are thought to influence the fluid and ion content in the outer tunnel that is located between the third row of OHCs and the third row of Deiter's cells (Lim, 2005). The cells of Claudius are located between the Deiter's cells and the lateral wall of the cochlea and provide no morphological evidence for a specialised function. The supporting cells in the vestibular system are also relatively unspecialised.

1.2.2 Hair bundles

The hair bundle is composed of actin-filled projections called stereocilia (see figure 1.3). The number of stereocilia in each hair bundle and the shape of the hair bundle vary between species and between different hair cell types within the same organ. In general, the hair bundle is made up of two or more rows of stereocilia of increasing height, with a single true cilium called a kinocilium situated adjacent to, and central with respect to, the tallest row (Slepecky, 1996; Lim, 2005). The kinocilium is absent in mature auditory hair cells. Deflections of the hair bundle along its axis of mechanosensitivity, toward or away from the kinocilium (if present) or the tallest row of stereocilia, regulate the opening and closing of the transducer channels (see figure 1.4). Thus, the hair bundle is a morphologically and functionally polarized structure with the position of the kinocilium (or the basal body) and the tallest row of stereocilia defining the hair cell's orientation or polarity (Slepecky, 1996; Lim, 2005).
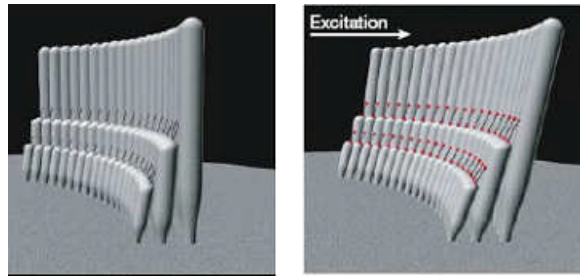
Figure 1.4: Hair cell depolarisation or excitation occurs when the hair bundle is deflected towards the tallest row of stereocilia. Deflection in the opposite negative direction is inhibitory. The picture is taken from Frolenkov et al., 2004

1.2.3 Hair bundle links

The stereocilia within a hair bundle are interconnected by several types of links whose occurrence and distribution varies with the hair cell type and position in the sensory organ (Goodyear et al., 2005). While one link type appears to be essential for mechanotransduction, the others are required for the development and maintenance of hair bundle integrity (Goodyear et al., 2005). From studies on avian and mammalian auditory and vestibular organs it is clear that there is a continuous change in the number and types of links associated with the developing hair bundle, up until its maturation (Pickles et al., 1991; Goodyear et al., 2005).

Tip links are a characteristic of all mechano-transducing acousticolateral hair cells and are essential for sensory transduction. The tip links are readily visualised by electron microscopy after fixation in the presence of tannic acid and appear as oblique strands of electron dense material connecting the tip of a stereocilium to the side of an adjacent taller stereocilium (see figure 1.5; Pickles et al., 1984; Furness and Hackney, 1985; Goodyear and Richardson, 1992). In the mature basilar papilla of the chick, besides tip links, three distinct link types have been described (see figure 1.5; Goodyear and Richardson, 1992). Horizontal top connectors occur just below the tip links and join adjacent stereocilia (see figure 1.5; Goodyear and Richardson, 1992). In samples fixed

in the presence of tannic acid, the horizontal top connectors are seen as plaques composed of 3-5 columns of short horizontal bars that connect nearby stereocilia (Goodyear and Richardson, 1992). Each top connector plaque can be 25-50 nm wide and up to 400 nm long (Goodyear and Richardson, 1992). Shaft connectors are seen in samples fixed in the presence of tannic acid or ruthenium red (Goodyear and Richardson, 1992). Tannic acid treatment reveals shaft connectors as a fine meshwork of fibres up to 7 nm in diameter, while ruthenium red staining (see figure 1.5) shows these connectors as dense spherical particles of about 20 nm diameter from which several fine strands emerge to interconnect adjacent stereocilia (Goodyear and Richardson, 1992; Goodyear et al., 2003). Depending upon the region under study, the shaft connectors are distributed either along part of or all along the entire length of the stereocilia (Goodyear and Richardson, 1992). Ankle links connect the stereocilia at their bases in the form of a web-like mesh made from thin stands that are up to 140 nm long, occupying a zone 200-400 nm from the apical surface (see figure 1.5; Goodyear and Richardson, 1992). These connectors appear similar with both tannic acid treatment and ruthenium red staining (Goodyear and Richardson, 1992). In contrast to the hair bundle links found in the mature basilar papilla, the OHCs in the mature mammalian cochlea have only the horizontal top connectors lying below the tip links (Pickles et al., 1984; Furness and Hackney, 1985; Hackney and Furness, 1986; Osborne et al., 1988; Goodyear et al., 2005). In addition, they have tectorial membrane attachment crowns (Tsuprun and Santi, 2002; Goodyear et al., 2005). When present, the kinocilium is connected to the tallest adjacent stereocilia via kinocilial links (Hillman, 1969; Hillman and Lewis, 1971).

The various interstereociliary link types are antigenically distinct and can be biochemically distinguished based on their relative sensitivity to the protease subtilisin

and the Ca^{2+} chelator BAPTA (for 1,2-bis (o-aminophenoxy) ethane-N,N,N',N'-tetraacetic acid) (Goodyear and Richardson, 1999; Goodyear et al., 2005). While tip links are sensitive to BAPTA and not to subtilisin, shaft connectors and tectorial membrane attachment crowns are lost only on subtilisin treatment (Goodyear and Richardson, 1999; Goodyear et al., 2005). The ankle links are sensitive to both agents and the horizontal top connectors resist both BAPTA and subtilisin treatment (Goodyear and Richardson, 1999; Goodyear et al., 2005). Kinocilial links have similar properties to tip links and are also BAPTA-sensitive, subtilisin-resistant structures (Goodyear and Richardson, 2003).
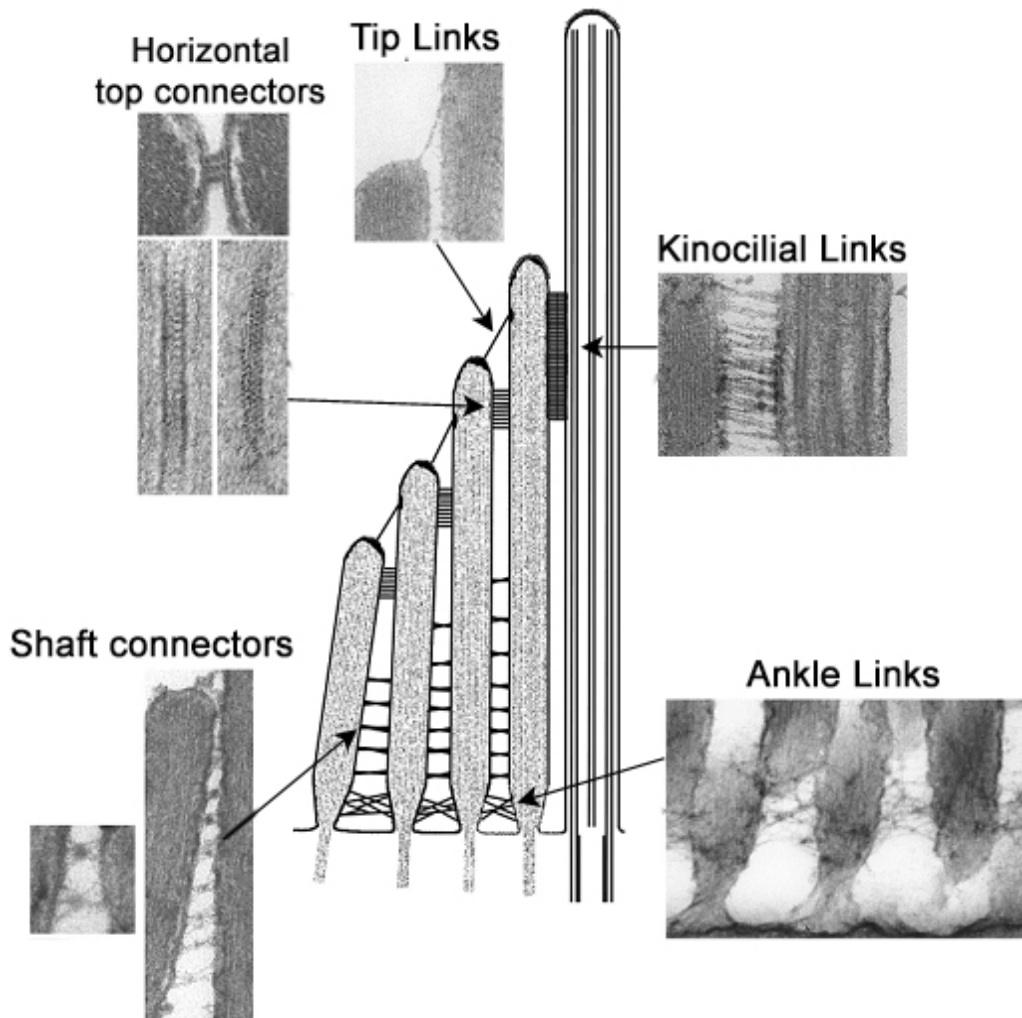
Figure 1.5: The various interstereociliary links seen in the hair bundles of the chick basilar papilla. This figure is from Nayak et al., 2007.

1.3 Development of the hair bundle

The development of the hair bundles has been extensively studied in the chick auditory organ, the basilar papilla, as well as in the vestibular and auditory organs of different mammals using scanning and transmission electron microscopy (Cotanche and Sulik, 1983; 1984; Tilney and DeRosier, 1986, Tilney et al., 1986; 1988; 1992a; 1992b; Li and Ruben, 1979; Anniko, 1983a; b; Lim and Anniko, 1985; Mbiene and Sans, 1986; Lavigne-Rebillard and Pujol, 1986; Lenoir et al., 1987; Kaltenbach et al., 1994; Zine and Romand, 1996). Although hair bundle morphology varies with the species and type of organ with variations occurring even within the same organ, the essential processes involved in the formation of the hair bundles appears to be similar. Hair bundle development in the avian basilar papilla can be divided into three phases (Tilney et al., 1992a). Before hair bundles develop, the apical surfaces of all the epithelial cells of the papilla have both numerous short microvilli and a single cilium (Cotanche and Sulik, 1984). During the first phase of hair bundle development, the microvilli on the apical surfaces of hair cells are only just distinguishable from those on the surrounding supporting cells (see figure 1.6, day 8; Tilney and DeRosier, 1986; Tilney et al., 1992a). The hair bundles at this stage are exceedingly short with no evidence of the staircase-like pattern (Tilney et al., 1986). Migration of the kinocilium to the periphery of the bundle determines the hair bundle polarity and the bundles then reorient and become aligned with those of neighbouring cells (See figure 1.6, day 9-10.5; Tilney et al., 1992a). Then, the hair bundles throughout the papilla begin to elongate, starting with the stereocilia nearest to the kinocilium followed by those progressively further away, resulting in rows of height-ranked stereocilia (Tilney et al., 1992a). In the second phase, elongation ceases and the stereocilia begin to increase in width owing to an increase in the number of actin filaments which become maximally cross-bridged (see figure 1.6;

day 13-16; Tilney and DeRosier, 1986; Tilney et al., 1986; 1992a). At the same time, the stereocilia begin to taper at the base and form rootlets that extend into the apical cytoplasm where the cuticular plate is developing (Tilney and DeRosier, 1986; Tilney et al., 1992a). In the final phase, stereocilia that have not attained their adult length re-initiate elongation (Tilney et al., 1986; Tilney et al., 1988; Tilney et al., 1992a). The growing stereocilia do not cease to elongate simultaneously. Instead, the shortest row of stereocilia ceases to elongate first, followed by successively taller and taller rows with the tallest row finishing last resulting in an increase in difference in height-ranking within the staircase (see figure 1.6, day 22; Tilney et al., 1988; Tilney et al., 1992a). Also, the stereocilia at the distal end of the cochlea are the last to stop elongating, so that these hair cells have longer stereocilia than those found at the proximal end (Tilney et al., 1988; Tilney et al., 1992a).

Hair bundle development in the mammalian cochlea (Mbiene and Sans, 1986; Zine and Romand, 1996; Denman-Johnson and Forge, 1999) is broadly similar to that observed in the avian basilar papilla. However, unlike in the bird, hair bundle development proceeds in the basal (high frequency) to apical (low frequency) direction in the mammalian cochlea (Lim and Anniko, 1985; Kaltenbach et al., 1994; Zine and Romand, 1996; Nishida et al., 1998). The taller, apical hair bundles of the postnatal hamster cochlea grow faster than their shorter, basal counterparts, and stereociliary elongation and increase in width occurs simultaneously rather than being separated into temporally distinct phases as in the avian basilar papilla (Kaltenbach et al., 1994). Recently, Lelli et al., (2009) reported a decrease in the height of hair bundles in the basal region of the cochlea between postnatal day (P)1 and P6, whilst the apical hair bundles showed a slight increase in their length during the same period. Thus, a gradient in hair bundle heights along the cochlea in mammals may be achieved by a combination

of different growth rates of stereocilia and a final refining of bundle heights by slight lengthening or shortening of the stereocilia.
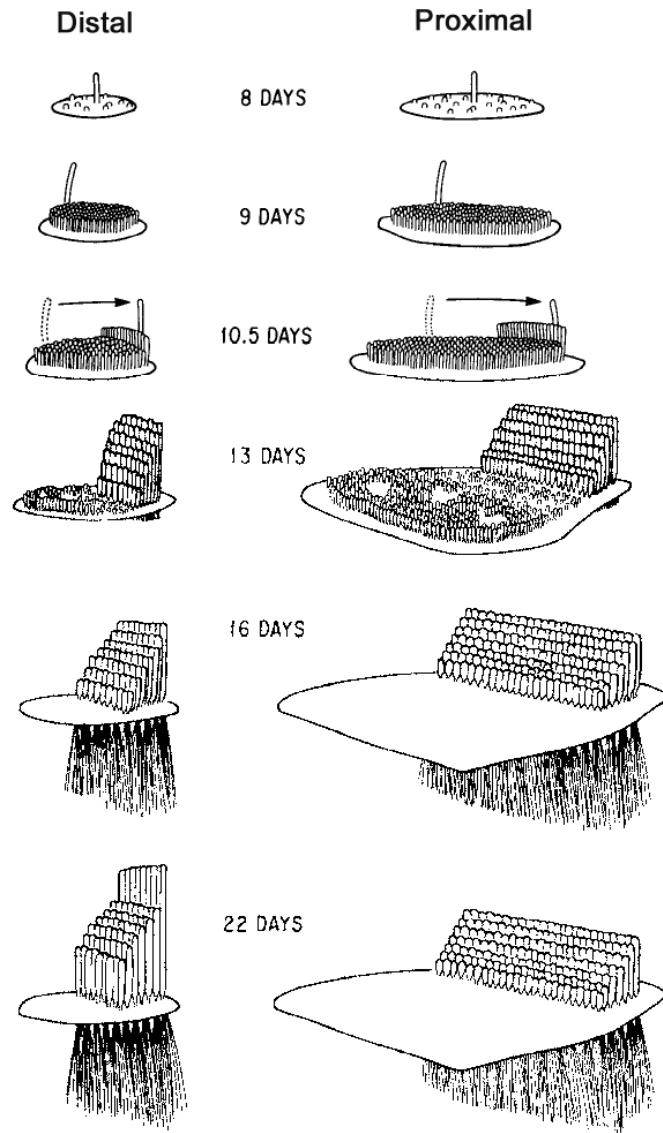
Figure 1.6: The various steps in the differentiation of the hair bundle and apical surface of the hair cell in the distal and proximal end of the basilar papilla. This figure is taken from Tilney et al., 1992a.

1.3.1 Stereociliary actin filaments are dynamic

An actin treadmill model has been proposed to describe the dynamic properties of the paracrystalline array of several hundred, uniformly polarized, cross-linked actin filaments that make up a stereocilium (Schneider et al., 2002; Rzadzinska et al., 2004; Lin et al., 2005). Recent evidence suggests that the stereocilia recycle their actin core

while maintaining a constant length (Rzadzinska et al., 2004; Lin et al., 2005). The rate of polymerisation at the tips of stereocilia equals the rate of actin depolymerisation at the base and the actin flux rates match the length of the individual stereocilia enabling them to maintain a steady-state structure (Rzadzinska et al., 2004). However, the rate of actin assembly and disassembly may actually be regulated independently of one another (Rzadzinska et al., 2004). The turnover of the actin bundling protein, espin, also matches the rate of actin incorporation at the stereocilia tips suggesting that the newly polymerised actin filaments are cross-linked as they are being formed (Rzadzinska et al., 2004; Lin et al., 2005).

A common occurrence in stereocilia and the two other actin protrusions they closely resemble, filopodia and microvilli, is that of an electron dense structure called the "tip complex" or "tip density" at the barbed ends of the actin filaments (Rzadzinska et al., 2004; Lin et al., 2005). The tip densities contain an organised assembly of proteins that include capping proteins, 'leaky caps', scaffold and motor proteins, intergrins and signalling proteins that are believed to mediate actin polymerisation and filament bundling (Rzadzinska et al., 2004; Lin et al., 2005). Although the exact composition of the tip complex at the distal ends of stereocilia is not known, some of the resident proteins have been uncovered (Belyantseva et al., 2005; Delprat et al., 2005). For example, myosin XVa has been shown to localise to the tip complex (Rzadzinska et al., 2004). The loss of myosin XVa in the shaker 2J mice resulting in short, rounded stereocilia lacking the tip complex is believed to reflect the role of this myosin in stereocilia elongation (Rzadzinska et al., 2004; Belyantseva et al., 2005). It was suggested that myosin XVa may regulate stereocilia elongation in conjunction with scaffold proteins and actin capping proteins (Rzadzinska et al., 2004). In support of this, myosin XVa has been suggested to be involved in transporting the PDZ-containing

scaffold protein, whirlin, to stereocilia tips (Kikkawa et al., 2005). Whirlin might be involved in the organization of the molecular complex necessary for actin polymerisation and stereocilia elongation (Kikkawa et al., 2005). Recently, Rzadzinska et al. (2009) showed the presence of twinfilin-2, an actin monomer binding protein, at the tips of shorter stereocilia within the hair bundle staircase. Twinfilin-2 may regulate actin polymerisation at the tips of these stereocilia either by maintaining the levels of the polymerisation competent ATP-actin monomers in the stereocilia or by capping the tips of actin filaments (Rzadzinska et al., 2009).

1.3.2 *Endocytosis at the apical non-stereociliary surface of hair cells*

In addition to stereocilia undergoing renewal of their actin filaments, there is also evidence that hair cells may be constantly turning over their apical membrane (Kachar et al., 1997; Grati et al., 2006). Apical endocytosis has been suggested to serve in the recycling and turnover of the membrane and its constituents, and also in transcytosis of proteins from the apical membrane to the basolateral surface (Forge and Richardson, 1993; Griesinger et al., 2004; Grati et al., 2006). Apical endocytosis and exocytosis is believed to occur at peripheral sites around the cuticular plate of the hair cell, above a region referred to as the pericuticular necklace where the apical plasma membrane is in direct contact with the underlying cytoplasm (Kachar et al., 1997; Grati et al., 2006). Several studies have reported the occurrence of membrane invaginations at the pericuticular surfaces and have described coated vesicles in the thin band of cytoplasm that connects the pericuticular surface to the cytoplasm below the cuticular plate (Forge and Richardson, 1993; Kachar et al., 1997; Richardson et al., 1997; Grati et al., 2006). As endocytic vesicles are observed mostly in the apical ends of neonatal mouse hair

cells and rarely encountered in the mature hair cells, apical endocytosis in the hair cells of mammals appears to be developmentally regulated (Forge and Richardson, 1993).

The concentration of microtubules in the infracuticular regions is suggestive of a pathway for transporting vesicles (Kaneko et al., 2006). Studies on adult cochlear hair cells using FM1-43, a cationic membrane marker, have suggested a role for calcium-dependent apical endocytosis in replenishing basal synaptic vesicular membrane in IHCs (Greisinger et al., 2002). In OHCs, FM1-43 and protein internalisation studies have revealed a pathway for calcium-dependent apically endocytosed membranes and proteins to be transported to specific intracellular and lateral wall compartments (Greisinger et al., 2004). Endocytosed material is first trafficked to the apical region of a tubulovesicular compartment located below the stereocilia and that is likely to correspond to the apical early endosome (Griesinger et al., 2004). Subsequent trafficking is directed to a central compartment that probably represents the common endosome which is known to function in endocytic sorting and transcytosis of proteins along the apical-basal axis (Griesinger et al., 2004). The lateral compartment to which the endocytosed material is trafficked is most likely the lateral cisternae.

1.4 Development of stereociliary links

In the basilar papilla of the chick, tip links can be observed by embryonic day (E)9 in some bundles as the stereocilia acquire graded lengths (Pickles et al., 1991). In the mouse, tip links first appear in the macular hair cells at E15.5 (Denman-Johnson and Forge, 1999) and may be present in the cochlear hair cells from as early as E17.5 (Goodyear et al., 2005). Rat IHCs develop tip links at P0 (Zine and Romand, 1996) and gerbil OHCs develop tip links at P2 (Souter et al., 1995). However, before the appearance of tip links, morphologically uncharacterised lateral links are found along

the length of the stereocilia (Pickles et al., 1991; Goodyear et al., 2005; Waguespack et al., 2007). Fine strands connecting adjacent stereocilia are seen in the avian basilar papilla at E7.5 and appear denser and more prominent towards the stereocilia tips, although the dense insertion points associated with tip links are not readily visible until E16 (Pickles et al., 1991). Based on the structure, location and data on tip link formation, many of the lateral links may in fact be excess tip links occurring along the entire bundle surface. A pruning process eliminates all but one of these links, the one that runs along the hair bundle's axis of sensitivity (Pickles et al., 1991; Goodyear et al., 2005; Waguespack et al., 2007).

Antigens that are specifically associated with the shaft connectors and ankle links are also initially expressed along the entire surface of the emerging stereocilia in the hair cells of the basilar papilla (Goodyear and Richardson, 1992; Goodyear and Richardson, 1999). The hair cell antigen (HCA) first appears at E6.5 along the stereocilia and only becomes restricted to the basal regions as the stereocilia grow in height during the final growth phase (Bartolami et al., 1991). The ankle link antigen (ALA) can be first seen at E7, becomes concentrated at the base of the hair bundle by E16 and eventually becomes restricted to the ankle region of the hair bundle by posthatch day 2 (Goodyear and Richardson, 1999).

In the mouse cochlea, cell-coat material with discrete puncta is first visible at E17.5 on the stereocilia of IHCs and OHCs, and between P0 and P2 on the apical non-stereociliary surfaces of these cells (Goodyear et al., 2005). Ankle links appear in the hair bundles of mouse basal-coil IHCs at P0 and become prominent on all hair bundles by P2. By this time the stereociliary cell coat becomes a dense uniform fuzz and only forms links between stereocilia where they are in relatively close proximity (Goodyear

et al., 2005). Ankle links begin to disappear around P9 concomitant with the initial appearance of the horizontal top connectors (Goodyear et al., 2005). By P12, ankle links are no longer seen in the cochlear hair bundles and the cell coat begins to recede (Goodyear et al., 2005). The horizontal top connectors continue to develop and attain their zipper-like mature appearance by P14 and the cell coat is lost by P19 (Goodyear et al., 2005).

Thus, from the limited information available, it seems likely that the development of these other interstereociliary links also seems to include a refining process wherein lateral connections initially observed along the entire stereociliary surface develop into their mature forms.

Recent studies have identified many of the proteins that are associated with the different link types. These include the cadherins, cadherin 23 (Cdh23) and protocadherin 15 (Pcdh15), two large cell-surface proteins, Vlgr1 and usherin, and the receptor-like phosphatase Ptprq. Animals with mutations in the genes encoding these proteins have revealed the significance of these links in the development, maintenance and functioning of the hair bundle.

1.4.1   The Cadherins, Cdh23 and Pcdh15

The cell surface proteins Cdh23 and Pcdh15 have numerous extracellular cadherin repeat sequences, a transmembrane region and a cytoplasmic domain (Di Palma et al., 2001; Adato et al., 2005a). The cytoplasmic domains of the two proteins interact with several hair bundle proteins in addition to interacting with each other and the PDZ (for Postsynaptic density, Discs large and Zona-occludens) domains of the scaffold protein harmonin (Xu et al., 2008; Sengupta et al., 2009; Siemens et al., 2004; Phillips et al., 2006; Senften et al., 2006; Kazmierczak et al., 2007; Boëda et al., 2002; Adato et al.,

2005a). Both Cdh23 and Pcdh15 are known to be associated with tip links and kinocilial links, while Cdh23 is also associated with the transient lateral links (Söllner et al., 2004; Siemens et al., 2004; Michel et al., 2005; Ahmed et al., 2006). From studies on mice lacking these proteins it is clear that the two cadherins are required for the normal development and maintenance of the hair bundle (Di Palma et al., 2001; Holme and Steel, 2002; Ahmed et al., 2003; Alagramam et al., 2001a; Alagramam et al., 2001b). The Cdh23 mutant mice, Waltzer, serve as a mouse-model for Usher syndrome, USH1D, while the Ames waltzer mice bear mutations in *Pcdh15*, the gene responsible for Usher syndrome, USH1F (Di Palma et al., 2001; Holme and Steel, 2002; Alagramam *et al.,* 2001a; Alagramam *et al.,* 2001b). In the Waltzer and Ames waltzer mice, stereocilia disorganisation occurs early in the development of the hair bundles and fragmentations leading to clumps of stereocilia, along with a misplaced kinocilia, are of common occurrence in these mice (Di Palma et al., 2001; Alagramam *et al.,* 2001a; Holme and Steel, 2002).

1.4.2 *Vlgr1 and usherin*

Vlgr1 is a member of the secretin family (family 2 or B) of G-protein-coupled receptors (McGee et al., 2006) and usherin is a large glycoprotein with several protein domains, including a laminin G-like domain, a laminin N-terminal domain, ten laminin-type EGF-like modules and four fibronectin type III (FNIII) repeats (Adato et al., 2005b). Both Vlgr1 and usherin are ankle-link associated proteins (McGee et al., 2006; Michalski et al., 2007; Adato et al., 2005b) and avian Vlgr1 is the ALA (McGee et al., 2006). The two proteins interact with scaffold proteins harmonin and whirlin, and may interact with each other to form ankle links (Adato et al., 2005b; Reiners et al., 2005b; van Wijk et al., 2006; McGee et al., 2006). Mutations in GPR98 (VLGR1) causes Usher

syndrome type USH2C (Weston et al., 2004) while mutations in the gene encoding usherin underlie USH2A, the most common genetic form of Usher syndrome (Eudy et al., 1998; Van Wijk et al., 2004). Loss of Vlgr1 and ankle links from the hair bundles of the Vlgr1 mutant mice results in loss of the characteristic V-shape and poor alignment of the two arms of the OHC hair bundles (McGee et al., 2006).

1.4.3   HCA/ Ptprq

The hair cell antigen (HCA) was first discovered in a screen for antibodies that specifically labelled hair bundles and was shown to be associated with shaft connectors (Richardson et al., 1990). Subsequent studies revealed that the HCA is Ptprq (Goodyear et al., 2003), a transmembrane phosphatase with several FNIII repeats in its extracellular domain (Wright et al., 1998). Studies on mice with functional-null mutations in the gene encoding Ptprq have revealed the importance of the protein in the maturation and maintenance of hair bundles (Goodyear et al., 2003).

1.5 Ptprq, a component of the shaft connectors

Ptprq (for protein tyrosine phosphatase receptor type Q) was identified in a search for protein tyrosine phosphatases (PTPases) involved in the mesangial cell response to glomerular injury in a rat model of glomerulonephritis (Wright et al., 1998). The protein was classified as a type III receptor PTPase based on its overall domain structure (Oganesian et al., 2003; Seifert et al., 2003). It was originally predicted to have an ectodomain with 18 FNIII repeats and 39 potential N-glycosylation sites, a single-pass transmembrane domain and an intracellular domain with PTPase activity (Wright et al., 1998). In addition, the intracellular region of Ptprq was reported to have 9 potential sites

for protein kinase C phosphorylation and 6 putative casein kinase II phosphorylation sites (Wright et al., 1998).

1.5.1 There are three known isoforms of Ptprq

So far, Ptprq has been shown to be expressed as three isoforms, resulting from alternative splicing as well as transcription from an alternative promoter (see figure 1.7; Seifert et al., 2003). One of these isoforms is the full length receptor-like phosphatase (Seifert et al., 2003). As a consequence of alternative splicing that removes the most 3` juxtamembrane exon and the most 5` catalytic domain exon, a premature stop codon is created in the transcript (Seifert et al., 2003). This alternatively spliced transcript encodes a transmembrane protein with a very short cytoplasmic region and no catalytic domain (Seifert et al., 2003). Transcription from an alternative promoter lying in the intron between exons encoding the transmembrane and juxtamembrane domains produces a short protein containing the cytoplasmic catalytic domain (Seifert et al., 2003).
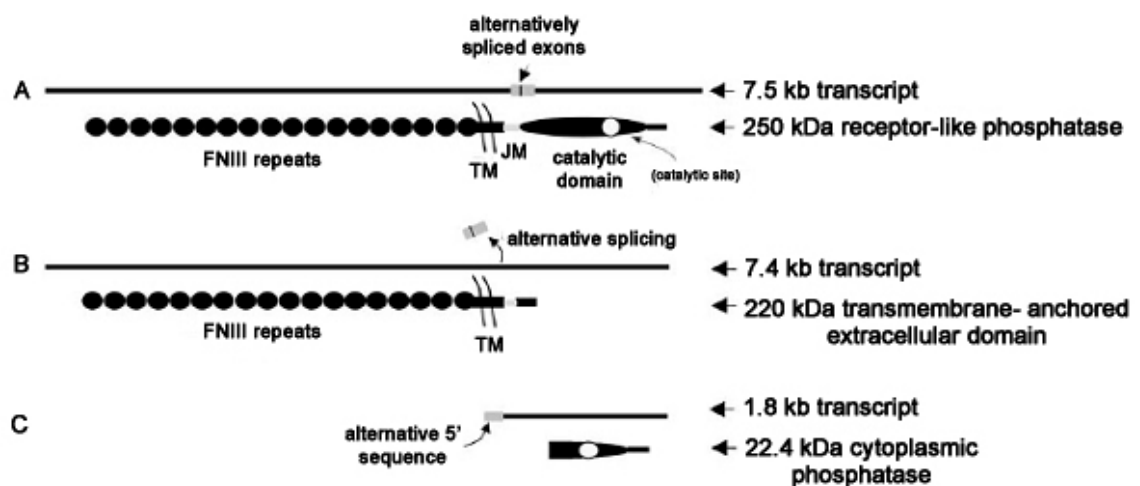
Figure 1.7: The three isoforms of Ptprq generated by alternative splicing and transcription from an alternative promoter. This figure is taken from Seifert et al., 2003.

Transcripts encoding the cytosolic and transmembrane form of Ptprq are differentially expressed in several adult human tissues tested (Seifert et al., 2003). RT-PCR analysis shows that the rat mesangial cells have higher levels of the shortest transcript, whereas fetal and adult human kidneys both mostly produce the full-length transmembrane protein (Seifert et al., 2003). While longer transcripts predominate in adult human lung, tissues such as testis and brain express shorter transcripts (Seifert et al., 2003). However, antibody staining suggests that Ptprq expression is restricted to the inner ear and the kidney (Richardson et al., 1990; Goodyear et al., 2003). In the latter organ it is associated with the podocytes of the glomeruli (Richardson et al., 1990; Goodyear et al., 2003).

1.5.2   *Distribution of Ptprq in the hair bundle*

In the chick, monoclonal antibody (mAb) D10 (anti-HCA) labelling is restricted to the base of hair bundles located in the basilar papilla, the striolar regions of the maculae, and the central regions of each crista (Goodyear and Richardson, 1992). In the extrastriolar regions of the maculae and the peripheral regions of the ampullae, the monoclonal stains the entire length of the stereocilia (Goodyear and Richardson, 1992). Labelling is also evident on the apical non-stereociliary surfaces of all these types of hair cells (Richardson et al., 1990; Goodyear and Richardson, 1992). These expression patterns correlate with the known distribution of shaft connectors as revealed by transmission electron microscopy (Goodyear and Richardson, 1992). Furthermore, immunogold labelling shows that mAb D10 specifically labels shaft connectors and shaft connector-like material at the apical non-stereociliary surfaces of hair cells in the chick inner ear (Goodyear and Richardson, 1992). Ptprq is also suggested to be

associated with the cell-coat puncta visible on the stereociliary surfaces of most hair cells in the mouse cochlea by E17.5 (see section 1.4; Goodyear et al., 2005).

1.5.3 Ptprq expression is only transient in the hair bundles of basal-coil OHCs

Ptprq expression begins early on in the differentiation of hair cells in the chick inner ear and the mouse vestibular system (Bartolami et al., 1991; Goodyear et al., 2003). In the mouse cochlea, however, there is a delay of about 48 hours between the emergence of hair bundles and the appearance of Ptprq (Goodyear et al., 2003). Thus, Ptprq is first detected in the mouse vestibule at E13.5, coincident with the onset of hair-cell differentiation as determined by myoVIIA expression (Goodyear et al., 2003). Within 2 days, all the vestibular hair cells that express myosin VIIA also express Ptprq (Goodyear et al., 2003). The IHCs of the cochlea begin to express Ptprq at E17.5, 2 days after the onset of hair cell differentiation, and Ptprq expression is first detected in the OHCs at E18.5 (Goodyear et al., 2003). In the hair cells at the very apical end of the cochlea Ptprq is detected only at P2 and the overall staining becomes stronger at this stage (Goodyear et al., 2003).

Although Ptprq is expressed throughout the lifetime of most hair bundles (i.e. in case of the chick inner ear, the mouse vestibular organs and most of the mouse cochlea) the protein is only a transient feature of mouse basal-coil OHC bundles (Goodyear et al., 2003). A decrease in the immunoreactivity for Ptprq in the basal-coil OHC bundles becomes apparent at P15 and, by P21, Ptprq is no longer detected in these cells (Goodyear et al., 2003).

1.5.4 Ptprq is required for maintenance of hair bundle structure

Ptprq-TM-KO mice lack the exon coding the transmembrane domain of the protein and flanking intronic sequences, while Ptprq-CAT-KO (Ptprq$^{CAT/CAT}$) mice lack two exons encoding part of the intracellular domain including the catalytic site as well as the flanking intronic sequences (Goodyear et al., 2003). These mutant mice lack both immunoreactivity to an antibody against the intracellular domain of Ptprq (anti-cytoPtprq) and shaft connectors (Goodyear et al., 2003). Compared to the wild-type and heterozygous mice, the Ptprq mutant mice have normal hair bundles at E18.5 (Goodyear et al., 2003). A cochlear hair bundle phenotype is first observable at P1 in the IHC bundles in the basal regions of the cochlea in Ptprq-TM-KO and Ptprq-CAT-KO mice (Goodyear et al., 2003). Varying degrees of hair bundle disorganization are seen in the cochlear hair bundles of the mutant mice at this age (Goodyear et al., 2003). By P8, in IHCs, stereocilia are missing and the remaining are misaligned and fused (see figure 1.8; Goodyear et al., 2003). The OHC hair bundles have shorter than normal stereocilia but fusion is hardly seen (see figure 1.8; Goodyear et al., 2003). The OHC bundles also lack the characteristic V- shape and appear to be more U-shaped than the normal wild-type or heterozygote hair bundles (Goodyear et al., 2003). While the cell bodies of the cochlear hair cells of the mutant mice appear normal until P22, the organ of Corti in the basal turn of the cochlea is completely lost by P80 (Goodyear et al., 2003). Intermediate stages have not been characterised but the hair cell death seen in the basal regions of the cochlea may result from the severity of the phenotype in this region which may prevent the hair cells from transducing (Goodyear et al., 2003). In ruthenium red stained preparations, the vestibular hair bundles of the mutant mice are devoid of shaft connectors and appear to be tightly packed together in an abnormal fashion (Goodyear et al., 2003). Specimens fixed in the presence of tannic acid, however, do not show any

such tight packing and have a normal appearance except for the lack of shaft connectors
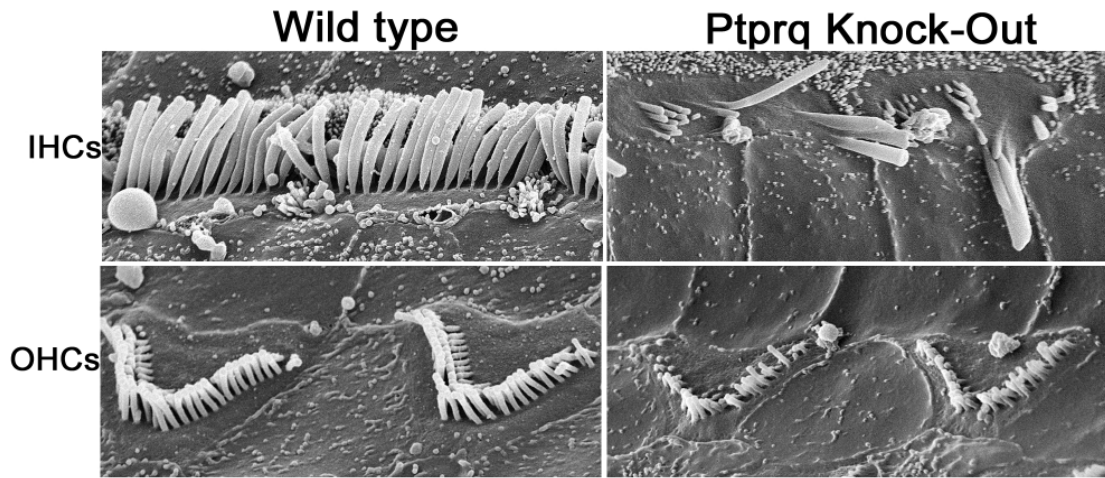
(Goodyear et al., 2003).

Figure 1.8: The stereociliary distruption seen in the Ptprq null mutant mice. This figure is from Goodyear et al., 2003.

1.5.5   Ptprq is a broad-spectrum phosphatidylinositol phosphatase

Although Ptprq was originally predicted to be a PTPase, it has a WPE motif in place of

the WPD motif that is present in the catalytic domains of active PTPases (Oganesian et

al., 2003). Introduction of the Asp to Glu substitution has been shown to reduce the

PTPase activity of other PTPases (Oganesian et al., 2003). This difference in a critical

residue in the catalytic domain of Ptprq makes it a phosphatidylinositol phosphatase

(PIPase) rather than a PTPase (Oganesian et al., 2003). Accordingly, the recombinant

glutathione S-transferase (GST) tagged intracellular domain of Ptprq has 100-fold less

activity than that of the control PTPase, the GST-tagged intracellular domain of PTPβ, a

receptor belonging to the same R3 subfamily of PTPases as Ptprq in the phylogenetic

classification of catalytic domain sequences (Oganesian et al., 2003). Ptprq removes the

phosphates from positions 3 and 5 of phosphatidylinositol 3,5–bisphosphate (PI 3,5 P_2)

and phosphatidylinositol 3,4,5–trisphosphate (PI 3,4,5 P_3), and only from position 5 of

phosphatidylinositol 4,5–bisphosphate (PI 4,5 P_2) (Oganesian et al., 2003; see figure

1.9). When the WPE motif is mutated to WPD, the PIPase activity of Ptprq is undetectable while the PTPase activity of Ptprq increases 10-fold (Oganesian et al., 2003). On increasing the expression levels of the intracellular domain of Ptprq in cultured cells, a dose-dependent reduction is seen in the phosphorylation of the serine/threonine kinase Akt/PKB, a kinase that is regulated by intracellular levels of PI 3,4,5 P_3 (Oganesian et al., 2003). Owing to its PIPase activity, Ptprq is able to inhibit cell proliferation and induce apoptosis in heterologous expression systems (Oganesian et al., 2003).
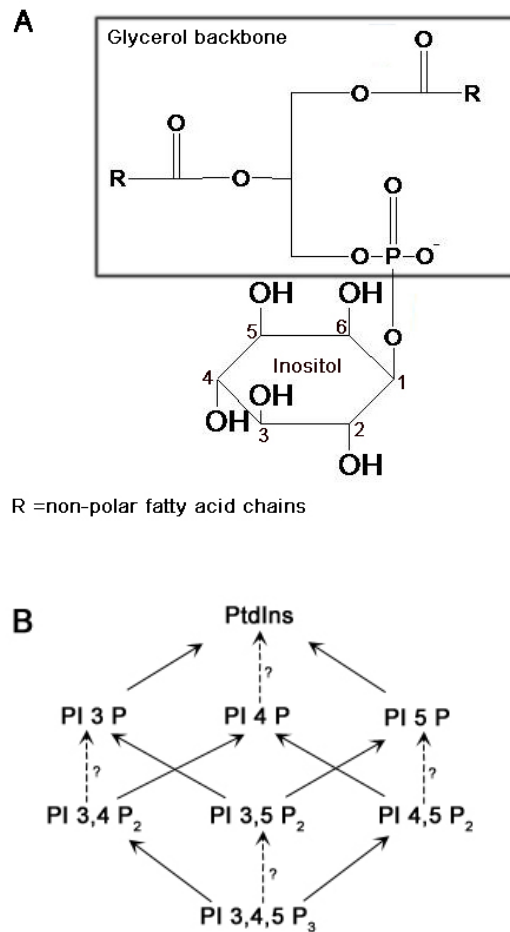
Figure 1.9: A: Structure of PtdIns. PtdIns is a glycerophospholipid and contains a glycerol backbone with two non-polar fatty acid chains and a phosphate group substituted with an inositol head group. The inositol head group can be phosphorylated on position 3, 4 and 5 in various combinations to give PI 3 P, PI 4 P, PI 5 P, PI 3,4 P_2 , PI 4,5 P_2, PI 3,5 P_2 and PI 3,4,5 P_3 . **B**: Ptprq can potentially dephosphorylate several PIs. *In vitro* studies have shown that Ptprq can remove the phosphate groups from positions 3 and 5 of the inositol moiety. Therefore, Ptprq has the potential to dephosphorylate and participate in the interconversion of the various PIs as shown in B.

1.5.5.1 Ptprq may control the PI levels in the hair bundle

Hirono et al. (2004) reported that Ptprq and PI 4,5 P_2 are reciprocally distributed in isolated bullfrog saccular hair cells, suggesting a role for Ptprq in maintaining PI 4,5 P_2 –free zones in the hair bundle and apical surface of these cells. Using antibodies for PI 4,5 P_2, Hirono et al (2004) showed the restriction of PI 4,5 P_2 to the distal end of the hair bundle, and its absence from the apical non-stereociliary surface and the lower regions of the hair bundle, regions where Ptprq is present. Inhibition of phosphatidylinositol 4-kinase, an enzyme required for the synthesis of PI 4,5 P_2, results in the loss of anti-PI 4,5 P_2 immunoreactivity suggesting that hair cells have a robust phosphoinositide (PI) flux (Hirono et al., 2004). A possible role for PI 4,5 P_2 in mechanotransduction and both fast and slow adaptation was shown by treating hair cells with inhibitors of PI 4,5 P_2 synthesis (Hirono et al., 2004).

Based on its phosphatase activity *in vitro,* Ptprq can potentially dephosphorylate most of the PIs (Oganesian et al., 2003; see figure 1.9). Thus, determining how the inositol phospholipid composition and dynamics of the stereocilia membrane are controlled is important for understanding mechanotransduction and its regulation in hair cells (Hirono et al., 2004).

1.6 Inositol phospholipids

PIs are versatile molecules involved in signalling and the regulation of various cellular functions (Downes et al., 2005; Varnai and Balla, 2006; Sasaki et al., 2007). There are 7 different types of PIs found in yeast to man (see figure 1.10), and they are located predominantly in the inner leaflet of virtually all cellular membranes (Downes et al., 2005). PIs are found in low abundance in eukaryotic cells, with PI 4 P and PI 4,5 P_2

being the major PIs after the parent molecule phosphatidylinositol (PtdIns) (Takenawa and Itoh, 2001). PI 3 P and PI 5 P are the next abundant monophosphorylated PIs, whilst PI 3,4 P_2 and PI 3,5 P_2 together make up about 0.2 % of the doubly phosphorylated PIs (Vanhaesebroeck et al., 2001). Levels of PI 3,4,5 P_3 can be very variable. They are nearly undetectable in quiescent cells and can increase 2- to 100-fold upon stimulation (Vanhaesebroeck et al., 2001; Downes et al., 2005; Sasaki et al., 2007).

A combination of various PI kinases and PIPases, under the control of external and internal cues, allows for a dynamic PI content in cells (Downes et al., 2005; see figure 1.10 below).
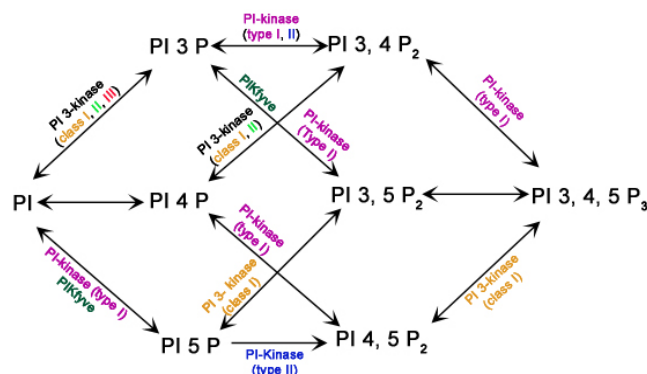
Figure 1.10: The various PI kinases and PIPases are responsible for the interconversions of the PIs. The figure is adapted from Halet, 2005.

PIs are known to perform various functions in cells, either in the form of second messengers, in the recruitment of cytosolic proteins to the membrane, or in binding directly to proteins and modulating their function at the membrane (Balla, 2005; Sasaki et al., 2007). Being a group of molecules that control nearly every signalling process associated with cellular membranes, PIs bind protein kinases, phospholipases, cytoskeletal and scaffold proteins, as well those involved in endocytosis, membrane trafficking and controlling the dynamics of the actin cytoskeleton (Sasaki et al., 2007).

It has therefore been suggested that Ptprq may influence the local PI content of the apical plasma membrane of hair cells, thereby regulating the actin cytoskeleton and membrane traffic, as well as the rates of membrane and actin turnover in developing cochlear hair bundles (Goodyear et al., 2003).

1.6.1   PIs regulate the dynamics of the actin cytoskeleton

PIs are potent regulators of actin binding proteins, and the control of the spatial and temporal distribution of the various PIs, as well as their phosphorylation status dictate the dynamics of the actin cytoskeleton (Janmey et al., 1999; Takenawa and Itoh, 2001; Hilpelä et al., 2004). Two of these lipids, PI 4,5 P_2 and PI 3,4,5 P_3, bind to and modulate the activity of various actin binding proteins (Janmey et al., 1999; Takenawa and Itoh, 2001; Hilpelä et al., 2004). These include actin capping proteins, severing proteins, monomer binding proteins, actin cross-linkers and several other proteins.

1.6.1.1 Actin capping and severing proteins

Capping proteins bind the barbed ends of actin filaments and prevent the addition of monomers, thereby promoting disassembly (Takenawa and Itoh, 2001; Hilpelä et al., 2004). The actin-severing proteins, the gelsolins, promote depolymerization by severing actin filaments and capping the barbed ends (Takenawa and Itoh, 2001; Hilpelä et al., 2004). PI 4,5 P_2 is the only known regulator that can dissociate the capping protein and gelsolin from actin *in vitro* (Takenawa and Itoh, 2001; Hilpelä et al., 2004). PI 4,5 P_2 also appears to inhibit the severing activity of all gelsolin family proteins (Hilpelä et al., 2004).

1.6.1.2 Actin monomer binding proteins

Actin monomer-binding proteins regulate the spatial and temporal availability of actin monomers for polymerization into filaments (Takenawa and Itoh, 2001; Hilpelä et al., 2004). Some actin-monomer binding proteins enhance polymerization while others sequester the monomers and promote actin filament depolymerization (Hilpelä et al., 2004). PI 4,5 P_2 and PI 3,4,5 P_3 interact with and prevent profilin, an actin-monomer binding protein, from sequestering actin monomers (Takenawa and Itoh, 2001; Hilpelä et al., 2004). ADF/cofilins, a group of proteins that bind to ADP-actin, promote filament depolymerization (Takenawa and Itoh, 2001; Hilpelä et al., 2004). All PIs, specially PI 4,5 P_2 and PI 3,4,5 P_3 are able to bind ADF/cofilins, and inhibit their actin binding and depolymerization activities, but PI 4,5 P_2 displays the highest affinity for these proteins (Hilpelä et al., 2004). The sequestration of actin monomers by twinfilin that leads to an inhibition of filament assembly is prevented by an interaction with PI 4,5 P_2 (Hilpelä et al., 2004).

1.6.1.3 Actin cross linking proteins

Actin-cross linking proteins perform the important function of creating higher order actin filament structures like bundles and networks by cross linking the filaments (Hilpelä et al., 2004). PI 4,5 P_2 binds to and enhances the cross linking activity of α actinin while inhibiting the cross-linking activity of filamin (Takenawa and Itoh, 2001; Hilpelä et al., 2004).

1.6.1.4 Other PI modulated proteins that regulate the actin cytoskeleton

On stimulation, Wiskott-Aldrich Syndrome Protein (WASP) and N-WASP activate Arp2/3, a nucleator of actin filaments (Hilpelä et al., 2004). PI 4,5 P_2 together with

Cdc42 is able to bind WASP and N-WASP, causing a conformational change that allows them to activate Arp2/3, thereby enabling actin filament nucleation (Takenawa and Itoh, 2001; Hilpelä et al., 2004).

Through binding and activation of the ezrin-radixin-moesin (ERM) family of proteins, PI 4,5 P_2 regulates the attachment of membrane proteins to actin filaments, a process defining the formation of cell shape and surface structures, motility, adhesion, phagocytosis etc. (Hilpelä et al., 2004). By binding and regulating the functions of vinculin, α-actinin and talin, PI 4,5 P_2 plays an important role in focal adhesion formation (Takenawa and Itoh, 2001). In response to PI 3 K signalling, PI 3,4,5 P_3 may restructure focal adhesions as the lipid is known to bind α actinin releasing it from an interaction with the integrin β subunit (Takenawa and Itoh, 2001; Hilpelä et al., 2004). PI 3,4,5 P_3 is an important regulator of the Rho family of small GTPases (Rho, Rac and Cdc 42) that are known to be involved in signaling to the actin cytoskeleton (Hilpela et al., 2004).

PI 3,4,5 P_3 interacts with Akt, a serine-threonine kinase necessary for cell survival and the interaction is regulated by the lipid phosphatase, PTEN (for Phosphatase and tensin homolog deleted on chromosome ten) (Sasaki et al., 2007). PI 3,4,5 P_3 mediates cellular polarization in different types of mammalian cells (Pinal et al., 2006; Martin-Belmonte and Mostov, 2007). The process of chemotaxis is also dependent on the polyphosphorylated products of PI 3 kinase (Halet, 2005). PI 3,4,5 P_3/ PI 3,4 P_2 have been shown to accumulate at the leading edge of the extending pseudopod in a chemotaxing neutrophil (Halet, 2005). Tandem pleckstrin homology (PH) domain containing protein (TAPP) 1 and 2 bind selectively to PI 3,4 P_2 (Dowler et al., 2000). It

has been suggested that TAPP1 and 2 may be involved in actin regulation, implying a role for PI 3,4 P_2 in the process (Hilpelä et al., 2004).

The above information highlights the role played by PIs in modulating the activity of the various proteins involved in actin filament assembly and cytoskeleton dynamics. Thus, if Ptprq can control the levels of the various PIs in the stereociliar membrane, it has also the potential to regulate actin polymerisation and cytoskeleton dynamics.

1.6.2 PIs are involved in endocytosis and membrane traffic

In addition to regulating actin dynamics, PI 4,5 P_2 plays a major role in endocytosis (Takenawa and Itoh, 2001). PI 4,5 P_2 binds the clathrin binding adaptor protein 2 (AP-2) and stabilizes its association with the membrane during clathrin-mediated endocytosis (Takenawa and Itoh, 2001). Further pinching off of the clathrin coated vesicle from the plasma membrane also requires activation of the GTPase dynamin by PI 4,5 P_2 (Takenawa and Itoh, 2001). Dynamin then activates endophilin which is necessary for the alteration in membrane shape and facilitates vesicle scission (Takenawa and Itoh, 2001). Epsin, an accessory protein required for the formation and invagination of coated pits, also binds to both clathrin and AP-2 and has a high affinity for PI 4,5 P_2 (Takenawa and Itoh, 2001). Thus, PI 4,5 P_2 is an important component necessary for the binding of clathrin and the accessory proteins to the plasma membrane (Takenawa and Itoh, 2001). However, the clathrin coat needs to be shed from the vesicle membrane following endocytosis (Takenawa and Itoh, 2001). The hydrolysis of PI 4,5 P_2 to PI 4 P by synaptojanin-I appears essential to this process (Takenawa and Itoh, 2001). There is a transient production of PI 3,4,5 P_3 in the plasma membrane during phagocytosis, a type of endocytosis (Halet, 2005). This PI 3,4,5 P_3 may activate

the actin cytoskeleton and membrane remodelling processes necessary for phagocytosis (Halet, 2005).

PI 3 P is predominantly found on vacuolar and endosomal membranes as well as those of the intralumenal vesicles of multivesicular bodies (MVB) (Downes et al., 2005; Halet, 2005; Sasaki et al., 2007). PI 3 P is essentially involved in the membrane recruitment of protein complexes that regulate the endosomal trafficking processes, as well as for sorting proteins from the Golgi to the lysosomes (Downes et al., 2005; Halet, 2005; Sasaki et al., 2007). Several proteins involved in the regulation of endosome membrane trafficking contain the FYVE domain (for Fab1p, YOTB, Vac1p and EEA1) that helps in their recruitment to the PI 3 P-containing endosomal membrane (Downes et al., 2005; Sasaki et al., 2007).

PI 4 P is essential for the recruitment of specific protein complexes to the Golgi membrane so as to modulate the traffic of membrane from the Trans Golgi Network (TGN) to the cell surface (Overduin et al., 2001; Downes et al., 2005; Sasaki et al., 2007). Membrane association of PI 4 P-effector proteins usually requires multiple interactions with other factors (Downes et al., 2005; D'Angelo et al., 2008). The clathrin adaptor-protein 1 (AP-1) complex that functions in the formation of clathrin coated vesicles at the TGN, binds to PI 4 P in the membrane, the small GTPase Arf1 and the cargo to be transported (Downes et al., 2005; Sasaki et al., 2007; D'Angelo et al., 2008). Two more PI 4 P binding proteins, the four-phosphatase-adaptor proteins FAPP1 and 2, also require Arf1 interaction in order to traffic vesicles from the TGN to the cell surface (Godi et al., 2004). Membrane recycling from the vacuoles/lysosmes to the Golgi and protein sorting into MVBs are some of the processes regulated by PI 3,5 P_2 (Roth, 2004; Downes et al., 2005; Halet, 2005; Sasaki et al., 2007).

Therefore, there is abundant evidence that the various steps of endocytosis and membrane turnover are regulated by local PI levels. Thus, Ptprq may serve to control the levels of the PIs involved in these processes at the apical surface of hair cells.

1.7 Ptprq is an apically targeted protein in the hair cell

As mentioned in section 1.5.2, Ptprq is restricted to the apical stereociliary and non-stereociliary surfaces of all hair cells during development and throughout life in most hair cells (Goodyear et al., 2003). The hair cells of the inner ear are polarized epithelial cells with their distinct apical and basolateral membrane surfaces performing specific cellular functions. As in all epithelial cells (Weimbs et al., 1997; Ellis et al., 2006), the functional asymmetry of the two plasma membrane domains of hair cells is reflected in their distinct molecular compositions. The apical surface is enriched in the hair bundle proteins including those of the mechanotransduction apparatus. For example, Ptprq, Cdh23, Pcdh15 and PMCA2a are all transmembrane proteins that are specifically targeted to the apical surface of hair cells (Goodyear et al., 2003; Michel et al., 2005; Senften et al., 2006; Kazmierczak et al., 2007; Grati et al., 2006; Hill et al., 2006). Potassium channels like KCNQ4, that are involved in shaping the receptor potential, are found specifically at the basal membrane of hair cells (Kharkovets et al., 2000).

The compositional asymmetry of the apical and basolateral domains of epithelial cells is brought about by asymetrical targeting of proteins and lipids to the two surfaces (reviewed in Mellman and Nelson, 2008). Tight junctions that seal together the apical ends of adjacent epithelial cells confine the proteins and lipids to their appropriate domains and prevent their lateral diffusion in the outer leaflet of the lipid bilayer (Mellman and Nelson, 2008). With the apical and the basolateral poles of the hair cell involved in very distinct functions, it is clear that the overall performance of the hair

cells must depend on efficient protein sorting machinery. With the exception of PMCA2, very little is known about polarized protein targeting in hair cells (Grati et al., 2006; Hill et al., 2006). However, apical targeting has been well studied in polarized epithelial cell lines (Brown and Breton, 2000; Mostov et al., 2000; Schuck and Simons, 2004; Mellman and Nelson, 2008).

1.8 Ptprq is an orphan receptor

As mentioned in section 1.2.3, electron micrographs of ruthenium red stained preparations show that shaft connectors are formed by numerous strands that extend from the surface of the stereocilia and coalesce in a dense particle (Goodyear et al., 2003). There are currently no known ligands for Ptprq and it is unknown whether Ptprq alone forms shaft connectors or if an associated protein interacts with and bridges the extracellular domains of several Ptprq molecules (Goodyear et al., 2003). It has been suggested that the dense particles associated with shaft connectors (see figure 1.5, inset) may be formed from keratan sulphate glycosaminoglycan (GAG) chains (Goodyear et al., 2003). Evidence in support of this suggestion comes from studies in which hair bundle staining resembling that seen with mAb D10 has been observed with a polyclonal antiserum to α–tectorin, a sulphated, keratanase-sensitive component of the tectorial membrane (Killick and Richardson, 1997). Also, in the guinea-pig cochlea, a mAb to keratan sulphate stains hair bundles (Katori et al., 1996).

1.9 Aims of the thesis

Currently, very little is known about the cellular function of Ptprq in hair cells. Although hair bundles in the Ptprq mutant mice are disorganised and the hair cells eventually die, the actual role Ptprq plays in maintaining hair bundles is unknown

(Goodyear et al., 2003). The current project was aimed at furthering our understanding of the function of Ptprq. The aims were four-fold. The PIPase activity of Ptprq has only been tested *in vitro* and whether Ptprq regulates the level of any PI in the hair bundle has remained unexplored. A first aim, therefore, was to investigate if the loss of Ptprq alters the normal distribution of PIs in the hair cell. No known protein-protein interaction domains are present in the intracellular domain of Ptprq and it is not known if Ptprq interacts with any of the hair bundle proteins that have been thus far identified or any other proteins. A second aim of this study was therefore to identify such potential interaction partners using yeast-two hybrid screening. A third aim was to determine how Ptprq is targeted to the apical surface of the sensory hair cell. Finally, various experiments were performed in order to determine if Ptprq is a proteoglycan.

CHAPTER 2

Materials and Methods

2.1   Gene cloning techniques

2.1.1 *Plasmid minipreparation*

Plasmid DNA was obtained from overnight cultures that had been prepared by inoculating single bacterial colonies into 5 ml of sterile lysogeny broth (LB) containing the appropriate antibiotic. All cultures were grown at 37°C for 12-16 hours and the plasmid DNA was prepared using a QiaPrep Spin miniprep kit (Qiagen, Germany). In brief, 3-5 ml volume of the culture was used to harvest the cells by centrifugation at 13000 rpm for 1 minute. The cell pellet was then re-suspended in 250 μl of re-suspension buffer (buffer P1) by pipetting until no clumps were visible. To this, 250 μl of lysis buffer (buffer P2) was added, and gently inverted 4-6 times to mix. To the lysate, 350 μl of neutralisation buffer (buffer P3) was added and gently inverted 4-6 times to mix. The off-white flocculate precipitate formed was pelleted by centrifugation at 13000 rpm for 10 minutes. The homogenous supernatant was then transferred to a spin column placed in the collecting tube and centrifuged at 13000 rpm for 1 minute. The flow through was discarded and 750 μl of wash buffer containing ethanol (buffer PE) was added. The spin column was centrifuged at 13000 rpm for 1 minute and the flow through discarded. To remove the wash buffer completely, the spin column was centrifuged again at 13000 rpm for 1 minute. After this, the spin column was transferred into a fresh, labelled microcentrifuge tube and 50 μl of the elution buffer (buffer EB) was added (for plasmids ≥ 10kb, buffer EB was warmed to 70°C) and the columns were

allowed to stand for one minute before collecting the eluate by centrifugation at 13000 rpm for one minute.

2.1.2 Plasmid maxipreparation

Maxipreparation of plasmid DNA was done using Nucleobond AX (Macherey-Nagel, Germany). A starter culture of 10 ml was used to inoculate 250 ml of LB containing the appropriate antibiotic, which was then grown overnight at 37°C (12-16 hours). The cells were harvested by centrifugation in a Sorvall GSA rotor at 5000 rpm for 10 minutes at 4°C. The bacterial cell pellet was re-suspended in 12 ml of re-suspension buffer (buffer S1) by pipetting till no clumps were seen. The cells were lysed by adding 12 ml of lysis buffer (buffer S2) and gently inverting 8 times. The lysate was neutralized by adding 12 ml of pre-chilled buffer S3 and gently inverting 8 times. The tube was incubated on ice for 5 minutes. Meanwhile, a folded filter paper was placed in a plastic funnel and wetted with a few drops of distilled water. The lysate was filtered through this and the filtrate was collected in a fresh beaker. This filtrate was then passed twice through an equilibrated AX500 Nucleobond column and the flow through was discarded. The DNA captured within the Nucleobond column was given a wash with 32 ml of wash buffer containing ethanol (buffer N3). A fresh 50 ml round-bottom centrifuge tube was placed under the column and 15 ml of elution buffer N5, pre-warmed to 45°C was added to the column. To the eluate collected in the centrifuge tube, 11 ml of isopropanol was added and mixed well by inversion several times to precipitate the plasmid DNA. It was then centrifuged at 12000 rpm for 30 minutes at 4°C. The supernatant was carefully discarded and the pellet was washed with 5 ml of 70% ethanol. It was centrifuged at 12000 rpm for at least 10 minutes at room temperature. The supernatant was discarded and the pellet was allowed to dry. To the tubes, 500 μl of 1x Tris EDTA buffer pH 8

was added and given a gentle shake. The tubes were left on ice for about 30 minutes after which the DNA concentration was estimated by measuring the absorbance at 260 nm (2.1.3).

2.1.3 Estimation of DNA concentration

The amount of DNA in a sample was estimated by measuring the absorbance at 260 nm and amount of protein at 280 nm. An OD_{260} of 1 for a 1 ml sample, in a cell with 1 cm path length, corresponds to 50 μg/ml of double stranded DNA. From this, the DNA concentration in any sample can be calculated using the dilution factor.

The ratio of absorbance at 260 nm to 280 nm reveals the purity of the DNA sample. A value between 1.8-2.0 implies the DNA is fairly pure.

2.1.4 Polymerase Chain Reaction (PCR)

PCR was performed with appropriate primer pairs and template DNA, using either Bioline *Taq* DNA polymerase (Bioline, London, UK) or *Pfu* turbo DNA polymerase (Stratagene, Netherlands).

A typical PCR reaction included the following reagents along with the appropriate template.

Reagents	Volume in μl per reaction	
	Bioline *Taq* DNA polymerase reaction (25 μl)	*Pfu* turbo DNA polymerase reaction (50 μl)
Supplied 10x buffer	2.5	5
Forward primer 25 pmol/μl	0.5	1

Reverse primer 25 pmol/µl	0.5	1
dNTPs 10 mM	0.5	1
MgCl$_2$ 50 mM	0.75	-
dH$_2$O	20.15	40.5
Polymerase	0.1	1

Table 2.1: Composition of a typical PCR reaction

In cases where PCR was performed in plates, 2 drops of mineral oil was added into each well before cycling to prevent evaporation of the reaction mixture during PCR.

A typical PCR cycle included the following steps

1. Melting-94°C for 1 minute

2. 94°C for 15 seconds

3. Annealing-50°C for 15 seconds

4. Extension-72°C for 1 minute/1 kb

5. Steps 2-4 were repeated 24 times

6. 72°C for 5 minutes

The annealing temperature and the number of cycles were varied in some cases to increase the yield of the product.

2.1.4.1 Insert amplification

All insert amplification reactions made use of *Pfu* turbo DNA polymerase that possesses 'proof reading' activity. The PCR products were separated on preparative TBE agarose gels (2.1.7), stained with ethidium bromide and the bands of interest were cut out of the gel and the DNA purified using Geneclean (Qbiogene, California; section 2.1.8.1) or the Nucleospin extraction kit (Macherey-Nagel, Germany; Section 2.1.8.2) .

2.1.4.2 Colony PCR

Bioline *Taq* DNA polymerase was used for colony PCR study to screen for presence of the desired insert in transformed colonies (2.1.10). Toothpicks were used to pick single colonies, which were first transferred onto a master plate and then into the appropriate well in the PCR plate containing 25 μl of the PCR reaction mixture. Master plates were incubated at 37°C overnight to allow the colonies to grow. The PCR products were analysed on TBE agarose gels stained with ethidium bromide (2.1.7).

2.1.5   Restriction enyzyme digestions

All restriction digests of DNA were done using enzymes supplied by New England Biolabs (Hitchin, UK) according to the manufacturer's specifications.

PCR products and vectors were typically digested in 50 μl and 20 μl volume reactions respectively. Double digestions were carried out simultaneously, as all of the enzyme pairs used had a common reaction buffer in which each enzyme was at least 75% active. Generally, 0.5-1 μg of DNA was digested in an appropriate volume of 1x reaction buffer containing 10 units (U) of restriction enzyme per μg of DNA. Reactions were carried out in microcentrifuge tubes at 37°C for one hour.

A typical restriction digestion reaction included the following reagents:

Reagents	Volume in μl per reaction	
	20μl	50μl
10x buffer (as per NEB recommendations)	2 μl	5 μl
BSA 10x (if required)	2 μl	5 μl
Sterile water	Made up to 20 μl	Made up to 50 μl
DNA	0.5-1 μg	0.5-1 μg
Enzyme/s	0.5-1 μl	0.5-1 μl

Table 2.2: Composition of typical restriction enzyme digestion reactions.

2.1.6 *Dephosphorylation*

In cases where the vector DNA was cut with a single restriction enzyme producing self-compatible ends, dephosphorylation was carried out to prevent vector re-ligation. Antarctic phosphatase (New England Biolabs, Hitchin, UK) was used in every such case using the buffer supplied by the manufacturer.

After the restriction digest reaction, 1/10 volume of the 10x Antarctic phosphatase buffer and 1 μl of Antarctic phosphatase was added. The reaction mixture was incubated at 37°C for 15 minutes after which another 1 μl of the enzyme was added, followed by further incubation for 15 minutes at 37°C. The reaction mixture was then placed at 65°C for 5 minutes to inactivate the enzyme.

2.1.7 Gel electrophoresis of DNA

Horizontal slab gels of TBE agarose were used for electrophoretic separation of DNA. Either 0.7% or 1% gels were used depending on the size of the DNA and the resolution required. 10x gel loading buffer (50% glycerol, 1 mM Tris-HCl, pH 8.0, 0.25% w/v bromophenol blue, 1 mM EDTA) was used at 1/10 of the volume of DNA sample. At least one lane of DNA size markers, either a 1 kb DNA ladder or a 100 bp DNA ladder as required, was always run alongside the samples. Electrophoresis was carried out in 1x TBE buffer (0.089 M Tris base, 0.088 M orthoboric acid, 0.002 M EDTA) at 80 volts for approximately 40 minutes.

After the electrophoretic separation, the gels were incubated in 0.5 μg/ml ethidium bromide in water for about 20 minutes before visualizing the DNA bands on a ultraviolet (UV) transilluminator. The gels were photographed with a CCD camera coupled to a thermal printer.

2.1.8 Purification of DNA from TBE agarose gels

A Geneclean II DNA purification kit (Qbiogene, California) or the Nucleospin extraction kit (Macherey-Nagel, Germany) was used to purify DNA separated on TBE agarose preparative gels.

After electrophoretic separation and ethidium bromide staining of the gel, the DNA bands of interest were excised from the gel while visualizing on a UV transilluminator. The gel pieces were collected in a labelled microcentrifuge tube, weighed and subjected to the various purification steps as recommended by the suppliers of the kits.

2.1.8.1 Using Geneclean

To the weighed gel pieces, 0.5 volume of TBE modifier was added followed by 4.5 volumes of NaI. This was mixed well and incubated at 45°C till the gel pieces dissolved completely. For volumes up to 1 ml, 10 μl of re-suspended glass milk was added, while 20 μl of glass milk was used for volumes up to 1.5 ml. To allow the DNA to bind to the glass beads, the tubes were incubated for at least 5 minutes depending on the volume (greater binding time of up to 15 minutes allowed for larger volumes). The glass beads were pelleted at 4500 rpm for 1 minute. The supernatant was discarded and the glass beads were re-suspended in 500 μl of New Wash buffer containing ethanol and were pelleted at 4500 rpm for 1 minute. Three such washes were given before finally vacuum drying the pellets for two minutes. The dried glass beads were then re-suspended in an equal volume of sterilised de-ionised water (dH_2O), incubated for 1 minute to allow DNA elution and then centrifuged at 13000 rpm for 1 minute. The supernatant containing the eluted DNA was collected in a fresh, labelled microcentrifuge tube. The elution process was repeated to ensure elution of ~90% of the DNA and the supernatants were pooled together. 2 μl of this gel-purified DNA was visualized by gel electrophoresis (2.1.7).

2.1.8.2 Using the NucleoSpin® extraction kit

To the weighed gel pieces, 3 volumes of lysis buffer (buffer NT1) was added and mixed well. The tube was placed at 50°C for 5-10 minutes with intermittent vortexing until the gel pieces dissolved completely. A NucleoSpin® column was placed in a 2 ml collecting tube and the sample was loaded on the column. The column was centrifuged at 9200 rpm for 1 minute and the flow through was discarded. 500 μl of binding buffer (buffer NT2) was added and the column was centrifuged at 10750 rpm for 1 minute.

The column was then washed with 600 μl of wash buffer (buffer NT3) and centrifuged at 10750 rpm for 1 minute and the flow through was discarded. The column was given a second wash with 200 μl of buffer NT3 and the column was centrifuged for 2 minutes at 10750 rpm to remove any residual NT3.The column was transferred to a fresh, labelled microcentrifuge tube and 25 μl of elution buffer NE (pre-warmed to 70°C) was added. The column was incubated at room temperature for 1 minute and centrifuged for 1 minute at 10750 rpm to collect the eluate. 2 μl of this eluted DNA was visualized by gel electrophoresis (2.1.7).

2.1.9   Ligation Reactions

Ligation reactions were performed using vector and insert DNA that had been digested (2.1.5) with the same enzyme/s and then purified from preparative gels (2.1.8). Ligations were carried out using vector and insert DNA at a 1:3 molar ratio, in 10 μl of 1x T4 DNA ligase buffer containing 0.5 μl of T4 DNA ligase from New England Biolabs (Hitchin, UK). This reaction was referred to as the +ligase+Insert (+L+I) reaction, to distinguish it from the two additional control reactions, with ligase (+L) and without ligase (-L), both of which contained only vector DNA and no insert DNA. All reactions were incubated at 14°C overnight. The ligation reaction +L+I, along with the controls –L and +L, were then transformed (2.1.10) into competent *Escherichia coli* cells of the appropriate strain. The ligation reactions with controls were perfomed as shown below.

	-L	+L	+L+I
10x ligase buffer	1 μl	1 μl	1 μl

Linearised Vector	1 μl	1 μl	1 μl
Insert	-	-	7.5 μl
eH2O	8 μl	7.5 μl	-
T4 DNA ligase	-	0.5 μl	0.5 μl

Table 2.3: Composition of a ligation reaction

2.1.10 Bacterial transformations

2.1.10.1   Bacterial culture media

2.1.10.1.1 <u>Lysogeny Broth or LB</u>

LB is a nutrient-rich medium for bacterial cultures that was originally developed by Bertani. To make up 1 litre of LB, 10 g of Tryptone, 5 g of yeast extract and 10 g of NaCl were dissolved in 900 ml of distilled water. The volume was then made up to 1000 ml with distilled water and the LB was sterilized by autoclaving at 121°C for at least 20 minutes.

2.1.10.1.2 <u>LB agar antibiotic selection plates</u>

To one litre of LB, 15 g of agar was added and the mixture was autoclaved as above. After cooling to 50°C, ampicillin (50 μg/ml), kanamycin (25 μg/ml) or chloramphenicol (50 μg/ml) were added and the bottle was swirled to mix the contents before pouring the mixture into bacterial culture plates.

2.1.10.1.3 <u>Super Optimal broth with Catabolite repression (SOC medium)</u>

To 800 ml of distilled water, 20 g tryptone, 5 g of yeast extract, 0.58 g of NaCl, 0.186 g of KCl and 0.952 g of MgCl$_2$ were added. Once dissolved, the solution was made up to 980 ml with distilled water and the medium was autoclaved as above. After cooling, 20 ml of filter-sterilized 1M glucose was added. The sterile SOC medium was then aliquoted into fresh 15 ml tubes for later use.

2.1.10.2 Protocol for bacterial transformations

Transformation of ligation reactions was done according to the supplier's instructions, using chemically competent XL1 blue or XL1 gold cells (both from Stratagene, Netherlands). The transformation protocol was as follows.

2.1.10.2.1 <u>Using XL1 blue competent cells</u>

For every three transformation reactions (-L, +L and +L+I), 1 vial (250 μl) of XL1 blue competent cells (from –80°C), was thawed out on ice and 4.5 μl of β-mercaptoethanol was added and swirled to mix. The cells were then incubated on ice for 10 minutes while swirling every two minutes. Meanwhile, 15 ml Falcon tubes (one for each reaction) were labelled appropriately and incubated on ice. Aliquots of 80 μl of the competent cells were transferred into the pre-chilled labelled Falcon tubes and 2 μl of the respective ligation mixtures were added to the cells. The tubes were incubated for 30 minutes on ice. The cells were then heat shocked at 42°C for 45 seconds and immediately placed on ice for 2 minutes. Pre-warmed SOC medium (900 μl) was added to the tubes and the tubes were incubated with shaking at 37°C for one hour. Each transformation reaction was then plated onto appropriately labelled LB agar plates containing the appropriate antibiotic, as 100 μl, 200 μl and 700 μl aliquots (the 700 μl

aliquot of cells was spun down and the pellet re-suspended in 200 μl of LB medium before plating).

2.1.10.2.2 <u>Using XL10 gold competent cells</u>

For every three transformation reactions (-L, +L and +L+I), 1 vial (100 μl) of XL1 gold competent cells (from –80°C) was thawed out on ice and 4 μl of β-mercaptoethanol was added and swirled to mix. The procedure here onward was the same as that for XL1 blue competent cells, except that 30 μl of the XL10 gold competent cells was used for each transformation reaction, and the heat shock at 42°C was for 30 seconds.

2.1.11 Glycerol stocks

Clones of all constructs were maintained as glycerol stocks. Cells were harvested from 1-3 ml of overnight cultures by centrifugation at 13000 rpm for 1 minute in microcentrifuge tubes. The cell pellet was re-suspended in 900 μl of sterile LB containing 12.5% glycerol. The microcentrifuge tubes were labelled appropriately and transferred to the -80°C freezer.

2.1.12 Gene cloning procedure

All of the gene cloning experiments followed these steps.

The vector plasmids were prepared by plasmid minipreparations (2.1.1) and the insert DNA was either amplified by PCR (2.1.4) or excised from a previous construct by restriction enzyme digestions (2.1.5). The vector and insert DNAs were digested (2.1.5) by the same restriction enzyme/s (as mentioned in the gene cloning strategies), followed by dephosphorylation (2.1.6) of the vector where necessary. Both vector and insert DNAs were then separated by electrophoresis on preparative gels (2.1.7) and purified

(2.1.8). The vector and insert DNAs were then ligated (2.1.9) and transformed into appropriate chemically competent bacterial host cells (2.1.10). The transformed colonies were then screened for the presence of insert DNA by colony PCR (2.1.4.2) and the PCR positive colonies or clones were used to make 5 ml overnight cultures. Plasmid DNA minipreparations (2.1.1) of these overnight cultures were digested (2.1.5) with appropriate restriction enzyme/s to confirm the size of the insert DNA. The DNA sequences of at least one of the clones was determined to confirm that the orientation of the insert with respect to the promoter was correct, and that no mutations were introduced during the cloning process. The positive clones were maintained as glycerol stocks (2.1.11). Plasmid maxipreparations (2.1.2) of the mammalian expression constructs were done and stored at -20°C.

2.2   Protein analysis

2.2.1 *Sodium dodecyl sulphate polyacrylamide gel electrophoresis (SDS PAGE)*

The BioRad (Hertfordshire, UK) mini gel system was used to make SDS PAGE mini gels. The gel plates were rinsed with 100% industrial methylated spirit (IMS) and wiped dry before use. The two glass plates were clamped to the stand and resolving gel solution (Table 2.4) was poured between the plates to a height of 5 cm. Water saturated N-butanol was layered on top of the gel solution to prevent O_2 mediated inhibition of polymerisation.

When the gels were completely polymerised, the butanol was poured out and un-polymerised acrylamide was washed out with distilled water. The stacking gel solution (Table 2.5) was then poured onto the polymerised resolving gel and the combs were put

in place. The gels were allowed to polymerise completely (15-20 minutes), before removing the combs. The gel plates were released from the clamp and the electrophoresis apparatus was set up and 1x SDS-PAGE running buffer (0.18 M Tris base, 0.19 M glycine, 0.01% SDS) was poured between the plates ensuring no leakage. The electrophoresis tank was filled with 1x SDS-PAGE running buffer to ¼ its level. The protein samples were mixed with equal volume of 2x reducing sample buffer (10% glycerol, 3% SDS, 12.5% stacking Tris, 0.1 M DTT) and boiled at 100°C for 5 minutes in microcentrifuge tubes. The microcentrifuge tubes were then given a quick spin to pellet protein precipitates and loaded into the wells and electrophoreses was carried out at 40 mA (for two gels) for approximately 40 minutes. Protein molecular weight markers, Precision Plus Protein Dual colour standards (Bio-Rad), were run alongside the samples in at least one lane in each gel.

Reagent	10% gel (2 gels)	7.5% gel(2 gels)
Acrylamide	2.66 ml	2 ml
4x Resolving gel buffer (1.5M Tris pH 8.8, 0.4% SDS)	2 ml	2 ml
Ammonium per sulphate (5mg/ml)	0.8 ml	0.8 ml
Distilled water	2.54 ml	3.2 ml
TEMED	10 µl	10 µl

Table 2.4: Resolving gel composition

Reagent	For 2 gels
Acrylamide	0.4 ml
Distilled water	2.2 ml
Ammonium per sulphate (5mg/ml)	0.4 ml
4x stacking buffer (0.5 M Tris pH 6.8, 0.4% SDS)	1 ml
TEMED	10 μl

Table 2.5: Stacking gel composition

2.2.2 Coomassie staining of proteins

Proteins separated on SDS-PAGE gels were stained using Coomassie stain (0.1% Brilliant blue, 50% methanol, and 10% acetic acid in distilled water) for 60 minutes on a rotating plate. The gels were then visualized after successive washes in destain (10% methanol and 10% acetic acid in distilled water). The gels were photographed and images stored on a CD.

2.2.3 Semi-dry western blotting and detection of proteins

The proteins separated on SDS-PAGE were transferred onto PVDF (Amersham Biosciences, Bucks, UK) protein transfer membranes by the semi-dry blotting method. For each gel, 10 sheets of Whatman 3MM papers of 10 X 8 cm were cut out. After the SDS-PAGE gel run, 3 sheets of the Whatman 3MM were soaked in anode buffer 1 (300 mM Tris, 20% methanol, pH 10.4) and placed on the anodal plate of the blotter after draining excess buffer. The next 2 were soaked in anode buffer 2 (25 mM Tris base,

20% methanol, pH 10.4) and placed on the first 3 pieces. Meanwhile the PVDF membrane (10 X 8 cm) was wetted in methanol and then soaked in anode buffer 2. The resolving gel was placed carefully on the PVDF membrane ensuring the gel did not slide on the membrane after initial contact (some protein transfer occurs soon after contact). The PVDF with the resolving gel on top of it was carefully transferred onto the stack of Whatman filter papers placed earlier on the blotter. The last 5 pieces of Whatman 3MM papers were soaked in cathode buffer (25 mM Tris Base, 40 mM 6-amino-n-hexanoic acid, 20% methanol, pH 9.4) and excess buffer was drained off before placing them on top of the resolving gel. The cathode was then placed on top after ensuring no air bubbles were trapped between the papers. The protein transfer was carried out at 40 mA per gel for 45 minutes.

After the transfer, the blot was placed in blocking buffer (3% skimmed milk powder, 0.2% Tween-20 in TBS (150 mM NaCl, 10 mM Tris-HCl, pH 7.4) with gentle shaking for one hour at room temperature. It was then probed with appropriately diluted primary antibody (antisera or monoclonal antibody) against the protein and left overnight on a shaker at 4°C. This was followed by three quick washes with TBS buffer and then three 5 minute washes with TBS containing 0.2% Tween-20 before incubating in alkaline phosphatase conjugated secondary antibody (DAKO, Germany) (raised against the IgG of the species that provided the primary antibody) at 1:1000 dilution for one hour at room temperature. The blot was then given three quick washes with TBS buffer and three 5-minute washes with TBS containing 0.2% Tween-20 followed by a 5 minute wash in alkaline phosphatase buffer (5% 1 M MgCl2, 10% 1 M Tris pH 9.5 and 0.25% 4 M NaCl). Meanwhile 20 ml of alkaline phosphatase buffer containing 20 μl of 5-bromo-4chloro-3-indolyl phosphate (BCIP), which is converted from colourless to insoluble blue product in presence of alkaline phosphatase, and 20 μl of nitro-blue

tetrazolium chloride (NBT), which helps intensify the colour and increase sensitivity, was prepared. The blot was finally incubated in this substrate solution, until the colour developed (~10 minutes). The reaction was then stopped by washing the blot several times with deionised water before drying on paper towels.

2.3   Immunofluorescence

2.3.1 *Paraformaldehyde fixation*

The specimens were first washed with 1 or 2 ml of HEPES buffered Hank's Balanced Salt Solution (HBHBSS) followed by three quick washes with phosphate-buffered saline (PBS; 1 x contains 150 mM NaCl, 10 mM sodium phosphate, pH of 7.4). The specimens were incubated in formaldehyde fixative (3.7% formaldehyde in 0.1 M sodium phosphate buffer, pH 7.4) for at least 30 minutes at room temperature. The fixed specimens were then washed 3 times for 5 minutes each to wash off the excess paraformaldehyde.

2.3.2 *Immunostaining*

2.3.2.1 Antibodies

mAb D10 (anti-HCA) has been described previously (Richardson et al., 1990). Briefly, mice were first immunised with a crude membrane fraction of lagena maculae obtained from posthatch day 1-3 domestic fowl. A mouse that was producing a polyclonal anti-lagena macula serum that could be made hair cell specific by absorption was used to make the mAb D10. Anti-cytoPtprq is a rabbit polyclonal that was raised to the recombinant intracellular domain of chick Ptprq (Dr. Kevin Legan, unpublished). The

anti-cytoPtprq polyclonal does not stain hair bundles in the Ptprq$^{CAT/CAT}$ mouse (Richardson, GP, unpublished).

2.3.2.2 Antibody staining

The fixed and washed specimens were incubated in pre-block (10% horse serum in TBS/PBS) for 1 hour. The specimens were permeabilized when detecting intracellular antigens by the addition of 0.1% Triton X-100 in the pre-block. The primary antibody was added at the appropriate dilution (indicated in the respective sections) and the specimens left on a rocker overnight at 4°C. The following day, the specimens were washed 3 times for 5 minutes each wash with TBS/PBS to wash off the primary antibody. The secondary antibody was added at the desired dilution (indicated in the respective sections) in 10% horse serum in TBS/PBS. If necessary, Texas Red®-X conjugated phalloidin (1:300 dilution; Molecular Probes, Invitrogen) or Rhodamine-conjugated phalloidin (at 1:500 dilution; Sigma) was used as counter stain. The specimens were incubated for at least 1 hour at room temperature on a rocker, followed by three 10 minute washes with TBS/PBS. The specimens were finally mounted on glass slides using Vectashield (Vector Laboratories, Peterborough, UK) mounting medium.

CHAPTER 3

Absence of Ptprq does not affect the distribution of inositol phospholipid reporters in hair cells

3.1 Introduction

Ptprq has PIPase activity *in vitro* and in bull frog saccular hair cell bundles, antibody staining reveals a reciprocal distribution of Ptprq and PI 4,5 P_2, with Ptprq confined to the basal part of the hair bundle and PI 4,5 P_2 found mostly in the apical part (Hirono et al., 2004; see section 1.5.5.1). As an inositol lipid phosphatase, Ptprq has the potential of regulating cellular processes involving these lipids (section 1.5.5; Goodyear et al., 2003). Therefore, an insight into all the PI targets of Ptprq may shed light on its role in the maintenance of cochlear hair bundles. Previous attempts to use antibodies to the different PIs on fixed cochlear hair cells have proved unsuccessful (Goodyear and Richardson, unpublished observation). Thus, several PI binding domains that have been previously used as reporters for specific PIs (see table 3.1; Dowler et al., 2000; Halet, 2005; Downes et al., 2005; Varnai and Balla, 2006) were used as probes to identify the potential PI targets of Ptprq in hair cells.

3.1.1 PI binding domains

PIs are embedded in membranes owing to their diacyglycerol (DAG) moiety, while their exposed polar head group interacts with specific lipid-binding domains of downstream effector proteins that mediate the PI signal (Downes et al., 2005). Thus, PIs serve to localise their effector proteins at the target membrane surfaces and modulate their function (Takenawa and Itoh, 2001; Downes et al., 2005). The fidelity of the PI-

dependent signalling relies on the affinity and specificity of the binding domains to the various PIs, as well as the differential distribution of the PIs in the subcellular membranes (Downes et al., 2005).

There are several different kinds of proteins that bind PIs using recognized domains (see table 3.1), as well as some proteins that bind PIs via a small patch of basic amino acids that display varying degrees of affinity for the PIs (Downes et al., 2005). The PI binding domains serve to recruit the protein to the various target membranes that are defined by their particular PI compositions (Parker, 2004). Beside membrane recruitment, interaction with the PI may also contribute to conformational changes in the protein (Parker, 2004). The PI binding domains currently known to recognise the various PIs with high specificity and affinity belong to the PH, FYVE , Epsin N-Terminal Homology (ENTH), Phagocyte Oxidase (PX), AP180 N-Terminal Homology (ANTH) and 4.1-Ezrin-Radixin-Moesin (FERM) domains (Lemmon, 2003).

PI	Reporter	Distribution
PI 4,5 P_2	PLC δ 1-PH	Plasma membrane
PI 3,4,5 P_3	GRP1-PH Btk-PH PKB-PH	Plasma membrane Plasma membrane Plasma membrane
PI 3,4 P_2	PKB-PH, TAPP1-PH	Plasma membrane Plasma membrane
PI 4 P	FAPP1-PH	Golgi and plasma membrane

PI 3 P	EEA1-FYVE, TAFF1	Endosomes Golgi
PI 5 P	None identified	-
PI 3,5 P_2	None identified	-

Table 3.1: The various proteins that are used to study the cellular distribution of the different PIs. (Lemmon et al., 2003; Downes et al., 2005; Varnai and Balla, 2007).

3.1.2　PI binding domains as reporters of the different PIs

Owing to their specificity and affinity for the target PI at levels that occur naturally in cellular membranes, several PI binding domains have been used as probes to detect the respective PI target in cells (see table 3.1; Irvine, 2004; Halet, 2005; Downes et al., 2005). Confocal microscopy has been employed to study PI dynamics in living cells by observing the distribution of the recombinant PI binding domains fused to GFP (for green fluorescent protein) or one of its variants (Irvine, 2004; Halet, 2005; Downes et al., 2005).

Historically, PI 4,5 P_2 has been known to play a major role in signal transduction, where phospholipase C $\delta1$ (PLC $\delta1$) acting downstream of membrane receptors, hydrolyses PI 4,5 P_2 to produce inositol 1,4,5 P_3 (IP_3) and DAG (Takenawa and Itoh, 2001; Parker, 2004; Downes et al., 2005; Sasaki et al., 2007). The products of PI 4,5 P_2 hydrolysis serve as second messengers, where IP_3 is involved in Ca^{2+} release from intracellular stores and DAG activates protein kinase C resulting in a variety of cellular responses (Takenawa and Itoh, 2001; Parker, 2004). Due to the abundance of PI 4,5 P_2 in the plasma membrane compared to the other PIs, the protein domains that bind PI 4,5 P_2 do not usually need a very high affinity for it (Lemmon, 2003). However, the PH domain of PLC $\delta1$, binds to PI 4,5 P_2 with exceptionally high affinity, and has been used to

monitor the cellular levels of this lipid in several studies (Stauffer et al., 1998; Lemmon, 2003; Downes et al., 2005; Halet, 2005). The PLC δ1-PH domain also binds the head group, IP_3, with some 20-fold higher affinity. This interaction might be necessary to downregulate the enzymatic activity of PLC δ1 by relocating it to the cytoplasm, away from the PI 4,5 P_2 -containing plasma membrane (Lemmon, 2003; Downes et al., 2005). When expressed in cells, the GFP-tagged PLC δ1-PH labels the plasma membrane where PI 4,5 P_2 is present and translocates to the cytoplasm upon activation of the PLC enzymes that degrade PI 4,5 P_2 (Stauffer et al., 1998; Downes et al., 2005). The translocation to the cytoplasm is a transient feature, as the protein re-labels the plasma membrane within 3-8 minutes perhaps due to re-synthesis of PI 4,5 P_2 (Stauffer et al., 1998). It has been argued however, that the localisation of PLC δ1-PH is dictated by the relative concentrations of PI 4,5 P_2 and IP_3 which vary during an experiment (Irvine, 2004; Downes et al., 2005).

Since PI 4,5 P_2 and PI 4 P are present at levels that are at least 25-fold higher than the other PIs, protein domains that recognise PI 3,4,5 P_3, PI 3,4 P_2 or PI 3 P must be able to select against the more common PIs (Lemmon, 2003, Downes et al., 2005). The PH domain of a guanine nucleotide exchange factor for small GTPases of the ARF family, the general receptor for phosphoinositides 1 (GRP1), and the PH domain of bruton's tyrosine kinase (Btk) are highly selective for PI 3,4,5 P_3 (Downes et al., 2005; Halet, 2005). These PH domains have been shown to label the PI 3,4,5 P_3 in the plasma membrane of cells that are stimulated by activation of the receptor tyrosine kinases or G protein coupled receptors that in turn activate the PI 3 kinase signalling pathways (Halet, 2005). Thus, PH domain reporters specific for PI 3,4,5 P_3 are found in the cytoplasm of unstimulated cells, but rapidly translocate to the plasma membrane on activation of the PI 3 kinases (Irvine, 2004; Halet, 2005). PI 3,4 P_2 is usually produced

from PI 3,4,5 P_3 by dephosphorylation and the two PIs occur in similar amounts (Downes et al., 2005). The PH domain of protein kinase B (PKB) recognises both PI 3,4,5 P_3 and PI 3,4 P_2 pools generated on activation of PI 3 kinase pathways (Halet, 2005). The C-terminal PH domain of TAPP1 (TAPP1-PH), however, is a well characterized domain that is selective for PI 3,4 P_2 (Dowler et al., 2000; Watt et al., 2004). Stimulation of fibroblasts with H_2O_2 or PDGF results in an increase in PI 3,4 P_2 levels and translocation of the yellow fluorescence protein-tagged TAPP1-PH domain from the cytoplasm to the plasma membrane of these cells (Halet, 2005). Also, B-cell receptor activation results in a delayed but more sustained plasma membrane accumulation of GFP-TAPP1 that correlates with PI 3,4 P_2 production, while GFP-Bkt-PH, a PI 3,4,5 P_3 reporter, displays a rapid and transient accumulation (Halet, 2005).

The PH domain of FAPP1 is known to specifically bind to PI 4 P, but the localization of the protein domain to the PI 4 P-rich Golgi is dependent on additional interactions (see section 1.6.2, Dowler et al., 2000; Halet, 2005). Nevertheless, FAPP1-PH has been used to study PI 4 P dynamics upon manipulating the activity of various PI 4 kinases (Balla et al., 2005).

FYVE domain proteins have been popularly used to study PI 3 P dynamics in living cells (Halet, 2005; Downes et al., 2005). While a patch of basic residues interacts with the monophosphorylated lipid, hydrophobic side chains penetrate into the membrane and strengthen the interaction (Halet, 2005). Duplicating the FYVE domain has been shown to increase the affinity of the domain for PI 3 P (Cheung et al., 2001; Halet, 2005). PI 3 P is enriched in vacuolar and endosomal membranes, and the GFP-tagged FYVE domain of early endosome autoantigen 1 (EEA1) colocalizes with endosomal markers (Downes et al., 2005; Halet, 2005). The protein tandem FYVE fingers-1

(TAFF1) contains two FYVE domains in tandem and has been shown to reveal PI 3 P-containing-Golgi structures (Cheung et al., 2001; Gillooly et al., 2001; Ridley et al., 2001). Although many FYVE domain proteins are known to bind PI 3 P specifically, not many PH domains exhibit such specificity for the lipid (Varnai and Balla, 2007). However, the PH domain of PI 3 P-binding PH-domain protein-1 (PEPP1), a protein expressed at high levels in a melanoma cancer cell line, is the only reported mammalian PH domain-containing protein that binds PI 3 P specifically (Dowler et al., 2000). Northern blotting suggests that the protein may be restricted to melanoma, although its homologue PEPP2 appears to be widely expressed (Dowler et al., 2000).

Unfortunately, not all PIs have specific recognition domains that can be used as probes for their distribution (see table 3.1) (Lemmon et al., 2003; Downes et al., 2005; Varnai and Balla, 2007). There are no reported protein domains that specifically recognise PI 5 P and PI 3,5 P_2 (and PtdIns) with high affinity and that can be used as probes for these PIs (Lemmon et al., 2003; Downes et al., 2005; Varnai and Balla, 2007).

3.2   Materials and Methods

3.2.1   PI reporter constructs

All the PI reporters used in this study were N-terminally EGFP (for enhanced GFP)-tagged. The mammalian expression construct, EGFP-PLC-δ1-PH (in pEGFPN1 vector; see below), and the bacterial expression constructs (in pGex4t vector) containing the DNA sequences for the full-length human TAFF1, human TAPP1, human FAPP1 and the PH domain sequence of human PEPP1 were a gift from Professor Peter Downes, University of Dundee, UK. The EGFP-GRP1-PH and EGFP-PKB-PH constructs (in pEGFPN1 vector) were gifts from Professor Mike Ashford, University of Dundee, UK.

Mammalian expression constructs containing EGFP-tagged PH domains of TAPP1, FAPP1 and PEPP1, as well as EGFP-tagged full-length TAFF1 were prepared using standard cloning techniques (see sections 2.1.12). The DNA sequence for each of these proteins was inserted in frame into XhoI and XbaI sites of pEGFPN1 (Clontech; see figure 3.1a and b; sections 3.2.1.1- 3.2.1.3).
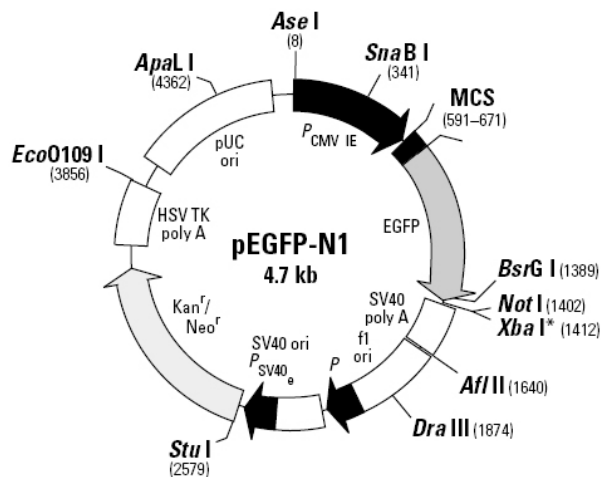
Figure 3.1a: pEGFPN1 (Clontech) vector map.
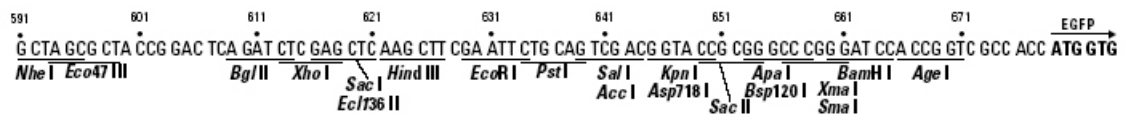
Figure 3.1b: the multiple cloning site of pEGFPN1.

Listed below are the primer sequences used to amplify the DNA sequences of the various PI reporters from their respective bacterial expression constructs mentioned above.

3.2.1.1 PI 4 P reporter – EGFP-FAPP1-PH

FAPP1-PH-F1 - CAGAT CTCGAG CTATGGAGGGGGTGTTGTACAA
Xhol
Sequence 238-257 of FAPP1 cDNA
(Accession number : AF286162)

FAPP1-PH-R1 - AGTTA TCTAGA TCA AGTCCTTGTATCAGTCA
Xbal
Reverse complement of sequence
521-537 of FAPP1 cDNA
(Accession number : AF286162)

The above primers were used to PCR amplify the PH domain of FAPP1 from the construct pGex4t- FAPP1.

3.2.1.2 PI 3 P reporters – EGFP-TAFF1 and EGFP-PEPP1-PH

TAFF1-F1 - CAGAT CTCGAG CT GCGCACAGCTCCTTTTTTCC
Xhol
Sequence 111-130 of TAFF1 cDNA
(accession number: AF311602)

TAFF1-R1 - AGTTA TCTAGA TTAAAGGTCACCGGGCTTTT
Xbal
Reverse complement of sequence
1177-1196 of TAFF1 cDNA
(Accession number: AF311602)

The above primers were used to PCR amplify full-length TAFF1 from the construct pGex4t-TAFF1.

PEPP-PH-F1 - CAGAT CTCGAG CT AGCGCCTCCACCATCTCCTC
Xhol
Sequence 568-587 of PEPP1 cDNA
(Accession number: AY007233)

PEPP1-PH-R1 - AGTTA TCTAGA TCA CTGGGGTCGTGCAGGTG
Xbal
Reverse complement of sequence
1016-1032 of PEPP1 cDNA
(Accession number : AY007233)

The above primers were used to PCR amplify the PH domain of PEPP1 from the construct pGex4t-PH -PEPP1.

3.2.1.3 PI 3,4 P₂ reporter-EGFP-TAPP1-PH
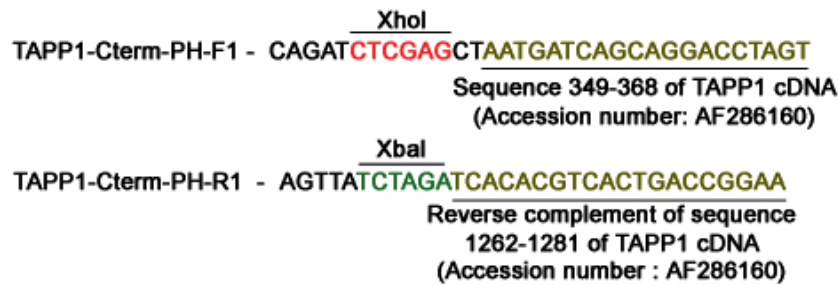
The above primers were used to PCR amplify only the C-terminal PH domain of TAPP1 from the pGex4t-TAPP1 construct.

3.2.2 Cochlear cultures

Cultures were prepared as described previously (Russell & Richardson, 1987). Briefly, the cochleae of P2 mouse pups obtained from matings set up between Ptprq$^{+/CAT}$ and Ptprq$^{CAT/CAT}$ pairs of mice were dissected in Hepes buffered (10mM, pH 7.2) Hanks' balanced salt solution (HBHBSS). After removal of the stria vascularis and the immature modiolar tissue, the cochlea was separated into apical- and basal-coils which were explanted onto collagen coated round glass coverslips. The cultures were incubated in ~1 drop of medium: DMEM F-12 Ham nutrient mixture containing 7% fetal bovine serum (Gibco) and 10 μg/ml ampicillin. All cultures were maintained in Maximow slide assemblies in the lying drop position at 37ºC for 24 hours before transfecting with the appropriate expression construct.

3.2.3 Gene gun transfections

3.2.3.1 Preparation of gene gun bullets

Microcarrier solution and bullets were prepared in accordance with the instructions in the Helios® Gene Gun system (Bio-Rad) handbook. 25 mg of gold microparticles (Bio-

Rad; particles of 1.0 µ in diameter) were mixed with 50 µl of 0.05 M spermidine (Sigma Aldrich), and sonicated 3 times for 3 seconds in an Eppendorf® tube (1.5 ml). 50 µg of the purified supercoiled plasmid DNA was added to the gold microparticle suspension (in a total volume of 100 µl). An equal volume of $CaCl_2$ (1 M) was then added drop-wise with continuous vortexing. The tubes were allowed to stand for 10 minutes at room temperature for precipitation. The gold microparticle-DNA suspension was washed three times with 1 ml of absolute ethanol (Sigma-Aldrich), and the sample was pelleted by centrifugation at 12,000 rpm for 1 minute. Finally, the pellet was resuspended in 3.5 ml of ethanol containing 0.1 mg/ml polyvinylpyrrolidone (PVP; MW 360,000) which is an adhesive and readily forms films. The inner surface of the Tefzel tubing (external size 10 mm; internal diameter 6 mm; Bio-Rad) was cleaned with 5 ml of absolute ethanol and dried with nitrogen in the rotating tubing holder for at least 5 minutes. The DNA microcarrier suspension was sonicated in ethanol for 3 seconds (to achieve a homogeneous solution) and loaded into the tubing using a syringe. The gold microparticle-DNA suspension was allowed to settle for 3 minutes and the ethanol solution was removed slowly. For drying the wall-attached particles, nitrogen gas was flushed through the tubing for 3 minutes at a flow rate of 0.35 l/min. Finally, the DNA microcarrier coated tubing was cut into individual cartridges of 16 mm in length to fit into the 12-shot barrels of the Helios gene gun (Bio-Rad). The cartridges were stored in labelled tubes containing a bed of silica gel particles.

3.2.3.2 Gene gun transfections

Figure 3.2 shows a schematic representation of the gene gun set up used in the current study. All cultures were incubated for 1 day *in vitro* before being transfected with a particular plasmid DNA, using a Helios™ gene gun (BioRad). Cochlear cultures were

removed from their Maximow slide assemblies and the excess culture medium was dried off using sterile filter paper. The Helios™ Gene Gun was connected to the helium source and an empty cartridge holder was inserted into the gun. The helium regulator was turned to select the appropriate pressure (120-130 bar) and the system was pressurized by a few "pre-shots". The cartridges of the plasmid DNA of choice were loaded into the cartridge holder and inserted into the gun. The coverslip containing a culture was placed at the centre of the pedestal under the gene gun and a fresh 3 µm cell culture insert was placed over the culture (see figure 3.2). The trigger was pressed to deliver the DNA microcarrier to the target culture that was placed about 3 cm below the gene gun. Each culture was "shot" once with a single bullet. The cultures were then incubated at 37ºC in 3 ml of medium for 24 hours in a CO_2 incubator to allow for gene expression, before being fixed and immunostained.
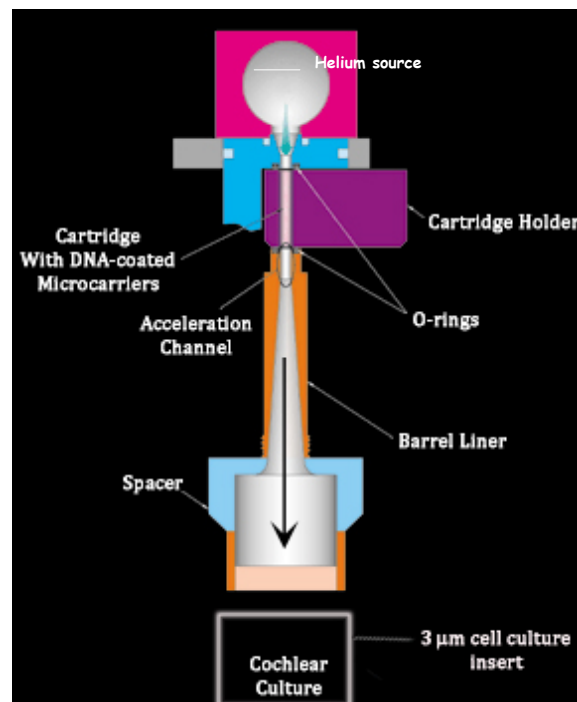
Figure 3.2: Schematic representation of the gene gun set up. The bulb at the top represents the Helium supply. A high pressure Helium pulse fires the DNA-microcarriers from their cartridges, through the acceleration channel and down the barrel of the gene gun, in the direction of the arrow. The spacer at the end of the gene gun barrel both moderates the Helium shock waves and maintains the optimal distance from the target. The cell culture insert placed over the cochlear culture serves as a screen to keep out the bigger gold particles and deliver the DNA into the cells.

3.2.4 Immunofluorescence and microscopy

After 24 hours at 37ºC, the cultures were fixed for 30 minutes in 4% paraformaldehyde (see section 2.3.1) and prepared for immunostaining with permeabilisation using 0.1% Triton X-100 as detailed in section 2.3.2. In order to prevent photobleaching of the GFP signal, a rabbit anti-GFP polyclonal serum (Invitrogen) was used as the primary antibody at 1 in 1000 dilution in pre-block. Alexa 488 conjugated goat anti-rabbit secondary antibody (Molecular Probes, Invitrogen) was used at 1 in 500 dilution in pre-block, along with Texas Red®-X phalloidin (Molecular Probes, Invitrogen) as counter-stain (see section 2.3.2).

After fixation and staining, transfected cells were imaged using a Zeiss LSM 510 Meta confocal microscope.

3.3   Results

Table 3.2 contains the list of the EGFP-tagged PI binding domains used as probes to detect the various PIs in the hair cells of Ptprq$^{+/CAT}$ and Ptprq$^{CAT/CAT}$ mice cochlear cultures.

PI	Binding domain	Reporter	Number of cells analysed	
			Ptprq$^{+/CAT}$	Ptprq$^{CAT/CAT}$
PI 4,5 P$_2$	PH domain of PLC δ 1	EGFP-PLC δ 1-PH	20	16
PI 3,4,5 P$_3$	PH domain of GRP1	EGFP-GRP1-PH	18	26
PI 3,4,5 P$_3$/ PI 3,4 P$_2$	PH domain of PKB	EGFP-PKB-PH	17	25
PI 3,4 P$_2$	C-terminal PH domain	EGFP-TAPP1-PH	16	23

	of TAPP1			
PI 4 P	PH domain of FAPP1	EGFP-FAPP1-PH	20	27
PI 3 P	Full-length TAFF1	EGFP-TAFF1	12	15
	PH domain of PEPP1	EGFP-PEPP1-PH	13	24
PI 5 P	None available	None available	-	-
PI 3,5 P_2	None available	None available	-	-

Table 3.2: List of the PI reporters used in the current study.

The subcellular localisation of each individual PI reporter in the cochlear hair cells of heterozygote, Ptprq$^{+/CAT}$ mice, was compared with that observed in the cochlear hair cells of the homozygote, Ptprq$^{CAT/CAT}$ mice. The results of the study are detailed below.

3.3.1 Absence of Ptprq does not alter the distribution of PI reporters in cochlear hair cells

3.3.1.1 PI 4,5 P_2 reporter, EGFP-PLCδ1-PH

Confocal microscopy imaging revealed that the distribution of EGFP-PLCδ1-PH in the hair bundles of both transfected Ptprq$^{+/CAT}$ and Ptprq$^{CAT/CAT}$ cochlear hair cells appears identical (see figure 3.3, panels B and B'). The protein is also found distributed evenly throughout the cytoplasm as well as the basolateral membrane of transfected cells (see figure 3.3, panels E and E'). The lack of Ptprq in the mutant Ptprq$^{CAT/CAT}$ cochlear hair cells does not affect the distribution of the PI 4,5 P_2 probe, EGFP-PLCδ1-PH, in the hair bundle.

3.3.1.2 PI 3,4 P_2 reporter, EGFP-TAPP1-PH

The recombinant EGFP-TAPP1-PH is found in the hair bundle, including the kinocilium, of transfected cells in both Ptprq$^{+/CAT}$ and Ptprq$^{CAT/CAT}$ cochlear cultures, as revealed by confocal microscopy (see figure 3.4, panels B and B'). A strong anti-GFP signal can also be seen at the level of the cuticular plate in the heterozygous mutant as well as the homozygous mutant hair cells (see figure 3.4; panels E and E'). The EGFP-TAPP1-PH reporter is also found in the cytoplasm and nucleus of all transfected hair cells (see figure 3.4, panels H and H'). The protein thus shows a similar distribution in both the Ptprq mutant and the heterozygote hair cells.

3.3.1.3 PI 3,4,5 P_3 reporter, EGFP-GRP1-PH

On examining the transfected hair cells using confocal microscopy it was found that EGFP-GRP1-PH is found abundantly in the hair bundles, including the kinocilium, of all transfected cells (see figure 3.5, panels B and B'). The reporter also labels the apical surface in the region of the kinocilium in all transfected cells (panels B and B'). EGFP-GRP1-PH is also seen in the cytoplasm and basolateral surface but not the nucleus of transfected Ptprq$^{+/CAT}$ and Ptprq$^{CAT/CAT}$ hair cells (see figure 3.5, panels E and E'). The PI 3,4,5 P_3 reporter thus, has a similar distribution in the cochlear hair cells of Ptprq$^{+/CAT}$ and Ptprq$^{CAT/CAT}$ mice.

3.3.1.4 PI 3,4 P_2/ PI 3,4,5 P_3 reporter, EGFP-PKB-PH

EGFP-PKB-PH when expressed in cochlear hair cells displays a similar distribution in both the Ptprq heterozygote and mutant hair cells (see figure 3.6). Anti-GFP labeling highlights the presence of the reporter in the hair bundles, including the kinocilium of all transfected cells (see figure 3.6, panels B and B'). EGFP-PKB-PH also displays both

cytoplasmic and nuclear localisation in all transfected cells (see figure 3.6, panels E and E').

Next, the distribution of the monophosphorylated derivatives of PI, PI 3 P and PI 4 P, was determined.

3.3.1.5 PI 3 P reporters, EGFP-PEPP1-PH and EGFP-TAFF1

Confocal microscopy images of transfected cells reveal no difference in the cellular distribution of two PI 3 P reporters, in Ptprq$^{+/CAT}$ and Ptprq$^{CAT/CAT}$ cochlear hair cells (see figures 3.7 and 3.8). EGFP-PEPP1-PH is found in the hair bundle of all transfected cells (see figure 3.7). The protein shows a strong localization at the apical junctions (panels B and B') and the basolateral membrane (panels E and E'), and is found in the nucleus of both transfected Ptprq$^{+/CAT}$ and Ptprq$^{CAT/CAT}$ hair cells (see panels E and E').

EGFP-TAFF1 on the other hand, is excluded from the hair bundles of transfected hair cells of both genotypes (see figure 3.8, panels B and B'). The protein is found in the form of dense granules in all transfected cells (see figure 3.8, panels E and E').

The localization of the PI 3 P reporters, EGFP-PEPP1-PH and EGFP-TAFFI appears unperturbed in the absence of Ptprq in hair cells.

3.3.1.6 PI 4 P reporter, EGFP-FAPP1-PH

EGFP-FAPP1-PH is found in the hair bundle, including the kinocilium of transfected Ptprq$^{+/CAT}$ and Ptprq$^{CAT/CAT}$ hair cells (see figure 3.9, panels B and B'). The reporter also localises to the apical surface around the region of the kinocilium (panels B and B'). EGFP-FAPP1-PH is diffusely distributed in the cytoplasm as well as localized to grouped puncti in the cytoplasm of all transfected cells (see figure 3.9, panels E and E').

Thus, there is no obvious difference in the distribution of the PI 4 P reporter, EGFP-FAPP1-PH, between transfected Ptprq heterozygote and mutant hair cells.

3.4   Discussion

In order to determine the PI targets of Ptprq, several EGFP–tagged protein domains that have been used as PI reporters (see table 3.2) were expressed in hair cells and their distribution compared in the cochleae of P1 Ptprq$^{+/CAT}$ and Ptprq$^{CAT/CAT}$ mice. It was expected that the absence of Ptprq would result in altered levels or distribution of the target PIs in the hair bundle.

Confocal imaging of all transfected hair cells reveals that the lack of Ptprq in the Ptprq$^{CAT/CAT}$ cochleae does not affect the distribution of any of the PIs, as judged by these reporters. The distributions of PI 3,5 P$_2$ and PI 5 P, however, have not been examined in this study due to a lack of specific reporters (Lemmon, 2003; Varnai and Balla, 2007). Thus, it is possible that one or both of these PIs may be the target of Ptprq in the hair cell.

Alternatively, functional compensation may account for the observed result, with the upregulation of another PIPase compensating for the loss of Ptprq in the Ptprq$^{CAT/CAT}$ hair cells. However, the Ptprq$^{CAT/CAT}$ mice begin developing a hair bundle phenotype in the cochlea from around P1 (see section 1.5.4; Goodyear et al., 2003). Thus, if there is functional compensation for the PIPase activity, the phenotype seen in the cochlea of the Ptprq$^{CAT/CAT}$ mice may be a direct consequence of the absence of the interstereociliary links formed by the extracellular domain of Ptprq.

It is also important to consider the limitations and disadvantages of using over-expressed reporters for studying PI dynamics in cells (Balla et al., 2000; Halet, 2005;

Varnai and Balla, 2006) while interpreting the results of this study. A possibility is that the technique may not be sensitive enough to detect the effects of the PIPase activity of Ptprq, a process that may be occurring very rapidly and localized to a very limited area. Although an *in vivo* PIPase activity of Ptprq has not been shown directly so far, Ptprq overexpression results in a dose-dependent reduction in phosphorylation of Akt/PKB most likely via a reduction in PI 3,4,5 P_3 (Oganesian et al., 2003). Ptprq may be involved in the maintenance of a fine balance of PIs, but not the complete exclusion of the target PIs as shown by Hirono et al. (2004) in isolated frog saccular hair cells. Thus, the difference in the levels of the target PIs in heterozygote and Ptprq mutant hair cells may not be large enough to result in an observable difference in the levels of their respective reporters.

A common problem encountered when using PI binding domains as reporters is that of sequestration (Halet, 2005; Lemmon, 2003; Varnai and Balla, 2006). By engaging the PI, over-expressed PI binding domains have the potential to sequester the binding site or the head group of the PI and thus prevent the PI from interacting with endogenous proteins (Varnai and Balla, 1998; Varnai and Balla, 2006). It is easy to imagine that Ptprq, as a PIPase, must have access to the head group in order to dephosphorylate the target PI. If the reporters used in this study bind and sequester the target PI, making it unavailable for interaction with Ptprq, then the distribution of the reporters would represent only the sequestered PI and therefore appear similar in both transfected Ptprq$^{+/CAT}$ and Ptprq$^{CAT/CAT}$ hair cells.

PI binding domains often recognize their target PI in conjunction with another co-localizing protein in the membrane, a process called coincidence detection (discussed in section 1.6.2; Lemmon, 2004; Irvine, 2004; Balla, 2005; Carlton and Cullen, 2005;

Varnai and Balla, 2006; Lemmon, 2007). Thus, the recruitment of a PI binding domain to the target PI in the membrane may not depend solely on the lipid-protein interaction. Multiple interactions with other proteins, especially those that are a part of the signaling complex involving the PI and the parent molecule of its reporter, may determine the specificity and the affinity of the recombinant reporter to its target PI (Lemmon, 2004; Parker, 2004; Varnai and Balla, 2006). Thus, a PI reporter is best suited to reveal the PI pool that is produced in the molecular context of the parent molecule of the reporter, and may not reveal the target PI pool produced elsewhere in the cell (Varnai and Balla, 2006). An example of this is the fact that PLCδ1-PH does not show Golgi or nuclear localization even though there is evidence of PI 4,5 P_2 in these locations (Irvine, 2004; Varnai and Balla, 2006). Similarly, GFP-tagged FAPPI-PH does not report the PI 4 P in the endocytic compartments (Varnai and Balla, 2006). The PI pool controlled by Ptprq could therefore be unavailable (probably due to lack of parallel interactions) to the various PI reporters. The phenomenon of coincidence detection may also explain the observed difference in the distribution of the two PI 3 P reporters, EGFP-PEPP1-PH and EGFP-TAFF1, used in the current study (compare figure 3.7 and 3.8). The reporters appear to be revealing different pools of the same PI within the hair cell. While EGFP-TAFF1 (see figure 3.8) appears to report the PI 3 P pool in the Golgi, EGFP-PEPP1-PH labelling seen in the basolateral membrane (see figure 3.7) probably reveals the PI 3 P known to occur in the plasma membrane (Sasaki et al., 2007).

In this context it is interesting to note that although the PI 3,4 P_2/PI 3,4,5 P_3 dual reporter, EGFP-PKB-PH, essentially shows a distribution similar to that seen with the PI 3,4,5 P_3 reporter, EGFP-GRP1-PH, there are also some differences. EGFP-PKB-PH is seen in the nucleus just like the PI 3,4 P_2 reporter, EGFP-TAPP1-PH, suggesting that both these reporters may be revealing the same nuclear PI 3,4 P_2 pools (compare figures

3.4 and 3.6). The PI 3,4,5 P_3 reporter, EGFP-GRP1-PH, does not label the nucleus (see figure 3.5). This suggests that the nuclear distribution of EGFP-PKB-PH may be due to the PI 3,4 P_2 binding activity of the protein and not its affinity for PI 3,4,5 P_3. In support of this, PKB-PH has been shown to reveal the sustained plasma membrane localization of PI 3,4 P_2 under conditions of oxidative stress, while GRP1-PH accumulates transiently at the plasma membrane, reflecting a similarly transient PI 3,4,5 P_3 production (Gray et al., 1999).

3.5   Conclusions

Ptprq may be required to maintain a fine balance of its target PIs in the hair bundle and the use of protein domains as specific reporters for the various PIs may not be a technique that is sensitive enough to detect fine changes in PI flux. Alternatively, in the absence of Ptprq, another PIPase may be upregulated to functionally compensate for the PIPase activity of Ptprq in the cochlear hair cells of Ptprq$^{CAT/CAT}$ mice. Thus, with the above knowledge it is impossible to exclude any of the PIs tested for in this study as the targets of Ptprq in hair cells. The current study does however, suggest that there is an enrichment of PI 4,5 P_2, PI 3,4 P_2, PI 3,4,5 P_3 and PI 4 P in the hair bundle as compared with the rest of the apical surface. This may represent the role of these lipids in the regulation of the actin cytoskeleton dynamics in the hair bundle.

3.6   Future Perspectives

Watt et al. (2002; 2004) have performed on-section labelling of PIs using GST-tagged PLC δ1-PH and TAPP1-PH. This involves decorating fixed cells with the tagged reporters and the method can be adapted for both immnuofluorescence and immunoelectronmicroscopy. This strategy could be applied to study and compare the

distribution of the various PIs in the hair cells of Ptprq$^{+/CAT}$ and Ptprq$^{CAT/CAT}$ mice. This would by-pass the problem of sequestration of the target PI by the reporter, but may not be useful in revealing a target PI that is bound by an endogenous effector.

Experiments to study PI 4,5 P$_2$ flux in the presence and absence of Ptprq could be used to reveal differences that might result from the PIPase activity of Ptprq. For example, activation of endogenous PLCs by ionophores or inhibition of PI 4 kinase by quercetin or phenylarsine oxide could be used to study PI 4,5 P$_2$-flux in control human embryonic kidney (HEK293) cells and HEK293 cells expressing recombinant full-length Ptprq. However, these chemicals are not very specific and they are known to affect various pathways and interfere with the normal functions of the cell (Varnai et al., 2006; Varnai and Balla, 2007). This caveat may be overcome by using a recently described approach for studying PI flux in which the immunosuppresant rapamycin or its analog iRap is used to chemically heterodimerize the protein domains from the FK506 binding protein (FKBP) and mTOR (FRB) at the plasma membrane (Varnai et al., 2006; Suh et al., 2006). FKBP can be fused to a specific enzyme involved in PI metabolism, and iRap-induced membrane-targeting of the enzyme results in changes in the levels of the target PI at the membrane (Varnai et al., 2006; Suh et al., 2006). The study by Suh et al., (2006) made use of PI 4 P 5-kinase type I–γ (PIPKI-γ), an enzyme that elevates PI 4,5 P$_2$ levels. Such a method to chemically induce the production of PI 4,5 P$_2$ at the plasma membrane via PIPKI-γ could be used to study PI 4,5 P$_2$ flux in HEK293 cells, with or without recombinant full-length Ptprq expression.

It will also be informative to determine if another PIPase is upregulated in the Ptprq$^{CAT/CAT}$ mice to compensate for the loss of Ptprq PIPase activity in the hair cells of these mice. PTEN is a PIPase that removes the phosphate from the D3 hydroxyl group

of the inositol moiety of PIs, including PI 3,4,5 P_3 (Maehama and Dixon, 1998; Leslie et al., 2000). PTEN is one of the most common tumor suppressors known and mutations of this gene are seen in many cancers (Myers et al., 1998). PTEN is also known to control the apical plasma membrane and lumen formation in polarised cells via its effect on PI distribution (Martin-Belmonte et al., 2007). Localisation of PTEN at the apical plasma membrane during epithelial morphogenesis results in preferential accumulation of PI 4,5 P_2 at the apical membrane and of PI 3,4,5 P_3 at the basolateral membrane, where the two PIs are suggested to be involved in the formation of the respective membranes (Gassama-Diagne et al., 2006). Determination of the levels of PTEN in the hair cells of the wild-type and Ptprq$^{CAT/CAT}$ cochlea may reveal if this PIPase functionally compensates for the loss of Ptprq in the mutant mice. However, it may be necessary to perform q-PCR analysis by designing individual primer pairs for each of the 28 known PIPases in the mammalian genome to determine if any of them are upregulated in the absence of Ptprq. Alternatively, PIPase gene expression profiling could be done using a microarray with probes specific for each of the known mammalian PIPases and RNA from hair cells of wild-type and Ptprq$^{CAT/CAT}$ mice to determine whether there is an upregulation of a particular PIPase in the Ptprq$^{CAT/CAT}$ hair cells.

CHAPTER 4

EHD3, a protein of the endocytotic pathway, interacts with Ptprq

4.1   Introduction

As discussed in section 1.5.5, the intracellular domain of Ptprq has PIPase activity. However, the possibility that this domain interacts with other components of the hair bundle, either known or unknown, has remained unexplored. Therefore, a yeast-two hybrid screen was performed to reveal the potential interaction partners of Ptprq.

4.1.1   The yeast-two hybrid technique

The yeast two-hybrid system was first described by Fields and Song (1989), as a technique to identify protein-protein interactions using the transcriptional activator protein GAL4, a protein required for the expression of enzymes essential for galactose utilisation in yeast. The system was based on the functional separability of the DNA binding domain and the transcriptional activator region of GAL4 (Fields and Song, 1989). The DNA binding domain can alone bind specific DNA sequences but needs the transcriptional activator region to form a functional unit (Fields and Song, 1989). Yeast cells deleted for GAL4 can be co-transformed with a 'bait' protein, a fusion of the DNA binding domain of GAL4 and the protein of interest, and a library of genomic or cDNA sequences fused to the transcriptional activator region of GAL4. These cells can then be screened for their ability to grow on galactose medium. Growth is only possible in the event of an interaction between the bait fusion protein and the transcriptional activator fusion protein (Fields and Song, 1989). The technique allows large scale screening for

potential interactors of the protein of interest within a library of cDNA or genomic DNA from the organism (Fields and Song, 1989).

4.1.2   The Sos recruitment system

Several variations of the above strategy are now available to identify protein-protein as well as protein-DNA interactions. The traditional yeast two-hybrid system described above requires interactions to occur in the nucleus and may not detect protein interactions that occur in the cytoplasm or at the membrane surface. Recently, a membrane-based yeast two-hybrid screen has been used to identify the binding partners of Cdh23 and the motor protein prestin, the latter being expressed exclusively in the OHCs (Zheng et al., 2009). The screen revealed that Cdh23 binds to several calcium-binding proteins while prestin interacts with proteins involved in electron transport (Zheng et al., 2009).

The CytoTrap® XR library yeast two-hybrid system from Stratagene employs a membrane-based Sos recruitment system (Aronheim et al., 1997). This system is based on the ability of the human Sos protein (hSos) to rescue its defective yeast homologue, Cdc25, in the *Saccharomyces cerevisiae* mutant strain cdc25H. hSos and its yeast homologue Cdc25 are guanyl nucleotide exchange factors that bind and activate Ras at the plasma membrane, initiating the Ras signalling pathway and thereby inducing cell growth. The mutated form of Cdc25 is able to induce growth at a permissive temperature of 25°C but not at 37°C. Expression of hSos complements the Cdc25 defect allowing the cdc25H yeast strain to grow at the restrictive temperature of 37°C, but only if hSos is localised to the plasma membrane. To perform a screen, hSos is fused with the 'bait' sequence and a cDNA library is made in an expression vector encoding a myristylation signal to target interactors to the plasma membrane. The bait and cDNA

library are co-transformed into cdc25H and in the event of an association of the bait with a myristylated interactor protein encoded by the cDNA expression library, hSos is recruited to the plasma membrane and activates Ras. Therefore, in the presence of a protein-protein interaction, the cdc25H colony is able to grow at 37°C, while the growth of a colony containing an irrelevant protein from the expression library will be inhibited at 37°C.

The pSos vector (figure 4.1) provided in the CytoTrap® XR library construction kit is designed to allow expression of the bait protein fused to hSos. Expression is driven by the yeast *ADH1* promoter and an ampicillin resistance gene allows selection of the pSos vector in bacteria. The pMyr vector (figure 4.2) is used to construct the cDNA library. This vector adds a myristylation (membrane localisation) signal to each of the proteins expressed. In the presence of galactose in the medium, the myristylated proteins will be expressed from the *GAL1* promoter. The chloramphenicol resistance gene allows selection of the pMyr vector in bacteria. The yeast biosynthetic genes *LEU2* and *URA3* are present in the pSos and the pMyr vector respectively. On co-transformation, only the yeast cells that contain both the pSos and pMyr constructs will be able to grow in the absence of leucine and uracil in the selection medium.
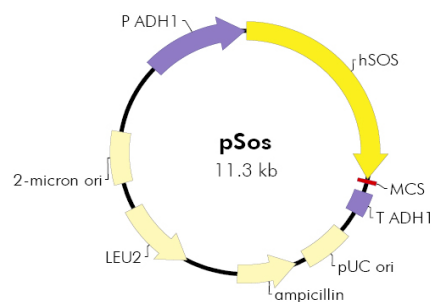
Figure 4.1: Schematic representation of the pSos vector. The human SOS (hSOS) protein is expressed from the yeast ADH1 promoter. A multiple cloning site (MCS) downstream of hSOS allows for insertion of bait DNA so that hSOS is fused to the bait protein. An ampicillin resistance gene allows for selection in bacteria while the LEU2 gene allows for the selection in yeast in the absence of leucine in the medium.
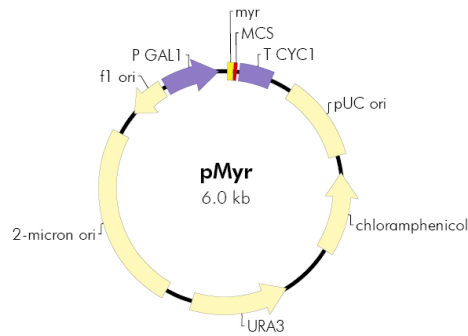
Figure 4.2: Schematic representation of the pMyr vector. The cDNA library is inserted in the MCS so that in the presence of galactose in the medium, the corresponding protein from the library is synthesized as a myristylated (myr) protein the GAL1 promoter (pGAL1). This vector can be selected in bacteria in the presence of chloramphenicol and in the absence of uracil (URA3) in the medium in yeast.

4.2   Materials and Methods

4.2.1   Yeast two-hybrid screen

4.2.1.1 Preparation of a pMyr cDNA library

As the DNA sequence encoding the Ptprq cytoplasmic domain (bait) was amplified from cDNA obtained from chick utricles, the same tissue was used to prepare the cDNA library. The cDNA library was prepared according to the procedure in the CytoTrap® XR library construction kit manual (Stratagene; see appendix 1). Total RNA was isolated from 20 posthatch day 1 chick utricles using the TRIZOL® reagent from Invitrogen according to the recommended protocol (see appendix 1.1). StrataScript™ reverse transcriptase and oligo (dT) linker-primers containing XhoI sites were used to obtain the first strand of cDNA. This reaction was performed using a nucleotide mixture containing dATP, dGTP, dTTP and 5-methyl dCTP, where the dCTP analog was used to protect the cDNA from the restriction enzymes used in the following steps. RNase H was used to create nicks in the RNA bound to the first strand cDNA. Second strand synthesis was then performed using DNA polymerase I that 'nick translates' the RNA fragments created by RNase H. Next, adapter sequences containing EcoRI sites were

ligated to the ends of the cDNA. The XhoI site created by the oligo (dT) linker primers (see above) and the EcoRI sites added by the adapters were cleaved using the restriction enzymes XhoI and EcoRI in order to obtain completed unidirectional cDNA. After size fractionation, the larger cDNA inserts were ligated (see appendix 1.3) into the pMyr XR vector that had been linearised with XhoI and EcoRI to allow insertion of the cDNA in a sense orientation in relation to the P_{GAL1} promoter (see figure 4.2).

The cDNA ligations were transformed (see section 2.1.10) into XL10-Gold® Kan Ultracompetent cells in order to obtain a primary cDNA library. After making glycerol stocks of half the transformed bacteria, the rest were used for alkaline lysis/CsCl gradient purification of plasmid DNA. The resultant DNA was used to transform a competent cdc25H strain of *S. cerevisiae* (see appendix 1.5 and 1.6).

4.2.1.2 Preparation of the bait plasmid vector

The intracellular domain of chick Ptprq was amplified by PCR (see section 2.1.4) using the following primers:

Forward primer (Ptprq sos F1):

maintains reading frame
GATCCGGATCCAGAGAATTAGGCAAAAGCAAAA
BamHI   Start of Ptprq
               intracellular domain

Reverse primer (Ptprq sos R1):

CGGTGCGGCCGCCTACATGGTAGTTTCTTCCCATT
Not1   Stop   Reverse complement of end of
          codon   Ptprq intracellular domain

The PCR product was then cloned into the pSos vector (see figure 4.1 section 2.1.12)

4.2.1.3 Library Screen

First, tests were performed to ensure that the yeast competent cell preparation (see appendix 1.5) and transformation reactions (see appendix 1.6) were efficient. In order to prevent a high rate of false positives, it was necessary to ensure that the number of temperature sensitive revertants was acceptably low. Next, it was confirmed that the Ptprq intracellular domain (bait) in the pSos plasmid did not itself interact with the myristylation introduced by the pMyr vector. Finally, the pMyr cDNA library was screened for potential interaction partners of the intracellular domain of Ptprq according to the protocol below.
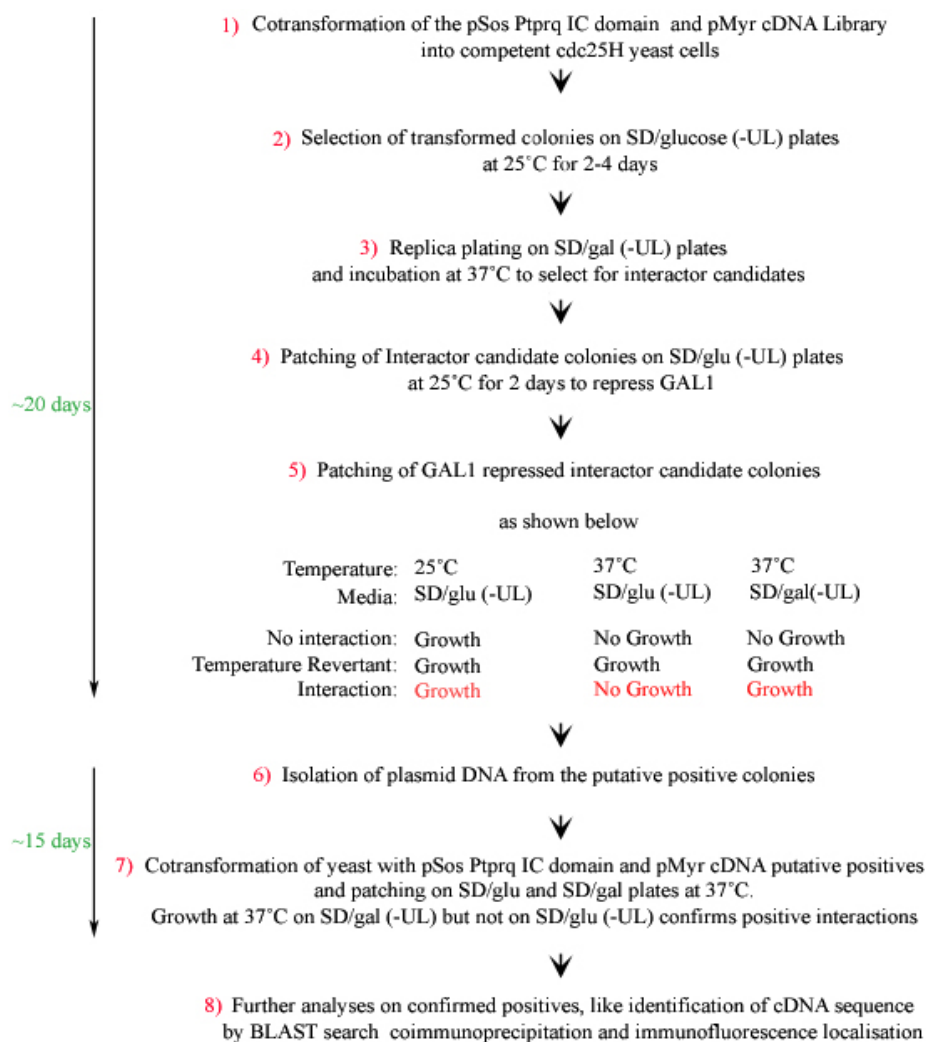
Figure 4.3: Flow chart of the yeast-two hybrid library screen using the CytoTrap® yeast two-hybrid kit, Stratagene. IC domain is intracellular domain.

On confirming the growth of the putative positive interactor colonies, the plasmid DNAs (pMyr cDNA) from these colonies were sequenced. A BLAST search was then done to determine the identity of the interacting cDNA sequences.

4.2.2 Co-immunoprecipitations

Potential interactions were confirmed by co-immunoprecipitations using the EGFP-tagged intracellular domain of chick Ptprq (Ic-Ptprq-EGFP) and myc-tagged interactor constructs.

HEK293 cells were transfected with 2.5 µg of each DNA (as indicated in section 4.3.2) using a modified version of the calcium phosphate method (George et al., 2007) and grown for 24 hours before lysing the cells using cold lysis buffer (1% Triton X-100, 150 mM NaCl, 50 mM Tris-HCl, pH 7.6) supplemented with 0.1 mM phenylmethylsulfonyl fluoride, 1 mM sodium orthovanadate, and 10 mM sodium fluoride. Cell lysates (1 mg) were then incubated overnight at 4°C with 3 µg of mAb 9E10 (anti-myc) and 20 µl of protein G sepharose beads. The bound beads were given at least 3 washes with PBS and eluted into reducing sample buffer. The samples were then separated on 8% SDS-PAGE gels (see section 2.2.1) followed by western blotting (see section 2.2.3). Myc-tagged proteins were detected using mAb 9E10 at 500 ng/ml and rabbit anti-mouse IgG (H+L)-horse radish peroxidase (HRP) conjugate (Zymed, San Fransisco, CA) at 1:25,000. GFP-tagged proteins were detected with rabbit anti-GFP (Santa Cruz Biotechnology, Santa Cruz, CA) at 200 ng/ml followed by Protein A-HRP (Zymed, San Fransisco, CA) at 1:25,000. Western Lightning Chemiluminescence Reagent Plus (PerkinElmer, Boston, MA) and Kodak X-Omat Blue XB-1 film (PerkinElmer, Boston, MA) were used to detect the HRP signals.

4.2.3 Immunohistochemistry

4.2.3.1 Cryosectioning

Tissues were fixed in 3.7% formaldehyde in 0.1 M sodium phosphate buffer, pH 7.4, for 1 hr at room temperature. The fixed tissues were then washed three times with PBS and equilibrated overnight at 4°C with 30% sucrose in PBS. The tissues were then imbedded in 1% low gelling point agarose (type VII; Sigma, Poole, UK) in PBS containing 18% sucrose. Agarose blocks containing the tissues were rapidly frozen onto cryotome chucks using Cryospray (Bright Instrument, Huntingdon, UK) and 10 μm thick sections were obtained at a temperature of -30°C. Sections were mounted onto gelatin-coated glass microscope slides, dried, and either used immediately or stored at -20°C until use.

4.2.3.2 Staining of cryosections for immunofluorescence

The cryosections were first blocked in TBS containing 10 % heat-inactivated horse serum (TBS/HS) for 30 minutes at room temperature, and then stained with the affinity purified anti-cytoPtprq antibody (see section 2.3.2.1) diluted to 1:100 in TBS/HS. The sections were incubated with the primary antibody overnight at room temperature in a humid chamber. The next day, the primary antibody was removed by 3 successive washes of 5 minutes each in TBS. The cryosections were then incubated for 1 hour with Alexa 488 goat anti-rabbit IgG (Molecular Probes, Invitrogen) at 1:500, diluted in TBS/HS. At this stage, Texas Red®-X conjugated phalloidin (Molecular Probes, Invitrogen) was added as a counter-stain (at 1:300) in order to visualize hair bundles clearly. The cryosections were finally mounted in Vectashield (Vector Laboratories, Peterborough, UK) and viewed using a Zeiss Axioplan 2 microscope equipped with a 100 W Attoarc epifluorescence illuminator.

4.3 Results

4.3.1 *The yeast-two hybrid results reveal an EH-domain protein as a potential interactor of Ptprq*

The yeast-two hybrid screen revealed several putative interactors of Ptprq. These are listed below in table 4.1 (Step 6 of figure 4.3).

Interactor	Mouse Gene symbols	Number of clones	
		Putative positives obtained in <u>step 6</u>	Positive interactors confirmed in <u>step 7</u>
Creatine Kinase, Brain	Ckb, B-CK, CK-3	15	15
EHD3	Ehd3	4	4
Hsp 70kDa	Hspa1b, hsp68, Hsp70, Hsp70-1, Hsp70.1, HSP70A1	1	1
Myosin Regulatory Light Chain Isoform L20B	Isoform L20-B1, MLC-2, DTNB, G1	1	1
Ribosome protein, large, P1	Rplp1, acidic ribosomal phosphoprotein P1, C430017H15Rik, 2410042H16Rik	1	None
Ribosomal protein S27a	Rps27a, 0610006J14Rik	1	None
Stromal derived factor 3 (SDF3)	Sdf3, EPC-1, Pedf, Pedfl, pigment epithelium derived factor,	1	None

Table 4.1: List of putative positives obtained in step 6 of the yeast-two hybrid screen (see figure 4.3). Out of the 7 putative positives, only 4 were confirmed as positives interactors of Ptprq in step 7 (see figure 4.3). Also included are the numbers of clones obtained for each interactor.

Figure 4.4 shows the results of the interaction test (step 7 in figure 4.3). Co-transformation with pSos and pMyr vectors is used to determine the transformation efficiency as well as to ensure that the number of temperature sensitive revertants is acceptably low (lane 1 in figures 4.4a and b). The positive control for the interaction study involves co-transforming yeast cells with two plasmids, pMyr MAFB and pSos MAFB. The positive control shows cell growth at 37°C on SD/Galactose (-UL) plates (lane 2, figure 4.4a), but not on SD/Glucose (-UL) plates at 37°C (lane 2, figure 4.4b). Co-transformation with plasmids, pSos MAFB and pMyr Lamin C, serves as a negative control as the proteins encoded by these plasmids do not interact and the cells do not grow at 37°C on either selection plate (see lane 3, figures 4.4a and b). Cells co-transformed with the bait plasmid (pSos cytoPtprq) and pMyr Lamin C show that the intracellular domain of Ptprq does not interact with the myristylation signal (see figure 4.4a and b, lane 4). All cells grow on SD/Glucose (-UL) at 25°C (see figure 4.4c) but not at 37°C (see figure 4.4b).

Lanes 5-19 in figure 4.4a and b show the results of co-transformations with pSos cytoPtprq and the pMyr cDNA clones that were found to encode overlapping regions of the brain isoform of creatine kinase (BCK) (see table 4.1). These cells show varying degrees of growth on the SD/Galactose selection plates at 37°C (see figure 4.4a, lanes 5-19). Colonies in lanes 20-23 of figure 4.4a show comparable growth on the SD/Galactose plates at 37°C. The pMyr cDNA from these colonies encode the EH (for Eps15 Homology) domain of EHD3 (Santolini et al., 1999; Pohl et al., 2000; see below and figure 4.8). Colonies in lanes 24 and 28 grow on SD/Galactose (see figure 4.4a), whilst colonies in lanes 25 to 27 do not grow on SD/Galactose plates (see figure 4.4a). Colonies in lanes 24 to 28 of figure 4.4a, b and c contain the pMyr cDNA plasmids

encoding Hsp70, ribosomal protein 27a, ribosomal protein large P1, SDF3 and myosin regulatory light chain isoform L20B respectively.

Interactions with heat shock proteins like Hsp70 (see table 4.1) can be considered to represent aspecific interactions due to the involvement of the proteins in general aspects of protein folding. Therefore, this interaction was not analysed further. The myosin regulatory light chain isoform L20-B (see table 4.1) is a vascular non-muscle isoform (Sobue et al., 1999) first isolated from embryonic chicken gizzard cDNA (Inoue et al., 1989). As the above isoform of myosin regulatory light chain maybe a contaminant from the vasculature of the chick utricles, it was not studied further. BCK has been shown to be abundant in chick vestibular hair bundles and it has been proposed that this enzyme may be responsible for maintaining ATP concentration in the hair bundle (Shin et al., 2007). Although unexpected, the interaction of BCK with Ptprq was studied further by immunofluorescence staining of inner ear sections with an antibody to BCK (see appendix 2). Appendix figure 2.1 shows that the antibody labels hair cells and hair bundles in the chick utricle. Further studies will be needed to confirm this interaction and determine its significance. The BCK antibody was a gift from Professor Theo Wallimann, Institute for Cell Biology, Zurich, Switzerland.

EHD3, the focus of the rest of this chapter, is a protein involved in endocytosis (Galperin et al. 2002; Naslavsky et al., 2006). Yeast colonies containing the pMyr EHD3 insert showed good growth on SD/Galactose (-UL) plates and no growth on SD/Glucose (-UL) plates at 37°C (see figure 4.4, lanes 20-23). The four independent clones of EHD3 obtained represented more than half the coiled-coil region and an entire EH domain (see figure 4.8; Pohl et al., 2000).

4.3.2 EHD3, an endocytosis protein interacts with Ptprq in vitro

The interaction between chick Ptprq and human EHD3 was studied further by immunoprecipitations of lysates from co-transfected HEK293 cells using mAb 9E10 (anti-myc). Figure 4.5a shows the co-expression of myc-tagged EHD3 with the GFP-tagged proteins, Ic-Ptprq-EGFP (GFP-tagged intracellular domain of Ptprq; see section 5.2.2.2 for the cloning strategy of the construct), EHD1-GFP and MTMR3-GFP. Also, a mutant form of EHD3 missing the EH domain, myc-EHD3ΔEH, was co-expressed with Ic-Ptprq-EGFP (see figure 4.5a). As shown in figure 4.5b, Ic-Ptprq-EGFP co-immunoprecipitates with myc-EHD3 (lanes 1 and 1'), as well as with myc-EHD3ΔEH, (lanes 2 and 2'). Co-immunoprecipitation of EHD1-GFP with myc-EHD3 was used as a positive control (see figure 4.5b, lanes 3 and 3'; George et al., 2007). MAb 9E10 does not co-immunoprecipitate an irrelevant GFP-tagged protein (GFP-myotubularin-related protein 3, MTMR3-GFP) co-transfected with Myc-EHD3 as shown in lanes 4 and 4' of figure 4.5b. Additional bands observed with anti-GFP are non-specific and are indicated by asterisk in figure 4.5b. Finally, as a negative control, lysates from Ptprq and myc-EHD3 co-transfections were incubated with an irrelevant antibody (anti-Cbl-b; for Casitas b-lineage lymphoma) which did not immunoprecipitate either protein (see figure 4.5b, lanes 5 and 5').

Thus, the intracellular domain of Ptprq interacts with EHD3 and the mutant form of EHD3 (EHD3ΔEH) from which the EH domain has been deleted (Lanes 1 and 2 in figure 4.5b).

4.3.3 Distribution of Ptprq is unaltered in EHD3 knock-out mice

Cochleae from EHD3 knock-out mice (unpublished) were obtained from Dr. Manju George, University of Nebraska Medical Center, Omaha. Western blotting analysis reveals the absence of the protein in all of the tissue lysates obtained from the knock-out mouse compared to those from the wild-type and the mice have no obvious phenotypes (Dr. Manju George, unpublished). Immunohistochemistry using the anti-cytoPtprq antibody shows that the hair bundles of IHCs are stained in the cochleae of EHD3 knock-out (kind gift from Dr. Manju George) and wild-type mice (see panel B and B' in figure 4.6). The anti-cytoPtprq staining in the knock-out cochlear hair bundles is qualitatively similar to that seen in wild-type hair bundles (see figure 4.6). Staining with the anti-cytoPtprq antibody is also evident in the utricular hair cell bundles of the EHD3 knock-out cochlea (see figure 4.7, panel B') and is similar to that observed in the hair cell bundles of the wild-type utricle (see figure 4.7; panel B).

4.4   Discussion

A yeast two-hybrid screen using the Sos recruitment system reveals that EHD3, a protein involved in endocytosis, is a potential cytoplasmic interactor of Ptprq. The interaction was further confirmed *in vitro* by immunoprecipitations. However, this interaction does not depend on the EH domain of EHD3, and the distribution of Ptprq is unaltered in the hair bundles of EHD3 knock-out mice.

EHD3 belongs to the subfamily of highly homologous mammalian C-terminal EH domain proteins (EHD) that is comprised of EHD 1-4 (Mintz et al., 1999; Pohl et al., 2000). The 4 EHD proteins have similar domain architecture, with a putative P-loop motif that is a nucleotide binding region at the N-terminus, a central coiled-coil region

and a C-terminal EH domain that binds calcium (Figure 4.8; Naslavsky and Caplan, 2005; Kieken et al., 2007). While the coiled-coil region is involved in homo- or heterodimerization of the EHDs, the ATP binding region, which is similar in structure to the G-domain of dynamin, is necessary for oligomerisation and association with membranes (Naslavsky and Caplan, 2005; Lee et al., 2005; Daumke et al., 2007; George et al., 2007; Grant and Caplan, 2008).
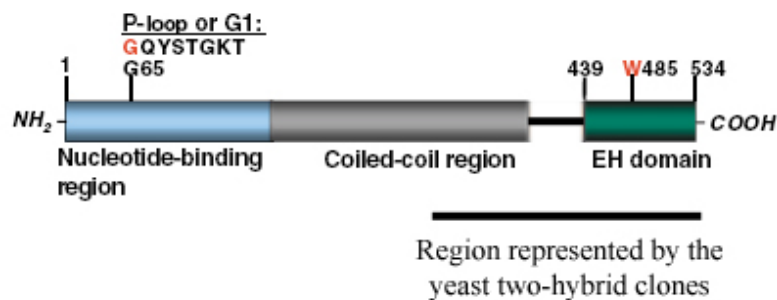
Figure 4.8: Schematic representation of the domain architecture of the EHD proteins. Also shown is the region represented by the EHD3 yeast two-hybrid clones.

The EH domain is an evolutionarily conserved protein-interaction domain that was originally identified in Eps15 (Santolini et al., 1999; Miliaras and Wendland, 2004). The overall structure of all of these EH domains appears to be similar and contains two EF-hands, potential calcium-binding helix-loop-helix motifs that are linked together by a short anti-parallel β-sheet (Confalonieri and Di Fiore, 2002; Kieken et al., 2007).

Based on the various interaction partners of the 4 EHD proteins reported so far, the main function of these proteins appears to be the regulation of endocytosis where they act at various stages of endocytic recycling (see figure 4.9a; Miliaras and Wendland, 2004; Naslavsky and Caplan, 2005; George et al., 2007; Grant and Caplan, 2008). EHD1/RME-1 is the best characterised protein among the EHDs (Grant and Caplan, 2008).

EHD3, which is most similar to EHD1, has been shown to interact and co-localise with EHD1 in tubulovesicular structures (Galperin et al., 2002; George et al., 2007). Rab4 and Rab11 are Rab-family GTPases whose activity is crucial for endocytic recycling (Seachrist and Ferguson, 2003). EHD1 and EHD3 both interact with rabenosyn-5, a Rab4 effector, and with Rab11-FIP2, a Rab 11 effector, with oligomerisation and ATP binding both being necessary for the latter interaction (Naslavsky et al., 2006). EHD3 depletion results in enlarged peripheral endosomes suggesting a role for EHD3 in the transfer of internalised cargo from the early endosome to the endocytic recycling compartment (ERC) (see figure 4.9a and b). In contrast, EHD1 depletion results in the accumulation of internalised transferrin in the ERC (Naslavsky et al., 2006; George et al., 2007). Thus, it appears that EHD1 and 3 have distinct functions in the endosomal recycling pathway and a model for their transient interaction facilitating transfer of cargo from the early endosome to the ERC has been proposed (Figure 4.9b; Naslavsky et al., 2006). In this model Rab4 and Rab11 containing early endosome vesicles employ rabenosyn-5 and Rab11-FIP2 as 'connector proteins' in order to recruit EHD3 that then hetero-oligomerises with EHD1 on the ERC allowing fusion of the early endosomal vesicle with the ERC (figure 4.9b; Naslavsky et al., 2006). A similar model involving EHD1-containing vesicles exiting the ERC may return the early endosomal proteins to the early endosome (Naslavsky et al., 2006). The interaction of EHD1 and EHD3 may provide the scaffolding necessary to facilitate the SNARE pairing and fusion of endosomal vesicles (Naslavsky et al., 2006).

The discovery of the potential interaction between Ptprq and a protein of the endocytotic pathway is interesting in the light of the localisation of Ptprq on the apical surfaces of hair cells (Richardson et al., 1990; Goodyear and Richardson, 1992; Goodyear et al., 2003), where endocytosis is known to occur (see section 1.3.2; Forge

and Richardson, 1993; Kachar et al., 1997; Richardson et al., 1997). Though the significance of the EHD3-Ptprq interaction is not obvious at the moment, it is easy to envisage a role for Ptprq in the endocytosis of the apical membrane in hair cells. Recent evidence shows that EHDs interact with PIs *in vitro* with varying degrees of affinity (Blume et al., 2007; Daumke et al., 2007; Naslavsky et al., 2007; Jović et al., 2009). There is also *in vivo* evidence for the association of EHDs with endosomal membranes containing specific PIs. Jović et al. (2009) have shown that EHD1 and EHD4 associate with tubules containing PI 4 P and PI 4,5 P_2 and the association of these EHDs with the tubules is lost on PI 4 P depletion. The authors suggest that a fine balance between PI 4 P and PI 4,5 P_2 might be necessary for the maintenance of the EHD1-associated tubular membranes (Jović et al., 2009).

From the above information, it appears that the sub-cellular distribution of the EHDs may be defined by specific PI compositions of the various cellular membranes. The specific localisation of the EHDs has been suggested to be essential for their functional role in endocytosis in cells (George et al., 2007). Thus, PI kinases and phosphatases may regulate the PI content of cellular membranes and determine where the different EHDs localise. For example, building on the model for the role of EHD3 in the early endosomal transport proposed by Naslavsky et al. (2006; Figure 4.9b), the specific PI content of the early endosomal membrane may differ from that of the ERC membrane and determine the localisation of EHD3 to the former and EHD1 to the latter. These two EHDs may then interact and bring about fusion between the respective membrane compartments. However, secondary interactions between other proteins residing in the endosomal membranes may also contribute in fine-tuning the specific localisation of the EHDs.

EHD3 may initially be recruited to sites of endocytosis at the apical surface of hair cells by an interaction with Ptprq (see figure 4.10a). In fact, occasional plasma-membrane localisation of EHD3 and its co-fractionation in both plasma membrane and cytosolic fractions are indicative of a transient interaction with membranes (Blume et al., 2007). As a broad specificity PIPase, Ptprq may dephosphorylate PI 4,5 P_2, PI 3,4 P_2 or even PI 3,4,5 P_3 that occur in the hair cell's apical plasma membrane to PI 4 P and thus regulate the PI levels in this region. On formation of endocytic vesicles, EHD3 may then reattach to these vesicular membranes when the clathrin complex falls apart, thus ensuring the entry of these vesicles into the endocytic pathway (see figure 4.10a). Interestingly, EHD3 is believed to assist in the transfer of internalised material from the early endosome to the ERC (Naslavsky et al., 2006; George et al., 2007) and the early endosome in hair cells lies close to the apical surface where Ptprq is found (Goodyear et al., 2003; Griesinger et al., 2004).

Alternatively, EHD3 may assist in transferring internalised Ptprq to the ERC in order to return it to the apical surface of hair cells (see figure 4.10b). As EHD3 also interacts with rabenosyn-5, which has been implicated in the 'fast recycling' of endocytic vesicles from the early endosome to the cell surface (de Renzis et al., 2002; Grosshans et al., 2006), endocytic recycling of internalised Ptprq may also occur via this pathway (see figure 4.10b). EHD3 may also regulate the internalisation of Ptprq, in addition to its recycling as described above. Transmembrane receptors are known to direct their own endocytosis by interacting with several cargo-recognising endocytic proteins (Conner and Schmid, 2003). Although EHD3 has not been reported to be a protein that recognises cargoes for endocytosis, by interacting with Ptprq it may mediate the assembly of the endocytic machinery at the apical surfaces in hair cells via EHD1 (see figure 4.10b). EHD1 is known to interact with the clathrin heavy chain and α-adaptin of

the AP-2 complex, both of which comprise the endocytic complex accompanied by accessory proteins (Rotem-Yehudar et al., 2001; Naslavsky and Caplan, 2005).

Like most EH domain proteins, the EHDs appear to interact with class I peptides containing asparagine-proline-phenylalanine (NPF) in their partner proteins (Confalonieri and Di Fiore, 2002). The intracellular domain Ptprq, however, does not have an NPF motif. Instead, Ptprq has a phenylalanine-tryptophan (FW) in the intracellular domain which belongs to the class II peptides known to bind EH domains (Confalonieri and Di Fiore, 2002). The co-immunoprecipitation results suggest that the intracellular domain of Ptprq also interacts with the EHD3 mutant lacking the EH domain (Figure 4.5b, lanes 1 and 2). The Ptprq interaction domain therefore must lie in the coiled-coil region of EHD3. The coiled-coil region of the EHDs is known to be important in mediating protein interactions by facilitating oligomerisation and, in the case of EHD1, the coiled-coil region itself mediates interaction with SNAP29 (Rotem-Yehudar et al., 2001; Naslavsky et al., 2006).

Although the normal distribution of Ptprq in the EHD3 knock-out cochleae does not indicate a lack of interaction between the two proteins, the results do suggest that EHD3 may not be required for the proper localisation of Ptprq. Alternatively, functional compensation by another EHD may account for the normal distribution of Ptprq in the EHD3 knock-out cochlea. It is known that the four mammalian EHDs share high levels of identity with each other, with EHD3 being most similar to EHD1 (Naslavsky and Caplan, 2005; Grant and Caplan, 2008). Such functional compensation has been suggested to occur in the EHD4 knock-out mice in which a hair bundle phenotype is not seen despite evidence for interactions between EHD4 and Cdh23 (Sengupta et al., 2009). Indeed, an increase in the expression levels of the EHD1 protein in the cochleae

of the EHD4 knock-out mice has been shown, suggestive of a functional compensation by EHD1 (Sengupta et al., 2009). Therefore, even though the EHDs may be involved at different stages of endocytosis, the high degree of similarity between these proteins allows for functional redundancy. RME-1 (receptor mediated endocytosis-1) is the *Caenorhabditis elegans* homologue of EHD1, and all four mammalian EHDs can rescue the basolateral endocytic trafficking and recycling defect in the *rme*-1 mutant worm (George et al., 2007).

4.5   Conclusions

In conclusion, whilst this study provides some of the first clues as to a possible role for Ptprq in regulating apical endocytosis, more studies are required to validate some of the proposals suggested.

4.6   Future Perspectives

The observed yeast-two hybrid and *in vitro* interaction of Ptprq and EHD3 needs to be supported by immunostaining experiments showing that EHD3 is expressed in hair cells. It has been difficult to determine the distribution of endogenous EHDs in tissues due to the high degree of similarity between their amino acid sequences (see appendix 3; Naslavsky et al., 2006; Sengupta et al., 2009). Several groups have now successfully prepared polyclonal antibodies to recombinant proteins as well as to peptides specific to each EHD (Naslavsky et al., 2006; Blume et al., 2007). However, a polyclonal antibody raised to recombinant mouse EHD3 (kind gift from Dr. Markus Plomann, Center for Biochemistry and Center for Molecular Medicine, University of Cologne, Cologne, Germany) and an EHD3 anti-peptide antibody (kind gift from Dr. Manju George) both showed staining in the inner ear tissue sections of EHD3 knock-out mice indicating that

these antibodies may not be suitable for immunohistochemistry studies (see appendix 3). As an alternative to immunofluorescence, mRNA expression of EHD3 in hair cells can be tested by *in situ* hybridization. As Ptprq is expressed only in the hair cells in the inner ear, co-expression of EHD3 in the hair cells will be further evidence that these two proteins could interact *in vivo.*

As functional compensation by another EHD may explain why the distribution of Ptprq in EHD3 knock-out cochlear hair cells is unchanged, analysis of double EHD knock-out mice may prove informative. Mice doubly mutant for EHD3 and one of the other EHDs could be used to study the expression and localisation of Ptprq, and measures of auditory performance in these mice could provide useful information regarding the possible functional significance of the observed interaction between EHD3 and Ptprq.

The interaction described above supports the suggestion that EHD3 regulates the endocytosis and/or recycling of Ptprq, or that Ptprq regulates the endocytotic pathway. It will be informative to examine how the overexpression of EHD3 influences the localisation of full-length recombinant Ptprq in HEK293 cells. If the internalisation of Ptprq is triggered by EHD3, decreased plasma membrane localisation and increased intracellular endosomal localisation of Ptprq might result from EHD3 co-overexpression. The ability of EHDs to interact with specific PIs and associate with membranes containing specific PIs makes Ptprq an attractive candidate for regulating these interactions. Transmission electron microscopy can be used to determine if there is a difference in the number of coated or uncoated vesicles at the apical ends of $Ptprq^{CAT/CAT}$ mutant hair cells compared to the wild-type. The result of such studies might reveal a defect in endocytosis in the Ptprq mutant hair cells as a result of a loss of the interaction of Ptprq with EHD3.

CHAPTER 5

N-glycosylation is essential for the apical targeting of Ptprq in polarized epithelial cells

5.1   Introduction

5.1.1   Polarized protein transport

Studies on polarized epithelial cell lines like Madin-Darby canine kidney (MDCK), the human intestinal cell lines Caco-2 and HT-29, and HepG2 hepatocytes have given rise to a general understanding of polarized protein trafficking. The polarized sorting of proteins involves simple variations in the working of common cellular machinery (Mellman and Nelson, 2008). Protein sorting begins with the recognition of intrinsic targeting signals by the cellular sorting machinery followed by protein trafficking to their respective membrane domains (Brown and Breton, 2000; Mellman and Nelson, 2008; figure 5.1). The polarized sorting may involve direct protein delivery or transcytosis, which involves the delivery of the proteins via vesicles to the target membrane following their initial delivery to the opposite surface (Weimbs et al., 1997; Mostov et al., 2000). Membrane protein trafficking involves a sequential protein transport via vesicles between the endoplasmic reticulum (ER), the Golgi complex, endosomes and the plasma membrane (see figure 5.1; Mellman and Nelson, 2008). Some of the protein complexes comprising these vesicular transport intermediates that shuttle membrane proteins between the different membrane compartments have been discovered. The protein complexes crucial for the trafficking process include receptor proteins involved in recognizing and selectively recruiting cargo proteins into the

vesicles, as well as structural proteins that are responsible for the formation of the vesicles (Mellman and Nelson, 2008).
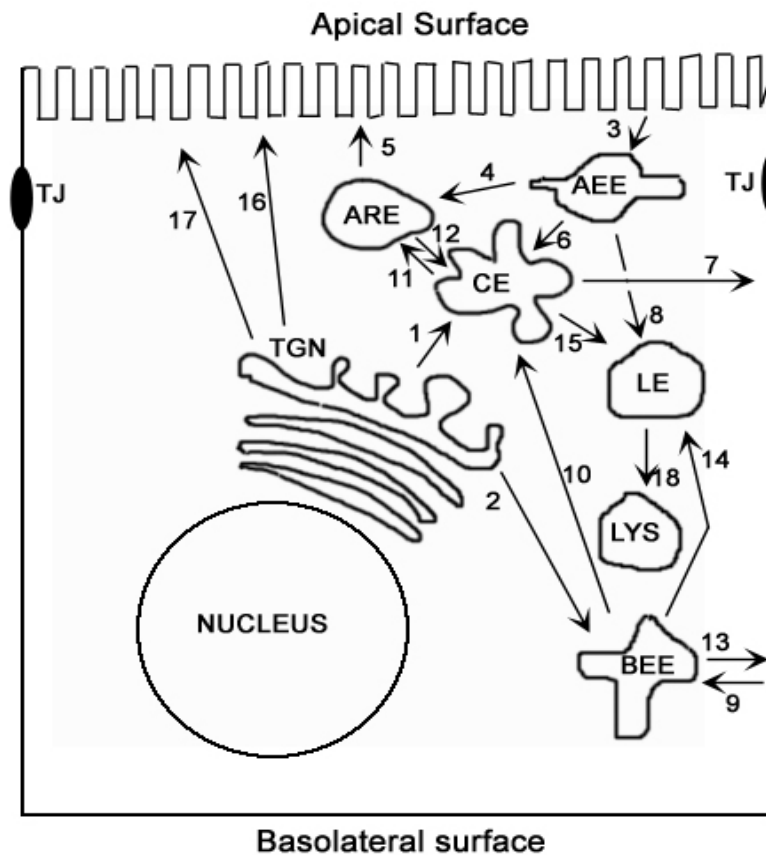
Figure 5.1: The various protein sorting pathways in polarised epithelial cells (Schuck and Simons, 2004; Mostov et al., 2000; Fölsch, 2008).

The cargo-filled vesicles travel along the actin and microtubule cytoskeleton and fuse

with the target plasma membrane domain in a process that is regulated by Rab GTPases,

tethering complexes and SNAREs (Hehnly and Stamnes, 2007; Grosshans et al., 2006; Rothman, 1994). On reaching the target plasma membrane domains, specific protein-protein and protein-lipid interactions stabilize the proteins at their respective membranes and help maintain the polarization of the membrane surfaces (Yeaman et al., 1999; Mellman and Nelson, 2008). The stabilization of membrane proteins involves specific interactions with cytoskeletal proteins, scaffolding proteins and signalling complexes, or lipid-raft clustering to ensure retention of correctly targeted proteins while removing mis-targeted proteins by endocytosis (Mays et al., 1994; Weimbs et al., 1997; Yeaman et al., 1999; Brown and Breton, 2000; Matter, 2000; Mellman and Nelson; 2008). Endocytic recycling of membrane proteins back to their target membranes is another mechanism for the preferential accumulation of proteins at the apical or basolateral domains but probably requires the binding of the particular protein to one or more scaffold proteins (Mellman and Nelson, 2008).

5.1.2 Intrinsic polarised sorting signals

Nearly all proteins destined for the apical or basolateral membrane depend on intrinsic sorting signals for their targeted delivery. The intrinsic sorting or targeting signals are a diverse group of determinants that are recognised and deciphered by the cellular sorting machinery (Mellman and Nelson, 2008). Targeting signals can be distinct cassettes of amino acids located in the intracellular or transmembrane region, or may be post translational modifications of the ectodomain like glycosylphosphatidylinositol (GPI) anchors and glycosylation motifs (Brown and Breton, 2000; Schuck and Simons, 2004; Mellman and Nelson, 2008). Deletion and site-directed mutagenesis have been used to locate targeting signals, as well as reveal hidden or recessive targeting signals that are functional only on removal of a more dominant targeting signal (Brown and Breton,

2000). Techniques used to characterize intrinsic targeting signals also include domain swapping, where the regions of two proteins believed to be involved in directing the respective proteins to opposing membrane surfaces are interchanged, resulting in new chimeric proteins with altered membrane sorting properties (Brown and Breton, 2000; Schuck and Simons, 2004; Mellman and Nelson, 2008).

5.1.2.1 Basolateral sorting signals

The well known basolateral signals are tyrosine or leucine based motifs that occur in the intracellular domains of the LDL-receptor, transferrin receptor and CD147 (Brown and Breton, 2000; Mellman and Nelson, 2008). The similarity of some basolateral signals with signals for endocytosis, and the maintenance of recycling receptors in their respective membrane domains suggest that these cytoplasmic signals may be recognized by adaptor protein complexes (Hunziker and Fumey, 1994; Mostov et al., 2000; Rodriguez-Boulan and Müsch, 2005; Mellman and Nelson, 2008; Fölsch, 2008). Indeed, μ1B, a recently identified isoform of μ1 subunit of AP-1, was found to mediate basolateral targeting in polarized epithelial cells (Fölsch et al., 1999). In addition to the Tyr and Leu based signals mentioned above, basolateral signals can also be encoded by a stretch of amino acids that probably confer an as yet undetermined property recognised by the cellular sorting machinery (Casanova et al., 1991; Mostov et al., 2000; Brown and Breton, 2000). In addition, PDZ-binding motifs have also been reported to function as basolateral signals for several proteins (Muth et al., 1998; Perego et al., 1999; Shelly et al., 2003; Schuck and Simons, 2004). However, it has been argued that PDZ binding domains act to retain the proteins at the target surface by binding to PDZ proteins and so the polarized distribution of the former may be due to a

combination of targeting and retention signals (Schuck and Simons, 2004; Brône and Eggermont, 2005).

5.1.2.2 Apical targeting signals

Apical signals, however, have proven more elusive. The apical targeting signals reported so far are quite varied and known to occur in the transmembrane region and intracellular domain of proteins (Lin et al., 1998; Dunbar et al., 2000; Muth et al., 1998; Milewski et al., 2001; Mostov et al., 2000; Mellman and Nelson, 2008). The best known apical targeting signals, however, are present in the post-translational modifications like GPI anchors and N- and O-linked glycans in the extracellular domain of proteins (Rodriguez-Boulan and Gonzalez, 1999; Urquhart et al., 2005; Delacour and Jacob, 2006). Apical sorting may occur by the clustering of GPI-anchors in lipid rafts, membrane domains enriched in glycosphingolipids, sphingomyelin and cholesterol (Weimbs et al., 1997; Paladino et al., 2007; Mostov et al., 2000; Mellman and Nelson, 2008). However, GPI-anchors are not always sufficient for apical sorting although they might confer raft association (Benting et al., 1999; Lipardi et al., 2000; Delacour and Jacob, 2006). Also, in Fischer rat thyroid cells, GPI-anchored proteins are targeted to the basolateral surface (Zurzolo et al., 1993).

Several apically directed proteins have been shown to rely on their N- and O-linked oligosaccharides for efficient targeting (Scheiffele et al., 1995; Yeaman et al., 1997; Benting et al., 1999; Mostov et al., 2000; Brown and Breton, 2000; Schuck and Simons, 2004; Urquhart et al., 2005; Delacour and Jacob, 2006; Mellman and Nelson, 2008). For example, occludin and the glycine transporter, GLYT2, depend on their N-glycans, while the neurotrophin receptor and podocalyxin require their O-glycosylated moieties for apical targeting (Schuck and Simons, 2004; Mellman and Nelson, 2008). Studies

done on glycosylation-deficient cell lines and on cells treated with glycosylation inhibitors have revealed the apical targeting potential of N-linked oligosaccharides (Le Bivic et al., 1993; Urban et al., 1987; Gut et al., 1998; Rodriguez-Boulan and Gonzalez, 1999).

Exactly how glycans are predicted to confer apical targeting is still not clear. It has been suggested that glycans might interact with hypothetical sorting lectins in the TGN that are required for the apical targeting of these proteins (Rodriguez-Boulan and Gonzalez, 1999; Mostov et al., 2000). Indeed, galectins, a family of lectins, have been shown to have a role in raft-dependent and raft-independent apical trafficking (Delacour and Jacob, 2005; Delacour et al., 2006; see figure 5.1). It has also been suggested that N-glycans may be required for the correct folding and thereby facilitating the apical delivery of the protein (Rodriguez-Boulan and Gonzalez, 1999; Mostov et al., 2000). Although one of the most commonly known apical targeting signals, N-linked sugars do not always signal sorting to the apical surface of polarized cells (Su et al., 1999; Larsen et al., 1999; Chmelar and Nathanson, 2006). It has also been suggested that not all cells recognise N-glycans as apical targeting signals (Su et al., 1999).

5.1.3 *Hierarchy of protein targeting signals*

From studies on protein targeting in polarized cells, it is clear that some sort of hierarchy exists among apical and basolateral targeting signals (Ikonen and Simons, 1998). The common belief for some time has been that basolateral targeting signals are dominant over apical ones (Gut et al., 1998; Matter, 2000; Schuck and Simons, 2004; Mellman and Nelson, 2008). However, recent data show that cytoplasmic basolateral targeting signals can be recessive to apical sorting determinants (Yeaman et al., 1997; Jacob et al., 1999; Ihrke et al., 2001).

The various types of apical and basolateral signals and the apparent hierarchy between them reflects the flexible phenotype of epithelial cells. The various apical and basolateral proteins are directed to their destinations to suit the cell type and its physiological context (Delacour and Jacob, 2006).

5.1.4 Protein targeting in the hair cell

Protein targeting in hair cells has not been studied in great detail and very little is known about the targeting signals in the various hair bundle proteins. However, targeting studies have been performed on the plasma-membrane Ca^{2+}-ATPase (PMCA) isoforms 1 and 2, the major Ca^{2+} pumps of mammalian sensory hair cells (Grati et al., 2006; Hill et al., 2006). PMCA2 is expressed in the stereocilia of hair cells of the inner ear, whereas PMCA1 is localized to the basolateral plasma membrane of hair cells (Dumont et al., 2001). They are predicted to contain ten membrane spanning segments, two large cytoplasmic loops as well as cytosolic N- and C-termini (Grati et al., 2006). Alternative splicing at their first cytosolic loop (A-site) and their C-terminal tail (C-site) generates several isoform variants of PMCA1 and 2 (Strehler and Zacharias, 2001). A Leucine-Isoleucine motif in a C-site splice variant (b-tail) was found to promote exclusive basolateral targeting of PMCA1b and PMCA2b isoforms, whilst the size of the insert (w) at the A-splice site was shown to regulate apical targeting (Grati et al., 2006). Thus, the isoform PMCA2w/a, is targeted exclusively to the apical surface and hair bundles of transfected hair cells, whilst the PMCA2x/b is targeted to the basolateral surface (Grati et al., 2006).

In hair cells, Ptprq is found restricted to the apical stereociliary and non-stereociliary surfaces (see section 1.5.2; Goodyear et al., 2003). In the human kidney, however, Ptprq

is found at the basal lamina of podocytes (Seifert et al., 2003). Thus far, no apical or basolateral targeting signals have been reported for Ptprq.

The aim of the current study was therefore to determine the localization of the targeting signal in Ptprq that is responsible for its exclusive apical localization in hair cells. Attempts to transfect hair cells in cultured mouse cochleae with Ptprq using the biolistic method were unsuccessful. Therefore, the targeting of the individual domains or combinations of the various domains of Ptprq was determined in the porcine kidney epithelial cell line, LLC-PK1 (CL4).

5.2 Materials and Methods

5.2.1 Mammalian expression constructs
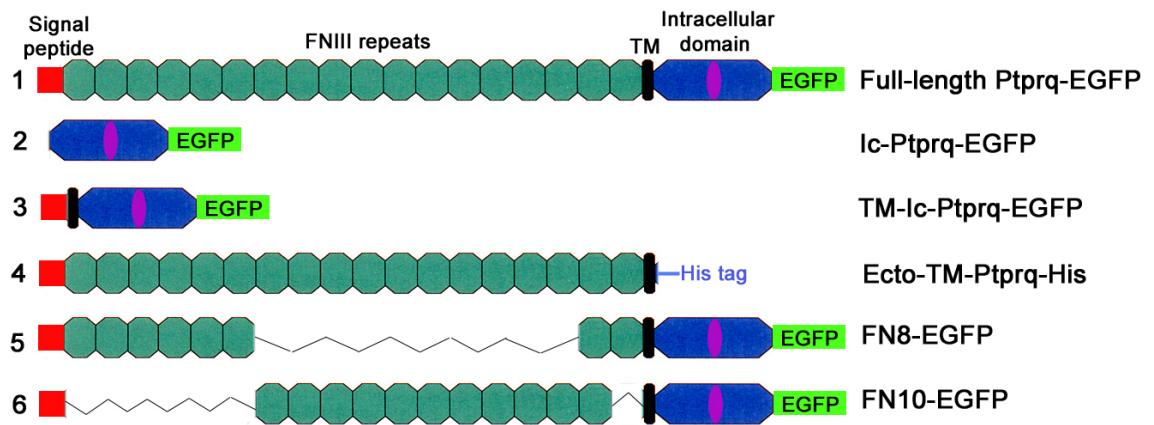
Figure 5.2: The various Ptprq constructs that are designed to express the different domains of Ptprq, either individually or in combinations. Ic is intracellular domain, TM is transmembrane domain, Ecto is ectodomain and FN refers to fibronectin type III repeats.

5.2.2 *Gene cloning strategies*

The cDNA made from total RNA of post hatch day 2 chick utricles was used as a template to amplify the Ptprq sequence. All constructs were made using the pEGFP actin vector (Clontech) and possess a C- terminal EGFP-tag. The pEGFP actin vector is designed to express the human cytoplasmic β-actin fused at its N-terminus to the human codon-optimised variant of GFP known as EGFP (see Figure 5.3). The constructs were designed to replace both β-actin and EGFP sequences with the Ptprq sequence of interest fused to a C-terminal EGFP tag. In some cases the C-terminal EGFP tag was amplified by PCR separately and inserted inframe at the end of the Ptprq DNA sequence. Others constructs were amplified by PCR using another EGFP-tagged Ptprq construct as a template (See below).
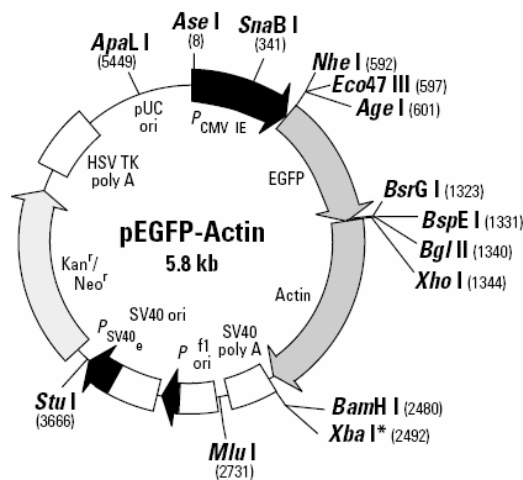
Figure 5.3: pEGFPActin vector map (Clontech).

5.2.2.1 TM-Ic-Ptprq-EGFP

The construct TM-Ic-Ptprq EGFP (see figure 5.2) expresses the transmembrane region (TM) of Ptprq fused to its intracellular domain (Ic) and a C-terminal EGFP tag. See below (figure 5.4).
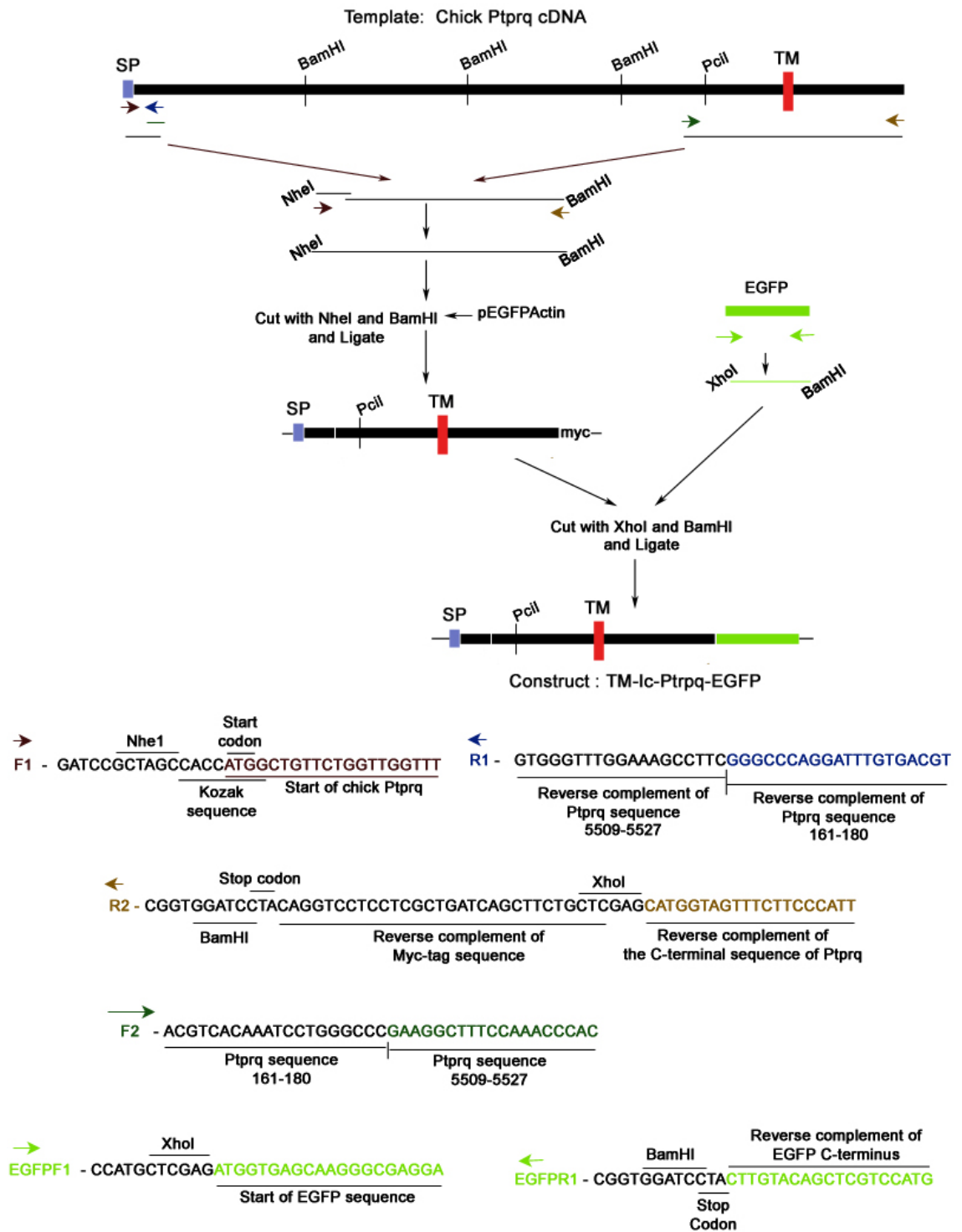
Figure 5:4: Strategy to clone the Ptprq sequence encoding the transmembrane region (TM) fused to the sequence encoding the intracellular domain (Ic) with a C- terminal EGFP tag.

Primers F1 and R1 were used to amplify the first 180 bp of chick Ptprq cDNA sequence (see figure 5.4). This region includes the signal peptide (SP) of Ptprq. Primers F2 and R2 were used to amplify the transmembrane and intracellular region of Ptprq (bases 5509-6945 of Ptprq). The reverse primer R2 adds a myc tag at the end of the amplified product. The products of the above PCR reactions were pooled and used as a template along with primers F1 and R2. As F2 sequence overlaps with R1, the product of this PCR will include the first 180 bp of Ptprq fused to the region from 5509 to 6945 of the Ptprq cDNA sequence. This final product was cut with restriction enzymes Nhe1 and BamHI and ligated into the pEGFPactin vector, also cut with NheI and BamHI. Cutting pEGFPActin with these enzymes removes the EGFP-actin sequence from the backbone of the vector. The construct obtained from transforming this ligation was called, TM-Ic-Ptprq-myc. To replace the myc-tag sequence with the EGFP sequence, a separate PCR was performed using primers EGFPF1 and EGFPR1 to amplify the EGFP sequence using pEGFPactin as a template. The EGFP PCR product and TM-Ic-Ptprq-myc were cut with XhoI and BamHI, and ligated. The final construct in this case was called TM-Ic-Ptprq-EGFP (See figure 5.2).

5.2.2.2 Ic-Ptprq-EGFP

The construct Ic-Ptprq-EGFP encodes the intracellular domain of Ptprq fused to the EGFP sequence (See figure 5.2).

The insert was amplified using the primers CytoF1 and EGFPR1, and TM-Ic-Ptprq-EGFP as template. The PCR product was cut with NheI and BamHI and ligated into pEGFPactin vector that was cut with the same enzyme pair. The new construct was called Ic-Ptprq-EGFP.
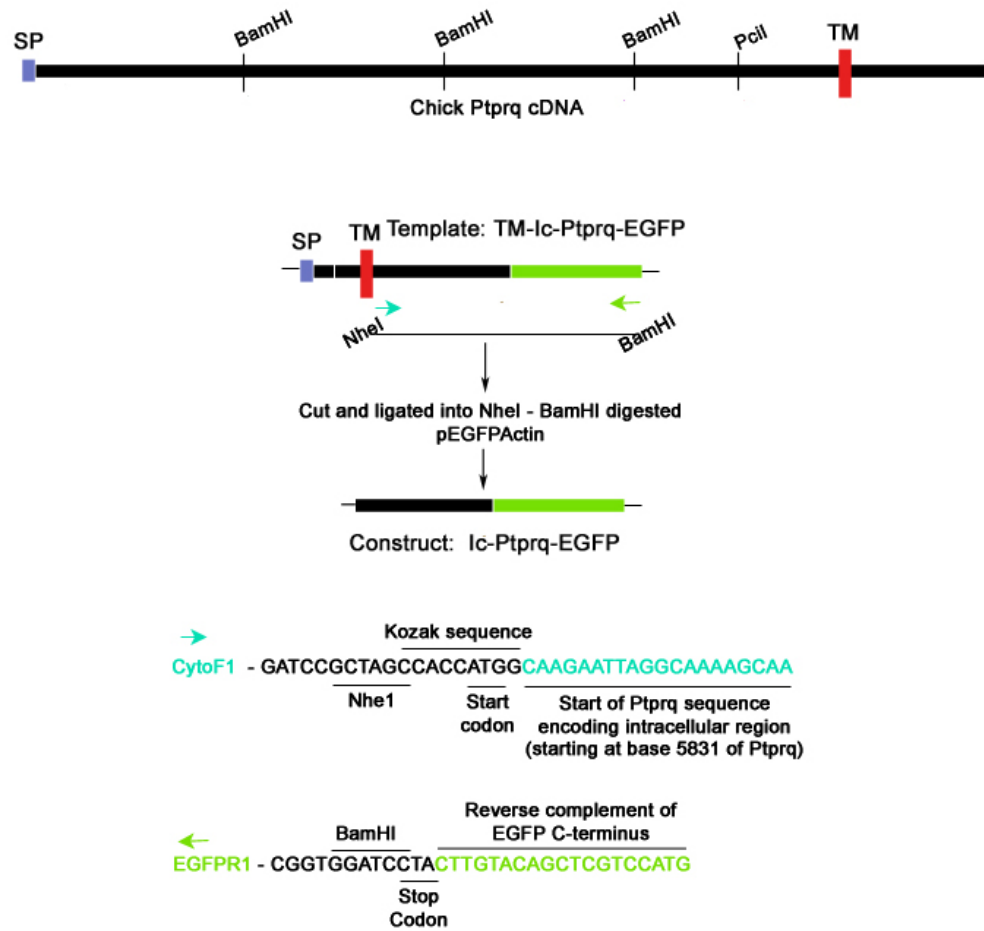
Figure 5.5: Strategy for cloning the DNA sequence encoding the intracellular domain of Ptprq with a C-terminal EGFP tag.

5.2.2.3 FN8-EGFP

The FN8-EGFP construct encodes the first 6 FNIII repeats in the ectodomain of Ptprq fused to the last 2 FNIII repeats followed by the remainder of the protein and a C-terminal EGFP tag (see figure 5.2). Figure 5.6 shows the strategy used to clone FN8-EGFP construct.
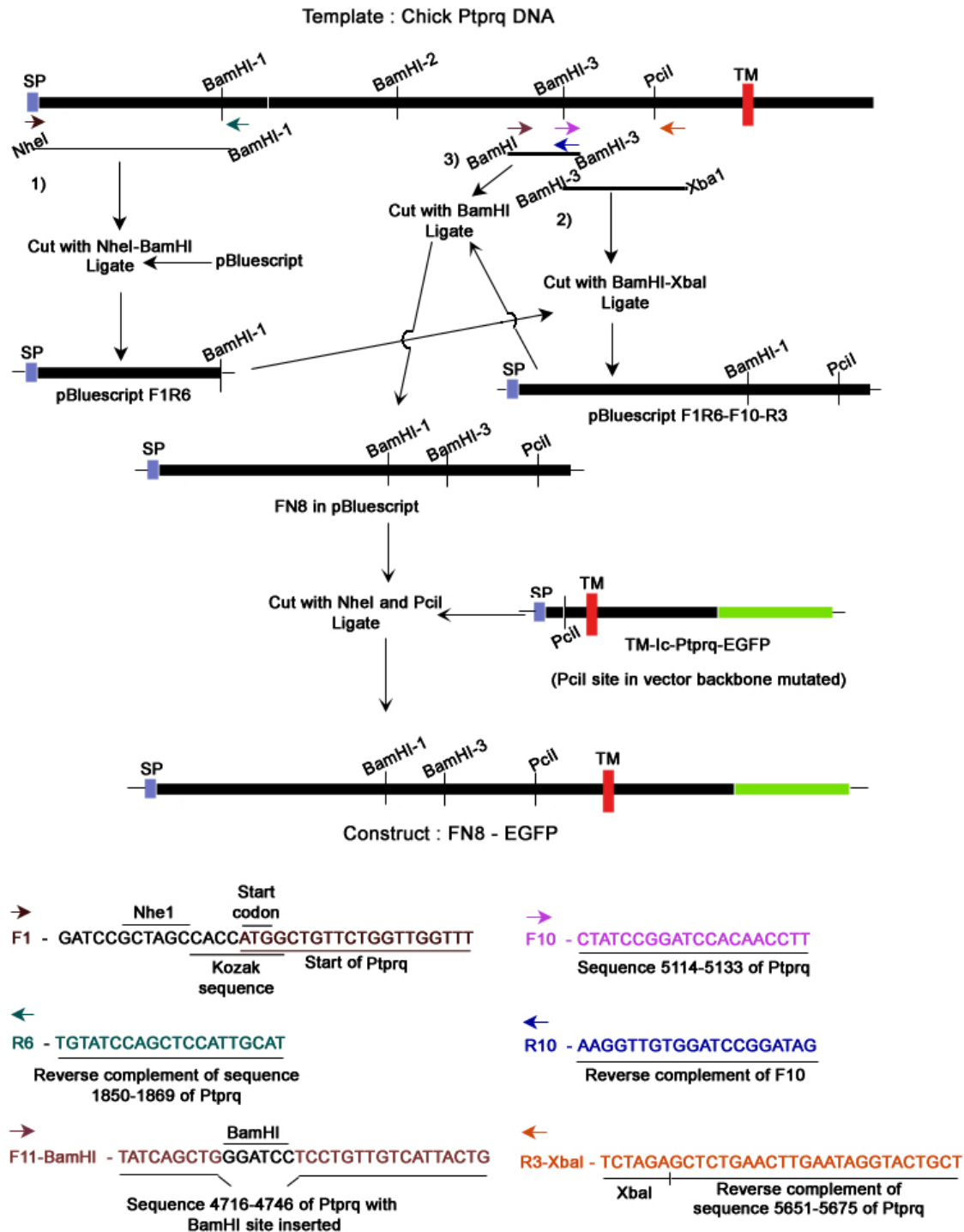
Figure 5.6: Strategy for cloning the FN8-EGFP construct.

Primers F1 and R6 was used to amplify a 5' region of Ptprq cDNA that included the first BamHI site. This product was cut with NheI and BamHI and ligated into pBluescript vector that was cut with the same pair of enzymes to obtain construct pBluescript F1R6. Next, primers F10 and R3-XbaI were used to amplify a short region

beginning from 5' of the third BamHI site and ending just after the PciI site. This product of ~500 bp length was cut with BamHI and XbaI (site added on by the reverse primer) and ligated into pBluescript F1R6 that was cut with the same enzymes. The resultant construct was called pBluescript F1R6-F10R3. Primers F11-BamHI and R10 were used to amplify another short region from 4716-5133 of Ptprq sequence. The F11 primer was designed such that it included a BamHI site within it. This enabled the PCR product to be cut with BamHI alone and ligated into pBluescript F1R6-F10-R3 that was linearised using BamHI. This FN8-pBluescript construct was finally cut with Nhe1 and PciI and ligated into Nhe1-PciI digested TM-Ic-Ptprq-EGFP (the PciI site in the pEGFPactin backbone was mutated prior to ligation). The new construct was called FN8-EGFP.

5.2.2.4 Full-length Ptprq EGFP

The construct full-length Ptprq-EGFP encodes the entire chick Ptprq sequence fused to a C-terminal EGFP tag (see figure 5.2).

Primers F5 and R12 were used to amplify the region from the first BamHI site to the second BamHI site in the ectodomain of Ptprq. Primers F13 and R10 were used to PCR amplify the region from the second BamHI site to the third BamHI site. Both these PCR products along with the FN8-pBluescript construct (see figure 5.6) were individually restriction digested with BamHI and used together in a ligation reaction. Several colonies were tested for the presence of both inserts in the right orientation by restriction digestions followed by DNA sequencing.
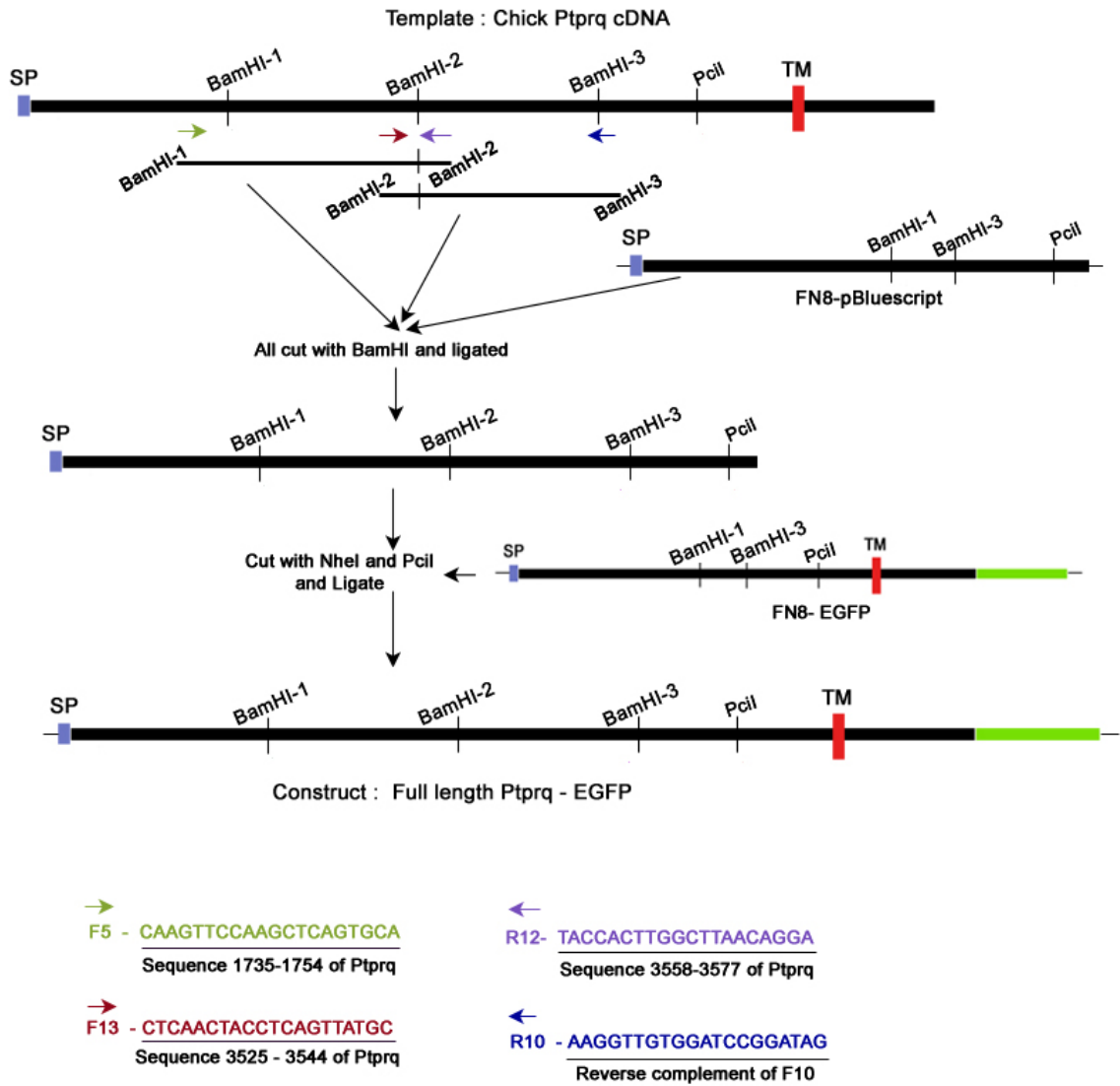
Figure 5.7: Strategy to clone the full-length Ptprq-EGFP construct.

One construct that was correctly ligated was restriction digested with NheI and PciI and the insert was ligated into the backbone of FN8-EGFP (after digestion with NheI and PciI). The construct resulting from this ligation was full-length Ptprq-EGFP which was confirmed by restriction digestion analysis and DNA sequencing.

5.2.2.5 FN10-EGFP

FN10-EGFP was designed to express the region from the 7th to the 17th FNIII repeats in the ectodomain of Ptprq fused to rest of the C-terminal region of the protein with a C-terminal EGFP-tag (see figure 5.2).
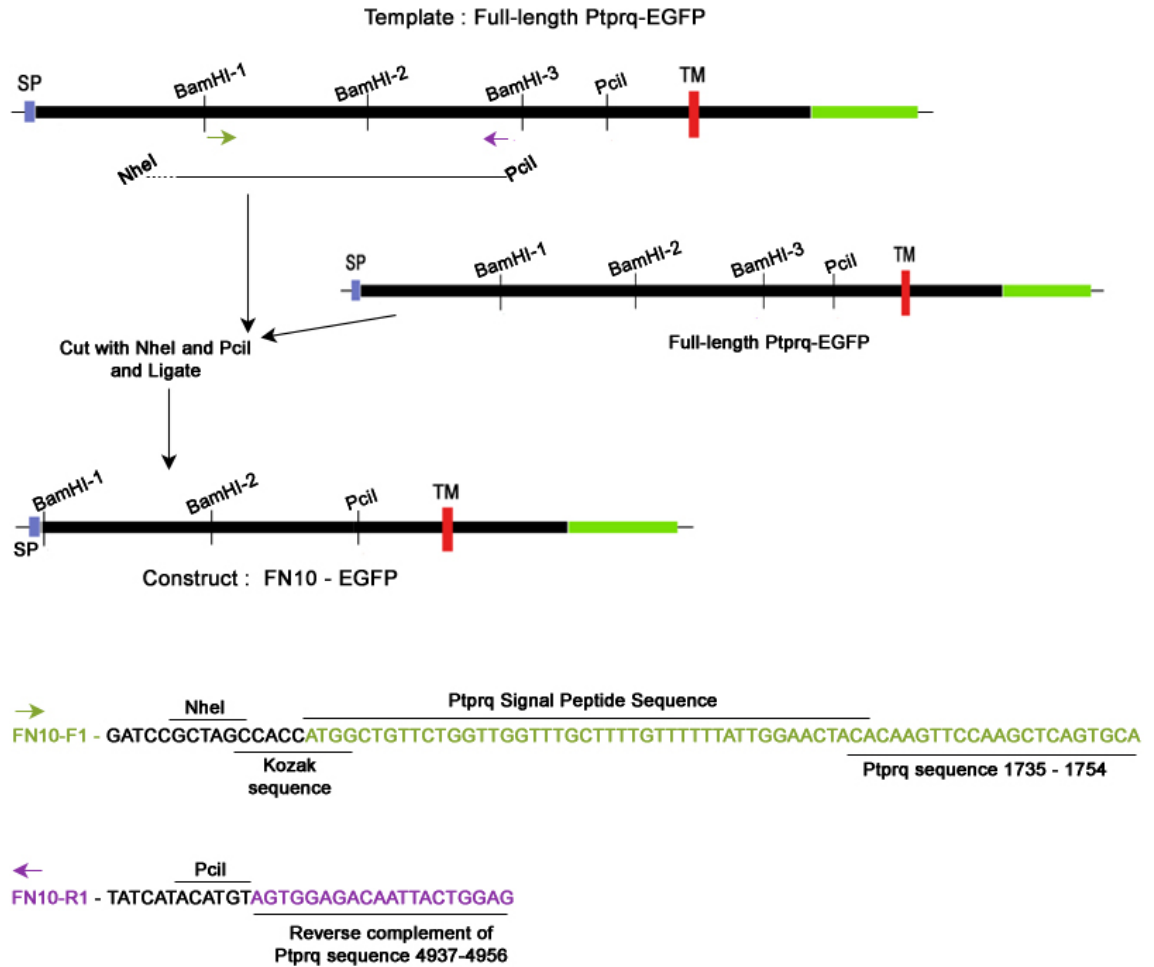
Figure 5.8: Strategy to clone the construct FN10-EGFP.

Primers FN10-F1 and FN10-R1 were used to PCR amplify the region from the first BamHI site to the third BamHI site in the ectodomain of Ptprq, with NheI and PciI sites added by the forward and reverse primers (as indicated in figure 5.8). The insert was digested with NheI and PciI and ligated into the backbone of the full-length Ptprq-EGFP

construct obtained after digestion with the same pair of enzymes. The resulting construct was called FN10-EGFP (see figure 5.2).

5.2.2.6 Ecto-TM-Ptprq-His

This construct encodes a recombinant protein that contains the ectodomain of Ptprq and the transmembrane domain but lacks the entire intracellular domain (see figure 5.2).
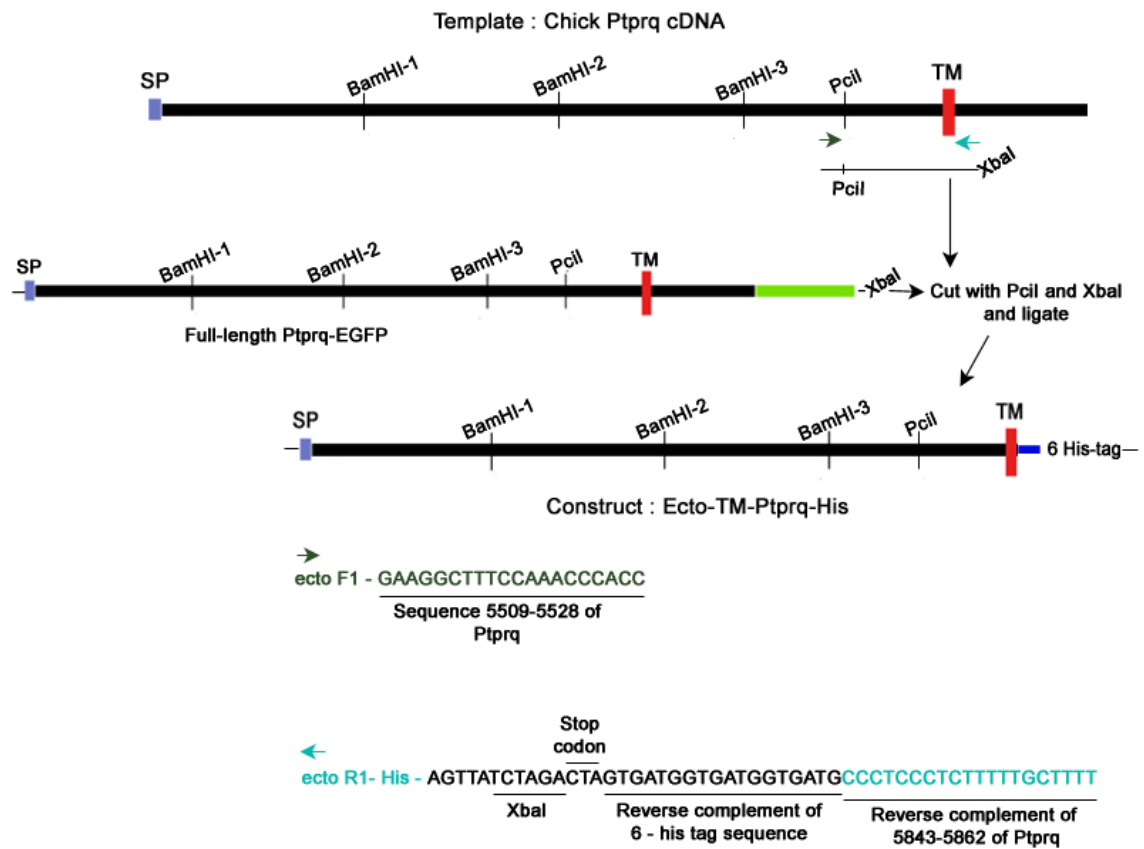
Figure 5.9: Strategy to clone the construct Ecto-TM-Ptprq-His.

Primers ectoF1 and ectoR1-his were used to amplify the region from just before the transmembrane domain encoding sequence to just after the transmembrane domain, with the XbaI site added by the reverse primer (see figure 5.9). The amplified PCR product contains an internal PciI site close to the 5` end. The PCR product was digested with PciI and XbaI restriction enzymes and ligated into the backbone of the full-length

Ptprq-EGFP construct obtained after digestion with the same pair of enzymes. The resulting construct was referred to as Ecto-TM-Ptprq-His.

5.2.3 Cell Culture

The CL4 cell line was a gift from Professor James R. Bartles, Northwestern University Medical School, Chicago, IL.

The CL4 cells were grown in Minimum Essential Medium Alpha Medium with L-glutamine and without ribonucleotides and deoxyribonucleotides (Gibco), containing 10% (v/v) fetal bovine serum (Gibco) and 1% of Penicillin/Streptomycin (Gibco). This medium is referred to as CL4 medium. For transfection studies, CL4 medium without Penicillin/Streptomycin, CL4 (-P/S), was used.

5.2.3.1 Passaging CL4 cells

The cells were grown in regular 75 cm^2 tissue culture flasks and passaged by trypsinization when they reached ~30-50% confluence. Typically, the medium was aspirated and the cells quickly rinsed in ~2 ml of 0.05% trypsin/EDTA, and then trypsinized with 1.8 ml of fresh aliquot of 0.05% trypsin/EDTA for 4 min at 37°C. Then, 8 ml of fresh CL4 medium was added and the bulk of the cells released by pipetting up and down with a 10 ml pipette.

5.2.3.2 Transfection studies

For transfection studies, cells were grown on sterile coverslips (standard no. 1) in 35 mm culture dishes. The cells were plated at a low density and grown for 2 days before transfecting them.

The transfections were done with Lipofectamine (Invitrogen) using the manufacturer's recommended conditions. All incubations were done at room temperature. For one 35-mm dish, 1.5 µg of the desired Ptprq construct was incubated for 15 minutes with 150 µl of CL4 (-P/S) medium in a 1.5 ml tube. In a fresh tube, 6 µl of Lipofectamine was incubated for 15 minutes with 150 µl of CL4 (-P/S) medium. The contents of both these tubes were mixed and incubated in a 2 ml tube for a further 30 minutes. The transfection mix was made up to 1.8 ml with fresh CL4 (-P/S) medium. Before adding the transfection medium, the cells were washed 3 times with CL4 (-P/S) medium. The transfection medium was then added on to the cells. After incubation for 3-4 hours the cells were washed twice with CL4 (-P/S) medium before adding back the complete CL4 medium. The cells were examined the following day (15-24 h later; see section 5.2.5).

5.2.4 Tunicamycin treatment

CL4 cells were grown on coverslips in two 35 mm dishes and transfected with the full-length Ptprq EGFP expression construct. After incubation for 3-5 hours in the transfection medium, the cells were washed thrice with CL4 (-P/S) medium. To one dish, marked control, CL4 medium containing 0.1% DMSO was added. To the other, CL4 medium containing 10 µg/ml tunicamycin (dissolved in DMSO) was added. The cells were incubated for at least 18 hours before processing them for immunofluorescence (see next).

5.2.5 Immunofluorescence

After 15-24 h following transfection, the cells were fixed in 4 % formaldehyde for 30 minutes, blocked and permeabilised with 0.1 % Triton X-100 (see section 2.3). The

cells were then probed with the appropriate antibodies (as indicated in the results) for immunofluorescence.

The rabbit polyclonal serum raised against GFP (anti-GFP; Invitrogen) was used at 1:1000 dilution. Culture supernatant from hybridomas expressing mAb D10 was used at 1:100 dilution. Appropriate Alexa 488 conjugated secondary antibodies (Molecular Probes, Invitrogen) were used to detect primary antibody labelling. Alexa 488 conjugated goat anti-rabbit (Molecular Probes, Invitrogen) was used for anti-GFP labelling, while Alexa 488 conjugated goat-anti mouse (Molecular Probes, Invitrogen) was used to detect mAb D10 labelling. In all cases, rhodamine-conjugated phalloidin (Sigma) was used as a counter-stain (1 in 500 dilution) to label filamentous actin.

5.3 Results

Figure 5.2 shows the different constructs used and the Ptprq domains they are designed to express.

5.3.1 CL4 cells target full-length recombinant Ptprq to the apical surface.

The full-length Ptprq-EGFP construct encodes all the domains of Ptprq including the signal peptide, the ectodomain, the transmembrane domain and the intracellular domain along with a C-terminal EGFP tag (see figure 5.2). On the basis of mAb D10 staining, the full-length form of Ptprq localises to the apical surface and is found in the membrane of the apical microvilli of transfected CL4 cells (see figure 5.10, panels B' and C'). Orthogonal z projections of the confocal images clearly reveal the accumulation of full-length Ptprq-EGFP at the apical surface (see figure 5.10, panels B'' and C''). The preferential sorting of the full-length protein to the apical half of transfected cells suggests that these cells have the cellular machinery necessary for the

apical targeting of Ptprq. The epithelial cell line CL4 thus appears to be suitable for determining the location of the apical targeting signal in Ptprq.

5.3.2 *The intracellular domain of Ptprq distributes in a non-polarized manner in CL4 cells.*

To determine if the intracellular domain of Ptprq on its own can target to the apical surface, the CL4 cells were transfected with the construct Ic-Ptprq-EGFP that encodes the recombinant intracellular domain of Ptprq with a C-terminal EGFP tag (see figure 5.2). Anti-GFP staining is seen throughout the cytoplasm suggesting that the intracellular domain alone is not sufficient for the apical targeting of Ptprq (see figure 5.11, panels B and B'). Interestingly, the recombinant intracellular domain of Ptprq is also found within the apical microvilli of the transfected cells (see figure 5.11). As no plasma membrane staining can be seen with this protein product, the apical microvilli labelling observed may be due to the presence of Ic-Ptprq-EGFP in the microvillar cytoplasm.

5.3.3 *The transmembrane domain of Ptprq does not confer apical targeting*

Next, the construct encoding the transmembrane and intracellular domain of Ptprq, TM-Ic-Ptprq-EGFP (see figure 5.2) was used to determine if the apical targeting signal lies in this region of the protein. When expressed in CL4 cells and visualised using anti-GFP polyclonal serum, the recombinant protein is distributed throughout a membranous system in the cytoplasm (see figure 5.12, panels B and B') but is excluded from the apical microvilli (see panel C', figure 5.12), implying that the transmembrane and intracellular domains are not sufficient for the apical targeting of Ptprq.

5.3.4 *The entire ectodomain is required for the delivery of Ptprq exclusively to the apical surface*

In order to test the ability of the ectodomain of Ptprq to target the recombinant protein to the apical surface of transfected CL4 cells, a construct that encodes the signal peptide, the ectodomain and the transmembrane region with the intracellular domain replaced by a 6-His tag was used (see figure 5.2)**.** mAb D10 staining showed that the membrane-tethered ectodomain of Ptprq is correctly targeted to the apical membrane including that of the microvilli (see figure 5.13a, panel B, B' and B'') revealing that the apical targeting signal resides in the ectodomain of Ptprq. However, the membrane-tethered ectodomain does not always target specifically to the apical surface. In some cells a non-polarised delivery of the protein to the plasma membrane including that of the microvilli as well as a diffuse distribution throughout the cytoplasm can be observed (see figure 5.13b, panels B, B' and B'').

In an attempt to delineate the region of the ectodomain containing the targeting signal two constructs that encode truncated ectodomains of Ptprq were designed (see section 5.2.2 and figure 5.2). The FN8-EGFP construct encodes the first 6 and the last 2 FNIII repeats, while the region from the 7th FNIII repeat to the 17th FN III repeat is encoded by the FN10-EGFP construct. Both these truncated ectodomain constructs also encode the signal peptide, the transmembrane region and the intracellular domain with a C-terminal EGFP tag.

On expression in CL4 cells FN8-EGFP is seen within a membranous system throughout the cytoplasm in a non-polarised fashion (see figure 5.14, panel B'') and is excluded from the plasma membrane and apical microvilli (see figure 5.14, panels C' and C''). The distribution of FN8-EGFP appears similar to that of TM-Ic-Ptprq-EGFP (compare

figures 5.12 and 5.14). The recombinant protein, FN10-EGFP, is also found distributed throughout the cytoplasm (see figure 5.15 panels B and B') and excluded from the plasma membrane and apical microvilli (see figure 5.15, panel C'). Since neither of the truncated ectodomain constructs target efficiently to the apical surface, the apical targeting signal must be distributed throughout the whole ectodomain. However, as the Ecto-TM-Ptprq-His also includes the transmembrane domain, it is possible that the apical targeting signal is localised along the whole ectodomain and transmembrane region.

5.3.5 *N-linked oligosaccharides in the ectodomain encode the apical targeting signal in Ptprq*

Tunicamycin is an analogue of N-acetyl glucosamine and acts as an inhibitor of N-linked glycosylation. N-linked glycosyl moieties are known to serve as apical targeting signals (Rodriguez-Boulan and Gonzalez, 1999; Urquhart et al., 2005). Therefore tunicamycin was used to determine if recombinant full-length Ptprq can be sorted to the apical surface of transfected CL4 cells in the absence of N-glycosyl moieties. CL4 cells transfected with the full-length Ptprq-EGFP construct were either incubated for 18 hours in DMSO or DMSO containing tunicamycin (Sigma Aldrich) at 10 μg/ml (see section 5.2.4). Confocal images of the transfected cells probed with mAb D10 reveal that the protein is efficiently targeted to the apical surface of control cells (see figure 5.16a, panel B, B' and B''), whilst the tunicamycin treated cells are unable to sort the expressed full-length Ptprq-EGFP to their apical surface and microvilli (see figure 5.16b, panel B'' and C').

Thus, N-glycosylation of the ectodomain of Ptprq appears to be at least a major part of the signal that is necessary for the targeting of the protein to the apical surface and microvillar membrane of transfected CL4 cells.

5.4   Discussion

Since Ptprq is expressed specifically at the apical stereociliary and non-stereociliary surface of the hair cell, the current study was aimed at understanding where the intrinsic apical targeting signal is located in Ptprq. To address the question, a series of mammalian expression constructs were designed to express the various domains of Ptprq, either individually or in different combinations (see figure 5.2), in CL4 cells. The cellular distribution of the various recombinant Ptprq products observed in transfected cells is summarised in figure 5.17.

Targeting signals may not be absolute and can be differentially interpreted by various cell types (reviewed in Brown and Breton, 2000). Therefore, the ability of the CL4 cells to apically target the recombinant full-length Ptprq was confirmed in order to ensure the suitability of this cell line for delineating the targeting signal. The results show that only the full-length protein and the product containing the ectodomain fused to the transmembrane domain (Ecto-TM-Ptprq-His) target successfully to the apical surface and microvillar membrane (see figures 5.10 and 5.13a). Apical targeting signals are known to occur in both ectodomains and transmembrane regions of plasma membrane proteins (Kundu et al., 1996; Scheiffele et al., 1997; Vogel et al., 1991; Yeaman et al., 1997). Although TM-Ic-Ptprq-EGFP which contained the transmembrane domain does not target specifically to the apical surface (see see figure 5.12), the apical targeting of Ecto-TM-Ptprq-His suggests that the targeting signal may be distributed along the entire ectodomain and transmembrane region of the protein. In order to delineate the region of

the ectodomain containing the apical targeting signal, two constructs that encode truncated ectodomains of Ptprq fused to the remainder of the protein were used. The results showed that neither the protein product containing the first 6 and the last 2 FNIII repeats (see figure 5.14) nor the product containing the region from the 7th FNIII repeat to the 17th FNIII repeat (see figure 5.15) are delivered specifically to the apical surface. This implies that the apical targeting signal contained in the ectodomain may be distributed along the entire length of the region. N-glycosylation has been shown to be the apical targeting signal for several proteins (Urban et al., 1987; Le Bivic et al., 1993; Scheiffele et al., 1995; Delacour and Jacob, 2006) and Ptprq has 39 potential sites for N-glycosylation (Wright et al., 1998). Apical targeting of Ptprq is lost in tunicamycin treated CL4 cells suggesting that indeed the carbohydrate moieties in the ectodomain of Ptprq encode a major part of the apical sorting signal (see figures 5.16a and b). The N-glycosylation process can result in a gamut of carbohydrate modifications. The apical sorting signal may be made up of a particular combination of the carbohydrate modifications at a few of the sites, or all of the 39 potential sites for N-glycosylation may be involved in the targeting of Ptprq.

Membrane targeting depends not just on intrinsic targeting signals but also on the protein trafficking machinery, intrinsic signalling complexes and the proteins involved in cell-cell and cell-substrate adhesion (Mellman and Nelson, 2008). The components of the sorting and trafficking machinery direct the proteins through distinct transport routes to the apical and basolateral cell surfaces and once the proteins reach the target membrane, selective retention may refine the polarized distribution brought about by targeting (Yeaman et al., 1999; Delacour and Jacob, 2006; Mellman and Nelson, 2008). The PDZ-binding domain in the cystic fibrosis transmembrane conductance regulator (CFTR) has been shown to be responsible for its retention at the apical membrane

although CFTR is delivered to both the apical and basolateral membranes (Swiatecka-Urban et al., 2002). The PDZ protein NHERF is believed to link CFTR to the apical cytoskeleton (Short et al., 1998). Several more PDZ proteins that accumulate preferentially at the apical surface have been reported (Altschuler et al., 2003). In recent years, many receptors and enzymes have been shown to interact with one or more PDZ proteins (Altschuler et al., 2003) supporting the theory that scaffolding proteins can selectively retain proteins destined for a particular membrane domain. In the hair bundle, the PDZ domains of the scaffold proteins, whirlin and harmonin are known to interact with several hair bundle proteins such as Pcdh15, Cdh23, Vlgr1, usherin and MyoVIIa via the PDZ-binding domains in these proteins (Adato et al., 2005a; Reiners et al., 2005a; Siemens et al. 2002; Boëda et al., 2002; Reiners et al., 2005b, van Wijk et al., 2006; Adato et al., 2005b). These interactions mediate the formation of the Usher protein network in the hair cell and defects in the above proteins underlie different forms of Usher syndrome (Kremer et al., 2006). The PDZ domains of whirlin and harmonin may therefore, also serve to retain these hair bundle proteins at the apical end of the hair cell.

Ptprq lacks a PDZ binding domain. However, the presence of an as yet undiscovered membrane-retention signal cannot be ruled out. In support of this, the recombinant intracellular domain of Ptprq was found in the apical microvillar cytoplasm although delivered in a non-polarized fashion when expressed in CL4 cells (see figure 5.11). None of the other recombinant products that were not specifically targeted to the apical surface were found in the apical microvilli. This suggests that the intracellular domain possesses a signal/interaction domain that is hidden or unavailable in the other products. Thus, when expressed on its own, the intracellular domain of Ptprq (Ic-Ptprq-EGFP) may interact with another protein found in the apical microvilli. As a result of this

interaction, Ic-Ptprq-EGFP may be taken by a "piggy back" method and retained in the apical microvillar cytoplasm. The full-length protein may however, require such an interaction domain for efficient apical targeting (see figure 5.10) as the membrane-tethered ectodomain of Ptprq does not always target to the apical surface (see figure 5.13b). This may be due to a lack of the intracellular region and the proposed membrane retention/interaction domain within it.

The selective retention of membrane proteins can also be modulated by altering the endocytosis and/or endocytotic recycling processes (Swiatecka-Urban et al., 2002). Clustering of proteins by interactions with lipids or cytosolic cytoskeletal components can result in either exclusion of the proteins from endocytic vesicles and retention in the membranes, or may signal their inclusion in vesicles and removal from the membrane as in receptor-mediated endocytosis (Mays et al., 1994). Membrane retention signals can also signal the recycling of the endocytosed protein (Swiatecka-Urban et al., 2002). The PDZ-binding domain of CFTR is believed to be responsible for the apical membrane retention of the protein by interaction with PDZ proteins involved in its endocytic recycling (Swiatecka-Urban et al., 2002). In view of this, it is interesting to note that the yeast-two hybrid screen using the intracellular region of Ptprq as bait, suggested EHD3, a protein involved in endocytosis, as a potential interaction partner of Ptprq (Discussed in chapter 4).

Being a broad specificity PIPase, Ptprq has the potential to regulate the PI content of the apical stereociliary and non-stereociliary membrane surface (Goodyear et al., 2003). PIs are a versatile group of membrane lipids implicated in a variety of cellular functions including specifying and maintaining epithelial polarity (section 1.6; Pinal et al., 2006; Comer and Parent, 2007; Martin-Belmonte and Mostov, 2007). As mentioned in section

3.6, the apical localization of the lipid phosphatase, PTEN, is necessary during the early stages of polarization (Martin-Belmonte et al., 2007). PTEN converts PI 3,4,5 P_3 at the apical membrane to PI 4,5 P_2, and the apical PI 4,5 P_2 then recruits several other proteins involved in the organization of the subapical cytoskeleton and formation of the apical surface (Martin-Belmonte et al., 2007).

Ptprq may have a similar function at the apical surface of hair cells. Ptprq expression begins at E13.5 in the mammalian inner ear, coinciding with the onset of hair-cell differentiation (Goodyear et al., 2003). In the avian inner ear, Ptprq positive hair cells appear at a time when hair bundles emerge (Bartolami et al., 1991). Expression of Ptprq at the apical surface from early in the development of hair cells gives it the potential to regulate the formation of the apical surface and the stereociliary bundle in hair cells. However, it is evident from studies in knock-out mice that although Ptprq is necessary for the maintenance of auditory hair cell bundles it is not essential for the initial stages of hair bundle development (Goodyear et al., 2003).

Interestingly, the apical targeting signal in Ptprq is not absolute. The protein is targeted to the basal membrane of podocytes in the human kidney (see above, Seifert et al., 2003). Tyrosine-based and dileucine-based basolateral targeting signals that are known to occur in a variety of proteins (reviewed in Brown and Breton, 2000; Mellman and Nelson, 2008) are also found in the intracellular domain of Ptprq (see figure 5.18).

Figure 5.18: The amino acid sequence of the intracellular domain of chick Ptprq starting with the first amino acid (black arrow) following the transmembrane region. The sequences that fit the consensus for the tyrosine-based and dileucine basolateral targeting motifs are shown in red and blue, respectively.

It is possible that the glycosylation of Ptprq in the glomerular podocytes differs from that occurring in the hair cells of the inner ear. Altered glycosylation may prevent Ptprq from reaching the apical plasma membrane in the glomerular podoctyes. Owing to the potential intrinsic basolateral targeting signals mentioned above, Ptprq may instead be directed to the basal membrane of the podocytes where it is needed. Yet, Ic-Ptprq-EGFP and TM-Ptprq-EGFP do not target to the basolateral surface of transfected CL4 cells. This however, may reflect the inability of CL4 cells to correctly sort many basolateral proteins (Fölsch et al., 1999). It has previously been shown that the exogenous addition of PI 4,5 P_2 at the basolateral surface of MDCK cells or PI 3,4,5 P_3 at the apical surface can result in the relocalization of the plasma membrane proteins from their respective domains to the opposite surface (Martin-Belmonte et al., 2007). With the potential to control the fine local distribution of PIs, it is clear that the mis-targeting of Ptprq to the basolateral domain of hair cells would have deleterious effects on the functioning of the hair cell. Any mutations that affect the type or distribution of the N-linked oligosaccharide moieties might result in the loss of apical targeting of Ptprq and

subsequent loss of stereocilia, leading to hair cell death. Thus, it seems likely that the apical targeting of Ptprq is crucial to the survival of at least the auditory hair cells.

5.5 Conclusions

As with hair cells, the CL4 cells preferentially sort recombinant full-length Ptprq to their apical surface. The current study reveals that the N-glycosylated moieties in the ectodomain of Ptprq are responsible for the apical targeting of the protein in CL4 cells. The N-glycosylated moieties may override the potential basolateral targeting signals in the intracellular domain of Ptprq and direct the protein to the apical ends of hair cells. Ptprq is necessary for the maintenance of hair bundles, and the process of targeting Ptprq to the apical surface of newly formed hair cells is likely to be an essential requirement for the proper functioning of the hair cell.

5.6 Future Perspectives

Although the results of this study suggest the involvement of N-glycans in the apical targeting of Ptprq, one cannot rule out the possibility that the tunicamycin treatment hampers the protein sorting machinery in such a way that the cell cannot target the apical proteins correctly. Therefore, it would be informative to determine if the targeting of other hair bundle proteins like, PMCA2a, occurs in the presence of tunicamycin. Additionally, antibodies to apical junction markers like zona occludens1, can be used to determine whether the tunicamycin-treated CL4 cells maintain their polarisation. Alternatively, the targeting of the protein products of the various Ptprq constructs can be tested in the glycosylation-deficient MDCK cell line, MDCK-RCA[r], as no sorting defects have been reported in these cells (Le Bivic et al., 1993).

CHAPTER 6

Ptprq is a chondroitin sulphate proteoglycan

6.1   Introduction

As mentioned in section 1.8, the dense particles associated with shaft connectors have been suggested to be keratan sulphate GAG moieties (Goodyear et al., 2003). Immunogold labelling reveals that a keratan sulphate antibody specifically labels the interstereociliary links in the cochlear hair bundles of the guinea pig (Katori et al., 1996). It was suggested that the lateral link-associated keratan sulphate GAG chains may participate in maintaining the spacing between adjacent stereocilia and/or the structural integrity of the hair bundle (Katori et al., 1996).

6.1.1 Shaft connectors in auditory and vestibular hair bundles are differentially glycosylated

Previous studies have shown that there are differences in the glycosylation of apical surface components in the vestibular and auditory hair cells of the chick (Goodyear and Richardson, 1994). These differences were revealed using the fluorescently labelled lectins, peanut agglutinin (PNA) and jacalin, both of which recognise the dissacharide Galβ1-3GalNAc (Goodyear and Richardson, 1994). The lectins were found to stain the vestibular hair bundles in a manner similar to that seen with the monoclonal antibody, mAb D10 that recognises an epitope in the ectodomain of Ptprq (Goodyear and Richardson, 1992; 1994; Goodyear et al., 2003). Like mAb D10, both lectins were found to stain the entire length of hair bundles in the extrastriolar regions of the maculae and the peripheral regions of the cristae, whilst only staining the base of the hair

bundles in the striolar regions of the maculae and central regions of the cristae (Goodyear and Richardson, 1994). However, neither lectin showed any staining at the base of the auditory hair bundles, where Ptprq is detected (Goodyear and Richardson, 1994). Immunogold labelling using PNA and mAb D10 matched the staining seen with immunofluorescence in the vestibular system, and the lectin was shown to label the shaft connectors and the apical, non-stereociliary surface in a manner similar to that seen with mAb D10 (Goodyear and Richardson, 1992; 1994). Moreover, it was shown that staining with both PNA and mAb D10 are lost on trypsin treatment, and that PNA blocks the mAb D10 staining, suggesting that PNA recognises a vestibular-specific form of Ptprq (Goodyear and Richardson, 1994).

The aim of the study described below was to determine whether Ptprq is itself a proteoglycan or whether it associates with another proteoglycan to form the shaft connectors.

6.2   Materials and Methods

6.2.1 Antibodies

mAb 473HD was obtained from Santa Cruz and mAb 5240 was obtained from Millipore. mAb 5240 was derived from a mouse immunised with a mixture of chick proteoglycans, and mAb 473HD was obtained from a rat that was immunised with a brain glycoprotein fraction enriched in the L2/HNK-1 epitope (Faissner et al., 1994). Both mAbs are IgM class antibodies and both are reported to recognise phosphacan (PTPζ/RPTPβ). MAb 5240 is reported to recognise the phosphacan core protein and mAb 473HD recognises the dermatan sulphate dependent epitope, DSD-1. mAb H10 is an IgM class mAb obtained from a mouse immunised with a mixture of formaldehyde-

fixed shark inner ear tissue and chick sensory organs (Goodyear and Richardson, unpublished).

6.2.2 *Immunoprecipitations*

Sensory organs were dissected from the inner ears of early posthatch chicks (1-4 days after hatching) in cold PBS containing a cocktail of protease inhibitors (1 mM PMSF, 2 mM benzaminidine, 1 μg/ml leupeptin and 1 μg/ml pepstatin). The tissues were frozen to -80°C soon after dissection. Frozen tissues were thawed in ~1.0 ml TBS containing 1% TX-100 (TBS/TX) and the same cocktail of inhibitors. Tissues were homogenised and centrifuged at 14,000 rpm for 10 minutes in a cold microcentrifuge. The supernatant was collected and 10 μg of affinity purified anti-cytoPtprq was added, followed by 20-50 μl of a 1:1 slurry of protein G-Sepharose that had been preblocked in TBS containing 25 mg/ml bovine serum albumin. After overnight incubation at 4°C, the protein-G Sepharose beads were washed 3 times with TBS/TX, and divided into aliquots. The aliquots were washed once with the appropriate digestion buffer and incubated in buffer alone or buffer containing chondroitinase ABC (1 mg/ml), endo-β-galactosidase (5 U/ml) or heparinase I (1 mg/ml) for 1 hour at 37°C. Beads were washed once with TBS/TX and eluted by heating for 4 minutes at 100°C in 10 μl of 2x concentrated SDS-PAGE sample buffer. Eluted samples were separated on 5% polyacrylamide gels and transferred to PVDF using semi-dry blotting (see section 2.2.3). PVDF membranes were preblocked in 3% low-fat dried milk powder in TBS/0.05% Tween-20, and incubated with anti-cytoPtprq (at 1:100 dilution) overnight at 4°C. Bound antibodies were detected with alkaline phosphatase conjugated goat anti-rabbit (Dako).

6.2.3 Electron microscopy

Utricular maculae were dissected from posthatch day 2 chickens in Hepes buffered (10 mM pH 7.2) Hanks' balanced salt solution (HBHBSS) and the otoconial membranes were gently removed with fine forceps. The maculae were transferred using micropipette tips to fresh HBHBSS (as a control) or HBHBSS containing 1 mg/ml chondroitinase ABC, and incubated at 37°C for 1 hour. Maculae were then washed twice in HBHBSS, fixed in 2.5% glutaraldehyde in 0.1 M sodium cacodylate buffer containing 0.5% ruthenium red for 2 hours, washed 3 times in buffer and postfixed for 1 hour in 1% osmium tetroxide. After a brief wash in buffer, samples were dehydrated through a series of ascending concentrations of ethanol, equilibrated with propylene oxide, infiltrated with and imbedded in Epoxy resin. Resin was polymerised at 60°C for 2 days. Thin sections were cut from the polymerised blocks with a diamond knife, mounted on copper mesh grids, double stained with uranyl acetate and lead citrate and viewed in a Hitachi 7100 microscope operating at 100 kV. Images were captured with a Gatan digital camera.

6.2.4 Cochlear cultures

The preparation of cochlear cultures is described in section 3.2.2. After 1 day *in vitro*, cultures were either fixed immediately, after a brief wash in HBHBSS, or treated with enzymes and fixed for immunofluorescence or electron microscopy as described above.

6.2.5 Immunofluorescence

Samples were fixed in 4% paraformaldehyde for 30 minutes and prepared for immunofluorescence as detailed in section 2.3. Cryosections were prepared and stained as described in section 4.2.3. mAb D10, mAb H10 and mAb 5240 culture supernatants

were used at 1 in 100 dilution. mAb 473HD was used at 1 in 200 dilution. Affinity purified anti-cytoPtprq was used at 1 in 200 dilution. To detect mouse mAb D10, Alexa 488 goat anti-mouse secondary antibody (Molecular Probes, Invitrogen) was used at 1 in 500 dilution. Mouse mAbs H10 and 5240 were detected using fluorescein isothiocyanate (FITC) conjugated goat anti-mouse IgM (Sigma-Aldrich) at 1 in 200 dilution. To detect rat mAb 473HD, FITC conjugated goat anti-rat secondary antibody (Sigma-Aldrich) was used at 1 in 200 dilution. Rabbit polyclonal anti-cytoPtprq was detected using Alexa 555 goat anti-rabbit secondary antibody (Molecular Probes, Invitrogen) which was used at 1 in 500 dilution. Texas Red®-X phalloidin (Molecular Probes, Invitrogen) was used at 1 in 300 dilution, and Alexa 647 conjugated phalloidin (Molecular Probes, Invitrogen) was used at 1 in 100 dilution. Images were taken with a Zeiss LSM 510 Meta confocal microscope.

6.3   Results

6.3.1 *Chondroitinase ABC digestion removes the dense particles that are associated with shaft connectors*

Electron micrographs of posthatch day 1 chick utricles that were incubated for 1 hour in HBHBSS at 37°C and fixed in the presence of ruthenium red reveal the appearance of shaft connectors (see figure 6.1, panel A). As reported previously (Goodyear and Richardson, 1992; Goodyear et al., 2003) shaft connectors are observed as dense particles that are suspended between stereocilia by several fine strands that emerge from the stereociliar membrane (see figure 6.1, panel A). Chondroitinase ABC treatment alters the appearance of the shaft connectors (see figure 6.1, panel B). It removes the interstereociliary dense particles but does not disrupt the distribution of the fine strands that interconnect adjacent stereocilia (see figure 6.1, panel B).

6.3.2 *Chondroitinase ABC treatment causes a shift in the electrophoretic mobility of Ptprq*

Ptprq was immunoprecipitated from lysates of inner ear sensory organs from early posthatch chicks using mAb D10 and the immunoprecipitates were digested with either chondroitinase ABC, endo-β-galactosidase (keratanase) or heparinase I. On electrophoresis and western blotting, a small but distinct shift in the electrophoretic mobility of Ptprq is observed in the samples digested with chondroitinase ABC but not in those treated with either keratanase or heparinase I (see figure 6.2).

6.3.3 *Chondroitinase ABC treatment does not abolish mAb D10 immunoreactivity in chick hair bundles*

Early posthatch chick utricles were incubated in either HBHBSS or HBHBSS containing 1 mg/ml chondroitinase ABC for 1 hour at 37°C to determine whether the ectodomain epitope in Ptprq recognised by mAb D10 is sensitive to chondroitinase ABC treatment.

As shown in figure 6.3, mAb D10 staining in the chondroitinase ABC treated utricles (panel B') was indistinguishable from that seen in the control, HBHBSS-treated samples (panel B).

6.3.4 *A mAb to a chondroitin sulphate epitope stains hair bundles in the mouse cochlea*

mAb 473HD is a rat IgM that recognises the dermatan sulphate-dependent epitope, DSD-1, that is present in the chondroitin sulphate proteoglycan (CSPG), PTPζ/RPTPβ (Garwood et al., 1999; von Holst et al., 2006). Immunostaining of cryosections of P2

mouse cochlea reveals intense staining of the hair bundles with mAb 473HD (see figure 6.4). mAb 473HD staining of hair bundles in wholemount preparations of P2 mice cochleae is shown in figure 6.5. Labelling is seen located between the stereocilia of IHCs and OHCs (see figure 6.5).

Cochleae dissected from P2 wild-type mice were incubated in HBHBSS or HBHBSS containing 1mg/ml chondroitinase ABC for 1 hour at 37°C and then fixed and stained with mAb 473HD. Figure 6.6 shows that hair bundle staining with mAb 473HD is lost after chondroitinase ABC treatment (compare panels B and B').

Cochleae from PTPζ /RPTPβ null-mutant mice were obtained from Prof. Masaharu Noda, Okazaki, Japan, to determine if the staining observed with mAb 473HD was due to the presence of this RPTP. Figure 6.7 shows that mAb 473HD staining is still present in the hair bundles of the PTPζ/RPTPβ null-mutant mice cochleae (panel B').

6.3.5 mAb 473HD stains developing mouse hair bundles in a manner similar to that seen with a Ptprq antibody

Figure 6.8 shows early postnatal mouse cochlear hair bundles double-labelled with mAb 473HD and anti-cytoPtprq. The mAb 473HD staining of cochlear hair bundles broadly co-localises with the anti-cytoPtprq staining (see figure 6.8). At higher magnification, it is evident that the staining seen with the two antibodies does not completely overlap (see figure 6.9, panels C and D) which would be consistent with mAb 473HD and anti-cytoPtprq recognising epitopes in the extracellular and intracellular regions, respectively, of the same molecule.

6.3.6   mAb 473HD immunoreactivity is absent from the cochlear hair bundles of the Ptprq mutant mouse

Cochlear wholemounts prepared from wild-type and homozygous (Ptprq$^{CAT/CAT}$) mice were stained with mAb 473HD. Figure 6.10 shows mAb 473HD staining of the hair bundles in wild-type mice cochlea (panel C) and the absence of immunoreactivity in the Ptprq$^{CAT/CAT}$ cochlear hair bundles (panel G). Hair bundle staining is seen in the cochleae of transgenic animals that are null mutants for other hair bundle proteins; MyoVIIa (panel L), Pcdh15 (panel R) and Vlgr1 (panel V), indicating that the loss of mAb 473HD immunoreactivity is not a consequence of general hair bundle disruption. Thus, the DSD-1 epitope might be present in a GAG moiety of Ptprq. However, it is also possible that a CSPG containing the DSD-1 epitope is associated with the shaft connectors via an interaction with Ptprq. Thus far attempts to either immunoblot or immunoprecipitate Ptprq from either mouse or chick inner ear tissues with mAb 473HD have not succeeded.

6.3.7   Chondroitinase ABC removes the dense particles from the apical surface of immature cochlear hair cells

Cochleae from P2 mice were treated with HBHBSS containing 0.1 mg/ml chondroitinase ABC or HBHBSS as a control for 1 hour at 37°C, and fixed for electron microscopy in the presence of ruthenium red. Figure 6.11, panel B shows that chondroitinase ABC treatment results in a loss of the dense particles that can be seen in the cell coat of the apical surfaces of hair cells in control samples (panel A). The dense cell coat is a transient feature of developing mouse cochlear outer hair cells and its loss from the basal-coil outer hair cells correlates with the loss of Ptprq from the hair bundles of these cells (Goodyear et al., 2003; 2005).

6.3.8 The DSD-1 epitope is transiently expressed in cochlear hair bundles and is lost before Ptprq

Figure 6.12 compares the temporal expression patterns of the DSD-1 epitope and Ptprq in mouse cochlear hair bundles. In cochlear basal coils, expression of the DSD-1 epitope can be seen in the hair bundles of IHCs and OHCs by E18.5, the time at which Ptprq first becomes detectable in these cells (see figure 6.12, panels A and B). In the apical coil, both DSD-1 and Ptprq are strongly expressed by P3 (see figure 6.13, panels A' and B'). The expression of both the DSD-1 epitope and Ptprq peak at around P3 throughout most of the length of the cochlea (see figure 6.12; figure 6.13, panels A' and B' in both). However, while the DSD-1 epitope is no longer detectable in the cochlear hair bundles by P9 (see figure 6.12; figure 6.13, panel A'' in both), Ptprq is expressed into maturity in IHCs and is lost by P21 in all OHCs except those in the apical-most region (Goodyear et al., 2003; panel B'' in figure 6.12 and figure 6.13 shows Ptprq expression in the cochlea at P9). Note that at E18.5, more hair bundles appear to stain with mAb 473HD than with the anti-cytoPtprq polyclonal (see figure 6.12, panels A and B). This suggests that mAb 473HD may be recognising the ectodomain isoforms of Ptprq lacking the intracellular domain (see section 1.5.1 for Ptprq isoforms), which may be the predominant isoform at this age. However, it is also possible that there may be another hair bundle protein carrying the DSD-1 epitope, and either the protein levels or the expression levels of the epitope are low at E18.5 and undetectable by P9 (see figure 6.12 and figure 6.13, panel A'' in both).

Ptprq is also expressed into adulthood in a subset of mouse vestibular hair bundles, which show an uneven expression of the DSD-1 epitope (see figure 6.14). While some

vestibular hair bundles lack mAB 473HD immunoreactivity, others show various degrees of DSD-1 epitope expression (see figure 6.14; panels A and E).

6.3.9   The DSD-1 epitope is also present in the avian inner ear

Basilar papilla and utricle wholemounts from chicks at various stages of development were stained with mAb 473HD to determine the temporal expression pattern of the DSD-1 epitope and compare it with the known expression pattern of Ptprq. Figure 6.15 shows that the DSD-1 epitope is detected in the hair bundles at the distal end of the basilar papilla by E7 (panel A'), the time at which Ptprq first becomes detectable (E6.5) using mAb D10 (Bartolami et al., 1991; Goodyear and Richardson, 1997). Nearly all hair bundles are DSD-1 positive at the distal end by E8 (see figure 6.15, panel C'). Several DSD-1 positive hair bundles can also be seen at the proximal end at this stage (see figure 6.15, panel C). DSD-1 labelling of hair bundles in the proximal end peaks at E10 (see figure 6.15, panel E). By E14, the expression of the DSD-1 epitope diminishes (see figure 6.15, panels G and G') and becomes nearly undetectable by E17 (panels I and I'). The DSD-1 epitope is not detected in wholemounts of posthatch day 2 basilar papilla (see figure 6.16, panel B).

In the chick utricle, DSD-1 expression is visible at E7 (see figure 6.17; panel A') and peaks at E10 (panel E'). The expression of the DSD-1 epitope appears to be more prominent in the extrastriolar than the striolar hair bundles (see figure 6.17). By E14, the expression of the DSD-1 epitope diminishes (panel G and G'). At E17 (panels I and I'), a few hair bundles in the striolar and extrastriolar regions are still DSD-1 positive and wholemounts of the early posthatch chick utricles show varying degrees of DSD-1 epitope expression that is mostly confined to the extrastriolar hair cell bundles (see figure 6.18, panels B and B').

6.3.10 A mAb that immunoblots Ptprq stains extrastriolar but not striolar or basilar papillar hair bundles

mAb H10 is a mouse IgM that reacts with numerous protein bands on western blots and stains many structures in the avian inner ear, including hair bundles (Richardson G.P., unpublished observation). The hair bundle staining observed with mAb H10 appears similar to that observed with the Ptprq mAb D10 (see figure 6.19). However, in contrast to mAb D10, mAb H10 only stains extrastriolar hair bundles (see figure 6.19). mAb H10 does not stain hair bundles in the striolar region of the utricle, basilar papillar hair bundles or the immature hair bundles scattered throughout the utricle (see figure 6.19). Unlike mAb D10, mAb H10 also stains the apical surfaces of the supporting cells in both the basilar papilla (see figure 6.19, panel B) and the striolar region of the utricle (panel E), but not those in the extrastriolar region of the utricular macula (panel H). Hair bundle staining with mAb H10 is unaffected by chondroitinase ABC treatment (see figure 6.20).

Ptprq is recognised by mAb H10 and the immunoreactivity of Ptprq with mAb H10 on immunoblots is retained following chondroitinase ABC digestion (see figure 6.21).

mAb 5240 is a mouse IgM that is reported to recognise an epitope in the protein core of PTPζ/ RPTPβ (Millipore technical bulletin for mAb 5240) . It stains hair bundles in the avian inner ear (see figure 6.22) in a manner similar to that observed with mAb H10 (see figure 6.19). Hair bundles in the extrastriolar regions of the utricular macula are stained by mAb 5240 whereas striolar, basilar papillar and immature hair bundles are not stained by this mAb (see figure 6.22). This mAb stains the tectorial membrane strongly and the staining seen at the tips of hair bundles in the basilar papilla (see figure 6.22, panels B and C) probably represent remains of the tectorial membrane in these

regions. mAb 5240 also stains the apical surface of supporting cells in the basilar papilla (panel B) and the striolar region of the maculae (panel E) but not in the extrastriolar regions of the utricle (panel H). Also, as observed with mAb H10, mAb 5240 immunoreactivity is not lost following chondroitinase ABC treatment (see figure 6.23, panel B'). Unlike mAb H10, however, mAb 5240 does not react with immunoprecipitated Ptprq on western blots (not shown).

6.3.11 The structure of the shaft connectors in extrastriolar and striolar hair bundles is different

Striolar hair bundles have stereocilia that are fatter and more widely spaced than those in the extrastriolar regions (see figure 6.24, panel A), and they have shaft connectors that are restricted to the basal regions of the stereocilia (Goodyear and Richardson, 1992; Goodyear et al., 2003). The narrower and more tightly-packed stereocilia of the extrastriolar hair bundles (see figure 6.24, panel B) have shaft connectors distributed along most/all of their length (Goodyear and Richardson, 1992; Goodyear et al., 2003).

Comparison of the ultrastructure of shaft connectors in the hair bundles from the striolar and extrastriolar regions of the chick utricle (see figure 6.24, panels A and B) reveals a correlation with the absence and presence respectively, of the Ptprq isoform that reacts with mAb H10 (see figure 6.19, panels E and H). Shaft connectors in the basal regions of the striolar hair bundles are usually long with distinct densities (see figure 6.24, panel A). Although the shaft connectors in the extrastriolar hair bundles also have associated dense particles (see figure 6.24; panel B), the length of the connectors is distinctly shorter than those in the striolar regions (see figure 6.24, compare double arrows in panels A and B).

6.4 Discussion

The dense particles associated with shaft connectors have been suggested to be formed either by the ectodomains of several Ptprq molecules interacting in *cis* (originating from the same stereocilium) and/or in *trans* (originating from adjacent stereocilia), or by an unknown ligand interacting with and bridging the ectodomains of several Ptprq molecules (Goodyear et al., 2003). It has also been suggested that the dense particles, which are only observed in samples fixed in the presence of ruthenium red, may result from the collapse of associated keratan sulphate GAG chains (Goodyear et al., 2003).

Three lines of evidence indicate that Ptprq is a CSPG. One, chondroitinase ABC treatment but not treatment with keratanase or heparinase I, results in a modest increase in the electrophoretic mobility of Ptprq on polyacrylamide gels. Two, chondroitinase ABC treatment eliminates the dense particles that are associated with both shaft connectors of chick hair bundles and the dense cell coat that is a transient feature of the apical surface and hair bundles of early postnatal mouse cochlear hair cells. This latter feature has been suggested to be formed from the ectodomains of Ptprq (Goodyear et al., 2005). Hair-bundle staining observed in chick utricles with mAb D10 is not abolished by chondroitinase ABC treatment suggesting that the removal of the dense particles from the shaft connectors is not due to contaminating proteolytic activity. Third, the chondroitin sulphate epitope DSD-1, is associated with early postnatal mouse hair bundles and its appearance and distribution in these hair bundles is strikingly similar to that of Ptprq. Moreover, mAb 473HD stains hair bundles in the PTPζ/RPTPβ mutant mouse but not those in the Ptprq mutant mouse. Therefore the labelling cannot be due to the presence of PTPζ/RPTPβ in the hair bundle and suggests that the DSD-1 epitope may be associated with Ptprq. The loss of mAb 473HD

immunoreactivity in the cochlear hair bundles of the Ptprq mutant mouse is unlikely to be a consequence of general hair bundle disruption as this mAb stains hair bundles in the cochleae of MyoVIIa, Pcdh15 and the Vlgr1 null-mutant mice.

Ptprq is expressed into maturity in all hair bundles of the chick and mouse inner ear, except those of OHCs in the basal region of the mouse cochlea. The DSD-1 epitope on the other hand, is only transiently expressed in the developing mouse cochlea and the developing avian basilar papilla. In older mice and the post hatch bird, the DSD-1 epitope is expressed only in a subset of vestibular hair bundles. These results suggest that there is likely to be a developmentally-regulated isoform of Ptprq that contains the DSD-1 glycosaminoglycan epitope. One cannot however, fully rule out the possibility that there is another DSD-1 epitope-containing protein in the hair bundle that is associated with Ptprq.

Several lines of evidence suggest also that there may be glycosylation variants of Ptprq that are distributed in an organ- and region-specific manner in the inner ear. First, reverse transcription PCR studies using total RNA prepared from early postnatal mouse inner ear tissues have revealed that several extracellular domain splice variants of Ptprq are expressed (Dr. Kevin Legan, unpublished observations). At least one of these splice variants is predicted to have an altered glycosylation status relative to full length Ptprq (Dr. Kevin Legan, unpublished observation; see figure 6.25). Second, two mAbs H10 and 5240 only stain hair bundles in the extrastriolar regions of the utricle and not those in the striolar regions or in the basilar papilla in the chick. Third, mAb H10 reacts with Ptprq on immunoblots. Fourth, both mAbs stain several structures in the inner ear in addition to hair bundles and mAb H10 recognises multiple bands in blot of inner ear lysates, suggesting that these mAbs most probably recognise glycosylation epitopes that

are common to many inner ear proteins. Thus, mAbs H10 and 5240 may recognise glycosylation dependent epitopes in the full-length isoform of Ptprq that are common to several inner ear proteins. As hair bundle staining with mAbs H10 and 5240 is only seen in extrastriolar regions of the maculae in the chick and not in the striolar regions or the basilar papilla, Ptprq isoforms bearing the epitopes for these mAbs may be differentially distributed between the inner ear organs and also between the different regions of the same organ. As chondroitinase ABC treatment does not remove the staining observed with either of the two mAbs, the epitopes are not likely to be chondroitin sulphate-dependent.

In addition to the hair bundles of striolar and extrastriolar hair cells exhibiting differential immunoreactivity to the two mAbs, the length of their shaft connectors also varies. The Ptprq isoform that reacts with mAb H10 is associated with the shorter connectors that are found between the narrowly spaced stereocilia of the extrastriolar bundles. On the other hand, the Ptprq isoform that lacks the mAb H10 epitope is associated with the longer connectors with distinct densities that are seen between the stereocilia of the striolar hair bundles. A role for negatively charged glycocalyces in preventing fusion of adjacent stereociliary membranes by repulsion and thereby maintaining the hair bundle structure has been suggested previously (Dolgobrodov et al., 2000). Variation in the glycosylation status of Ptprq ectodomain splice variants may therefore be responsible for the differential appearance of the shaft connectors (see figure 6.26). In this respect, it is important to recall that the absence of Ptprq in the Ptprq$^{CAT/CAT}$ mice leads to stereociliary fusion seen in the IHCs (Goodyear et al., 2003). The splice variant from which exons 21 and 22 are deleted will lack the 11th and 12th FNIII repeats and will lack any GAG chains that may be attached to any of the Ser and Thr residues in this region (see figure 6.25). The position of the GAG chains in the final

Ptprq product could potentially dictate the spacing between the respective stereocilia (see figure 6.26). Alternatively spliced isoforms of Ptprq with differing glycosylation status may also occur in the avian inner ear. The extrastriolar hair bundles may largely contain a Ptprq isoform that reacts with mAbs H10 and 5240 and has GAG chains closer to the stereociliar membrane. The repulsive forces would act at shorter distances between adjacent stereocilia, resulting in shorter connectors and closely spaced stereocilia in extrastriolar bundles, as shown in figure 6.26. On the other hand, striolar hair bundles may express another glycosylation variant of Ptprq that provides a wider spacing between stereocilia due to the repulsion between GAG chains located at the ends of opposing Ptprq molecules (see figure 6.26).

Lastly, based on the identical hair bundle staining patterns seen with mAbs 5240 and H10, it appears that mAb 5240 may also recognise an epitope in Ptprq. However, as mAb 5240 does not react with immunoprecipitated Ptprq on Western blots (not shown), it may recognise an epitope that is sensitive to denaturation by SDS. Thus, it appears that Ptprq may have at least two epitopes in common with PTPζ/RPTPβ, the DSD-1 epitope recognised by mAb 473HD and that recognised by mAb 5240. The DSD-1 epitope was first recognised as an epitope associated with the extracellular isoform of PTPζ/RPTPβ (phosphacan) and is composed of hexa- or larger oligosaccharides which contain the chondroitin sulphate A- and D-units (Clement et al., 1998; Ito et al., 2005). The DSD-1 epitope is known to overlap the neuritogenic region of the protein, as mAb 473HD strongly inhibits the neurite-outgrowth promoting ability of phosphacan (Clement et al., 1998; Ito et al., 2005). However, the process by which the DSD-1 epitope promotes neurite outgrowth is not known. It has been suggested that the epitope might function by eliciting a second-messenger response and that a balance between the concentration of the DSD-1 epitope and other inhibitory molecules or motifs might

define the final response elicited (Clement et al., 1998). The DSD-1 epitope is expressed early during hair bundle development in the avian and mouse inner ear. Therefore, it is possible that the DSD-1 epitope might regulate the development of the hair bundle in a similar way to that suggested for its neurite outgrowth promoting activity (Clement et al., 1998).

6.5   Conclusions

The current study reveals that Ptprq is a chondroitin sulphate proteoglycan, and that there is most likely a developmentally regulated isoform that shares an epitope, DSD-1, in common with PTPζ/RPTPβ. The chondroitin sulphate GAG chains in Ptprq may occupy space between stereocilia and prevent the fusion of adjacent stereociliar membranes by the electrostatic repulsive forces generated between GAG chains of opposing molecules. A model has been suggested to explain the observed variation in the shaft connector morphology. The position of the GAG chains in the Ptprq ectodomain may depend on which extracellular splice variant is expressed and this may determine the spacing between the stereocilia.

6.6   Future Perspectives

In order to test the model suggested to explain the function of GAG chains in preventing stereociliary fusion, it will be interesting to determine if stereociliary fusion can be seen in chondroitinase ABC treated cultures that have been maintained for various periods of time. As the mAb H10 and mAb 5240 epitopes are not chondroitinase sensitive, it will be informative to determine if they are removed by either N- or O-glycosidase treatment. As in the mouse, total RNA from chick inner ear tissues should be used to determine which Ptprq splice variants are expressed. Antibodies to specific peptides

from the 11th and 12th FNIII repeats of mouse Ptprq would be useful to determine if the full-length isoform and an alternatively spliced variant lacking these FNIII repeats are differentially expressed in the mouse inner ear. HEK293 cells transiently transfected with full-length Ptprq could be stained with mAbs 473HD, H10 and 5240 to see if recombinant Ptprq contains the epitopes for these mAbs.

CONCLUSIONS

Previous studies have shown that Ptprq is required for the maturation and maintenance of sensory hair bundles. Although the precise role played by Ptprq in maintaining hair bundles remains unclear, the current study has provided further information on the potential function and structure of this hair bundle protein. The major findings of this thesis are summarised below:

- The absence of Ptprq does not affect the distribution of many of the PIs that are abundant in the hair bundle. Its effects may therefore be subtle.

- EHD3, a protein of the endocytotic pathway interacts with the intracellular domain of Ptprq *in vitro* suggesting Ptprq is either actively recycled or regulates apical endocytosis in hair cells.

- The targeting of Ptprq to the apical membrane of sensory hair cells is directed by carbohydrate moieties that are distributed throughout the ectodomain. Similar posttranslational modifications may direct apical targeting of other hair bundle membrane proteins.

- Ptprq is a chondroitin sulphate proteoglycan and there are likely to be isoforms that are substituted with the DSD-1 epitope expressed during the early stages of hair bundle maturation. There is also evidence for the presence of additional glycosylation variants of Ptprq that are expressed in an organ- and region-specific manner in the inner ear. Such carbohydrate modifications may regulate the spacing between stereocilia.

Future work needs to be directed towards testing the hypotheses herewith put forth.

REFERENCES

1. Adato, A., Michel, V., Kikkawa, Y., Reiners, J., Alagramam, K. N., Weil, D., Yonekawa, H., Wolfrum, U., El-Amraoui, A. and Petit, C. (2005a). Interactions in the network of Usher syndrome type 1 proteins. Hum Mol Genet. *14*, 347-356.

2. Adato, A., Lefevre, G., Delprat, B., Michel, V., Michalski, N., Chardenoux, S., Weil, D., El-Amraoui, A. and Petit, C. (2005b). Usherin, the defective protein in Usher syndrome type IIA, is likely to be a component of interstereocilia ankle links in the inner ear sensory cells. Hum. Mol. Genet., *14*, 3921–3932

3. Ahmed, Z. M., Riazuddin, S., Ahmad, J., Bernstein, S. L., Guo, Y., Sabar, M. F., Sieving, P., Griffith, A. J., Friedman, T. B., Belyantseva, I. A. and Wilcox, E. R. (2003). PCDH15 is expressed in the neurosensory epithelium of the eye and ear and mutant alleles are responsible for both USH1F and DFNB23. Hum Mol Genet. *12*, 3215-3223.

4. Ahmed, Z. M., Goodyear, R., Riazuddin, S., Lagziel, A., Legan, P. K., Behra, M., Burgess, S. M., Lilley, K. S., Wilcox, E. R., Griffith, A. J., Frolenkov, G. I., Belyantseva, I. A., Richardson, G. P. and Friedman, T. B. (2006). The tip-link antigen, a protein associated with the transduction complex of sensory hair cells, is protocadherin-15. J Neurosci. *26*, 7022-7034.

5. Alagramam, K. N., Murcia, C. L., Kwon, H. Y., Pawlowski, K. S., Wright, C. G. and Woychik, R. P. (2001a). The mouse Ames waltzer hearing-loss mutant is caused by mutation of Pcdh15, a novel protocadherin gene. Nat Genet. *27*, 99-102.

6. Alagramam, K. N., Yuan, H., Kuehn, M. H., Murcia, C. L., Wayne, S., Srisailpathy, C. R., Lowry, R. B., Knaus, R., Van Laer, L., Bernier, F. P., Schwartz, S., Lee, C., Morton, C. C., Mullins, R. F., Ramesh, A., Van Camp, G., Hageman, G. S., Woychik, R. P. and Smith, R. J. (2001b). Mutations in the

novel protocadherin PCDH15 cause Usher syndrome type 1F. Hum Mol Genet. *10*, 1709-1718.

7. Altschuler, Y., Hodson, C. and Milgram, S.L. (2003). The apical compartment: trafficking pathways, regulators and scaffolding proteins. Curr Opin Cell Biol. *15,* 423-429.

8. Anniko, M. (1983a). Postnatal maturation of cochlear sensory hairs in the mouse. Anat Embryol. *166*, 355-368.

9. Anniko, M. (1983b). Cytodifferentiation of cochlear hair cells. Am J Otolaryngol. *4*, 375-388.

10. Aronheim, A., Zandi, E., Hennemann, H., Elledge, S.J. and Karin, M. (1997). Isolation of an AP-1 repressor by a novel method for detecting protein-protein interactions. Mol Cell Biol. *17*, 3094-3102.

11. Balla, T., Bondeva, T. and Várnai, P. (2000). How accurately can we image inositol lipids in living cells? Trends Pharmacol Sci. *21*, 238-241.

12. Balla, A., Tuymetova, G., Tsiomenko, A., Várnai, P. and Balla, T. (2005). A plasma membrane pool of phosphatidylinositol 4-phosphate is generated by phosphatidylinositol 4-kinase type-III alpha: studies with the PH domains of the oxysterol binding protein and FAPP1. Mol. Biol. Cell. *16*, 1282-1295.

13. Balla, T. (2005). Inositol-lipid binding motifs: signal integrators through protein-lipid and protein-protein interactions. J Cell Sci. *118*, 2093-2104.

14. Bartolami, S., Goodyear, R. and Richardson, G. (1991). Appearance and distribution of the 275 kD hair-cell antigen during development of the avian inner ear. J Comp Neurol. *314,* 777-788.

15. Belyantseva, I.A., Boger, E.T., Naz, S., Frolenkov, G.I., Sellers, J.R., Ahmed, Z.M., Griffith, A.J. and Friedman, T.B. (2005). Myosin-XVa is required for tip localization of whirlin and differential elongation of hair-cell stereocilia. Nat Cell Biol. *7*, 148-156.

16. Benting, J.H., Rietveld, A.G. and Simons, K. (1999). N-Glycans mediate the apical sorting of a GPI-anchored, raft-associated protein in Madin-Darby canine kidney cells. J Cell Biol. *146*, 313-320.

17. Blume, J. J., Halbach, A., Behrendt, D., Paulsson, M., and Plomann, M. (2007). EHD proteins are associated with tubular and vesicular compartments and interact with specific phospholipids. Exp Cell Res. *313*, 219-231.

18. Boëda, B., El-Amraoui, A., Bahloul, A., Goodyear, R., Daviet, L., Blanchard, S., Perfettini, I., Fath, K. R., Shorte, S., Reiners, J., Houdusse, A., Legrain, P., Wolfrum, U., Richardson, G., Petit, C.l. (2002). Myosin VIIa, harmonin and cadherin 23, three Usher I gene products that cooperate to shape the sensory hair cell bundle. Embo J. *21*, 6689-6699.

19. Brône, B. and Eggermont, J. (2005). PDZ proteins retain and regulate membrane transporters in polarized epithelial cell membranes. Am J Physiol Cell Physiol. *288*, C20-29.

20. Brown, D. and Breton, S. (2000). Sorting proteins to their target membranes. Kidney Int. *57*, 816-824.

21. Carlton, J.G. and Cullen, P.J. (2005). Coincidence detection in phosphoinositide signaling. Trends in Cell Biology. *15*, 540-547.

22. Casanova, J.E., Apodaca, G. and Mostov, K.E. (1991). An autonomous signal for basolateral sorting in the cytoplasmic domain of the polymeric immunoglobulin receptor. Cell. *66*, 65-75.

23. Cheung, P.C., Trinkle-Mulcahy, L., Cohen, P. and Lucocq, J.M. (2001). Characterization of a novel phosphatidylinositol 3-phosphate-binding protein containing two FYVE fingers in tandem that is targeted to the Golgi. Biochem J.*355*, 113-121.

24. Chmelar, R.S and Nathanson, N.M. (2006). Identification of a novel apical sorting motif and mechanism of targeting of the M2 muscarinic acetylcholine receptor. J Biol Chem. *281*, 35381-35396.

25. Clement, A.M., Nadanaka, S., Masayama, K., Mandl, C., Sugahara, K. and Faissner, A. (1998). The DSD-1 carbohydrate epitope depends on sulfation, correlates with chondroitin sulfate D motifs, and is sufficient to promote neurite outgrowth. J Biol Chem. *273*, 28444-28453.

26. Comer, F.I. and Parent, C.A. (2007). Phosphoinositides specify polarity during epithelial organ development. Cell. *128*, 239-240.

27. Confalonieri, S., and Di Fiore, P. P. (2002). The Eps15 homology (EH) domain. FEBS Lett *513*, 24-29.

28. Conner, S.D. and Schmid, S.L. (2003). Regulated portals of entry into the cell. Nature. *422*, 37-44.

29. Cotanche, D.A. and Sulik, K.K. (1983). Early differentiation of hair cells in the embryonic chick basilar papilla. A preliminary report. Arch Otorhinolaryngol. *237*, 191-195.

30. Cotanche, D.A. and Sulik, K.K. (1984). The development of stereociliary bundles in the cochlear duct of chick embryos. Brain Res. *318*, 181-193.

31. D'Angelo, G., Vicinanza, M., Di Campli, A. and De Matteis, M.A. (2008). The multiple roles of PtdIns(4) P– not just the precursor of PtdIns(4,5) P_2. J Cell Sci.*121*, 1955-1963.

32. Daumke, O., Lundmark, R., Vallis, Y., Martens, S., Butler, P. J., and McMahon, H. T. (2007). Architectural and mechanistic insights into an EHD ATPase involved in membrane remodelling. Nature. *449*, 923-927.

33. de Renzis, S., Sönnichsen, B. and Zerial, M. (2002). Divalent Rab effectors regulate the sub-compartmental organization and sorting of early endosomes. Nat Cell Biol. *4*, 124-133.

34. Delacour, D. and Jacob, R. (2006). Apical protein transport. Cell Mol Life Sci. *63,* 2491-2505.

35. Delacour, D., Cramm-Behrens, C.I., Drobecq. H., Le Bivic, A., Naim, H.Y. and Jacob, R. (2006). Requirement for galectin-3 in apical protein sorting. Curr Biol. *16*, 408-414.

36. Delprat, B., Michel, V., Goodyear, R., Yamasaki, Y., Michalski, N., El-Amraoui, A., Perfettini, I., Legrain, P., Richardson, G., Hardelin, J.P. and Petit, C. (2005). Myosin XVa and whirlin, two deafness gene products required for hair bundle growth, are located at the stereocilia tips and interact directly. Hum Mol Genet. *14*, 401-410.

37. Denman-Johnson, K, and Forge, A. (1999). Establishment of hair bundle polarity and orientation in the developing vestibular system of the mouse. J Neurocytol. *28*, 821-835.

38. Di Palma, F., Holme, R.H., Bryda, E.C., Belyantseva, I.A., Pellegrino, R., Kachar, B., Steel, K.P. and Noben-Trauth, K. (2001). Mutations in Cdh23, encoding a new type of cadherin, cause stereocilia disorganization in waltzer, the mouse model for Usher syndrome type 1D. Nat Genet. *27*, 103-107.

39. Dolgobrodov, S.G., Lukashkin, A.N. and Russell, I.J. (2000). Electrostatic interaction between stereocilia: I. Its role in supporting the structure of the hair bundle. Hear Res. *150*, 83-93.

40. Dowler, S., Currie, R.A., Campbell, D.G., Deak, M., Kular, G., Downes, C.P. and Alessi, D.R. (2000). Identification of pleckstrin-homology-domain-containing proteins with novel phosphoinositide-binding specificities Biochem J. *351*, 19-31.

41. Downes, C.P., Gray, A. and Lucocq, J.M. (2005). Probing phosphoinositide functions in signaling and membrane trafficking. Trends Cell Biol. *15*, 259-268.

42. Dumont, R.A., Lins, U., Filoteo, A.G., Penniston, J.T., Kachar, B. and Gillespie, P.G. (2001). Plasma membrane Ca2+-ATPase isoform 2a is the PMCA of hair bundles. J Neurosci. *21*, 5066-5078.

43. Dunbar, L.A., Aronson, P. and Caplan, M.J. (2000). A transmembrane segment determines the steady-state localisation of an ion-transporting adenosine triphosphatase. J Cell Biol. *148*, 769-778.

44. Ellis, M.A., Potter, B.A., Cresawn, K.O., Weisz, O.A.(2006). Polarized biosynthetic traffic in renal epithelial cells: sorting, sorting, everywhere. Am J Physiol Renal Physiol. *291*, F707-713.

45. Eudy, J.D., Yao, S., Weston, M.D., Ma-Edmonds, M., Talmadge, C.B., Cheng, J.J., Kimberling, W.J., Sumegi, J., 1998. Isolation of a gene encoding a novel member of the nuclear receptor superfamily from the critical region of Usher syndrome type IIa at 1q41. Genomics. *50*, 382-384.

46. Faissner, A., Clement, A., Lochter, A., Streit, A., Mandl, C. and Schachner, M. (1994). Isolation of a neural chondroitin sulfate proteoglycan with neurite outgrowth promoting properties. J Cell Biol. *126*, 783-799.

47. Fettiplace, R. and Hackney, C.M. (2006). The sensory and motor roles of auditory hair cells. Nat Rev Neurosci. *7*, 19-29.

48. Fields, S. and Song, O. (1989). A novel genetic system to detect protein-protein interactions. Nature. *340*, 245-246.

49. Fölsch, H., Ohno, H., Bonifacino, J.S. and Mellman, I. (1999). A novel clathrin adaptor complex mediates basolateral targeting in polarized epithelial cells. Cell. *99*, 189-198.

50. Fölsch, H. (2008). Regulation of membrane trafficking in polarized epithelial cells. Curr. Opin. Cell Biol. *20*, 208-213.

51. Forge, A. and Richardson, G.P. (1993). Freeze fracture analysis of apical membranes in cochlear cultures: differences between basal and apical coil outer hair cells and effects of neomycin. J Neurocyt. *22*, 854-867.

52. Frolenkov, G.I., Belyantseva, I.A., Friedman, T.B. and Griffith, A.J. (2004). Nat Rev Genet. *5*, 489-498.

53. Furness, D.N. and Hackney, C.M. (1985). Cross-links between stereocilia in the guinea pig cochlea. Hear Res. *18*, 177-188.

54. Galperin, E., Benjamin, S., Rapaport, D., Rotem-Yehudar, R., Tolchinsky, S., and Horowitz, M. (2002). EHD3: a protein that resides in recycling tubular and vesicular membrane structures and interacts with EHD1. Traffic. *3*, 575-589.

55. Garwood, J., Schnädelbach, O., Clement, A., Schütte, K., Bach, A. and Faissner, A. (1999). DSD-1-proteoglycan is the mouse homolog of phosphacan and displays opposing effects on neurite outgrowth dependent on neuronal lineage. J Neurosci. *19*, 3888-3899.

56. Gassama-Diagne, A., Yu, W., ter Beest, M., Martin-Belmonte, F., Kierbel, A., Engel, J., and Mostov, K. (2006). Phosphatidylinositol-3, 4, 5-trisphosphate regulates the formation of the basolateral plasma membrane in epithelial cells. Nat. Cell Biol. *8*, 963–970.

57. George, M., Ying, G., Rainey, M. A., Solomon, A., Parikh, P. T., Gao, Q., Band, V., and Band, H. (2007). Shared as well as distinct roles of EHD proteins revealed by biochemical and functional comparisons in mammalian cells and C. elegans. BMC Cell Biol. *8*, 3.

58. Gillooly, D.J., Simonsen, A., Stenmark, H. (2001). Cellular functions of phosphatidylinositol 3-phosphate and FYVE domain proteins. Biochem J. *355*, 249-258.

59. Godi, A., Di Campli, A., Konstantakopoulos, A., Di Tullio, G., Alessi, D. R., Kular, G. S., Daniele, T., Marra, P., Lucocq, J. M. and De Matteis, M. A. (2004). FAPPs control Golgi-to-cell-surface membrane traffic by binding to ARF and PtdIns(4)P. Nat. Cell Biol. *6*, 393-404.

60. Goodyear, R. and Richardson, G. (1992). Distribution of the 275 kD hair cell antigen and cell surface specialisations on auditory and vestibular hair bundles in the chicken inner ear. J Comp Neurol. *325*, 243-256.

61. Goodyear, R. and Richardson, G. (1994). Differential glycosylation of auditory and vestibular hair bundle proteins revealed by peanut agglutinin. J Comp Neurol. *345*, 267-278.

62. Goodyear, R. and Richardson, G. (1997). Pattern formation in the basilar papilla: evidence for cell rearrangement. J Neurosci. *17*, 6289-62301.

63. Goodyear, R. and Richardson, G. (1999). The ankle-link antigen: an epitope sensitive to calcium chelation associated with the hair-cell surface and the calycal processes of photoreceptors. J Neurosci.*19*, 3761-3772.

64. Goodyear, R. J., Legan, P. K., Wright, M. B., Marcotti, W., Oganesian, A., Coats, S. A., Booth, C. J., Kros, C. J., Seifert, R. A., Bowen-Pope, D. F., and Richardson, G. P. (2003). A receptor-like inositol lipid phosphatase is required for the maturation of developing cochlear hair bundles. J Neurosci. *23*, 9208-9219.

65. Goodyear, R. J., Marcotti, W., Kros, C. J., and Richardson, G. P. (2005). Development and properties of stereociliary link types in hair cells of the mouse cochlea. J Comp Neurol. *485*, 75-85.

66. Grant, B. D., and Caplan, S. (2008). Mechanisms of EHD/RME-1 protein function in endocytic transport. Traffic. *9*, 2043-2052.

67. Grati, M., Schneider, M.E., Lipkow, K., Strehler, E.E., Wenthold, R.J. and Kachar, B. (2006). Rapid turnover of stereocilia membrane proteins: evidence from the trafficking and mobility of plasma membrane Ca(2+)-ATPase 2. J Neurosci. *26*, 6386-6395.

68. Gray, A., Van Der Kaay, J. and Downes CP. (1999). The pleckstrin homology domains of protein kinase B and GRP1 (general receptor for phosphoinositides-1) are sensitive and selective probes for the cellular detection of phosphatidylinositol 3,4-bisphosphate and/or phosphatidylinositol 3,4,5-trisphosphate in vivo. Biochem J. *344*, 929-936.

69. Griesinger, G.B., Richards, C.D. and Ashmore, J.F. (2002). FM1-43 Reveals Membrane Recycling in Adult Inner Hair Cells of the Mammalian Cochlea. J. Neur. *22*, 3939-3952.

70. Griesinger, G.B., Richards, C.D. and Ashmore, J.F. (2004). Apical endocytosis in outer hair cells of the mammalian cochlea. Eur.J.Neur. *20*, 41-50.

71. Grosshans, B.L., Ortiz, D. and Novick, P. (2006). Rabs and their effectors: achieving specificity in membrane traffic. Proc Natl Acad Sci U S A. *103*, 11821-11827.

72. Gut, A., Kappeler, F., Hyka, N., Balda, M.S., Hauri, H.P. and Matter, K. (1998). Carbohydrate-mediated Golgi to cell surface transport and apical targeting of membrane proteins. EMBO J. *17*, 1919-1929.

73. Hackney, C.M. and Furness, D.N. (1986). Intercellular cross-linkages between the stereociliary bundles of adjacent hair cells in the guinea pig cochlea. Cell Tissue Res. *245*, 685-688.

74. Halet, G. (2005). Imaging phosphoinositide dynamics using GFP-tagged protein domains. Biol Cell. 97, 501-518.

75. Hehnly, H. and Stamnes, M. (2007). Regulating cytoskeleton-based vesicle motility. FEBS Lett. *581,* 2112-2118.

76. Hill, J.K., Williams, D.E., LeMasurier, M., Dumont, R.A., Strehler, E.E. and Gillespie, P.G. (2006). Splice-site A choice targets plasma-membrane Ca2+-ATPase isoform 2 to hair bundles. J Neurosci. *26*, 6172-6180.

77. Hillman, D.E. (1969). New ultrastructural findings regarding a vestibular ciliary apparatus and its possible functional significance. Brain Res. *13*, 407-412.

78. Hillman, D.E. and Lewis, E.R. (1971). Morphological basis for a mechanical linkage in otolithic receptor transduction in the frog. Science. *174*, 416-419.

79. Hilpelä P, Vartiainen MK, Lappalainen P. (2004). Regulation of the actin cytoskeleton by PI(4,5)P2 and PI(3,4,5)P3. Curr Top Microbiol Immunol. *282*, 117-163.

80. Hirono, M., Denis, C.S., Richardson, G.P. and Gillespie, P.G. (2004). Hair cells require phosphatidylinositol 4,5-bisphosphate for mechanical transduction and adaptation. Neuron. *44*, 309-320.

81. Holme, R.H. and Steel, K.P. (2002). Stereocilia defects in waltzer (Cdh23), shaker1 (Myo7a) and double waltzer/shaker1 mutant mice. Hear Res. *169*, 13-23.

82. Hunziker, W. and Fumey, C. (1994). A di-leucine motif mediates endocytosis and basolateral sorting of macrophage IgG Fc receptors in MDCK cells. EMBO J. *13*, 2963-2996.

83. Ihrke, G., Bruns, J. R., Luzio, J. P. and Weisz, O. A. (2001). Competing sorting signals guide endolyn along a novel route to lysosomes in MDCK cells. EMBO J. *20*, 6256-6264.

84. Ikonen, E. and Simons, K. (1998). Protein and lipid sorting from the trans-Golgi network to the plasma membrane in polarized cells. Semin Cell Dev Biol. *9*, 503-509.

85. Inoue, A., Yanagisawa, M., Takano-Ohmuro, H. and Masaki, T. (1989). Two isoforms of smooth muscle myosin regulatory light chain in chicken gizzard. Eur J Biochem. *183*, 645-651.

86. Irvine, R. (2004). Inositol lipids: to PHix or not to PHix? Curr Biol. *14*, R308-310.

87. Ito, Y., Hikino, M., Yajima, Y., Mikami, T., Sirko, S., von Holst, A., Faissner, A., Fukui, S. and Sugahara, K. (2005). Structural characterization of the epitopes of the monoclonal antibodies 473HD, CS-56, and MO-225 specific for chondroitin sulfate D-type using the oligosaccharide library. Glycobiology. *15*, 593-603.

88. Jacob, R., Preuss, U., Panzer, P., Alfalah, M., Quack, S., Roth, M. G., Naim, H. and Naim, H. Y. (1999). Hierarchy of sorting signals in chimeras of intestinal lactase-phlorizin hydrolase and the influenza virus hemagglutinin. J. Biol. Chem. *274*, 8061-8067.

89. Janmey, P.A., Xian, W. and Flanagan, L.A. (1999). Controlling cytoskeleton structure by phosphoinositide-protein interactions: phosphoinositide binding protein domains and effects of lipid packing. Chem Phys Lipids.*101*, 93-107.

90. Jović, M., Kieken, F., Naslavsky, N., Sorgen, P. L., and Caplan, S. (2009). Eps15 homology domain 1-associated tubules contain phosphatidylinositol-4-phosphate and phosphatidylinositol-(4,5)-bisphosphate and are required for efficient recycling. Mol Biol Cell *20*, 2731-2743.

91. Kachar, B., Battaglia, A. and Fex, J. (1997). Compartmentalized vesicular traffic around the hair cell cuticular plate. Hear. Res. *107*,102-112.

92. Kaltenbach, J.A., Falzarano, P.R. and Simpson, T.H. (1994). Postnatal development of the hamster cochlea. II. Growth and differentiation of stereocilia bundles. J Comp Neurol. *350*, 187-198.

93. Kaneko, T., Harasztosi, C., Mack, A.F. and Gummer, A.W. (2006). Membrane traffic in outer hair cells of the adult mammalian cochlea. Eur. J. Neur. *23*, 2712–2722.

94. Katori, Y., Hackney, C.M. and Furness, D.N. (1996). Immunoreactivity of sensory hair bundles of the guinea-pig cochlea to antibodies against elastin and keratan sulphate. Cell Tissue Res. *284*, 473-479.

95. Kazmierczak, P., Sakaguchi, H., Tokita, J., Wilson-Kubalek, E.M., Milligan, R.A., Müller, U. and Kachar, B. (2007). Cadherin 23 and protocadherin 15 interact to form tip-link filaments in sensory hair cells. Nature. *449*, 87-91.

96. Kharkovets, T., Hardelin, J.P., Safieddine, S., Schweizer, M., El-Amraoui, A., Petit, C. and Jentsch, T.J. (2000). KCNQ4, a K+ channel mutated in a form of dominant deafness, is expressed in the inner ear and the central auditory pathway. Proc Natl Acad Sci USA. *97*, 4333-4338.

97. Kieken, F., Jovic, M., Naslavsky, N., Caplan, S., and Sorgen, P. L. (2007). EH domain of EHD1. J Biomol NMR. *39*, 323-329.

98. Kikkawa, Y., Mburu, P., Morse, S., Kominami, R., Townsend, S. and Brown, S.D. (2005). Mutant analysis reveals whirlin as a dynamic organizer in the growing hair cell stereocilium. Hum Mol Genet. *14*, 391-400.

99. Killick, R. and Richardson, G.P. (1997). Antibodies to the sulphated, high molecular mass mouse tectorin stain hair bundles and the olfactory mucus layer. Hear Res. *103*, 131-141.

100. Kremer, H., van Wijk, E., Marker, T., Wolfrum, U. and Roepman, R. (2006). Usher syndrome: Molecular links of pathogenesis, proteins and pathways. Hum Mol Genet. *15*, R262-270.

101. Kundu, A., Avalos, R.T., Sanderson, C.M. and Nayak, D.P. (1996) .Transmembrane domain of influenza virus neuraminidase, a type II protein, possesses an apical sorting signal in polarized MDCK cells. J Virol. *70*, 6508-6515.

102. Larsen, J.E., Avvakumov, G.V., Hammond, G.L. and Vogel, L.K. (1999). N-glycans are not the signal for apical sorting of corticosteroid binding globulin in MDCK cells. FEBS Lett. *451*, 19-22.

103. Lavigne-Rebillard, M. and Pujol, R. (1986). Development of the auditory hair cell surface in human fetuses. A scanning electron microscopy study. Anat Embryol. *174*, 369-377.

104. Le Bivic, A., Garcia, M. and Rodriguez-Boulan, E. (1993). Ricin-resistant Madin-Darby canine kidney cells missort a major endogenous apical sialoglycoprotein. J Biol Chem. *268,* 6909-6916.

105. Lee, D. W., Zhao, X., Scarselletta, S., Schweinsberg, P. J., Eisenberg, E., Grant, B. D., and Greene, L. E. (2005). ATP binding regulates oligomerization and endosome association of RME-1 family proteins. J Biol Chem. *280*, 17213-17220.

106. Lelli, A., Asai, Y., Forge, A., Holt, J.R. and Géléoc, G.S. (2009). Tonotopic gradient in the developmental acquisition of sensory transduction in outer hair cells of the mouse cochlea. J Neurophysiol. *101*, 2961-2973.

107. Lemmon, M.A. (2003). Phosphoinositide recognition domains. Traffic. *4,* 201-213.

108. Lemmon, M.A. (2004). Pleckstrin homology domains: not just for phosphoinositides. Biochem Soc Trans.32, 707-711.

109. Lemmon, M.A. (2007). Pleckstrin homology (PH) domains and phosphoinositides. Biochem Soc Symp. *74*, 81-93.

110. Lenoir, M., Puel, J.L. and Pujol, R. (1987). Stereocilia and tectorial membrane development in the rat cochlea. A SEM study. Anat Embryol. *175*, 477-487.

111. Leslie, N.R., Gray, A., Pass, I., Orchiston, E.A. and Downes, C.P. (2000). Analysis of the cellular functions of PTEN using catalytic domain and C-terminal mutations: differential effects of C-terminal deletion on signalling pathways downstream of phosphoinositide 3-kinase. Biochem J. *346*, 827-833

112. Li, C.W. and Ruben, R.J. (1979). Further study of the surface morphology of the embryonic mouse cochlear sensory epithelia. Otolaryngol Head Neck Surg. *87*, 479-485.

113. Lim, D.J. and Anniko, M. (1985). Developmental morphology of the mouse inner ear. A scanning electron microscopic observation. Acta Otolaryngol Suppl. *422*, 1-69.

114. Lim, D.J. (2005). Ultrastructural anatomy of the cochlea. In Otolaryngology: basic science and clinical review. Edited by Van de Water, T.R. and Staecker, H. Thieme; 1 edition., pp 314-331.

115. Lin, S., Niam, H.Y., Rodriguez, A.C. and Roth, M.G. (1998). Mutations in the middle of the transmembrane domain reverse the polarity of transport of the influenza virus hemagglutinin in MDCK epithelial cell. J Cell Biol. *142,* 51-57.

116. Lin, H.W., Schneider, M.E. and Kachar, B. (2005). When size matters: the dynamic regulation of stereocilia lengths. Curr. Opin. Cell Biol. *17*, 55-61.

117. Lipardi, C., Nitsch, L. and Zurzolo, C. (2000). Detergent-insoluble GPI-anchored proteins are apically sorted in fischer rat thyroid cells, but interference

with cholesterol or sphingolipids differentially affects detergent insolubility and apical sorting. Mol Biol Cell. *11*, 531-542.

118. Maehama, T. and Dixon, J.E. (1998). The tumor suppressor, PTEN/MMAC1, dephosphorylates the lipid second messenger, phosphatidylinositol 3,4,5-trisphosphate. J Biol Chem. *273*, 13375-13378.

119. Martin-Belmonte, F. and Mostov, K. (2007). Phosphoinositides control epithelial development.Cell Cycle.*6*, 1957-1961.

120. Martin-Belmonte, F., Gassama, A., Datta, A., Yu, W., Rescher, U., Gerke, V. andMostov, K. (2007). PTEN-mediated apical segregation of phosphoinositides controls epithelial morphogenesis through Cdc42. Cell. *128,* 383-397.

121. Matter, K. (2000). Epithelial polarity: sorting out the sorters. Curr Biol.*10*, R39-42.

122. Mays, R.W., Beck, K.A. and Nelson, W.J. (1994). Organization and function of the cytoskeleton in polarized epithelial cells: a component of the protein sorting machinery. Curr Opin Cell Biol. *6*, 16-24.

123. Mbiene, J.P. and Sans, A. (1986). Differentiation and maturation of the sensory hair bundles in the fetal and postnatal vestibular receptors of the mouse: a scanning electron microscopy study. J Comp Neurol. *254*, 271-278.

124. McGee, J., Goodyear, R. J., McMillan, D. R., Stauffer, E. A., Holt, J. R., Locke, K. G., Birch, D. G., Legan, P. K., White, P. C., Walsh, E. J. and Richardson, G. P. (2006). The very large G-protein-coupled receptor VLGR1: a component of the ankle link complex required for the normal development of auditory hair bundles. J Neurosci. *26*, 6543-6553.

125. Mellman, I. and Nelson, W.J. (2008). Coordinated protein sorting, targeting and distribution in polarized cells. Nat Rev Mol Cell Biol. *9,* 833-845.

126. Michalski, N., Michel, V., Bahloul, A., Lefèvre, G., Barral, J., Yagi, H., Chardenoux, S., Weil, D., Martin, P., Hardelin, J.P., Sato, M. and Petit, C.

(2007). Molecular characterization of the ankle-link complex in cochlear hair cells and its role in the hair bundle functioning. J Neurosci. *27*, 6478-6488.

127. Michel, V., Goodyear, R. J., Weil, D., Marcotti, W., Perfettini, I., Wolfrum, U., Kros, C. J., Richardson, G. P. and Petit, C. (2005). Cadherin 23 is a component of the transient lateral links in the developing hair bundles of cochlear sensory cells. Dev Biol. *280,* 281-294.

128. Milewski, M.I., Mickle, J.E., Forrest, J.K., Stafford, D.M., Moyer, B.D., Cheng, J., Guggino, W.B., Stanton, B.A. and Cutting, G.R. (2001). A PDZ-binding motif is essential but not sufficient to localize the C terminus of CFTR to the apical membrane. J Cell Sci. *114*, 719-726.

129. Miliaras, N. B., and Wendland, B. (2004). EH proteins: multivalent regulators of endocytosis (and other pathways). Cell Biochem Biophys. *41*, 295-318.

130. Mintz, L., Galperin, E., Pasmanik-Chor, M., Tulzinsky, S., Bromberg, Y., Kozak, C. A., Joyner, A., Fein, A., and Horowitz, M. (1999). EHD1-an EH-domain-containing protein with a specific expression pattern. Genomics. *59*, 66-76.

131. Mostov, K.E., Verges, M. and Altschuler, Y. (2000). Membrane traffic in polarized epithelial cells. Curr Opin Cell Biol. *12*, 483-490.

132. Muth, T.R., Ahn, J. and Caplan, M.J. (1998). Identification of sorting determinants in the C-terminal cytoplasmic tails of the gamma-aminobutyric acid transporters GAT-2 and GAT-3. J Biol Chem. *273*, 25616-25627.

133. Myers, M.P., Pass, I., Batty, I.H., Van der Kaay, J., Stolarov, J.P., Hemmings, B.A., Wigler, M.H., Downes, C.P. and Tonks, N.K. (1998). The lipid phosphatase activity of PTEN is critical for its tumor supressor function. Proc Natl Acad Sci U S A. *95*, 13513-13518.

134. Naslavsky, N., and Caplan, S. (2005). C-terminal EH-domain-containing proteins: consensus for a role in endocytic trafficking, EH? J Cell Sci. *118*, 4093-4101.

135. Naslavsky, N., Rahajeng, J., Sharma, M., Jovic, M., and Caplan, S. (2006). Interactions between EHD proteins and Rab11-FIP2: a role for EHD3 in early endosomal transport. Mol Biol Cell. *17*, 163-177.

136. Naslavsky, N., Rahajeng, J., Chenavas, S., Sorgen, P. L., and Caplan, S. (2007). EHD1 and Eps15 interact with phosphatidylinositols via their Eps15 homology domains. J Biol Chem. *282*, 16612-16622.

137. Nayak, G.D., Ratnayaka, H.S., Goodyear, R.J. and Richardson, G.P. (2007). Development of the hair bundle and mechanotransduction. Int J Dev Biol. *51*, 597-608.

138. Nishida, Y., Rivolta, M.N. and Holley, M.C. (1998). Timed markers for the differentiation of the cuticular plate and stereocilia in hair cells from the mouse inner ear. J Comp Neurol. *395*, 18-28.

139. Oganesian, A., Poot, M., Daum, G., Coats, S.A., Wright, M.B., Seifert, R.A. and Bowen-Pope, D.F. (2003). Protein tyrosine phosphatase RQ is a phosphatidylinositol phosphatase that can regulate cell survival and proliferation. Proc Natl Acad Sci U S A. *100*, 7563-7568.

140. Osborne, M.P., Comis, S.D. and Pickles, J.O. (1988). Further observations on the fine structure of tip links between stereocilia of the guinea pig cochlea. Hear Res. *35*, 99-108.

141. Overduin, M., Cheever, M.L. and Kutateladze, T.G. (2001). Signaling with phosphoinositides: better than binary. Mol Interv. *1*, 150-159.

142. Paladino, S., Sarnataro, D., Tivodar, S. and Zurzolo, C. (2007). Oligomerization is a specific requirement for apical sorting of glycosyl-phosphatidylinositol-anchored proteins but not for non-raft-associated apical proteins. Traffic. *8*, 251-258.

143. Parker, P.J. (2004). The ubiquitous phosphoinositides. Biochem Soc Trans. *32*, 893-898.

144. Perego, C., Vanoni, C., Villa, A., Longhi, R., Kaech, S.M., Fröhli, E., Hajnal, A., Kim, S.K. and Pietrini, G. (1999). PDZ-mediated interactions retain the epithelial GABA transporter on the basolateral surface of polarized epithelial cells. EMBO J. 18, 2384-2393.

145. Phillips, K. R., Tong, S., Goodyear, R., Richardson, G. P. and Cyr, J. L. (2006). Stereociliary myosin-1c receptors are sensitive to calcium chelation and absent from cadherin 23 mutant mice. J Neurosci. *26*, 10777-10788.

146. Pickles, J.O., Comis, S.D. and Osborne, M.P. (1984). Cross-links between stereocilia in the guinea pig organ of Corti and their possible relation to sensory transduction. Hear Res. *15*, 103-112.

147. Pickles, J.O., von Perger, M., Rouse, G.W. and Brix. J. (1991). The development of links between stereocilia in hair cells of the chick basilar papilla. Hear Res. *54*, 153-163.

148. Pinal, N., Goberdhan, D.C., Collinson, L., Fujita, Y., Cox, I.M., Wilson, C. and Pichaud, F. (2006). Regulated and polarized PtdIns (3,4,5)P3 accumulation is essential for apical membrane morphogenesis in photoreceptor epithelial cells. Curr. Biol. *16,* 140-149.

149. Pohl, U., Smith, J.S., Tachibana, I., Ueki, K., Lee, H.K., Ramaswamy, S., Wu, Q., Mohrenweiser, H.W., Jenkins, R.B. and Louis, D.N. (2000). EHD2, EHD3, and EHD4 encode novel members of a highly conserved family of EH domain-containing proteins. Genomics. *63*, 255-262.

150. Reiners, J., Marker, T., Jurgens, K., Reidel, B. and Wolfrum, U. (2005a). Photoreceptor expression of the Usher syndrome type 1 protein protocadherin 15 (USH1F) and its interaction with the scaffold protein harmonin (USH1C). Mol Vis. *11,* 347-355.

151. Reiners, J., van Wijk, E., Marker, T., Zimmermann, U., Jurgens, K., te Brinke, H., Overlack, N., Roepman, R., Knipper, M., Kremer, H. and Wolfrum, U. (2005b). Scaffold protein harmonin (USH1C) provides molecular links between Usher syndrome type 1 and type 2. Hum Mol Genet. *14*, 3933-3943.

152. Richardson, G.P., Bartolami, S. and Russell, I.J. (1990). Identification of a 275-kD protein associated with the apical surfaces of sensory hair cells in the avian inner ear. J Cell Biol. *110*, 1055-1066.

153. Richardson, G.P., Forge, A., Kros, C.J., Fleming, J., Brown, S.D.M. and Steel, K.P. (1997). Myosin VIIa Is Required for Aminoglycoside Accumulation in Cochlear Hair Cells. J. Neur. *17*, 9506-9519.

154. Ridley, S.H., Ktistakis, N., Davidson, K., Anderson, K.E., Manifava, M., Ellson, C.D., Lipp, P., Bootman, M., Coadwell, J., Nazarian, A., Erdjument-Bromage, H., Tempst, P., Cooper, M.A., Thuring, J.W., Lim, Z.Y., Holmes, A.B., Stephens, L.R. and Hawkins, P.T.(2001). FENS-1 and DFCP1 are FYVE domain-containing proteins with distinct functions in the endosomal and Golgi compartments. J Cell Sci. *114*, 3991-4000.

155. Rodriguez-Boulan, E. and Gonzalez, A. (1999). Glycans in post-Golgi apical targeting: sorting signals or structural props? Trends Cell Biol. *9*, 291–294.

156. Rodriguez-Boulan, E. and Müsch, A. (2005). Protein sorting in the Golgi complex: Shifting paradigms. Biochim. Biophys. Acta. *1744,* 455-464.

157. Rotem-Yehudar, R., Galperin, E., and Horowitz, M. (2001). Association of insulin-like growth factor 1 receptor with EHD1 and SNAP29. J Biol Chem. *276*, 33054-33060.

158. Roth, M.G. (2004). Phosphoinositides in constitutive membrane traffic. Physiol Rev.84, 699-730.

159. Rothman, J.E. (1994). Mechanisms of intracellular protein transport. Nature. *372,* 55-63.

160. Rzadzinska ,A.K., Schneider, M.E., Davies, C., Riordan, G.P. and Kachar, B. (2004). An actin molecular treadmill and myosins maintain stereocilia functional architecture and self-renewal. J. Cell Biol. *164*, 887-897.

161. Rzadzinska, A.K., Nevalainen, E.M., Prosser, H.M., Lappalainen, P. and Steel, K.P. (2009). MyosinVIIa interacts with Twinfilin-2 at the tips of mechanosensory stereocilia in the inner ear. PLoS One. *4(9)*, e7097.

162. Santolini, E., Salcini, A. E., Kay, B. K., Yamabhai, M., and Di Fiore, P. P. (1999). The EH network. Exp Cell Res. *253*, 186-209.

163. Sasaki, T., Sasaki, J., Sakai, T., Takasuga, S. and Suzuki, A. (2007). The physiology of phosphoinositides. Biol Pharm Bull. *30*, 1599-1604.

164. Scheiffele, P., Peranen, J. and Simons, K. (1995). N-glycans as apical sorting signals in epithelial cells. Nature. *378,* 96-98.

165. Scheiffele, P., Roth, M.G. and Simons, K. (1997). Interaction of influenza virus haemagglutinin with sphingolipid-cholesterol membrane domains via its transmembrane domain. Embo J. *16*, 5501-5508.

166. Schneider,M.E., Belyantseva, I.A., Azvedo, R.B. and Kachar, B. (2002). Rapid Renewal of Auditory Hair Bundles. Nature. *418*, 837-838.

167. Schuck, S. and Simons, K. (2004). Polarized sorting in epithelial cells: raft clustering and the biogenesis of the apical membrane. J Cell Sci. *117*, 5955-5964.

168. Seachrist, J.L., Ferguson, S.S. (2003). Regulation of G protein-coupled receptor endocytosis and trafficking by Rab GTPases. Life Sci. *74*, 225-235.

169. Seifert, R.A., Coats, S.A., Oganesian, A., Wright, M.B., Dishmon, M., Booth, C.J., Johnson, R.J., Alpers, C.E. and Bowen-Pope, D.F. (2003). PTPRQ is a novel phosphatidylinositol phosphatase that can be expressed as a cytoplasmic protein or as a subcellularly localized receptor-like protein. Exp Cell Res. *287*, 374-386.

170. Senften, M., Schwander, M., Kazmierczak, P., Lillo, C., Shin, J. B., Hasson, T., Geleoc, G. S., Gillespie, P. G., Williams, D., Holt, J. R. and Muller, U. (2006). Physical and functional interaction between protocadherin 15 and myosin VIIa in mechanosensory hair cells. J Neurosci. *26,* 2060-2071.

171. Sengupta, S., George, M., Miller, K. K., Naik, K., Chou, J., Cheatham, M. A., Dallos, P., Naramura, M., Band, H., and Zheng, J. (2009). EHD4 and CDH23 are interacting partners in cochlear hair cells. J Biol Chem. *284*, 20121-20129.

172. Shelly, M., Mosesson, Y., Citri, A., Lavi, S., Zwang ,Y., Melamed-Book, N., Aroeti, B. and Yarden, Y. (2003). Polar expression of ErbB-2/HER2 in epithelia. Bimodal regulation by Lin-7. Dev Cell. *5*, 475-486.

173. Shin, J.B., Streijger, F., Beynon, A., Peters, T., Gadzala, L., McMillen, D., Bystrom, C., Van der Zee, C.E., Wallimann, T. and Gillespie, P.G. (2007). Hair bundles are specialized for ATP delivery via creatine kinase. Neuron. *53,* 371-386.

174. Short, D.B., Trotter, K.W., Reczek, D., Kreda, S.M., Bretscher, A., Boucher, R.C., Stutts, M.J. and Milgram, S.L. (1998). An apical PDZ protein anchors the cystic fibrosis transmembrane conductance regulator to the cytoskeleton. J Biol Chem. *273*, 19797-19801.

175. Siemens, J., Kazmierczak, P., Reynolds, A., Sticker, M., Littlewood-Evans, A. and Muller, U., (2002). The Usher syndrome proteins cadherin 23 and harmonin form a complex by means of PDZ domain interactions. Proc. Natl. Acad. Sci. U.S.A. *99*, 14946-14951.

176. Siemens, J., Lillo, C., Dumont, R. A., Reynolds, A., Williams, D. S., Gillespie, P. G. and Muller, U. (2004). Cadherin 23 is a component of the tip link in hair-cell stereocilia. Nature. *428*, 950-955.

177. Slepecky, N.B. (1996). Structure of the mammalian cochlea. In *The Cochlea*. Edited by Dallos, P. , Popper, A.N. and Fay, R.R. Springer-Verlag New York, Inc. , pp 44-129.

178. Sobue, K., Hayashi, K. and Nishida, W. (1999). Expressional regulation of smooth muscle cell-specific genes in association with phenotypic modulation. Mol Cell Biochem. *190*, 105-118

179. Söllner, C., Rauch, G. J., Siemens, J., Geisler, R., Schuster, S. C., Muller, U. and Nicolson, T. (2004). Mutations in cadherin 23 affect tip links in zebrafish sensory hair cells. Nature. *428*, 955-959.

180. Souter, M., Nevill, G. and Forge, A. (1995). Postnatal development of membrane specialisations of gerbil outer hair cells. Hear Res. *91*, 43-62.

181. Stauffer, T.P., Ahn, S. and Meyer, T. (1998). Receptor-induced transient reduction in plasma membrane PtdIns(4,5)P_2 concentration monitored in living cells. Curr. Biol. *8,* 343-346.

182. Strehler, E.E. and Zacharias, D.A. (2001). Role of alternative splicing in generating isoform diversity among plasma membrane calcium pumps. Physiol Rev. *81*, 21-50.

183. Su, T., Cariappa, R. and Stanley, K. (1999). N-glycans are not a universal signal for apical sorting of secretory proteins. FEBS Lett. *453*, 391-394.

184. Suh, B.C., Inoue, T., Meyer, T. and Hille, B. (2006). Rapid chemically induced changes of PtdIns (4,5)P2 gate KCNQ ion channels. Science.*314*, 1454-1457

185. Swiatecka-Urban, A., Duhaime, M., Coutermarsh, B., Karlson, K.H., Collawn, J., Milewski, M., Cutting, G.R., Guggino, W.B., Langford, G., Stanton, B.A. (2002). PDZ domain interaction controls the endocytic recycling of the cystic fibrosis transmembrane conductance regulator. J Biol Chem. *277*, 40099-40105.

186. Takenawa, T. and Itoh, T. (2001). Phosphoinositides, key molecules for regulation of actin cytoskeletal organization and membrane traffic from the plasma membrane. Biochim Biophys Acta. *1533*, 190-206.

187. Tilney, L.G. and DeRosier, D.J. (1986). Actin filaments, stereocilia, and hair cells of the bird cochlea. IV. How the actin filaments become organized in developing stereocilia and in the cuticular plate. Dev Biol. *116*, 119-129.

188. Tilney, L.G., Tilney, M.S., Saunders, J.S. and DeRosier, D.J. (1986). Actin filaments, stereocilia, and hair cells of the bird cochlea. III. The development and differentiation of hair cells and stereocilia. Dev Biol. *116*, 100-118.

189. Tilney, L.G., Tilney, M.S. and Cotanche, D.A. (1988). New observations on the stereocilia of hair cells of the chick cochlea. Hear Res. *37*, 71-82.

190. Tilney, L.G., Tilney, M.S. and DeRosier, D.J. (1992a). Actin filaments, Stereocilia, and Hair cells: How cells count and measure. Annu. Rev. Cell. Biol. *8,* 257-274.

191. Tilney, L.G., Cotanche, D.A. and Tilney, M.S. (1992b). Actin filaments, stereocilia and hair cells of the bird cochlea. VI. How the number and arrangement of stereocilia are determined. Development. *116*, 213-226.

192. Tsuprun, V. and Santi, P. (2002). Structure of outer hair cell stereocilia side and attachment links in the chinchilla cochlea. J Histochem Cytochem. *50*, 493-502.

193. Urban, J., Parczyk, K., Leutz, A., Kayne, M. and Kondor-Koch, C. (1987). Constitutive apical secretion of an 80-kD sulfated glycoprotein complex in the polarized epithelial Madin-Darby canine kidney cell line. J Cell Biol. *105,* 2735-2743.

194. Urquhart, P., Pang, S. and Hooper, N.M. (2005). N-glycans as apical targeting signals in polarized epithelial cells. Biochem Soc Symp. *72*, 39-45.

195. van Wijk, E., Pennings, R.J., te Brinke, H., Claassen, A., Yntema, H.G., Hoefsloot, L.H., Cremers, F.P., Cremers, C.W. and Kremer, H. (2004). Identification of 51 novel exons of the Usher syndrome type 2A (USH2A) gene that encode multiple conserved functional domains and that are mutated in patients with Usher syndrome type II. Am. J. Hum. Genet. *74,* 738–744.

196. van Wijk, E., van der Zwaag, B., Peters, T., Zimmermann, U., Te Brinke, H., Kersten, F. F., Marker, T., Aller, E., Hoefsloot, L. H., Cremers, C. W., Cremers, F. P., Wolfrum, U., Knipper, M., Roepman, R. and Kremer, H. (2006). The DFNB31 gene product whirlin connects to the Usher protein network in the cochlea and retina by direct association with USH2A and VLGR1. Hum Mol Genet. *15*, 751-765.

197. Vanhaesebroeck, B., Leevers, S.J., Ahmadi, K., Timms, J., Katso, R., Driscoll, P.C., Woscholski, R., Parker, P.J. and Waterfield, M.D. (2001). Synthesis and function of 3-phosphorylated inositol lipids. Annu. Rev. Biochem. *70,* 535-602.

198. Várnai, P. and Balla, T. (1998). Visualization of phosphoinositides that bind pleckstrin homology domains: calcium- and agonist-induced dynamic changes and relationship to myo-[3H] inositol-labeled phosphoinositide pools. J Cell Biol.*143*, 501-510.

199. Várnai, P. and Balla, T. (2006). Live cell imaging of phosphoinositide dynamics with fluorescent protein domains. Biochim Biophys Acta. *1761*, 957-967.

200. Várnai, P. and Balla, T. (2007). Visualization and manipulation of phosphoinositide dynamics in live cells using engineered protein domains. Pflugers Arch. *455*, 69-82.

201. Varnai, P., Thyagarajan, B., Rohacs, T. and Balla T. (2006). Rapidly inducible changes in phosphatidylinositol 4,5-bisphosphate levels influence multiple regulatory functions of the lipid in intact living cells. J Cell Biol. *175*, 377-382.

202. Vogel, L.K., Spiess, M., Sjostrom, H. and Noren, O. (1992). Evidence for an apical sorting signal on the ectodomain of human aminopeptidase N. J Biol Chem. *267*, 2794-2797.

203. von Holst, A., Sirko, S. and Faissner, A. (2006). The unique 473HD-Chondroitinsulfate epitope is expressed by radial glia and involved in neural precursor cell proliferation. J Neurosci. *26*, 4082-4094.

204. Waguespack, J., Salles, F.T., Kachar, B. and Ricci, A.J. (2007). Stepwise morphological and functional maturation of mechanotransduction in rat outer hair cells. J Neurosci. *27*, 13890-13902.

205. Watt, S.A., Kular, G., Fleming, I.N., Downes, C.P. and Lucocq, J.M. (2002). Subcellular localization of phosphatidylinositol 4,5-bisphosphate using the pleckstrin homology domain of phospholipase C delta1. Biochem J. 363, 657-666.

206. Watt, S.A., Kimber, W.A., Fleming, I.N., Leslie, N.R., Downes, C.P. and Lucocq, J.M. (2004). Detection of novel intracellular agonist responsive pools of phosphatidylinositol 3,4-bisphosphate using the TAPP1 pleckstrin homology domain in immunoelectron microscopy. Biochem J. *377*, 653-663.

207. Weimbs, T., Low, S.H., Chapin, S.J. and Mostov, K.E. (1997). Apical targeting in polarized epithelial cells: There's more afloat than rafts. Trends Cell Biol. *7*:393-399.

208. Weston, M.D., Luijendijk, M.W., Humphrey, K.D., Möller, C. and Kimberling, W.J. (2004). Mutations in the VLGR1 gene implicate G-protein signaling in the pathogenesis of Usher syndrome type II. Am J Hum Genet. *74*, 357-366.

209. Wright, M.B., Hugo, C., Seifert, R., Disteche, C.M. and Bowen-Pope, D.F. (1998). Proliferating and migrating mesangial cells responding to injury express a novel receptor protein-tyrosine phosphatase in experimental mesangial proliferative glomerulonephritis. J Biol Chem. *273*, 23929-23937.

210. Xu, Z., Peng, A.W., Oshima, K. and Heller, S. (2008). MAGI-1, a candidate stereociliary scaffolding protein, associates with the tip-link component cadherin 23. J Neurosci. *28*, 11269-11276.

211. Yeaman, C., Le Gall, A.H., Baldwin, A.N., Monlauzeur, L., Le Bivic, A. and Rodriguez-Boulan, E. (1997). The O-glycosylated stalk domain is required for apical sorting of neurotrophin receptors in polarized MDCK cells. J Cell Biol. *139,* 929-940.

212. Yeaman, C., Grindstaff, K.K. and Nelson, W.J. (1999). New perspectives on mechanisms involved in generating epithelial cell polarity. Physiol. Rev. *79,* 73-98.

213. Zheng, J., Anderson, C.T., Miller, K.K., Cheatham, M. and Dallos, P. (2009). Identifying components of the hair-cell interactome involved in cochlear amplification. BMC Genomics. *10*, 127.

214. Zine, A. and Romand, R. (1996). Development of the auditory receptors of the rat: a SEM study. Brain Res. *721*, 49-58.

215. Zurzolo, C., Lisanti, M.P., Caras, I.W., Nitsch, L. and Rodriguez-Boulan, E. (1993). Glycosylphosphatidylinositol-anchored proteins are preferentially targeted to the basolateral surface in Fischer rat thyroid epithelial cells. J. Cell Biol. 121: 1031-1039.

APPENDIX

1. Preparation of the pMyr cDNA library

1.1 RNA Isolation

TRIZOL® reagent was added at 1000 μl for every 100 mg of tissue and homogenized by pipetting. The tubes were allowed to stand for 5 minutes to permit dissociation of nucleoprotein complexes. To separate the RNA, chloroform was added, followed by vigorous mixing and centrifugation. The upper aqueous layer containing the RNA was transferred into a fresh tube leaving behind the lower organic phase. The RNA was precipitated by addition of isopropyl alcohol, mixing and incubating for 10 minutes at 15 to 30˚C followed by centrifugation at 13000 rpm for 10 minutes. The gel-like pellet of precipitated RNA was collected into a fresh tube for an ethanol wash. The pellet was washed with 70% ethanol by vortexing and centrifugation at 13000 rpm for 10 minutes. The final pellet was vacuum-dried and redissolved in RNAse free water by incubating for 10 minutes at 55-60˚C.

1.2 cDNA preparation

The reagents for the first-strand synthesis were added to a microcentrifuge tube as follows:

Reagent	Volume
10✕ first-strand buffer	5 μl
first-strand methyl nucleotide mixture	3 μl

linker–primer (1.4 μg/μl)	2 μl
Poly(A) RNA from posthatch day 1 chick utricles in DEPC-treated water	37.5 μl
RNase Block Ribonuclease Inhibitor (40 U/μl)	1 μl

The reaction was incubated for 10 minutes to allow the primers to anneal to the RNA template. Then, 1.5 μl of StrataScript reverse transcriptase (50 U/μl) was added to the tube. The reaction was gently mixed and spun down. As control, 5 μl of this reaction mixture was added to a separate tube containing 0.5 μl of $[\alpha\text{-}^{32}P]dNTP$ (800 Ci/mmol). Both first-strand synthesis reactions were incubated for an hour at 42°C. The control radioactive sample was run on an agarose gel, while the nonradioactive sample (45 μl) was placed on ice and the following reagents were added to it.

Reagent	Volume
10× second-strand buffer	20 μl
second-strand dNTP mixture	6 μl
Sterile water	114 μl
$[\alpha\text{-}^{32}P]dNTP$ (800 Ci/mmol)	2 μl
RNase H (1.5 U/μl)	2 μl
DNA polymerase I (9.0 U/μl)	11 μl

The tube was gently vortexed and given a quick spin in the microcentrifuge. The reaction was then incubated for 2.5 hours at 16°C. The tube was placed on ice. In order to blunt the cDNA termini, the following two components were added to the tube.

Reagent	Volume
Blunting dNTP mix	23 µl
Pfu DNA polymerase	2 µl

After a quick vortex and a spin in the microcentrifuge, the tube was placed for 30 minutes at 70°C. Keeping the tube at room temperature, 200 µl of phenol–chloroform [1:1 (v/v)] (equilibrated to pH 7-8) was added, and vortexed and spun for 2 minutes. The aqueous upper layer containing the cDNA was removed to another tube. An equal volume of chloroform was added and vortexed. The tube was spun in a microcentrifuge for 2 minutes and the aqueous upper layer was transferred to another tube. The cDNA (200 µl) was precipitated by adding the following:

Reagent	Volume
3M sodium acetate	20 µl
100% (v/v) ethanol	400 µl

The tube was vortexed and incubated overnight at -20°C. The next day, the tube was spun for 60 minutes at 4°C. The radioactive supernatant was carefully discarded and the pellet was washed with 500 µl of 70 % (v/v) ethanol. The tube was spun at maximum speed for 2 minutes in a microcentrifuge at room temperature. The ethanol wash was aspirated and the pellet was dried by vacuum centrifugation. The cDNA pellet was resuspended in 9 µl of a solution containing *Eco*RI adapters (0.4 µg/µl) and incubated for 30 minutes at 4˚C. While keeping 1 µl of the above reaction as the second-strand synthesis control, the rest of the reaction (8 µl) was ligated to the *Eco*RI adapters using the following reagents:

Reagent	Volume
10 x Ligase Buffer	1 µl
10 mM rATP	1 µl
T4 DNA Ligase (4U/µl)	1 µl

The reaction was incubated overnight at 8˚C and the ligase inactivated by incubating for 30 minutes at 70˚C. After the cooling the reaction, the *Eco*R1 adaptors were phosphorylated by adding the following reagents:

Reagent	Volume
10 x Ligase Buffer	1 µl
10 mM rATP	2 µl
Sterile water	5 µl
T4 polynucleotide kinase (5.0 U/µl)	2 µl

The phosphorylation reaction was incubated for 30 minutes at 37˚C and the kinase then inactivated by incubating for 30 minutes at 70˚C. The reaction was cooled to room temperature. To digest the Xho1 sites introduced by the linker-primer, the following reagents were added to the reaction:

Reagent	Volume
Xho I buffer supplement	28 µl
Xho I (40 U/µl)	3 µl

The reaction was incubated for 1.5 hours at 37˚C, after which 5 µl of 10 X STE buffer and 125 µl of 100 % (v/v) ethanol was added and the DNA was precipitated overnight at –20˚C. Following precipitation, the reaction was centrifuged at 13000 rpm for 60 minutes at 4˚C. The supernatant was discarded and the pellet vacuum dried before resuspending in 14 µl of 1 X STE buffer and adding 3.5 µl of column-loading dye to each sample. The cDNA inserts were size fractionated on a drip column containing Sepharose® CL-2B gel filtration medium (all part of the CytoTrap® XR library construction kit). In total, 12 fractions of ~100 µl were collected. The first 4 fractions were not radioactive. The last 2 yielded high counts per second, suggesting that these contained unincorporated dNTPs, oligonucleotides and short transcripts. These were therefore discarded. On electrophoresis and ethidium bromide staining, fractions 5 to 10 had a clear gradient of cDNA sizes ranging from ~8-9 kb to ~200 bp. cDNA from each of these fractions were extracted by adding 100 µl of phenol: chloroform [1:1 (v/v)]. After vortexing and centrifugation for 2 minutes at 13000 rpm, the aqueous layer containing the cDNA was transferred to a fresh tube. An equal volume of chloroform was added to the aqueous layer and after vortexing and centrifugation the cDNA was collected in a fresh tube. Finally, the cDNA was precipitated with 100 % ethanol overnight at –20˚C. The tubes were centrifuged for 60 minutes at 4˚C and the pellets were washed with 70 % ethanol without mixing or vortexing. The tubes were centrifuged at 13000 rpm for 2 minutes at room temperature and the pellets were air-dried after discarding the supernatants. Each cDNA pellet was resuspended in 3.5 µl of sterile water. Based on the autoradiography signals and quantitation on ethidium bromide plates, cDNA fractions 5, 6, 7 and 8 were pooled together and ligated into the pMyr vector.

1.3   pMyr cDNA ligation and transformation

For ligating the cDNA into the pMyr XR Vector, the following reactions were set up:

Reagents	Control	pMyr cDNA ligations
pMyr XR vector	0.3 µl	1 µl
XR LacZ	1 µl	-
cDNA	-	2.5 µl
10 x Ligase Buffer	0.5 µl	0.5 µl
10mM rATP	0.5 µl	0.5 µl
Sterile water	2.2 µl	-
T4 DNA Ligase	0.5 µl	0.5 µl

The ligations (1 µl) were transformed (see section 2.1.10) into XL10-Gold® Kan Ultracompetent cells (Stratagene) and the transformation efficiency determined. The ligations were then scaled up and used to transform XL10-Gold® Kan Ultracompetent cells, Stratagene. After determining the transformation efficiency, the primary transformants were pooled and plated on fifteen 15 cm LB chloramphenicol plates so that each plate would have 20000 to 30000 colonies. After overnight incubation at 37˚C, the colonies on each plate were scraped into 8 ml of fresh LB medium for each. Colonies from all plates were then pooled together in a single sterile flask. Half of this bacterial suspension was used for alkaline lysis/CsCl gradient purification of plasmid DNA and the rest were made in to 1 ml glycerol stocks. The bacterial titer of each glycerol aliquot was determined by thawing out a single aliquot and diluting with LB to obtain a 10^{-6} dilution and plating out a certain amount on 15 cm LB chloramphenicol

plates. The cfu/µl was determined from these plates. Alkaline lysis/CsCl gradient purification of the plasmid DNA yielded 700 µg of DNA that was made into 1 µg/µl aliquots.

1.4 Yeast culture and media preparation

1.4.1 YPAD Broth

1% yeast extract

2% Bacto® peptone

2% dextrose

40 mg adenine sulfate

Deionized water to a final volume of 1 litre

1.4.2 YPAD Agar (30–40 Plates/Liter)

YPAD broth

2% Bacto® agar

Autoclave and pour in to plate

1.4.3 1 M sorbitol

1.4.4 LiSORB (per litre)

100 mM LiOAc

10 mM Tris-HCl (pH 8.0)

1 mM EDTA

1 M sorbitol

Add water to a volume of 1 liter

pH 8.0

Autoclave

1.4.5 20 mg/ml sheared salmon sperm DNA

1.4.6 PEG/LiOAc solution

10 mM Tris-HCl (pH 8.0)

1 mM EDTA (pH 8.0)

100 mM LiOAc (pH 7.5)

40% (w/v) PEG 3350

Autoclave

1.4.7 1.4 M β-mercaptoethanol

1.4.8 Synthetic Glucose Minimal Medium [SD/Glucose (–UL)]

1.7 g of yeast nitrogen base without amino acids

5 g of ammonium sulfate

20 g of dextrose

17 g of Bacto agar for SD dropout agar plates

Total volume to 900 ml with water

Autoclave.

100 ml of the appropriate filter-sterilized 10× dropout solution

(see *10× Dropout Solution*).

1.4.9 Synthetic Galactose Minimal Medium [SD/Galactose (–UL)]

1.7 g of yeast nitrogen base without amino acids

5 g of ammonium sulfate

20 g of galactose

10 g of raffinose

17 g of Bacto agar for SD dropout agar plates

Total volume to 900 ml with water

Autoclave.

100 ml of the appropriate filter-sterilized 10× dropout solution

(see *10× Dropout Solution*).

1.4.10 Yeast Lysis Solution for DNA Isolation

2.5 M LiCl

50 mM Tris-HCl (pH 8.0)

4% Triton X-100

62.5 mM EDTA

1.4.11 10 X dropout solution

Components	Weight (mg/liter)	Sigma Catalog #
L-Isoleucine	300	I 2752
L-Valine	1500	V 0500
L-Adenine hemisulfate salt	200	A 9126
L-Arginine HCl	500	A 5131
L-Histidine HCl monohydrate	200	H 8125
L-Leucine	1000	L 8000
L-Lysine HCl	500	L 5626
L-Methionine	200	M 9625
L-Phenylalanine	500	P 2126
L-Threonine	2000	T 8625
L-Tryptophan	500	T 0254
L-Tyrosine	500	T 3754
L-Uracil	200	U 0750
L -Glutamic acid	1000	G 1251
L -Aspartic acid	1000	A 9256
L -Serine	400	S 4500

To make the SD/Glucose (-UL) or SD/Galactose (-UL) media, amino acids leucine and uracil were left out of the 10x solution. Omission of leucine allows selection of the pSos vector while leaving out uracil allows pMyr vector selection.

1.5   *Yeast competent cell preparation*

A fresh plate of cdc25H (*a* or α) was prepared from a glycerol stock. The plate was incubated at room temperature for about 4 days until colonies appeared. Four to five tubes of 1 ml YPAD were inoculated with a single colony each and the tubes were vortexed to obtain a clear suspension of the colonies. The resuspended colonies were used to inoculate 50 ml YPAD in 250 ml flasks and were incubated at room temperature with shaking (220-250 rpm) for 14-16 hours. Once the OD exceeded 1, the starter cultures were diluted to obtain 300 ml cultures of OD 0.2. These cultures were incubated for 3 hours at room temperature with shaking (220-250 rpm). On reaching an OD > 0.7, 75 μl of the culture was plated on a YPAD plate to check for temperature-sensitive revertants, while the rest of the culture was pelleted down by centrifugation at 5000 x g for 5 minutes at room temperature. The supernatant was discarded and the cell pellet resuspended in 50 ml of distilled water. The cells were pelleted by centrifugation at 5000 x g for 10 minutes at room temperature. After discarding the supernatant, the cell pellet was resuspended in 50 ml of LiSORB and incubated for 30 minutes at room temperature. For each culture, 400 μl of 20 mg/ml salmon sperm DNA was boiled in a water bath for 30 minutes and 600 ml of LiSORB was added to each. At the end of the 30 minute incubation in LiSORB (step 6), the cells were pelleted and resuspended in 300 μl of LiSORB and 600 μl of salmon sperm DNA-LiSORB mix from step 7 was added. 5.4 ml of PEG/LiOAc and 530 μl of DMSO was added to each yeast preparation

and mixed gently. The competent cells were then aliquoted in to 1.5 ml centrifuge tubes as required for transformation.

1.6   Yeast transformation

To the required aliquot of freshly prepared yeast competent cells (see above), a suitable amount of DNA was added. A positive and a negative control provided in the CytoTrap® kit was included with every transformation. 1.4 M β-mercaptoethanol was added at a rate of 2 μl /100 μl of competent cells. The transformation reactions were incubated for 30 minutes at room temperature with occasional tapping. The reactions were heat shocked for 20 minutes at 42 ˚C. The transformation reactions were placed on ice for 3 minutes and the cells collected by centrifugation for 30 seconds at 14000 rpm at room temperature. The supernatant was discarded and the cells resuspended in 0.5 ml of 1 M sorbitol. The transformation reactions were then plated on suitable media.

1.7   Isolation of pMyr cDNA plasmid DNA from yeast

Each putative positive clone was used to inoculate 5ml of SD/Glucose (-UL) media in a 50-ml conical tube. The cultures were incubated at room temperature (22–25°C) with vigorous shaking (~250 rpm) until they were saturated (2-3 days, $OD_{600}>1.0$). The yeast cultures were pelleted at $1000 \times g$ for 5 minutes at room temperature. The yeast pellets were resuspended in 0.3 ml of Yeast Lysis Solution (see *appendix 1.4.10*). The suspensions were transferred to a 1.5-ml microcentrifuge tube and 50 μl of acid-washed glass beads (0.5 mm) and 300 μl of phenol/chloroform were added to the microcentrifuge tubes. The tubes were vortexed vigorously for one minute and the suspensions were centrifuged at $14,000 \times g$ for 5 minutes at room temperature. In each case the top aqueous phase containing the DNA was transferred to a fresh

microcentrifuge tube. The DNAs were precipitated with 600 μl of 100% (v/v) ice-cold ethanol at –20°C overnight. The suspensions were centrifuged at 14,000 × *g* for 10 minutes at 4°C and the supernatants were discarded. The DNA pellets were washed with 1 ml of 70% (v/v) ethanol and centrifuged at 14,000 × *g* for 5 minutes at room temperature. The supernatants were discarded and the DNA pellets were dried under vacuum. The DNA pellets were resuspended in 40 μl of distilled water. The DNAs were precipitated with 4.8 μl of 3 M NaOAc (pH 5.2) and 100 μl of ethanol. The suspension was centrifuged at 14,000 × *g* for 10 minutes at 4°C and the supernatant was discarded. The DNA pellets were washed with 1 ml of 70% (v/v) ethanol and centrifuged at 14,000 × *g* for 5 minutes at room temperature. The supernatants were discarded and the DNA pellets were dried under vacuum. The DNA pellets were resuspended in 20 μl of distilled water.

2. BCK is present in hair bundles of the chick inner ear

BCK was found to be a potential interactor of Ptprq according to a yeast-two hybrid screen. An affinity purified polyclonal antibody to chick BCK was used to stain chick utricle sections. Appendix figure 2.1 shows the results of the observed staining pattern.

BCK is present in the hair bundles of the chick innear ear where Ptprq is present. The significance of the interaction between the two proteins has to be determined by further experiments.

3. Currently available EHD3 antibodies are not suitable for Immunohistochemistry

Two EHD3 antibodies were tested on cryosections of wild-type and EHD3 knock out cochleae. Appendix figure 3.1 shows the labelling seen with a polyclonal antibody

raised to recombinant EHD3 and appendix figure 3.2 shows staining seen with a polyclonal antibody to an EHD3 peptide.

The results reveal that both EHD3 antibodies show non-specific labelling in the inner ear.

4. Ic-Ptprq-EGFP interacts with EHD3-myc

The results of immunoprecipitations performed by Dr. Manju George (see section 4.3.2) were repeated.

HEK 293 EBNA cells were cultured in Dulbecco's Minimal Essential Medium F12-HAM (Sigma) containing 10% fetal bovine serum (Gibco), 1 % Pencillin/Streptomycin (Gibco) and 1% L-Glutamine (Gibco). Cells grown to 90 % confluence in 60 mm dishes were transfected with myc-tagged EHD3 (from Dr. Manju Geroge) and Ic-Ptprq-EGFP using Lipofectamine^{TM} 2000 (Invitrogen). Two dishes were co-transfected with Ic-Ptprq-EGFP and myc-tagged EHD3. The following day, cells were lysed in buffer containing 1 % Triton X 100 + 150 mM NaCl, 50 mM Tris HCl pH 7.6 with 0.1 mM PMSF, 10 mM NaF, 1 mM sodium orthovanadate, 2 mM benzamidine for 1 hour at 4˚C. Lysates were centrifuged for 10 mins and supernatants were collected in fresh tubes. The protein G-sepharose (pG) beads were first washed thrice in PBS and blocked with 3 % BSA in PBS for at least half an hour before being used for preclearing. Supernatants were pre-cleared with blocked pG beads (10 μl) for about an hour. The tubes were centrifuged and supernatants collected in fresh tubes. 15 μl of each sample was transferred to a fresh tube to be used as loading controls. To each of the supernatants, 50 μl of 9E10 (anti-myc) was added and left overnight on a rotator at 4˚C.

The following day, ~10 μl bed volume of pG beads (blocked with 3 % BSA and washed thrice with PBS and resuspended in lysis buffer) was added to each sample and left on the rotator for at least 1 hour at room temperature. The beads were then pelleted and washed (three 5 minute washes in lysis buffer) and the immunoprecipitated proteins from each sample were eluted into 20 μl of 2x RSB. The samples were separated by SDS-PAGE on a 15% gel.

The results show that Ic-Ptprq-EGFP co-immunoprecipitates with myc-EHD3 from lysates of co-transfected cells.

5. Attempts to improve the efficiency of recombinant Ptprq expression in CL4 cells.

Several attempts to optimise the transfection conditions to improve the efficiency of recombinant full-length Ptprq expression in CL4 cells were unsuccessful. Oganesian et al., (2003) reported that the full-length form of Ptprq displayed a higher proapoptotic activity than the cytoplasmic isoform, consistent with the activity of the former against membrane PIs. Similarly, the expression of recombinant full-length Ptprq at the apical surface of transfected CL4 cells may create a great growth disadvantage resulting in very low expression levels of the recombinant protein. Therefore, the WPE motif that is reported to be responsible for the PIPase activity of Ptprq was mutated to WPD using a site-directed mutagenesis kit (Promega). A similar mutant cytoplasmic isoform of Ptprq was reported to have no effect on the growth rate of transfected cells compared to that of the wild-type isoform. However, transfection of CL4 cells with the mutant full-length construct did not increase the expression levels of the protein.
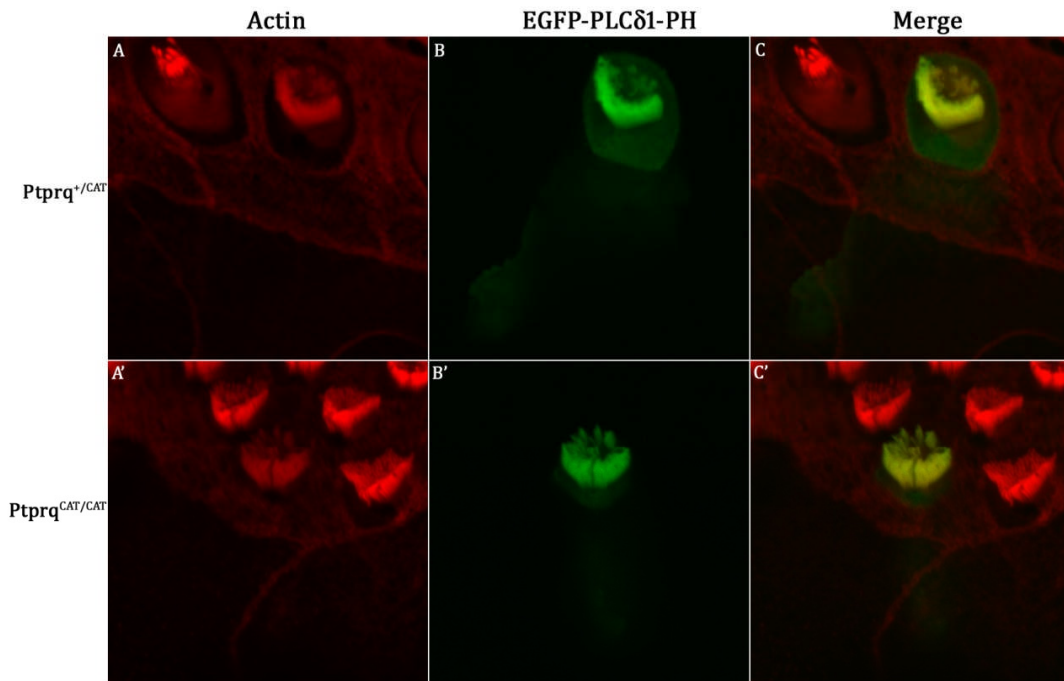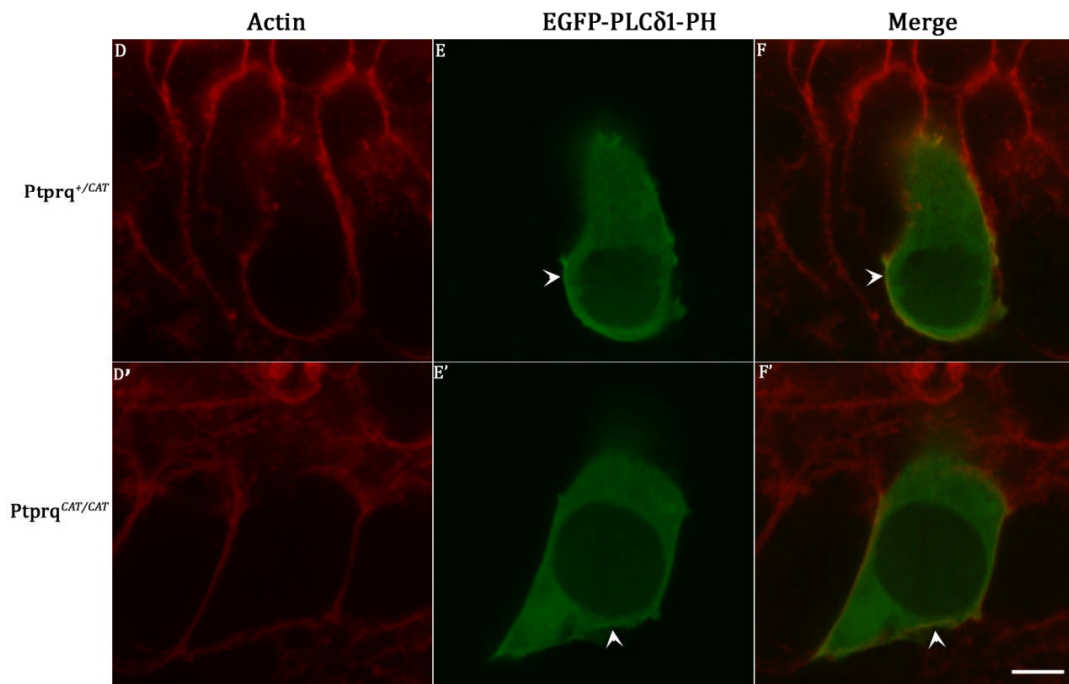
Figure 3.3: Distribution of EGFP-PLCδ1-PH in the cochlear hair cells of Ptprq$^{+/CAT}$ (panels A-F) and Ptprq$^{CAT/CAT}$ mice (panels A'-F'). Red represents phalloidin counter-stain and green represents anti-GFP labeling of transfected cells. Panels B, C and B', C' show that this reporter is present in the hair bundles of Ptprq$^{+/CAT}$ and Ptprq$^{CAT/CAT}$ hair cells, respectively. The protein is diffusely distributed in the cytoplasm (panels E, F and E', F') and localised to the basolateral surface (arrowheads) of these cells. Scale bar 5 μm.
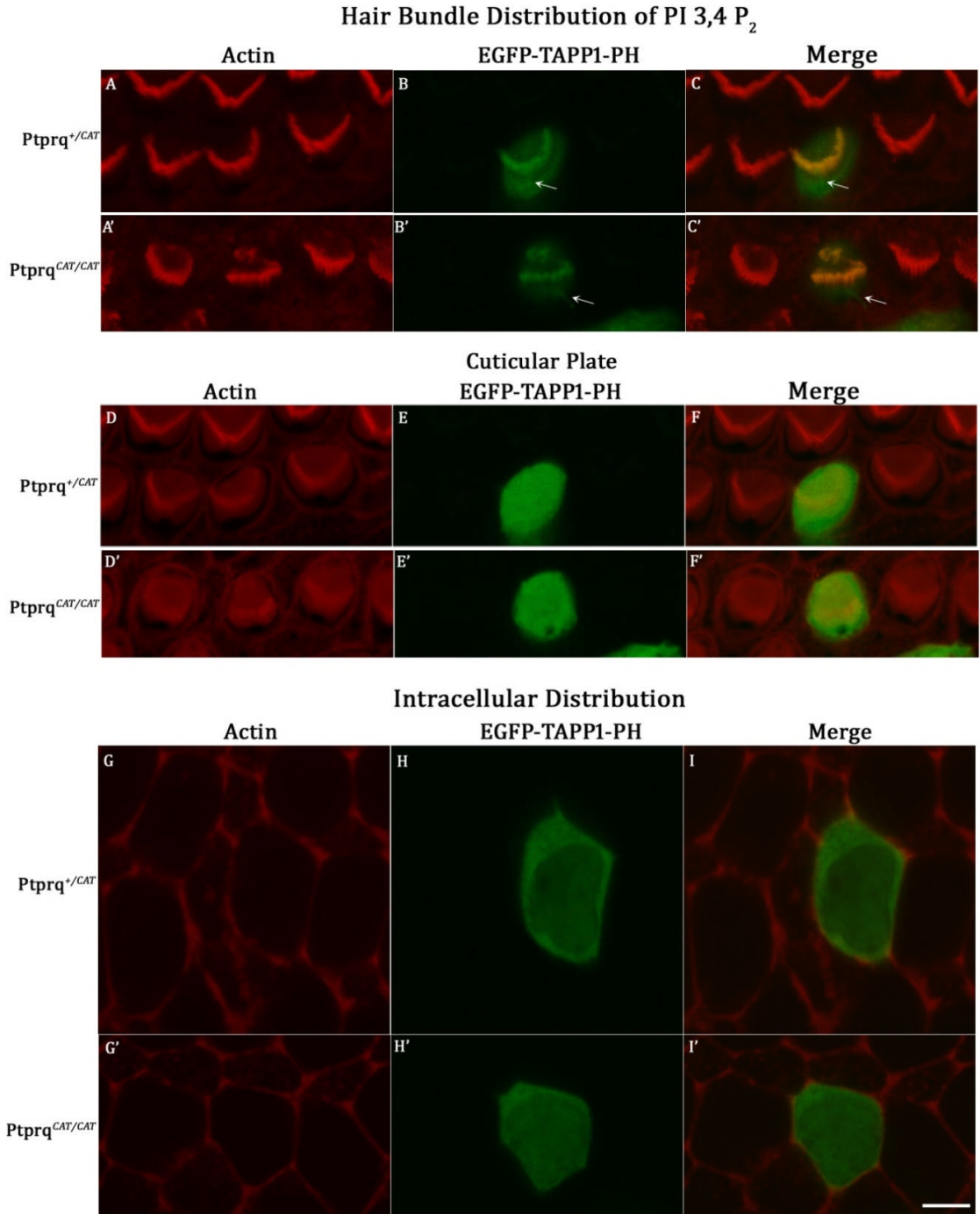
Figure 3.4: Distribution of EGFP-TAPP1-PH in the cochlear hair cells of Ptprq$^{+/CAT}$ (panels A-I) and Ptprq$^{CAT/CAT}$ mice (panels A'-I'). Red represents phalloidin counter-stain and green represents anti-GFP labeling of transfected cells. Panels B, C and B', C' show that this reporter is present in the hair bundles, including the kinocilium (arrows) of Ptprq$^{+/CAT}$ and Ptprq$^{CAT/CAT}$ hair cells, respectively. A strong anti-GFP signal is seen at the level of the cuticular plate (panels E, F and E',F') in these cells. EGFP-TAPP1-PH is also diffusely distributed in the cytoplasm and nucleus of transfected hair cells (panels H, I and H', I'). Scale bar 5 µm.
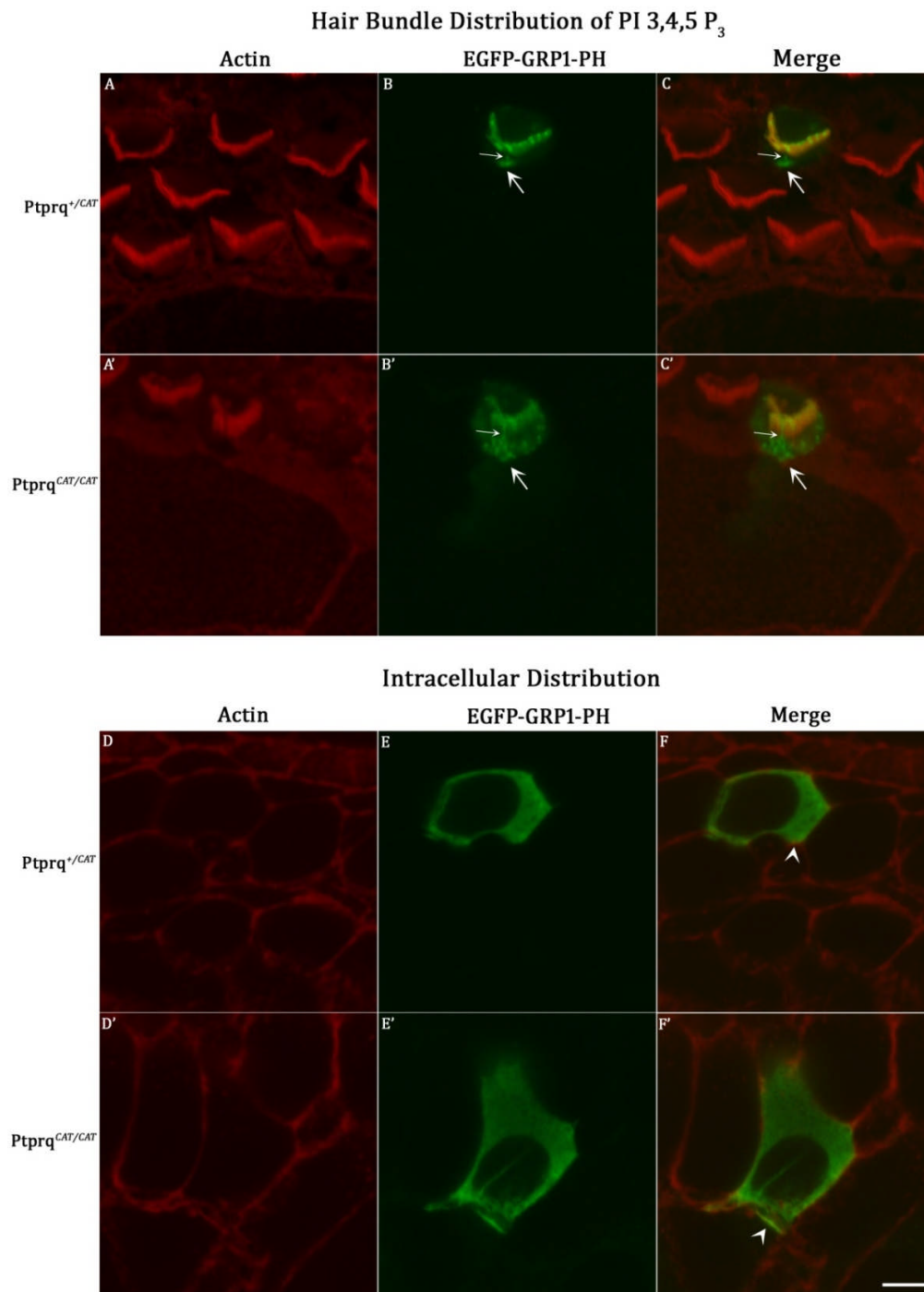
Figure 3.5: Distribution of EGFP-GRP1-PH in the cochlear hair cells of Ptprq$^{+/CAT}$ (panels A-F) and Ptprq$^{CAT/CAT}$ mice (panels A'-F'). Red represents phalloidin counter-stain and green represents anti-GFP labeling of transfected cells. Panels B, C and B', C' show that this reporter is distributed in the hair bundle, kinocilium (small arrows) and in the apical surface around the region of the kinocilium (large arrows) of Ptprq$^{+/CAT}$ and Ptprq$^{CAT/CAT}$ hair cells, respectively. The protein is also distributed in the cytoplasm (panels E and E') and basolateral surface (arrowheads in panels F and F') of these cells. Scale bar 5 μm.
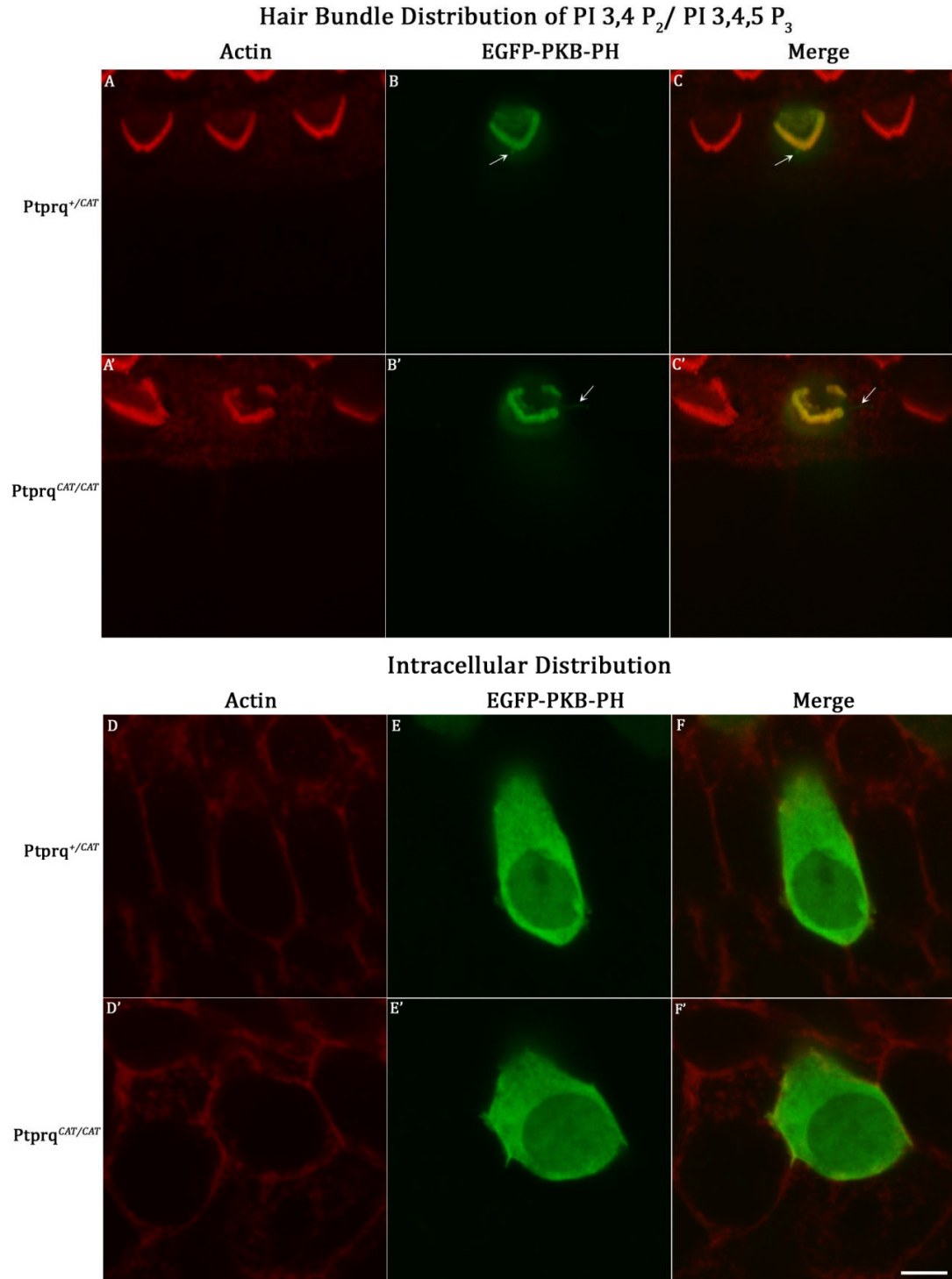
Figure 3.6: Distribution of EGFP-PKB-PH in the cochlear hair cells of Ptprq$^{+/CAT}$ (panels A-F) and Ptprq$^{CAT/CAT}$ mice (panels A'-F'). Red represents phalloidin counter-stain and green represents anti-GFP labeling of transfected cells. Panels B, C and B', C' show that this reporter is present in the hair bundle, including kinocilium (arrows) of Ptprq$^{+/CAT}$ and Ptprq$^{CAT/CAT}$ hair cells, respectively. The protein is also distributed in the cytoplasm and nucleus (panels E, F and E', F') of these cells. Scale bar 5 μm.

Hair Bundle Distribution of PI 3 P
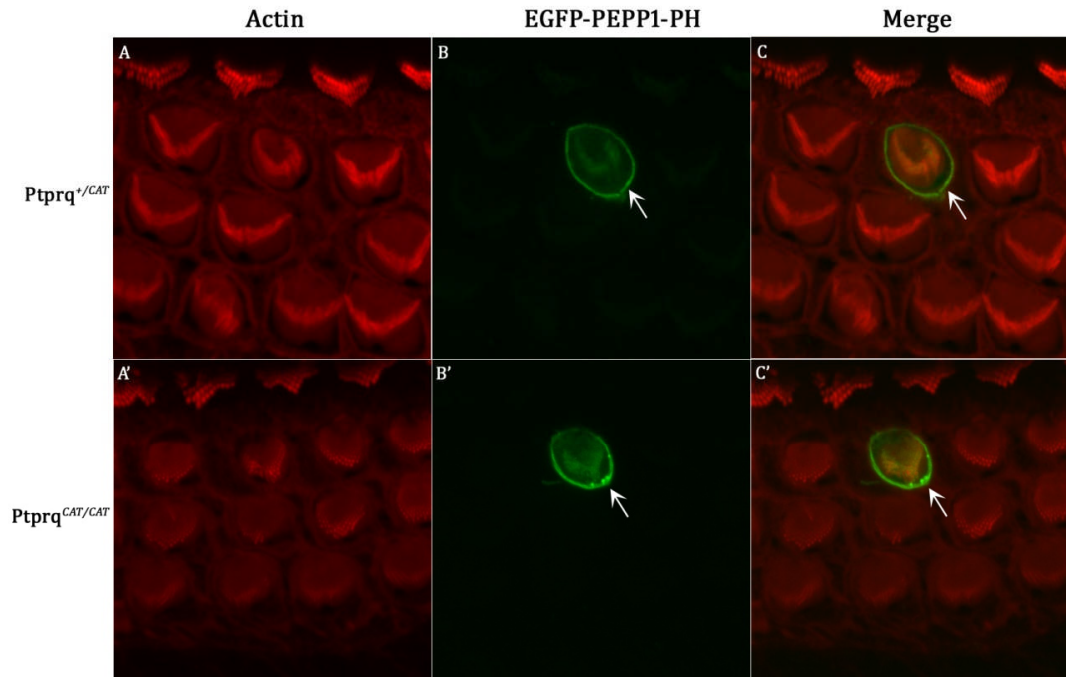
Intracellular Distribution
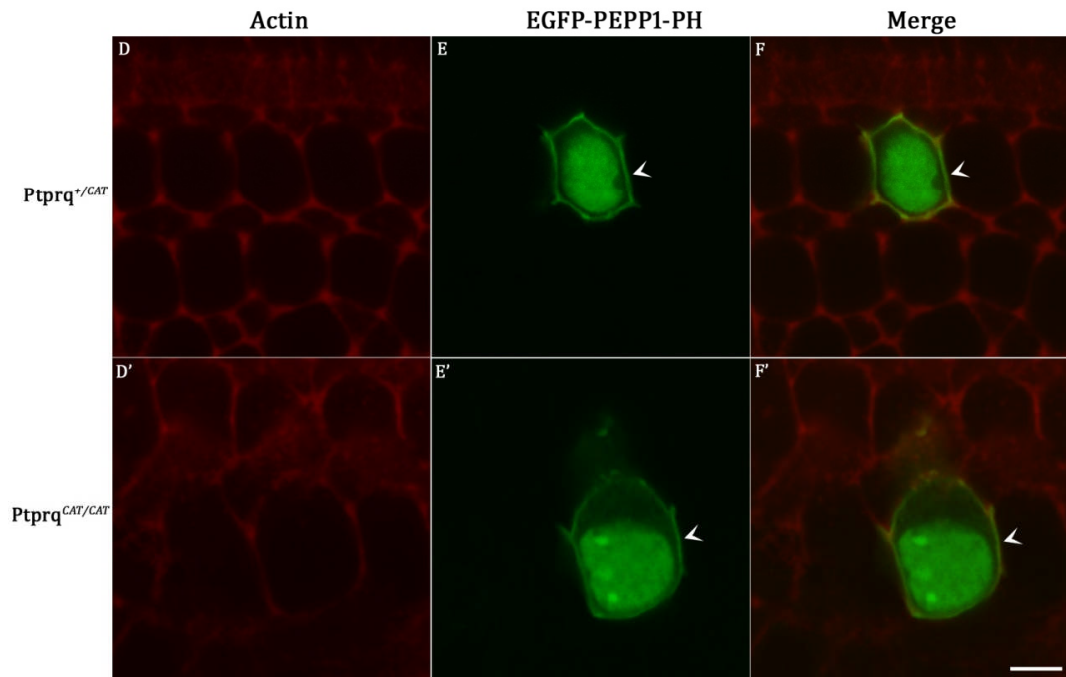
Figure 3.7: Distribution of EGFP-PEPP1-PH in the cochlear hair cells of Ptprq$^{+/CAT}$ (panels A-F) and Ptprq$^{CAT/CAT}$ mice (panels A'-F'). Red represents phalloidin counter-stain and green represents anti-GFP labeling of transfected cells. Panels B, C and B', C' show that this reporter is present in the hair bundle and apical junction (arrows) of Ptprq$^{+/CAT}$ and Ptprq$^{CAT/CAT}$ hair cells, respectively. The protein is also distributed in the nucleus (panels E, F and E', F') and basolateral surface (arrowheads) of these cells. Scale bar 5 μm.
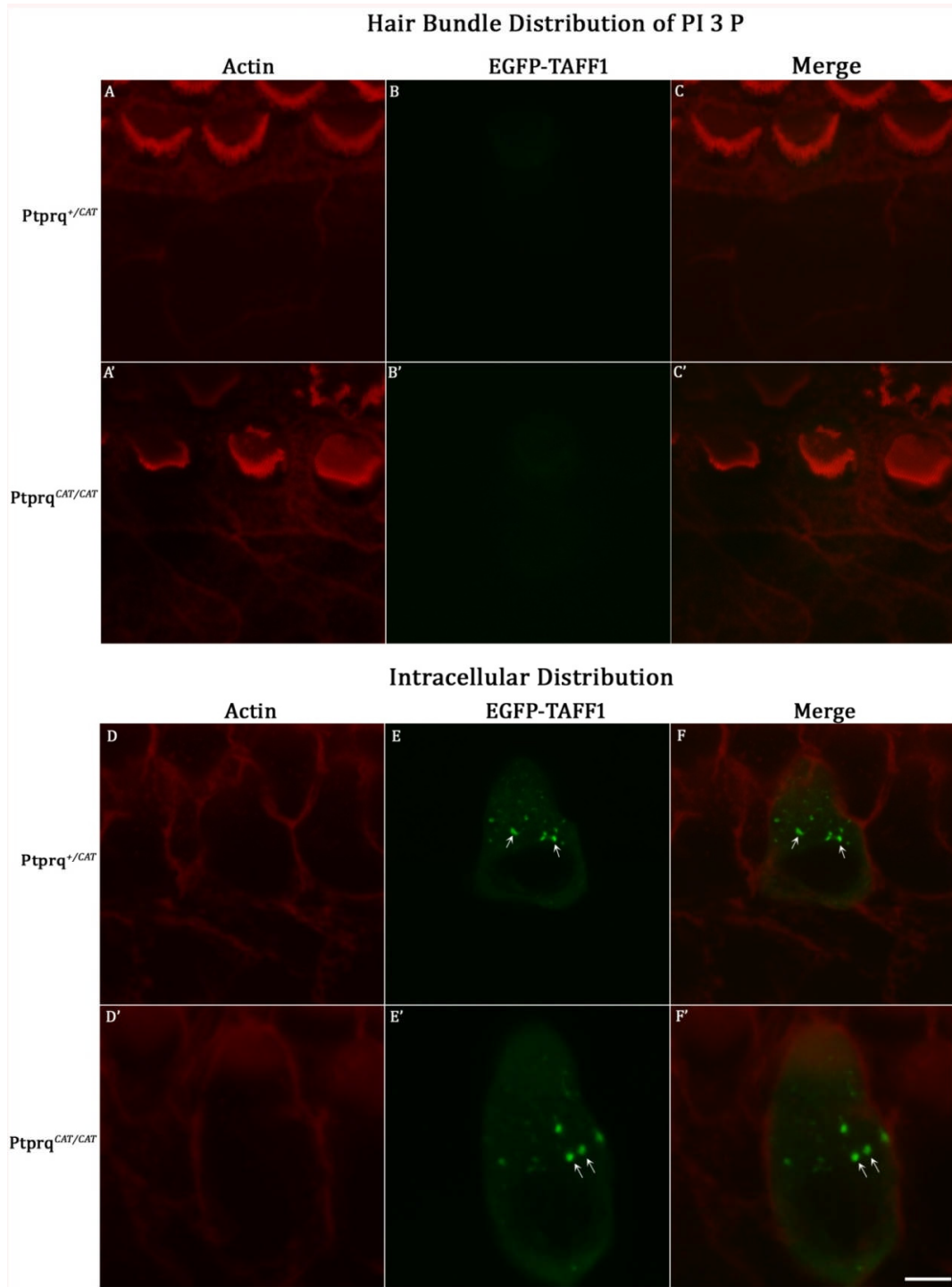
Figure 3.8: Distribution of EGFP-TAFF1 in the cochlear hair cells of Ptprq$^{+/CAT}$ (panels A-F) and Ptprq$^{CAT/CAT}$ mice (panels A'-F'). Red represents phalloidin counter-stain and green represents anti-GFP labeling of transfected cells. Panels B, C and B', C' show that this reporter is excluded from the hair bundles of Ptprq$^{+/CAT}$ and Ptprq$^{CAT/CAT}$ hair cells, respectively. The protein is found as dense granules in the cytoplasm (arrows in panels E, F and E', F') of these cells. Scale bar 5 μm.

Hair Bundle Distribution of PI 4 P

Actin	EGFP-FAPP1-PH	Merge

Intracellular Distribution

Actin	EGFP-FAPP1-PH	Merge
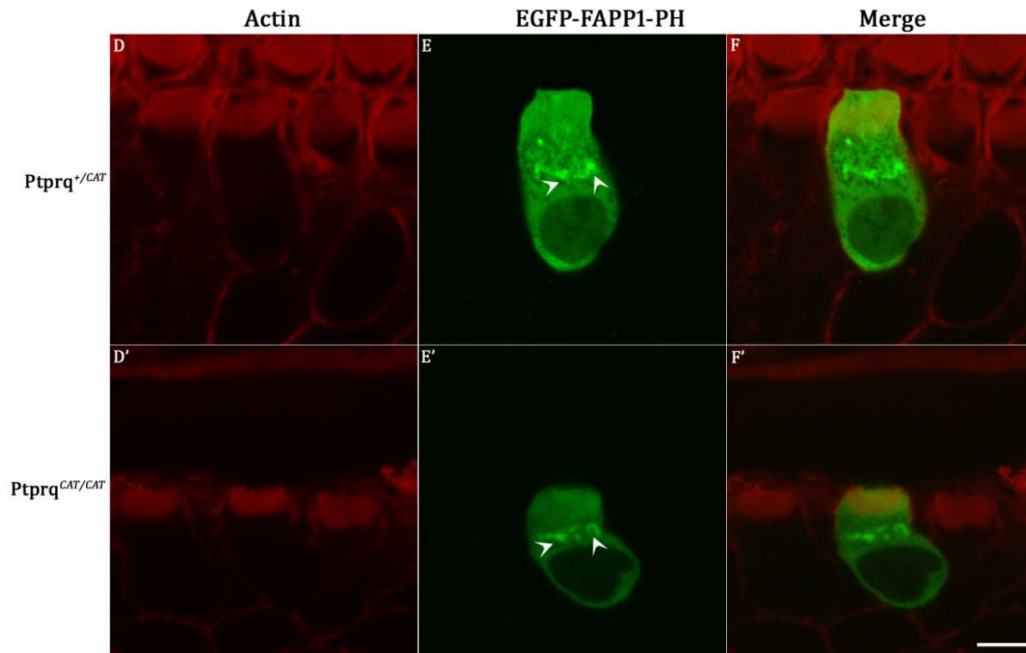
Figure 3.9: Distribution of EGFP-FAPP1-PH in the cochlear hair cells of Ptprq[+/CAT] (panels A-F) and Ptprq[CAT/CAT] mice (panels A'-F'). Red represents phalloidin counter-stain and green represents anti-GFP labeling of transfected cells. Panels B and B' show that this reporter is distributed in the hair bundle, kinocilium and in the apical surface around the region of the kinocilium (arrows) of Ptprq[+/CAT] and Ptprq[CAT/CAT] hair cells, respectively. The protein is also localized to grouped puncti in the cytoplasm (arrowheads in panels E and E') of these cells. Scale bar 5 μm.

SD-Galactose (-UL) plate at 37°C
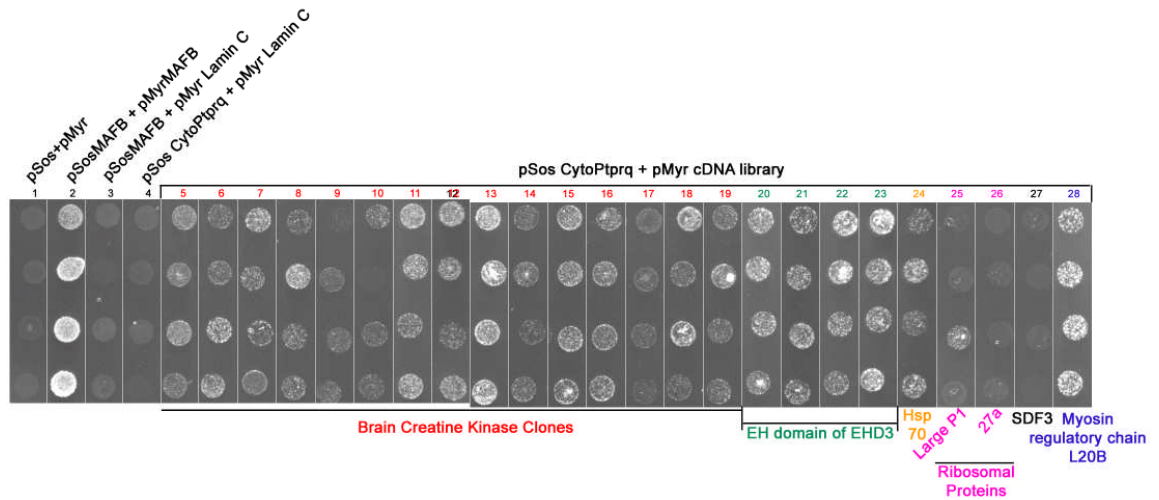
Figure 4.4a: Growth of the co-transformants on SD/galactose plates at 37°C. Lane1 is temperature revertant control, lane 2 is positive control, lane 3 is negative control, lane 4 shows that Ic domain of Ptprq does not interact with the myristylation signal. The lanes coloured in red (5-19) represent clones expressing the brain isoform of creatine kinase, the lanes in green (20-23) represent the clones expressing the EH domain of EHD3, lane 24 represents the clone expressing Hsp70, lanes 25 and 26 represent the clones expressing two ribosomal proteins, lane 27 represents a clone expressing SDF3 and lane 28 represents the clone expressing the myosin regulatory light chain L20B.

SD-Glucose (-UL) plate at 37°C
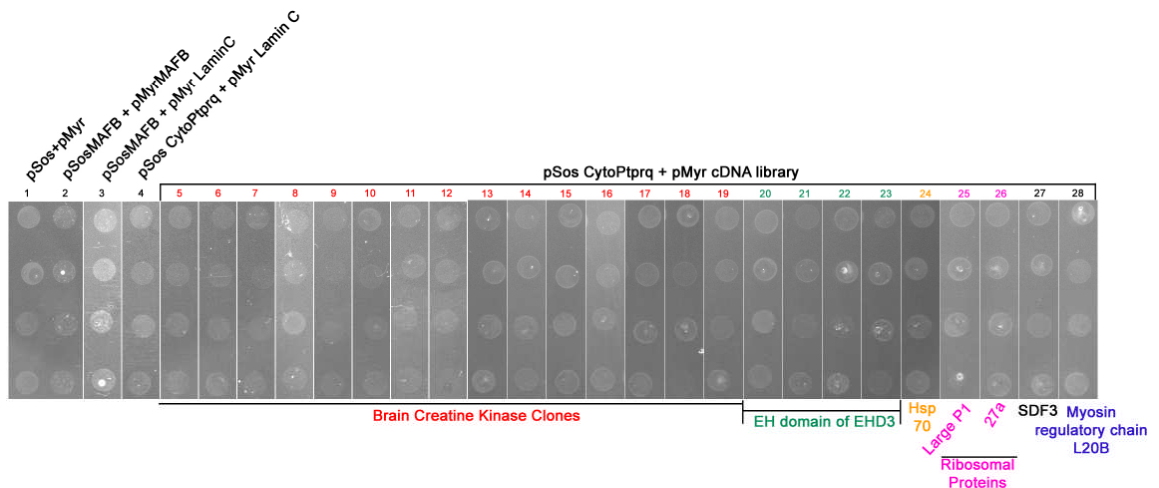
Figure 4.4b: Growth of the co-transformants on SD/glucose plates at 37°C. Lanes as above.
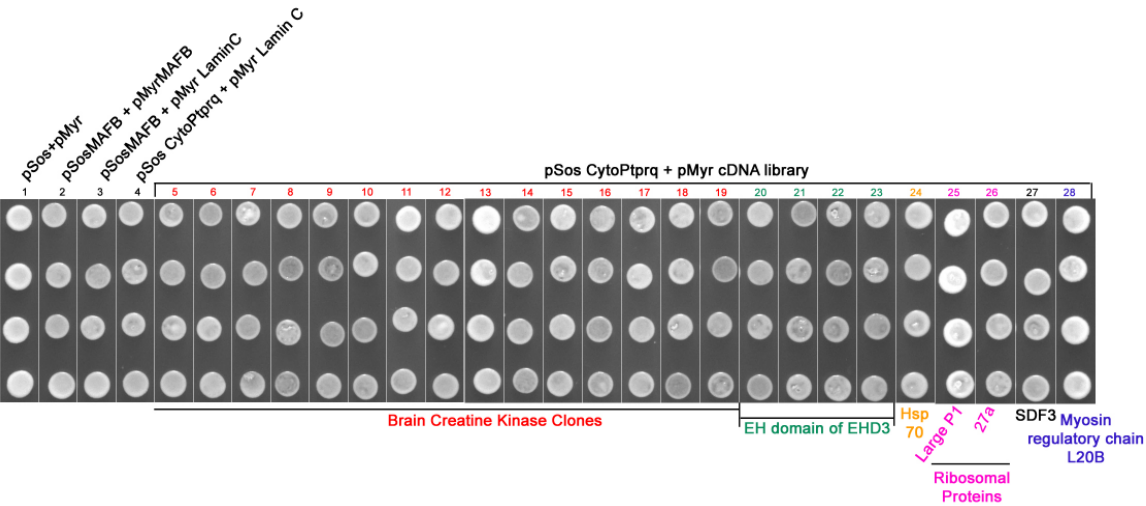
Figure 4.4c: Growth of the co-transformants on SD/glucose plates at 25°C. Lanes as above.
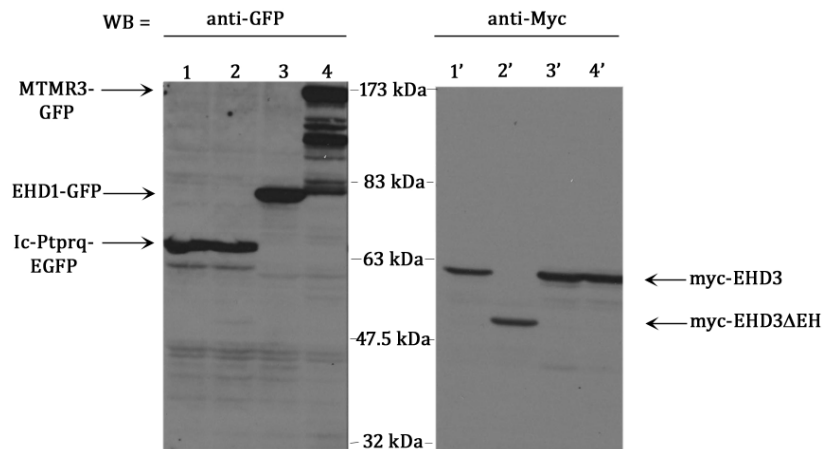
Figure 4.5a: Western blots of lysates (1 mg) of co-transfected HEK293 cells blotted with anti-GFP (lanes 1-4) and anti-myc (lanes 1'-4'). Lanes 1 and 1' represent lysates of cells co-transfected with Ic-Ptprq-EGFP and myc-EHD3. Lanes 2 and 2' represent lysates of cells co-transfected with Ic-Ptprq-EGFP + myc-EHD3ΔEH. Lanes 3 and 3' represent lysates of cells co-transfected with EHD1-GFP + myc-EHD3. Lanes 4 and 4' represent lysates from cells co-transfected with MTMR3-GFP + myc-EHD3.
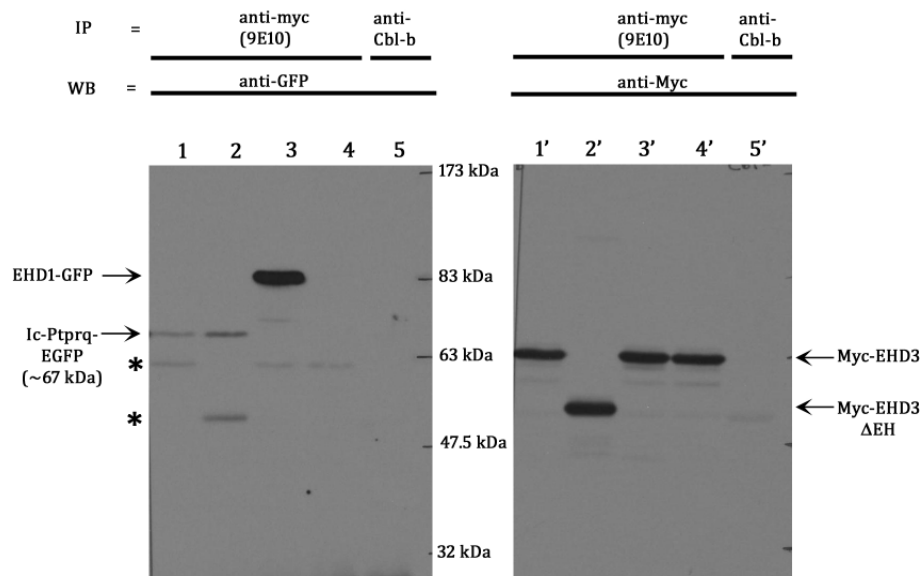
Figure 4.5b: Results of co-immunoprecipitations of lysates from co-transfections as above. Lanes 1 and 1', and 5 and 5' represent co-transfection of Ic-Ptprq-EGFP + myc-EHD3. Lanes 2 and 2' represent c-transfection of Ic-Ptprq-EGFP and myc-EHD3ΔEH. Lanes 3 and 3' represent co-transfections of EHD1-GFP + myc-EHD3. Lanes 4 and 4' represent co-transfection of MTMR3-GFP + myc-EHD3. Lysates from all co-transfections were immunoprecipitated with anti-myc (9E10) (lanes 1-4 and 1'-4'). Lysate from Ic-Ptprq-EGFP + myc-EHD3 co-transfection was also subjected to immunoprecipitation with a control antibody, anti-Cbl-b (lanes 5 and 5'). Lanes 1-5 were immunoblotted with anti-GFP and lanes 1'-5' were immunoblotted with anti-myc. Asterisk in anti-GFP blot indicates non-specific bands observed on immunoblotting with anti-GFP.
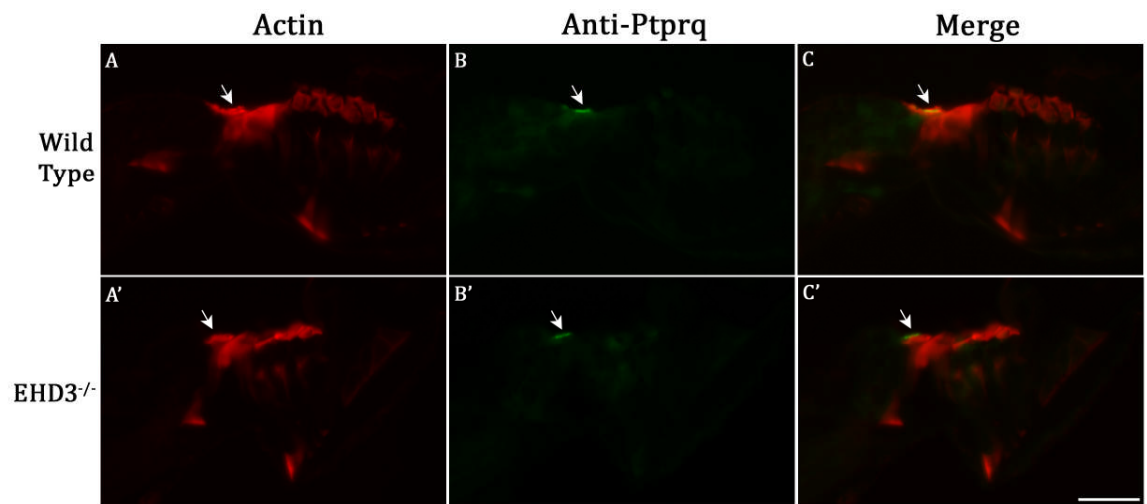
Figure 4.6: Anti-cytoPtprq staining in P30 wild-type (panels A-C) and EHD3$^{-/-}$ (panels A'-C') cochlea. Red represents phalloidin counter-stain and green represents anti-cytoPtprq labeling. Arrows in panels A-C and A'-C' show that the antibody labels the hair bundles of the IHC in the cochlea of wild-type and EHD3$^{-/-}$ mice, respectively. Scale bar is 25 μm.
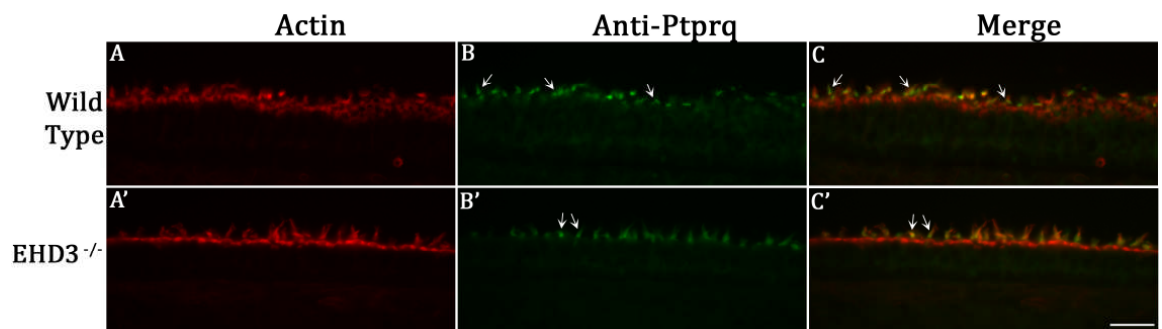
Figure 4.7: Anti-cytoPtprq staining in P30 wild type (panels A-C) and EHD3$^{-/-}$ (panels A'-C') utricular maculi. Red represents phalloidin counter-stain and green represents anti-cytoPtprq labeling. Arrows in panels B, C and B', C' show that the antibody labels hair bundles in the maculi of wild-type and EHD3$^{-/-}$ mice, respectively. Scale bar is 25 μm.
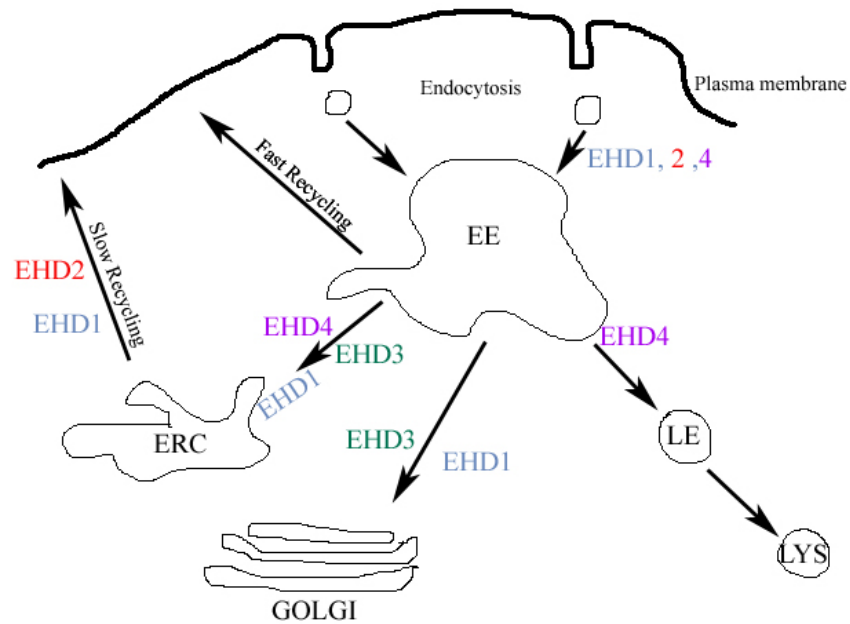
Figure 4.9a: The EHDs are involved in the various steps in the endocytic recycling in cells. The diagram is adapted from Naslasky and Caplan, 2005; Naslavsky et al., 2006; George et al., 2007; Caplan and Grant 2008. ERC is endocytic recycling compartment; EE is early endosome; LE is late endosome and LYS is lysosome.
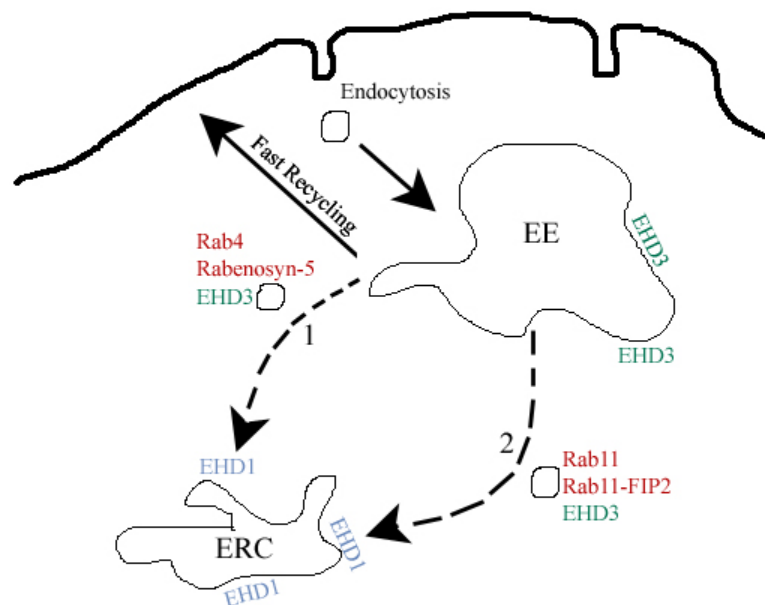
Figure 4.9b: Model to depict the transient interaction between EHD1 and 3 that facilitates the transfer of cargo from the early endosome (EE) to the endocytic recycling complex (ERC). The diagram is adapted from Naslavsky et al., 2006.
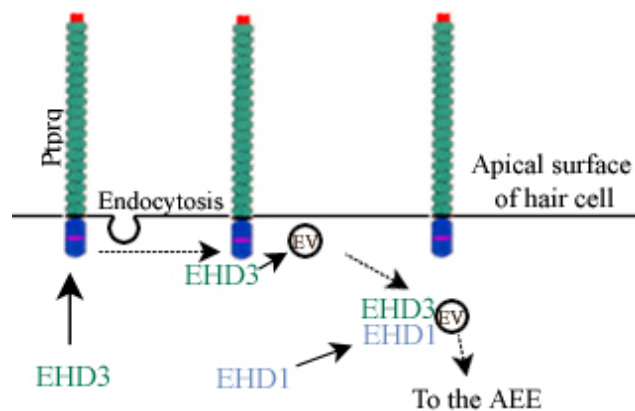
Figure 4.10a: Model suggesting the role of Ptprq in regulating endocytosis at the apical surface of hair cells. EHD3 may be recruited to the site of endocytosis by an interaction with the intracellular domain of Ptprq. EHD3 may then reattach to the endocytic vesicle (EV) and direct it to the apical early endosome (AEE) via an interaction with EHD1 which is known to be involved in the transfer of endocytosed material to the EE.
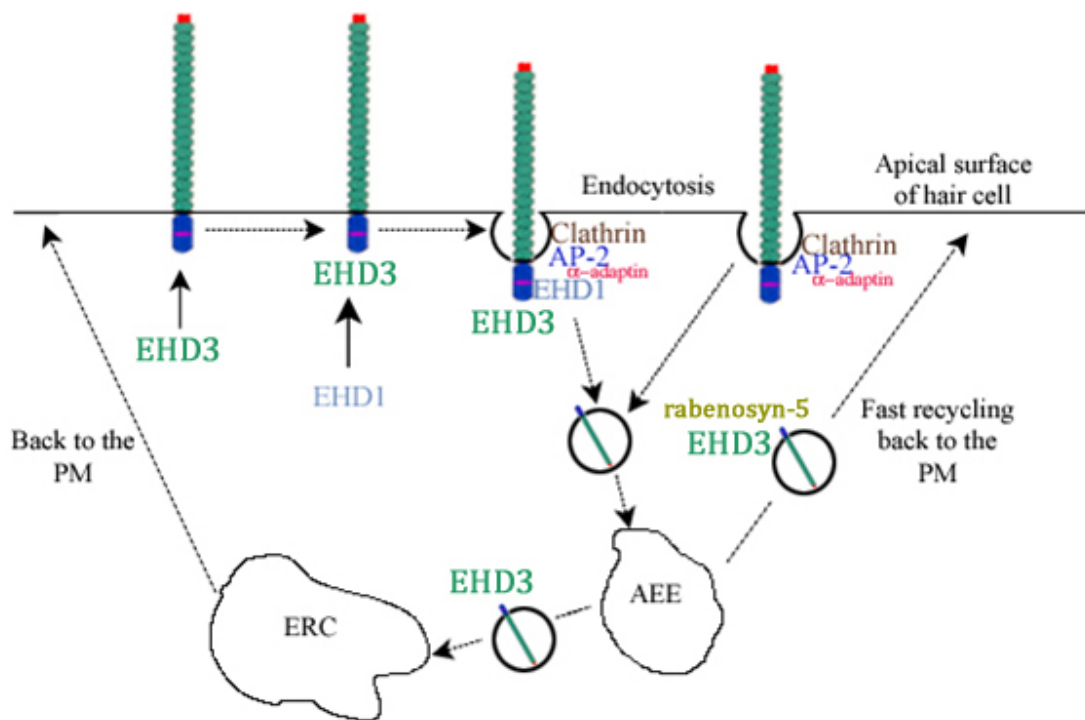
Figure 4.10b: Model suggesting the role of EHD3 in the endocytic recycling of Ptprq at the apical surface of hair cells. EHD3 may be involved in recycling of internalised Ptprq back to the plasma membrane either after delivery to the endocytic recycling complex (ERC) or by the 'fast recycling pathway' (see text). In addition, EHD3 may be recruited to the apical surface via an interaction with Ptprq, where EHD3 may direct the assembly of the endocytic machinery via EHD1 (see text). The endocytosed Ptprq may be recycled back to the plasma membrane (PM) as above.
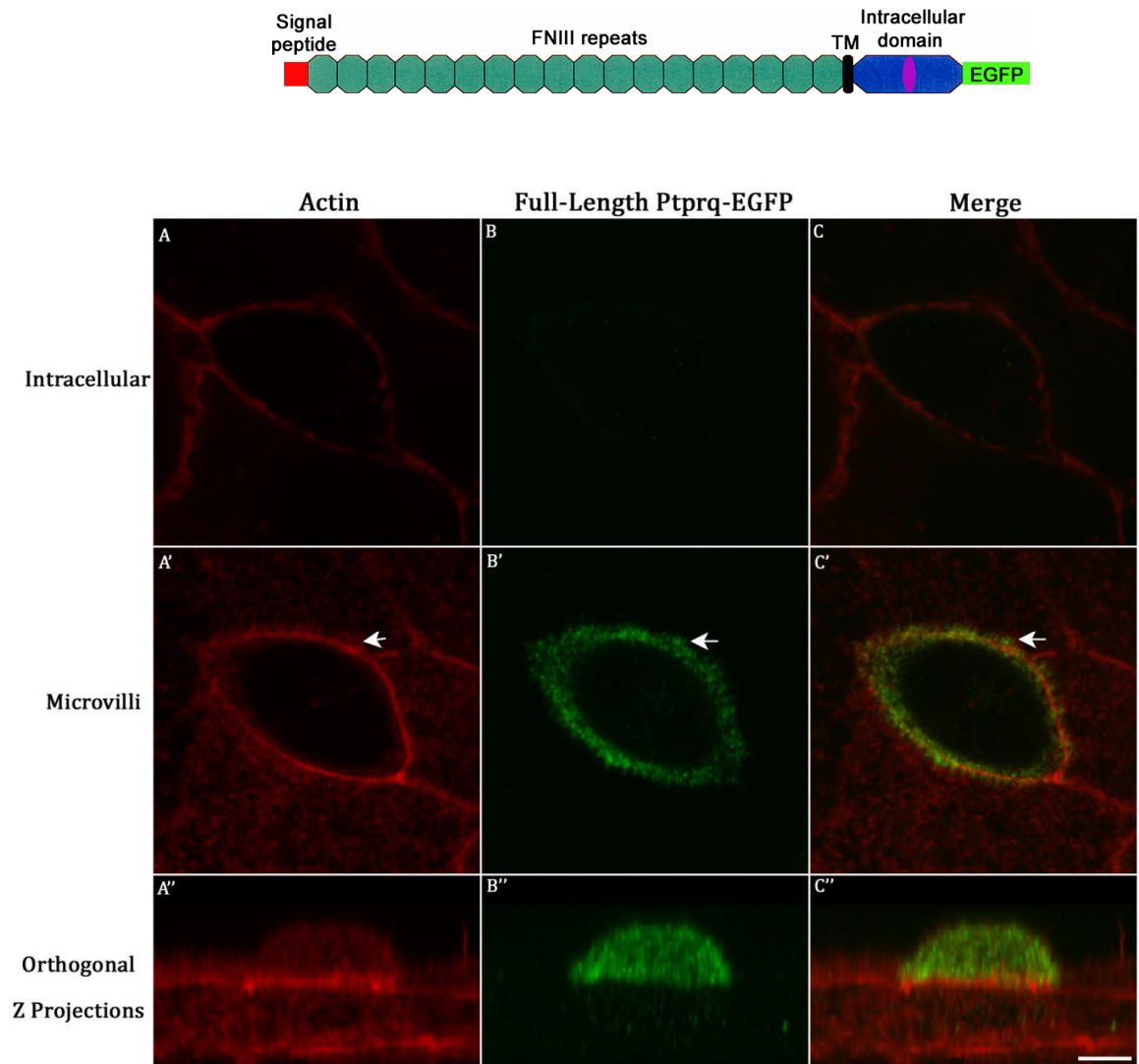
Figure 5.10: Distribution of full-length Ptprq-EGFP in transfected CL4 cells. Panels B, B' and B'' show that the recombinant protein is targeted to the apical surface of the cell. The arrows in panels A', B' and C' point to the apical microvilli that label with anti-GFP. 5 μm scale bar.
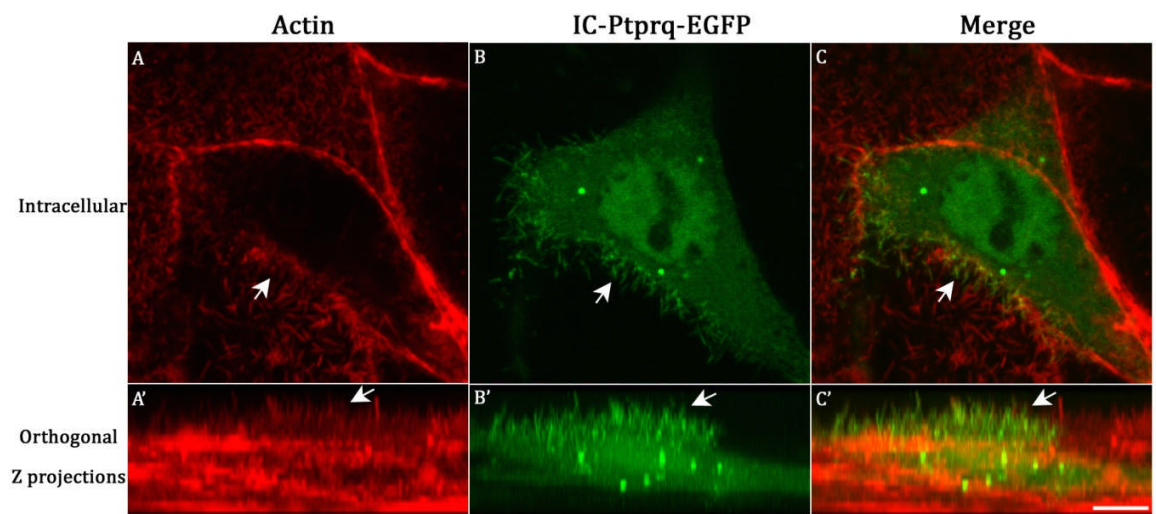
Figure 5.11: Distribution of EGFP-tagged intracellular domain of Ptprq in transfected CL4 cells. Panels B and B' show that the recombinant protein is distributed throughout the cell. The arrows in all panels point to the apical microvilli that are labeled by anti-GFP. 5 μm scale bar.

	Actin	TM-IC-Ptprq-EGFP	Merge
Intracellular	A	B	C
Orthogonal Z projections	A'	B'	C'
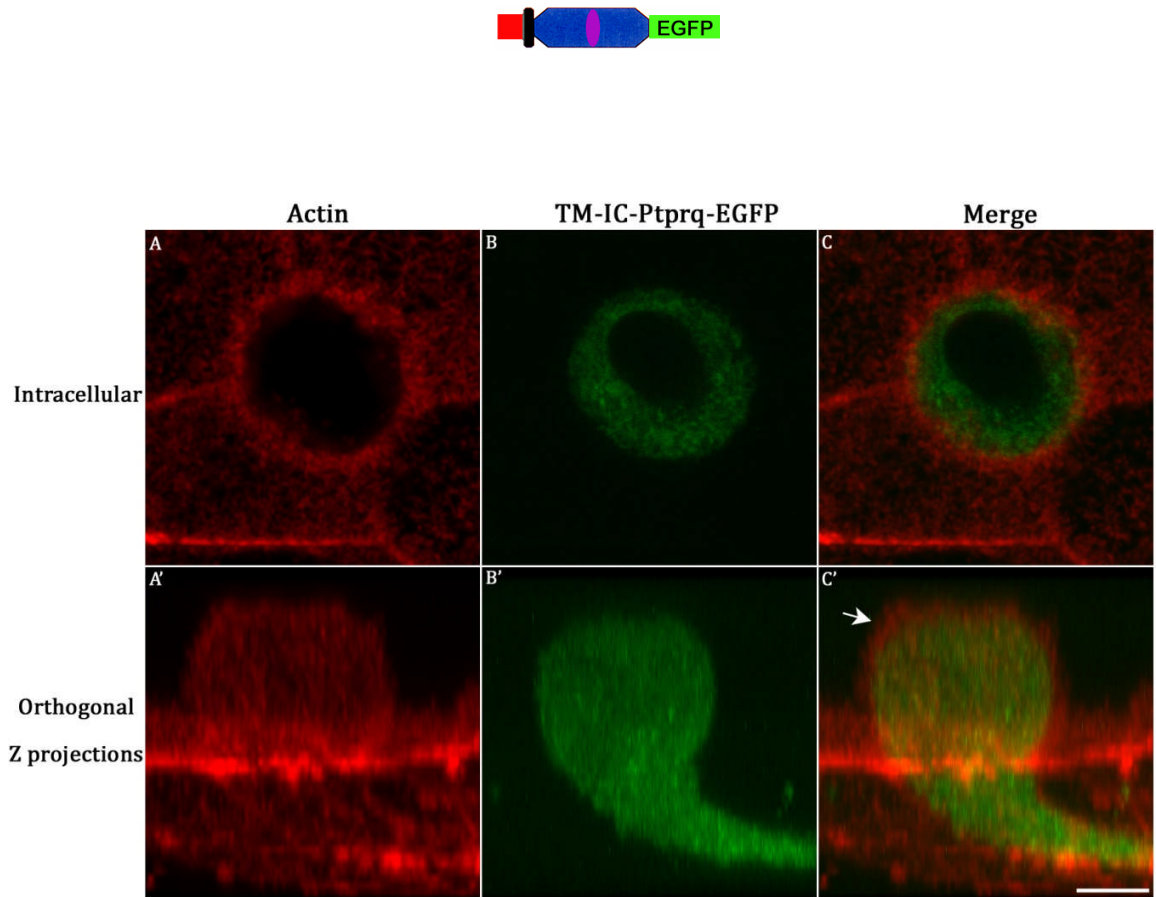
Figure 5.12: Distribution of TM-Ic-Ptprq-EGFP in transfected CL4 cells. Panels B and B' show that the recombinant protein is distributed throughout the cell. The arrow in panel C' points to the apical microvilli that do not label with anti-GFP. 5 μm scale bar.
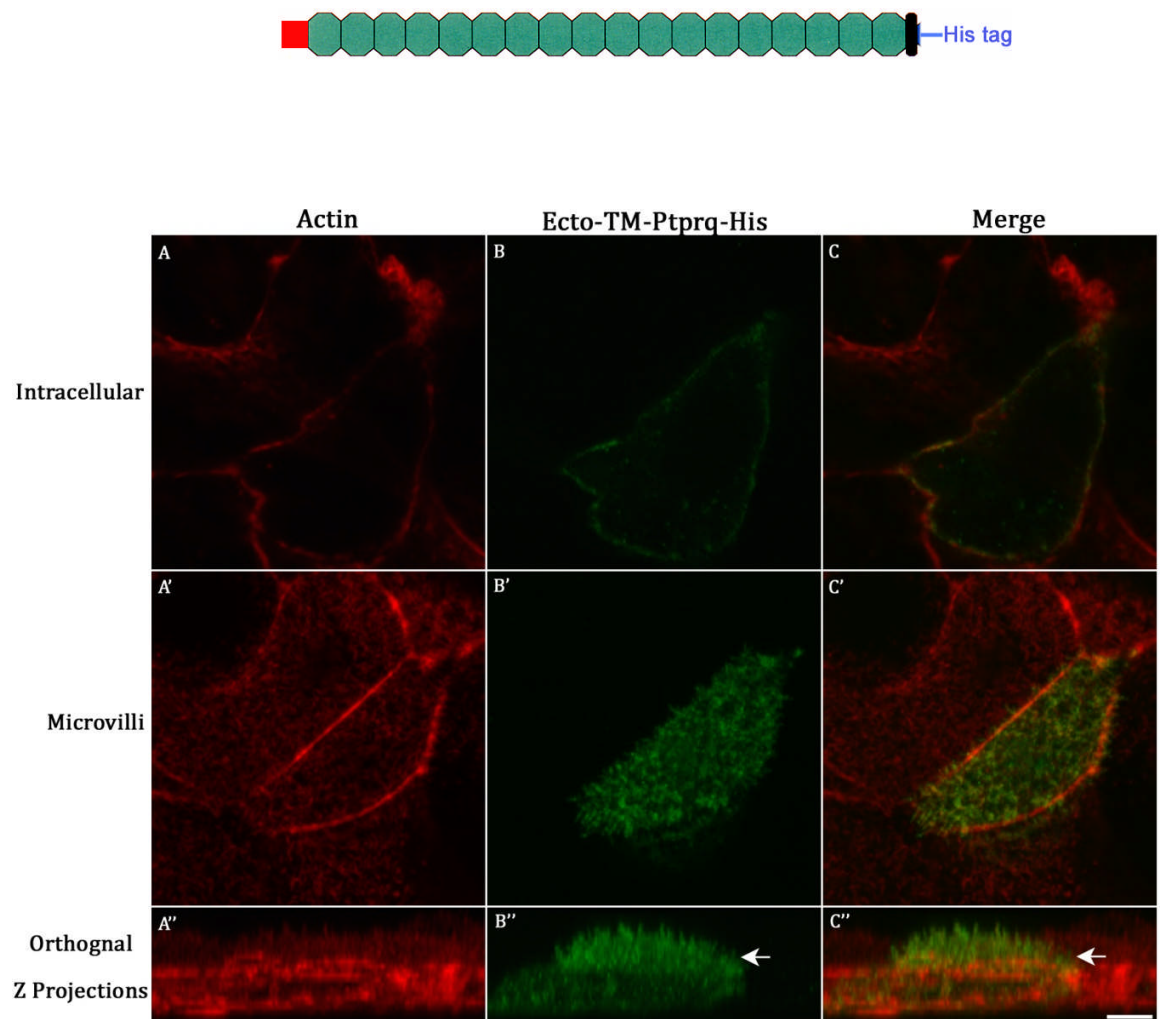
Figure 5.13a: Distribution of Ecto-TM-Ptprq-His in transfected CL4 cells. Panels B, B' and B'' show that the recombinant protein is targeted to the apical surface of the cell. The arrows in panels B'' and C'' point to the apical microvilli that label with anti-GFP. 5 μm scale bar.
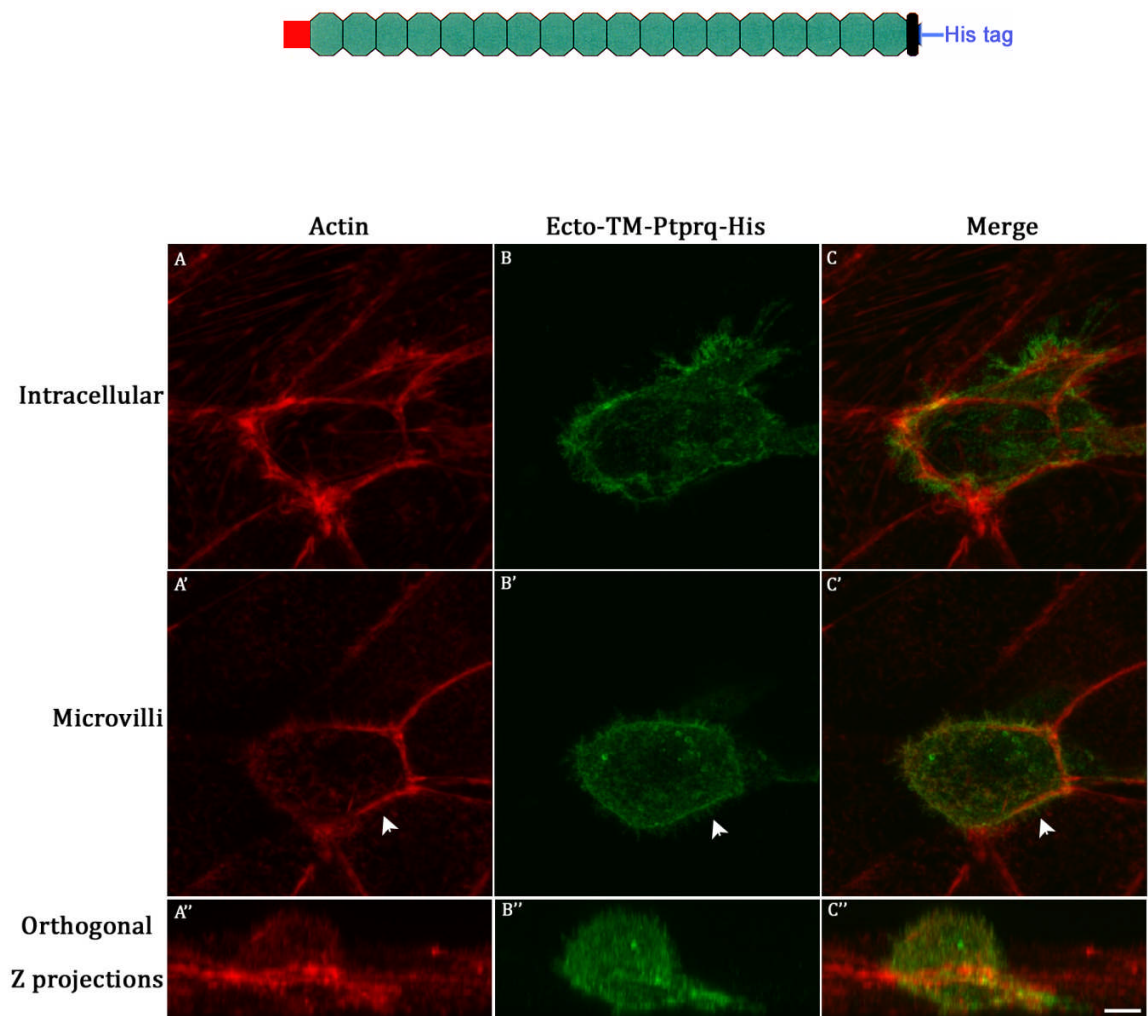
Figure 5.13b: Distribution of Ecto-TM-Ptprq-his in transfected CL4 cells. Panels B, B' and B'' show that the recombinant protein is distributed throughout the cell. The arrows in panels A', B' and C' point to the apical microvilli that label with anti-GFP. 5 μm scale bar.
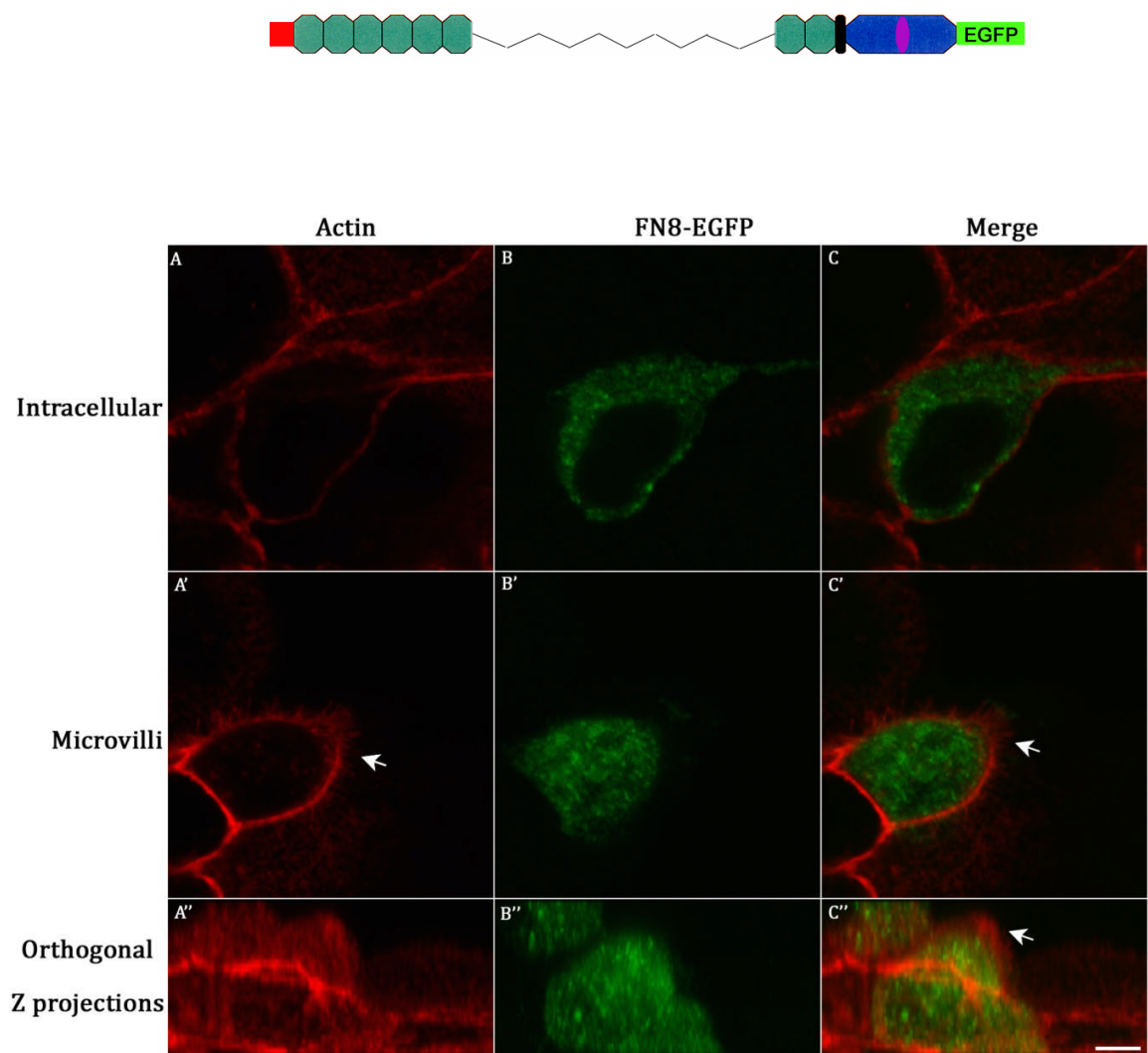
Figure 5.14: Distribution of FN8-EGFP in transfected CL4 cells. Panels B, B' and B'' show that the recombinant protein is distributed throughout the cell. The arrows in panels A', C' and C'' point to the apical microvilli that do not label with anti-GFP. 5 μm scale bar.
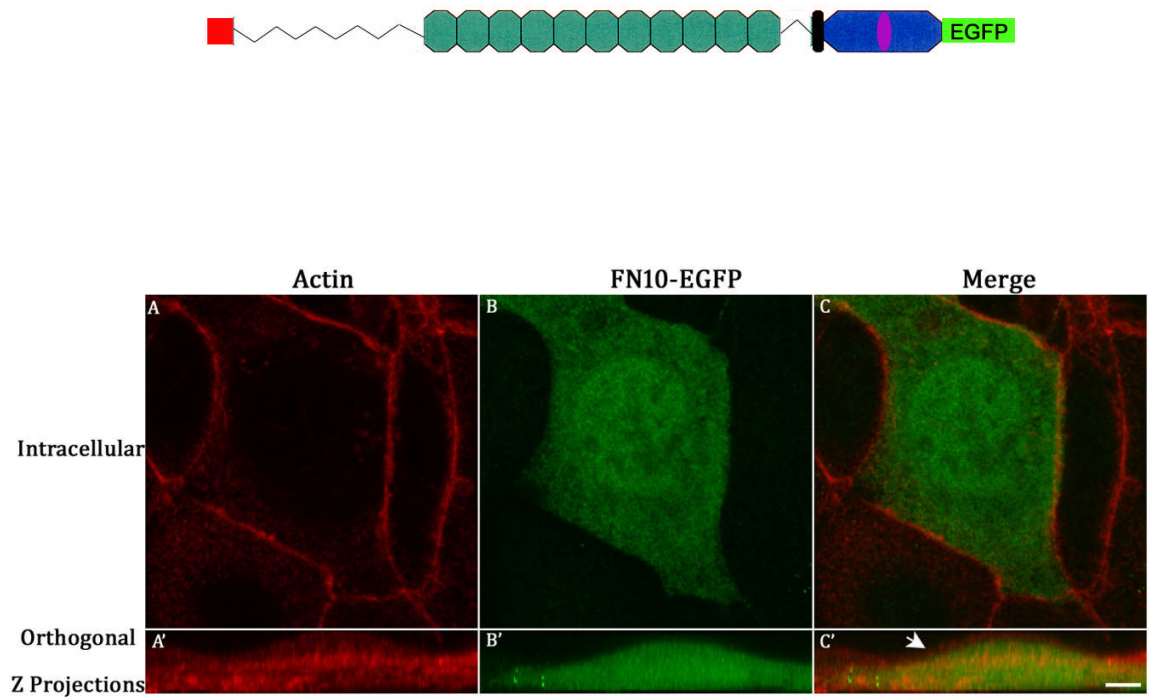
Figure 5.15: Distribution of FN10-EGFP in transfected CL4 cells. Panels B and B' show that the recombinant protein is distributed throughout the cell. The arrow in panel C' points to the apical microvilli that do not label with anti-GFP. 5 μm scale bar.

Full-Length Ptprq EGFP
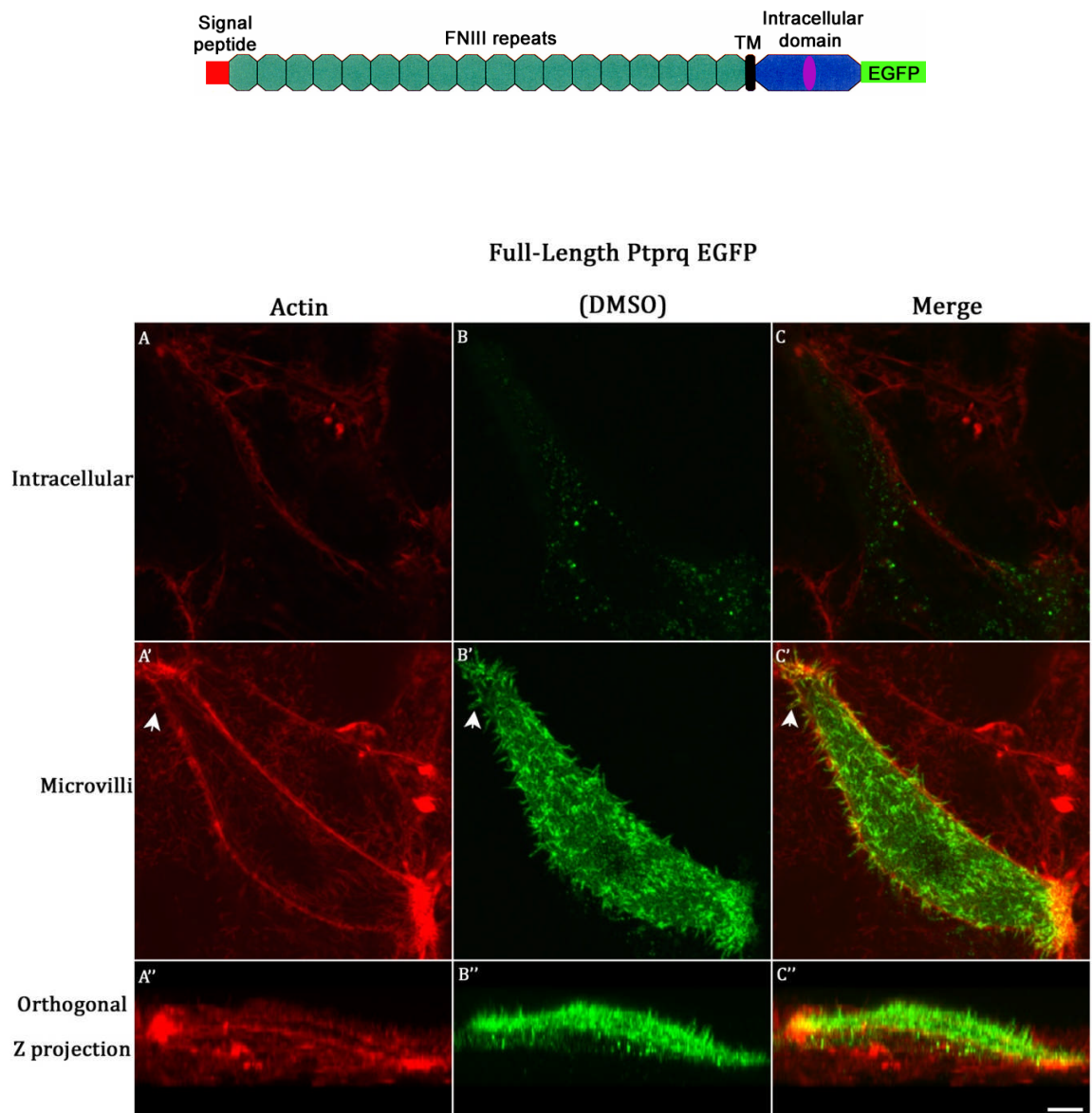
Figure 5.16a: Full-length Ptprq-EGFP expressed in control CL4 cells (DMSO-treated). Panels B, B' and B''
show that the recombinant protein is targeted to the apical surface of the cell. The arrows in panels A', B' and
C' point to the apical microvilli that label with anti-GFP. 5 μm scale bar.

Full-length Ptprq EGFP

	Actin	(tunicamycin)	Merge

Intracellular

Microvilli

Ortogonal
Z projections
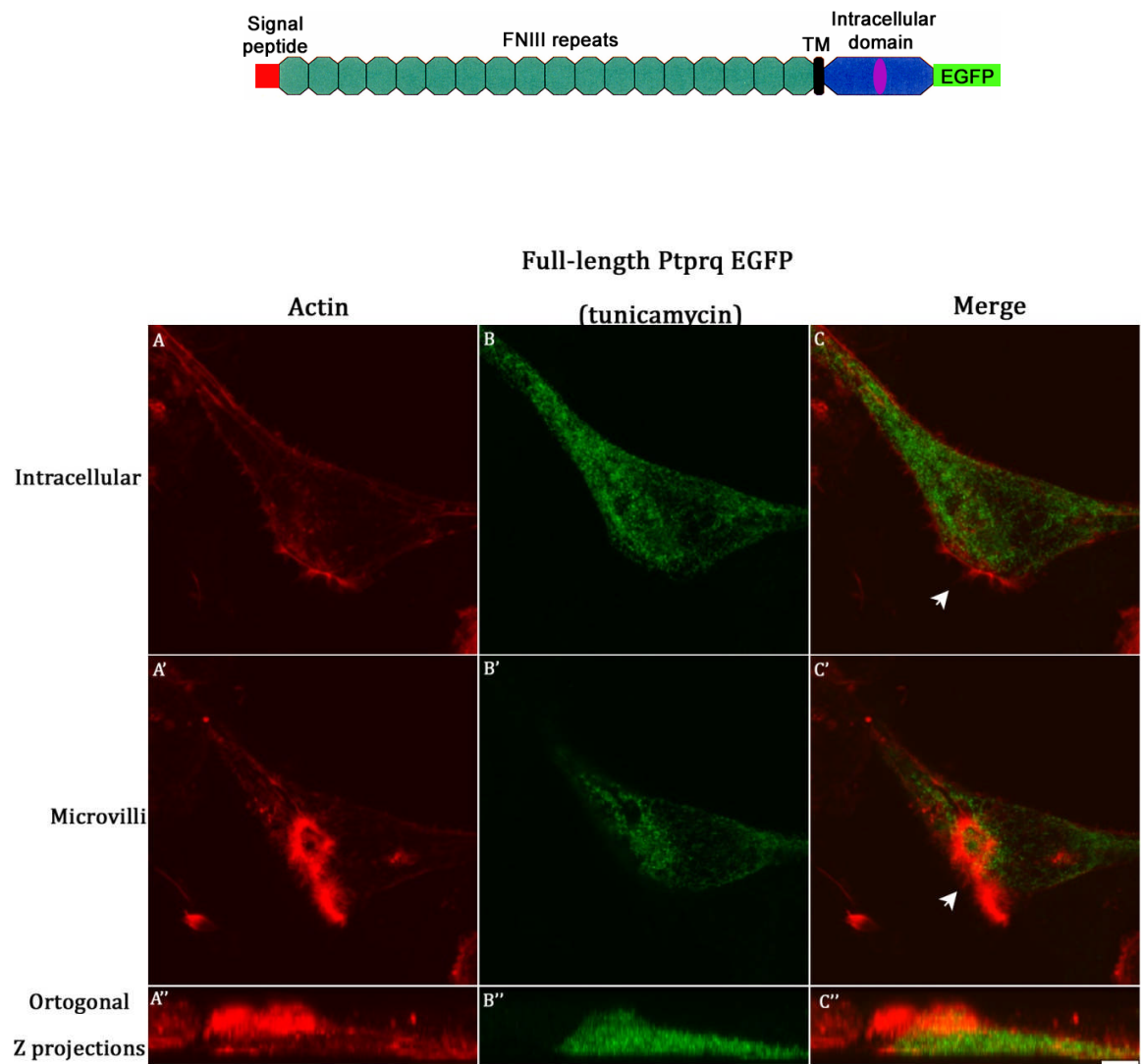
Figure 5.16b: Distribution of full-length Ptprq-EGFP in tunicamycin treated CL4 cells. Panels B, B' and B''
show that the recombinant protein is distributed throughout the cell. The arrows in panels C and C'point to the
microvilli that do not label with anti-GFP. 5 μm scale bar.
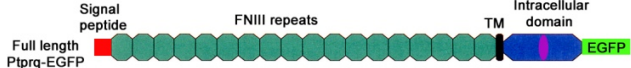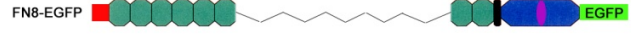
Constructs	Distribution	Number of cells analysed
Full length Ptprq-EGFP	Targets specifically to the apical surface and is found in the microvillar membrane	25
Ic-Ptprq-EGFP	Distributed throughout the cell and is found in the microvillar cytoplasm	20
TM-Ic-Ptprq-EGFP	Distributed throughout the cell but does not reach the microvilli	18
Ecto-TM-Ptprq-His	Targets to the apical surface and is found in the microvillar membrane. Occasional loss of apical targeting observed.	15
FN8-EGFP	Distributed throughout the cell but does not reach the microvilli	19
FN10-EGFP	Distributed throughout the cell but does not reach the microvilli	9
Full length Ptprq-EGFP (In control cells)	Targets to the apical surface and is found in the microvillar membrane	3
Full length Ptprq-EGFP (In tunicamycin-treated cells)	Distributed throughout the cell and does not reach the microvilli	4

Figure 5.17: Results of the Ptprq targeting study. Only full-length Ptprq-EGFP and Ecto-TM-Ptprq-His were able to target specifically to the apical surface of transfected CL4 cells. Therefore, the apical targeting signal may lie along the entire length of the ectodomain and may include the transmembrane domain. In the presence of tunicamycin, full-length Ptprq-EGFP was distributed throughout the cell suggesting that N-glycans in the ectodomain of Ptprq are a major part of the apical targeting signal. Also shown are the number of cells analysed for each construct and condition.
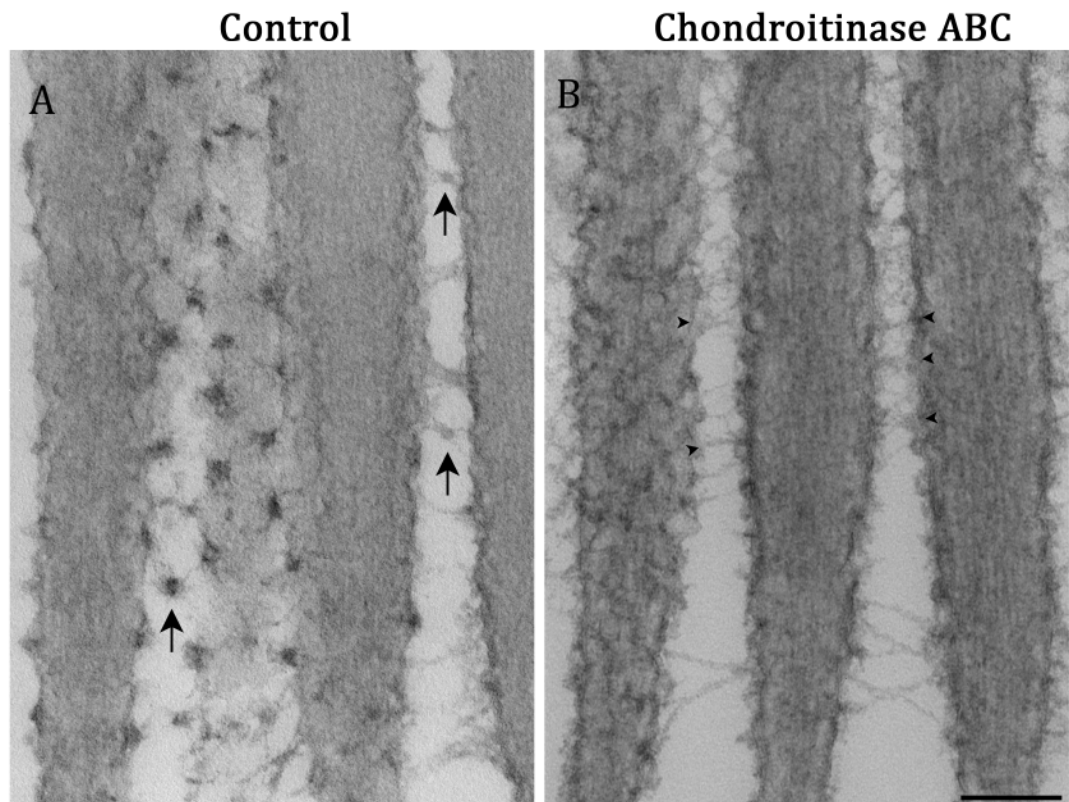
Figure 6.1: Appearance of shaft connectors following chondroitinase ABC treatment of early posthatch chick utricles. Chondroitinase ABC removes the dense particles associated with shaft connectors (compare panels A and B). The arrows in panel A point to dense particles that are suspended from fine strands emerging from adjacent stereocilia. No such dense particles are visible in the chondroitinase ABC treated chick utricles (panel B). The arrowheads in panel B show the fine strands that remain after chondroitinase ABC digestion. Scale bar 200 nm.
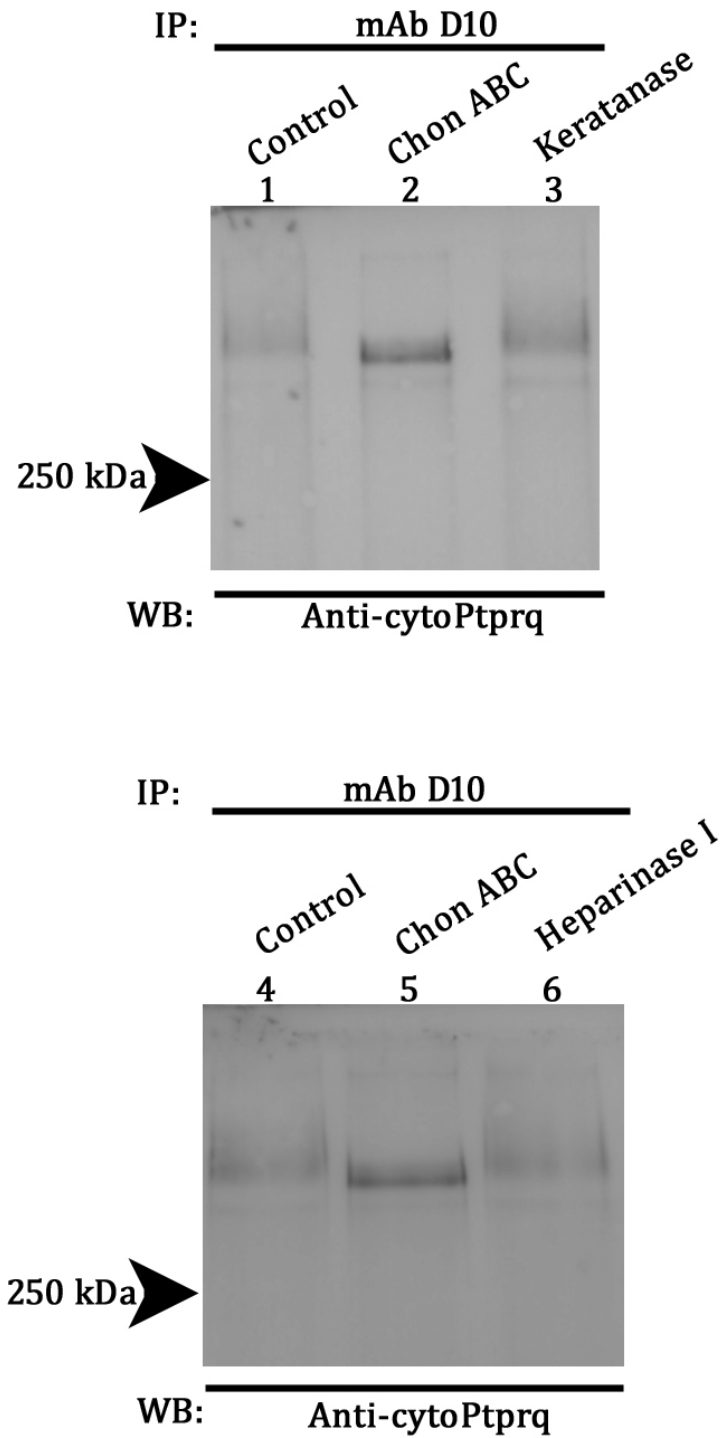
Figure 6.2: Digestion of immunoprecipitated chick Ptprq with chondroitinase ABC (lanes 2 and 5), endo-β galactosidase or keratanase (lane 3) and heparinase I (lane 6). Lanes 1 and 4 are controls. In all cases, mAb D10 was used for immunoprecipitation and anti-cytoPtprq was used for immunoblotting.
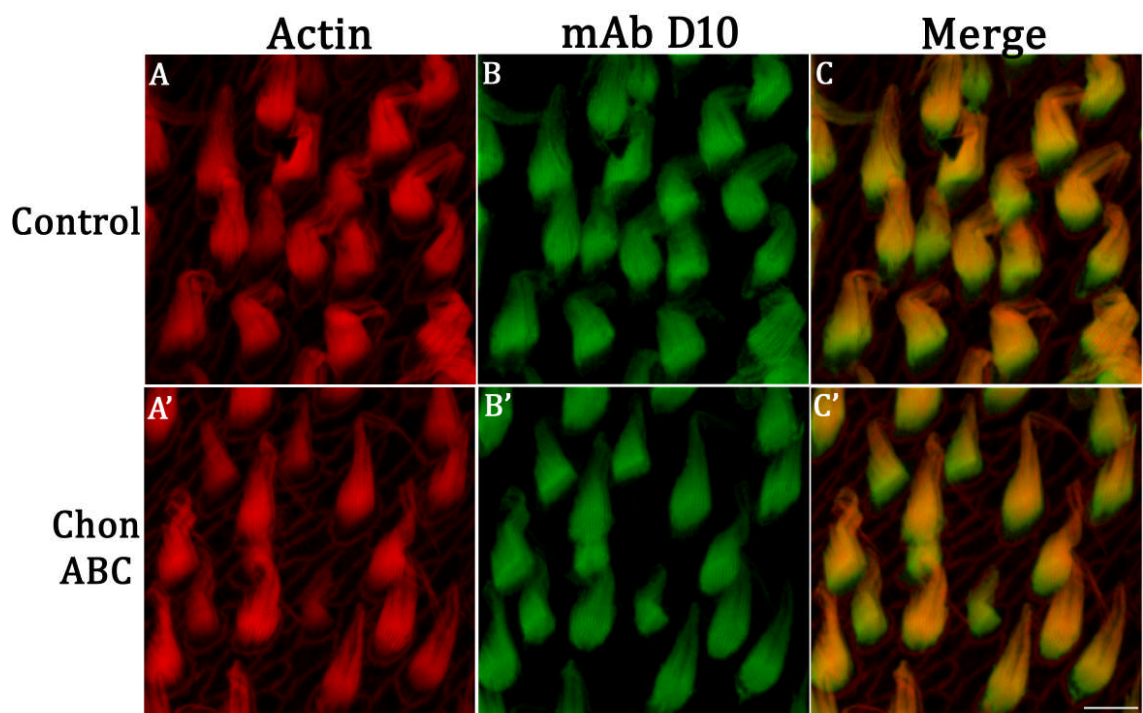
Figure 6.3: Hair bundle staining with mAb D10 after chondroitinase ABC treatment of early posthatch chick utricles. Red represents phalloidin counter stain and green represents mAb 473HD labelling of hair bundles. Chondroitinase ABC does not reduce mAb D10 staining of chick utricular hair bundles (compare panels B and B'). Scale bar 5 μm.
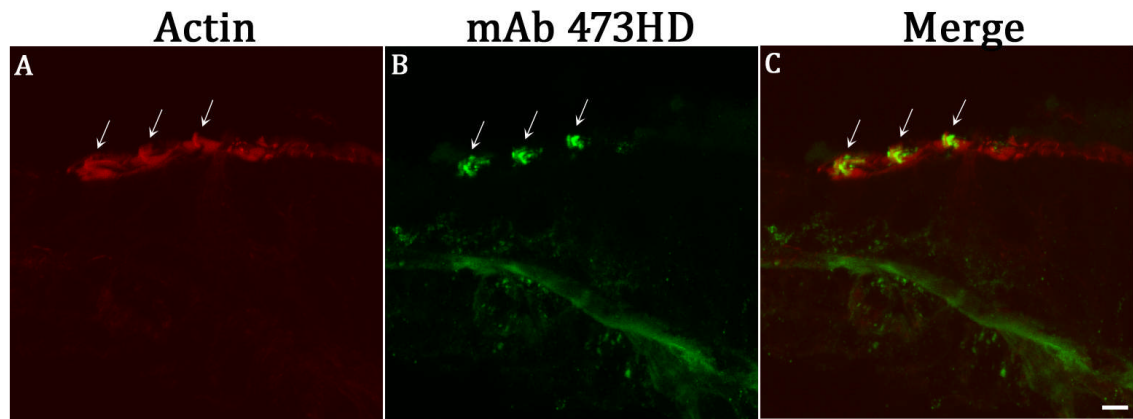
Figure 6.4: Hair bundle staining with mAb 473HD in mouse cochlear sections. Red represents phalloidin counter-stain and green represents mAb 473HD labelling of hair bundles. The arrows in panel A point to three outer hair bundles seen with phalloidin staining. Panel B shows staining of the same hair bundles as in A with the mAb. Panel C is a merge of images from the two channels and shows that the mAb staining of hair bundles overlaps with the phalloidin staining. Scale bar 5 μm.
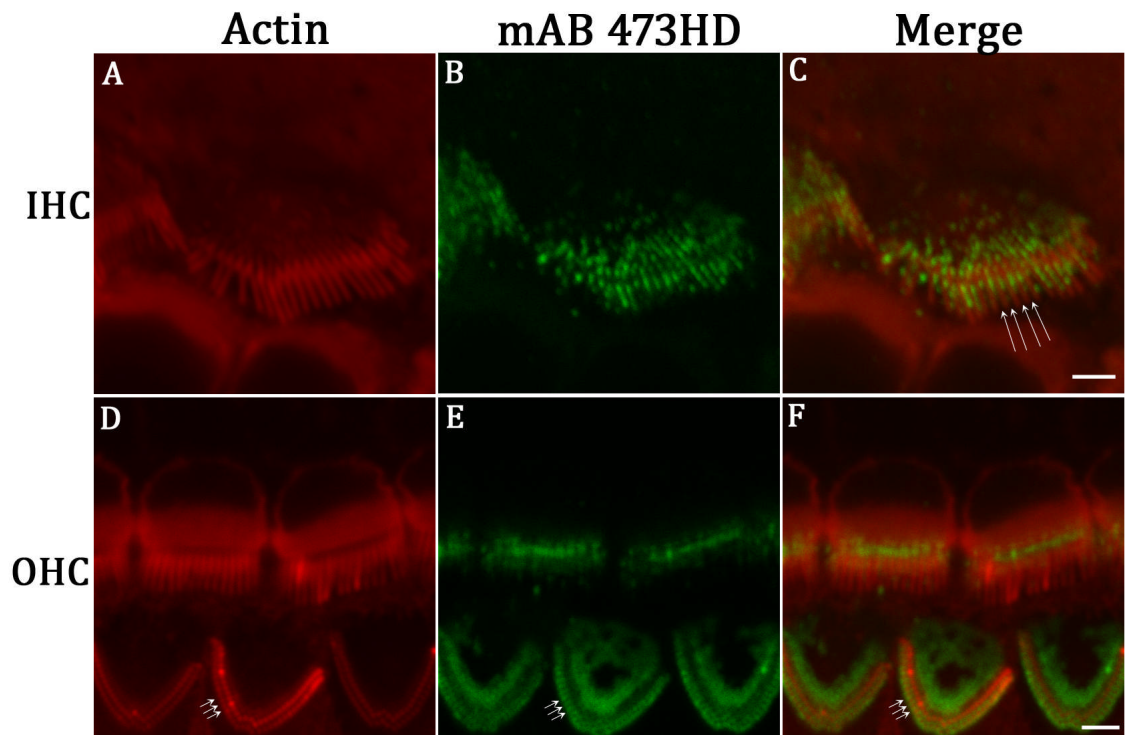
Figure 6.5: mAb 473HD staining in mouse cochlear wholemount preparations. Red represents phalloidin counter-stain and green represents mAb 473HD labelling of hair bundles. Large arrows in panel C show the staining between stereocilia in the IHC hair bundle. The small arrows in panel D indicate the space between stereocilia as seen with phalloidin staining of actin in the OHC hair bundle. The location of these arrows in panel E coincides with mAb 473HD staining suggesting that the staining is located between adjacent stereocilia. The hair bundle staining pattern in panel E suggests that the mAb 473HD epitope is found on the outer surface of the stereociliar membrane. The arrows in panel F show the same region as in panels D and E. Panels C (merge of A and B) and panel F (merge of D and E) clearly show that the mAb staining and phalloidin staining lie adjacent to each other. 2 μm scale bar.
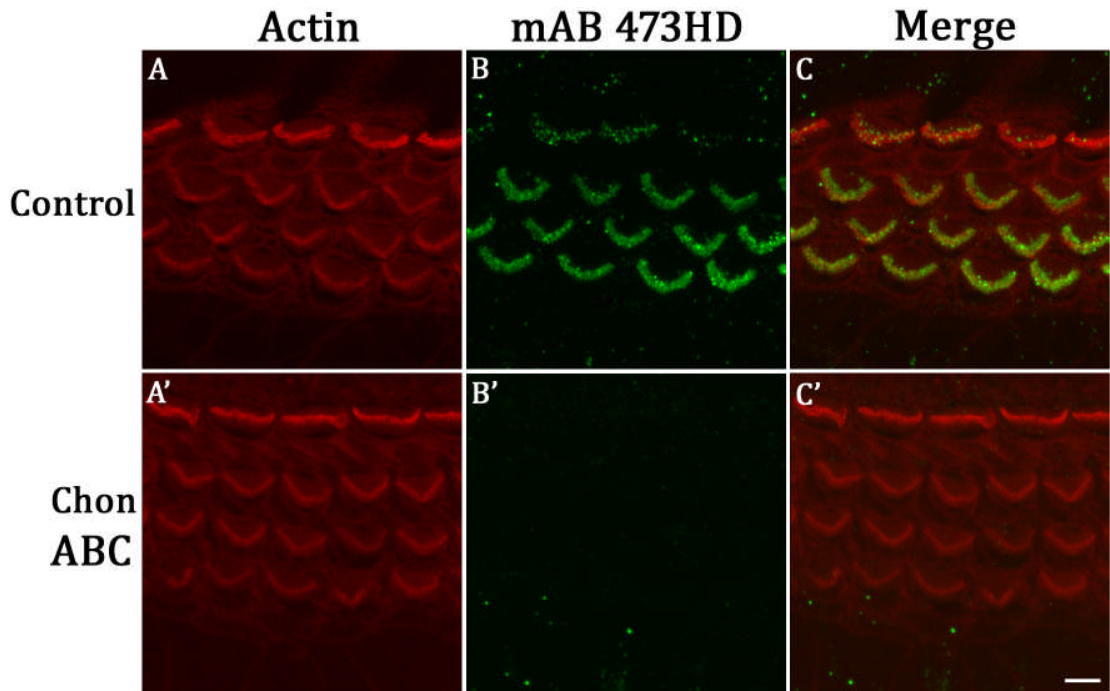
Figure 6.6: mAb 473HD staining of hair bundle upon chondroitinase ABC treatment of mouse cochleae. Red represents phalloidin counter-stain and green represents mAb 473HD labelling of hair bundles. The mAb stains hair bundles in the control cochlea (panel B) but not in those treated with chondroitinase ABC as shown in panel B'. 5 μm scale bar.
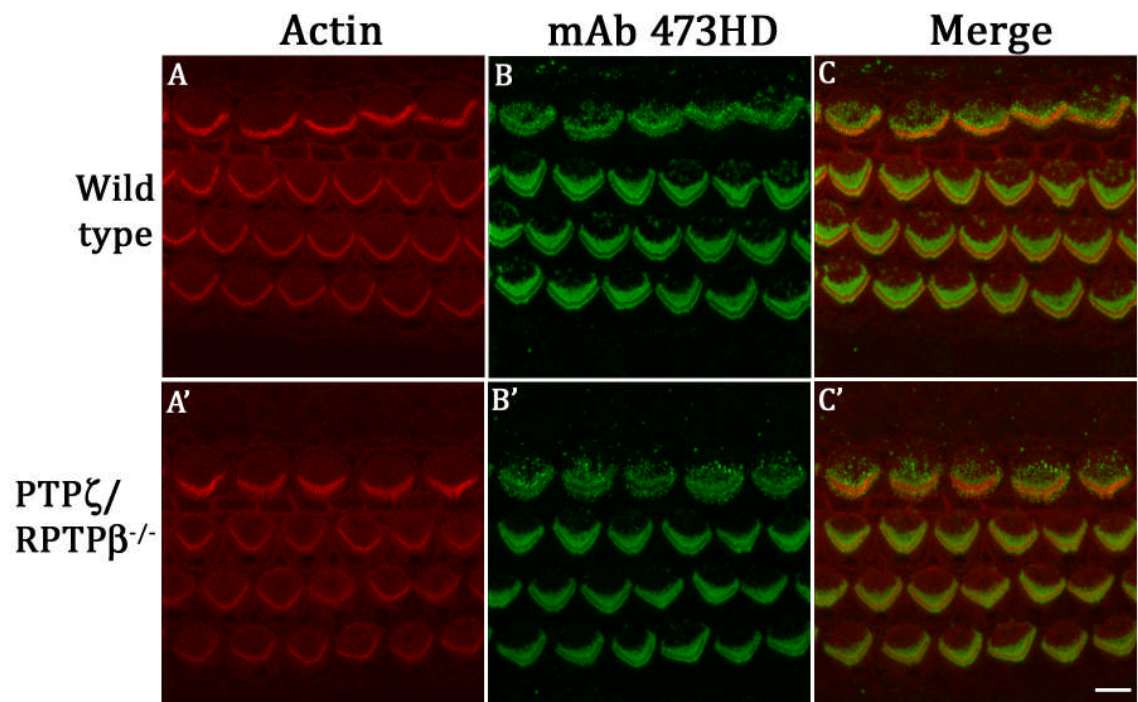
Figure 6.7: Comparison of mAb 473HD staining in wild-type (panels A-C) and PTPζ/RPTPβ knock-out mice (panels A'-C') cochleae. Red represents phalloidin counter-stain and green represents mAb 473HD labelling of hair bundles. The mAb stains hair bundles in the knock-out mice cochlea (panel B') in a manner similar to that seen in wild type cochlea (panel B). 5 μm scale bar.
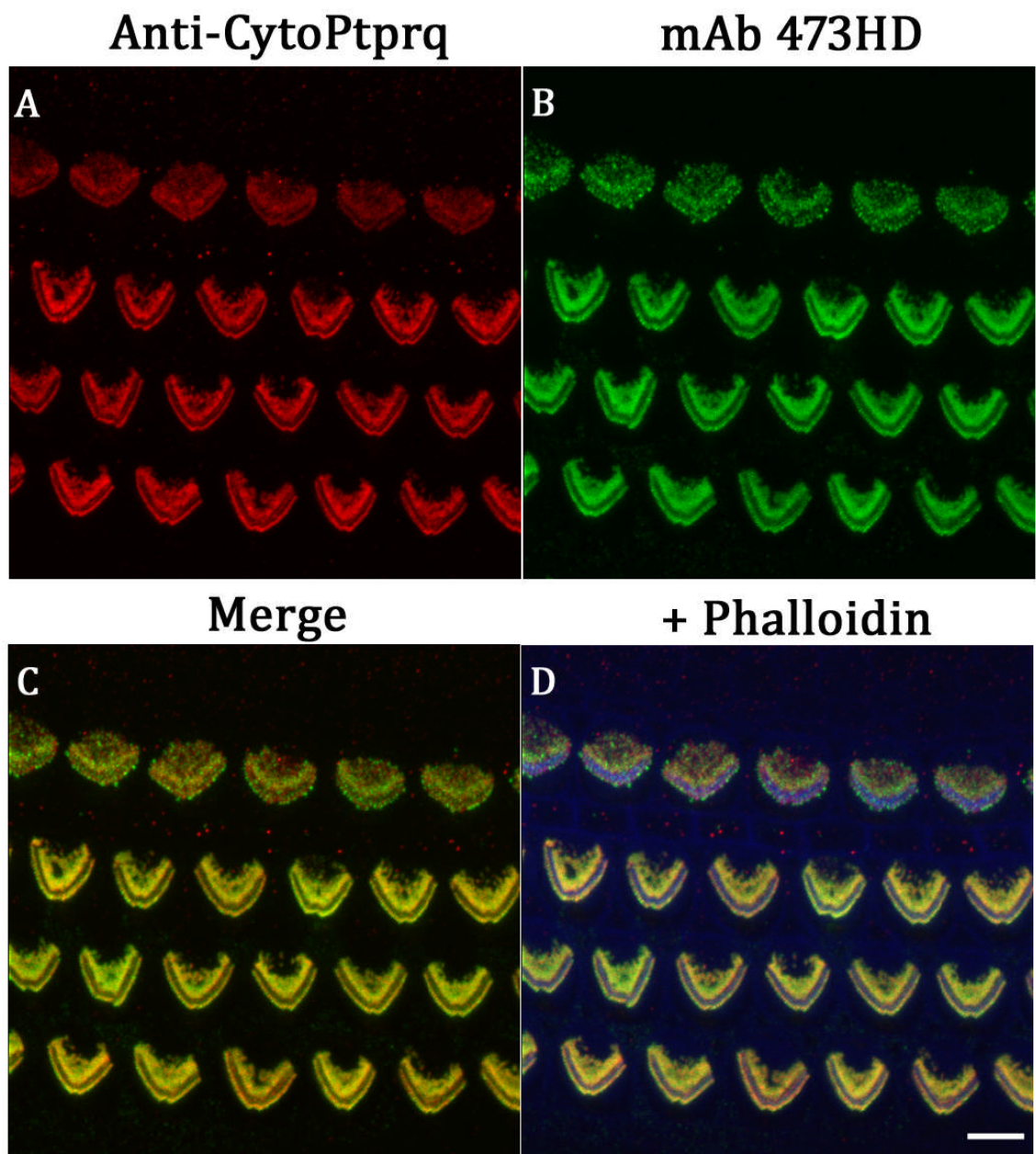
Figure 6.8: Comparison of anti-cytoPtprq (panel A) and mAb 473HD (panel B) staining of hair bundles in early postnatal wild-type cochlea. A merge of the two images shows that the staining patterns of the two antibodies broadly co-localise (panels C and D). Blue represents phalloidin staining. 5 μm scale bar.
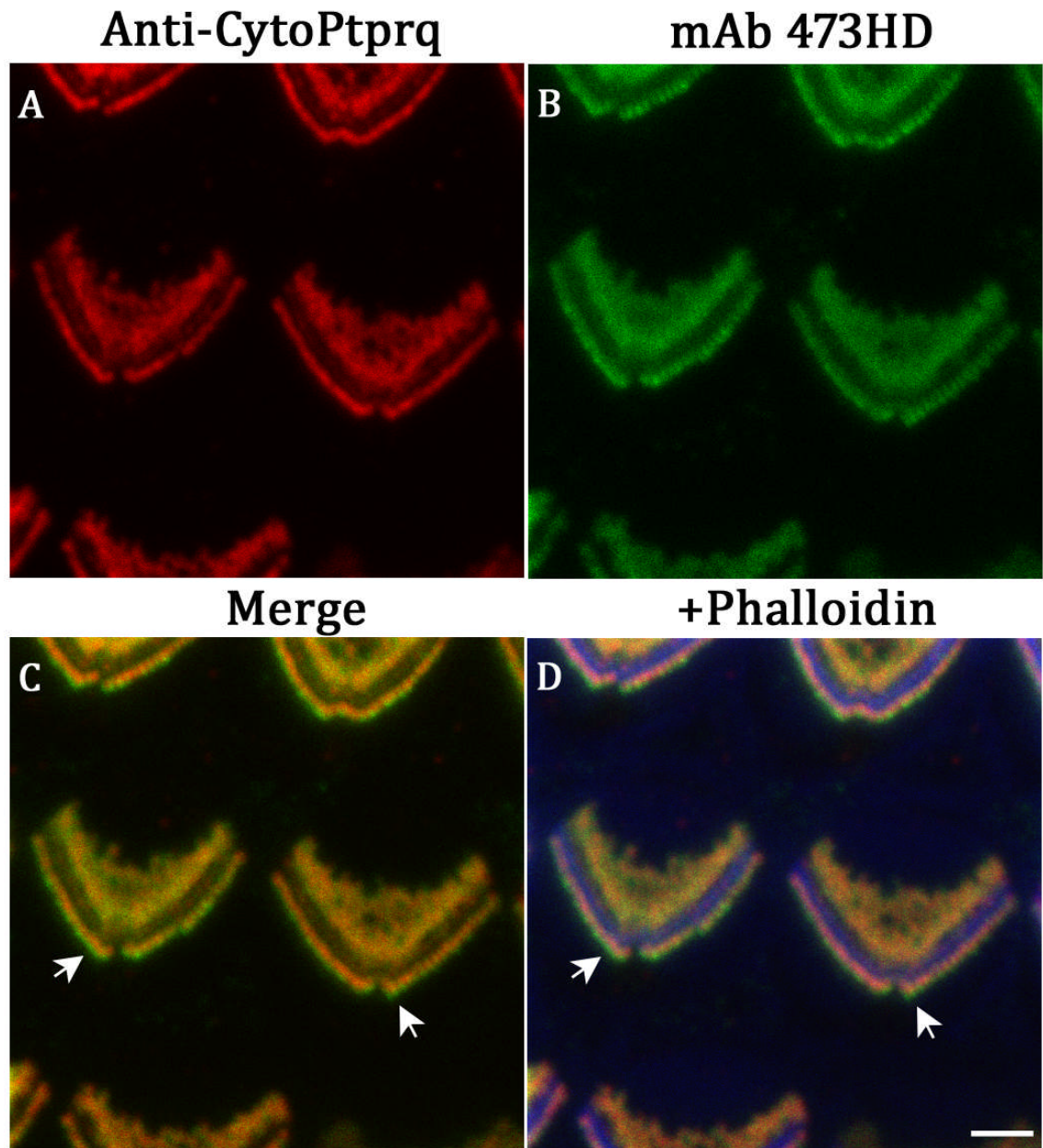
Figure 6.9: Higher magnification images of hair bundle staining with the anti-cytoPtprq polyclonal (red) and mAb 473HD (green). Panels A (anti-cytoPtprq) and B (mAb 473HD) reveal that the two antibodies stain hair bundles very similarly. However, the staining does not completely overlap. The arrows in panel C and D show two regions where mAb 473HD staining lies adjacent to, but outside with respect to that seen with the anti-cytoPtprq polyclonal and phalloidin (blue). 2 μm scale bar.
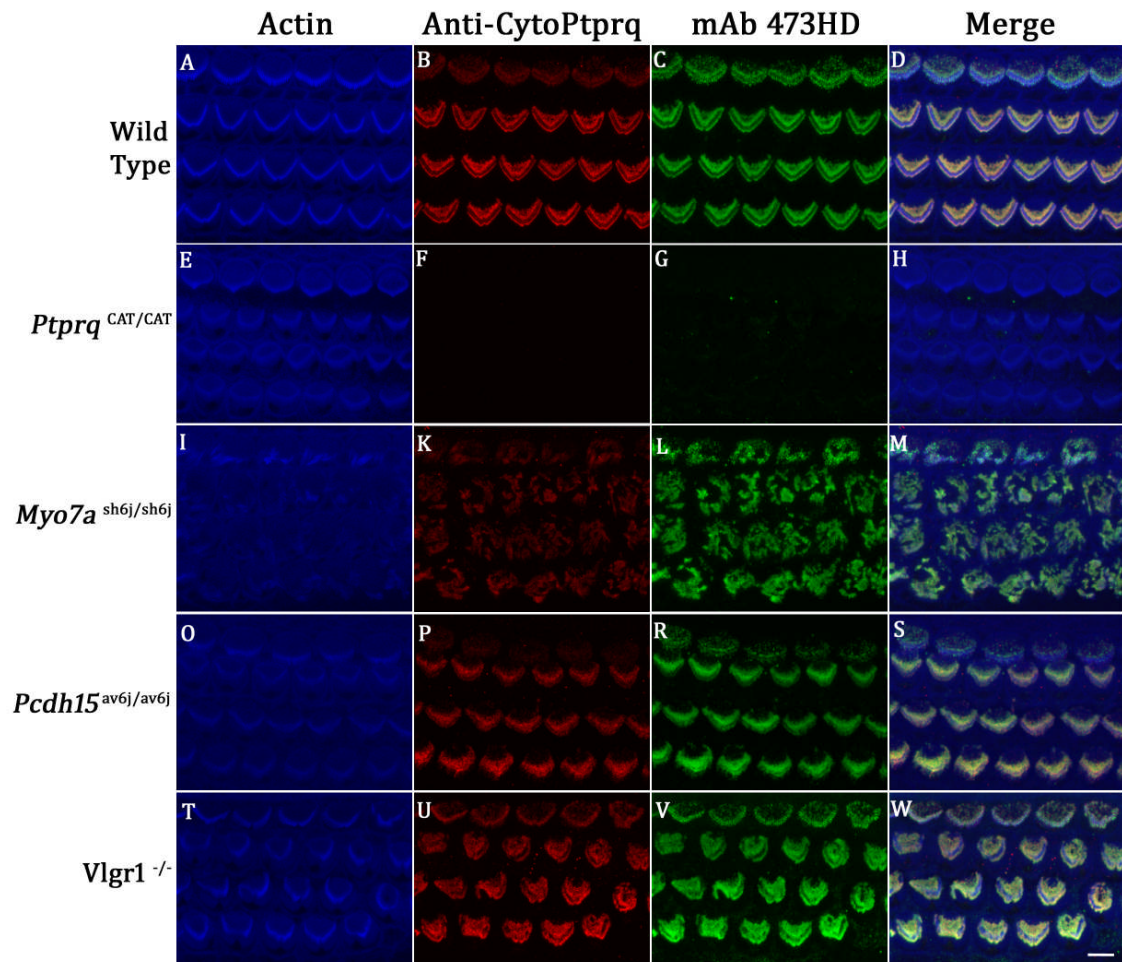
Figure 6.10: mAb 473HD staining of hair bundles in the wild-type cochlea (panel C) and cochleae of knock-out mice for several hair bundle proteins (listed on the left of the figure). Blue represents phalloidin counter stain, red represents anti-cytoPtprq labelling and green represents mAb 473HD labelling. mAb 473HD stains hair bundles in the cochleae of wild-type (panel C) and all mutants examined (panels L, R and V) except those in the cochleae of Ptprq$^{CAT/CAT}$ mice (panel G). Scale bar 5 μm.

Control
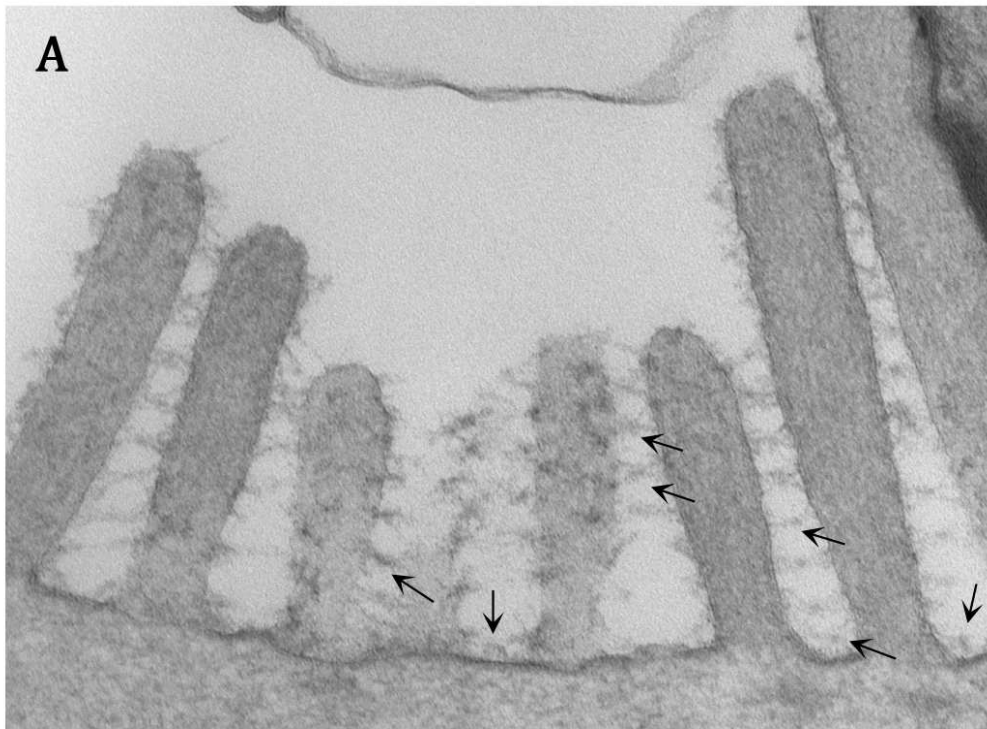
Chondroitinase ABC
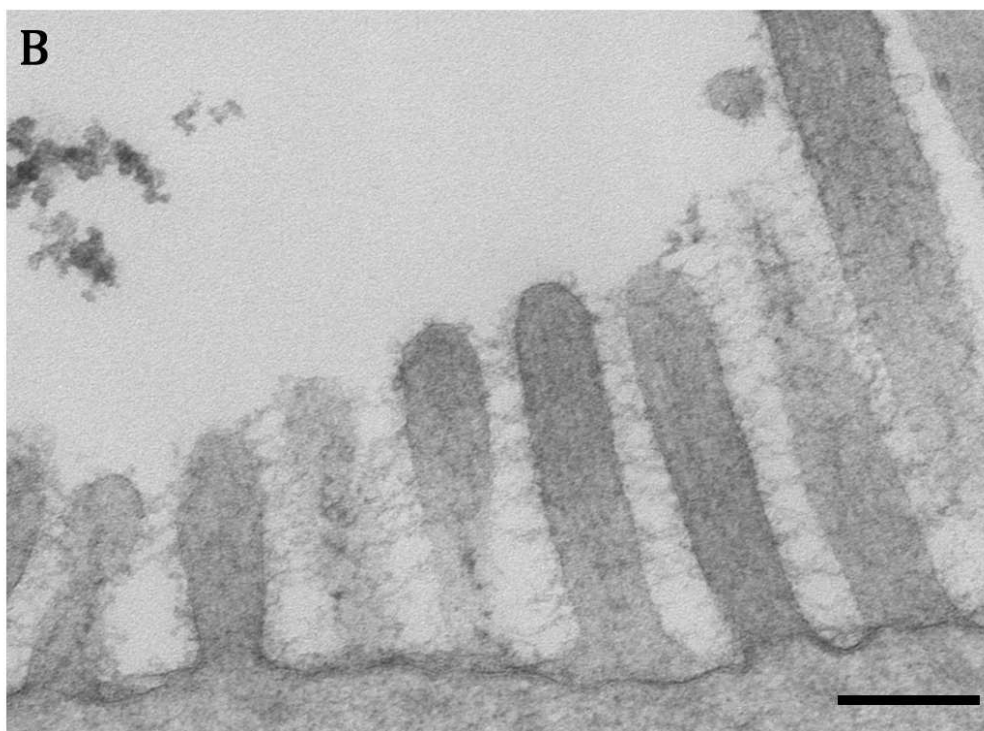
Figure 6.11: Ultrastructural changes in the appearance of cell-surface specialisations seen in early postnatal mouse cochleae following chondroitinase ABC treatment. The dense particles associated with hair bundles and the apical cell-coat of early postnatal mouse cochlear hair cells (panel A) are removed by chondroitinase ABC (panel B). The arrows in panel A show the dense particles that are absent from the chondroitinase ABC treated samples (panel B). 200 nm scale bar.
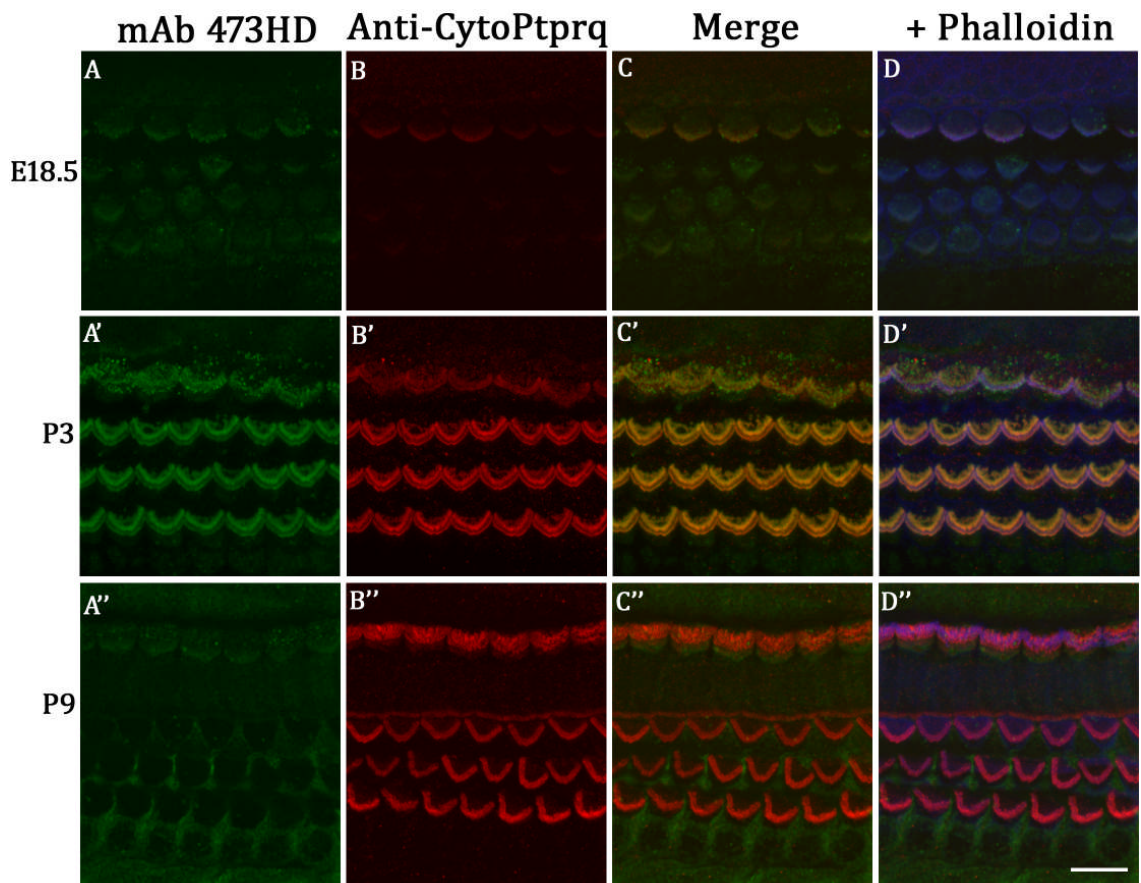
Figure 6.12: Temporal expression of the DSD-1 epitope (mAb 473HD) and Ptprq in the basal-coil of the mouse cochlea. Green represents mAb 473HD labelling, red represents anti-cytoPtprq labelling and blue represents phalloidin counter-stain. Staining with both mAb 473HD and anti-cytoPtprq is detectable by E18.5 (panels A and B). Both Ptprq and the DSD-1 epitope expressions peaks at P3 (panels A' and B'). Ptprq is still present in the hair bundles of P9 mouse cochlea (panel B'') while mAb 473HD staining is undetectable in the hair bundle at this age (panel A''). 10 μm scale bar.
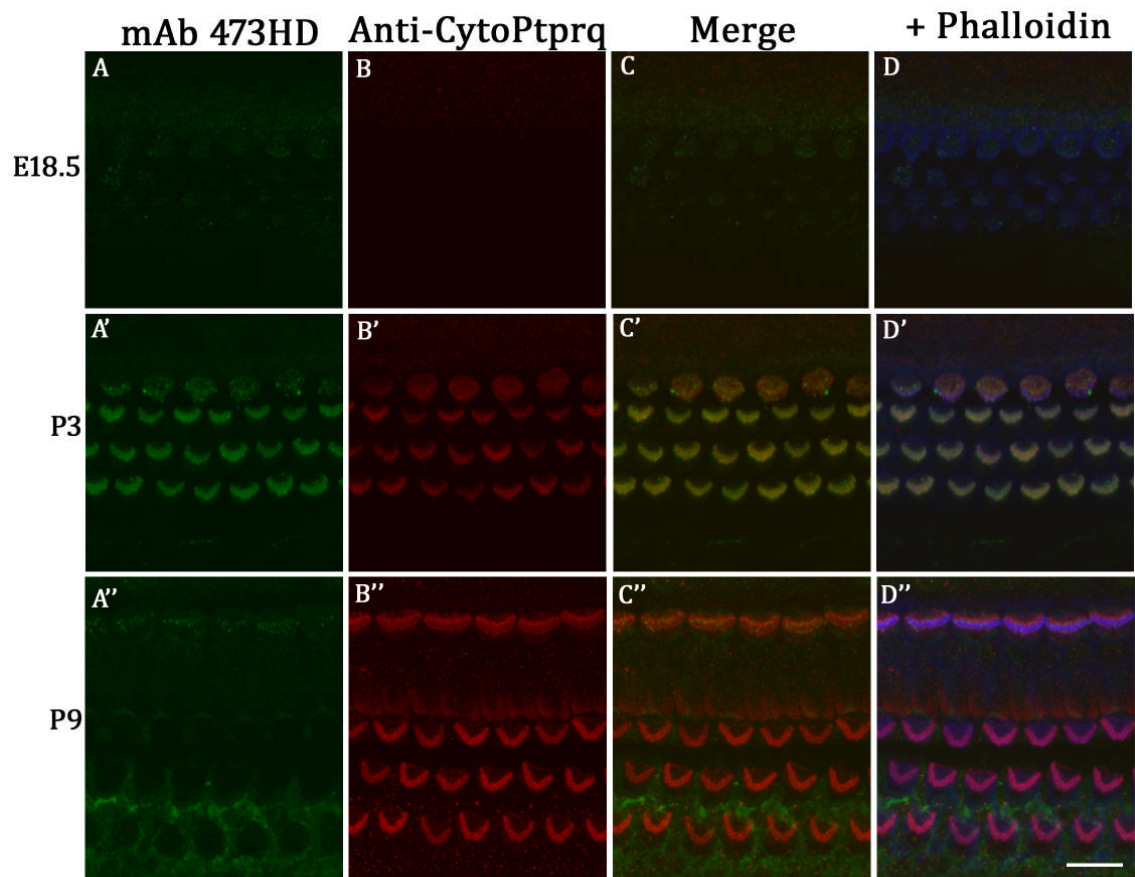
Figure 6.13: Temporal expression of the DSD-1 epitope (mAb 473HD) and Ptprq in the apical-coil of the mouse cochlea. Green represents mAb 473HD labelling, red represents anti-cytoPtprq labelling and blue represents phalloidin counter-stain. Staining with both mAb 473HD and anti-cytoPtprq is detectable by P3 (panels A' and B'). Ptprq is still present in the hair bundles of P9 mouse cochlea (panel B'') while mAb 473HD staining is undetectable in the hair bundle at this age (panel A''). 10 μm scale bar.
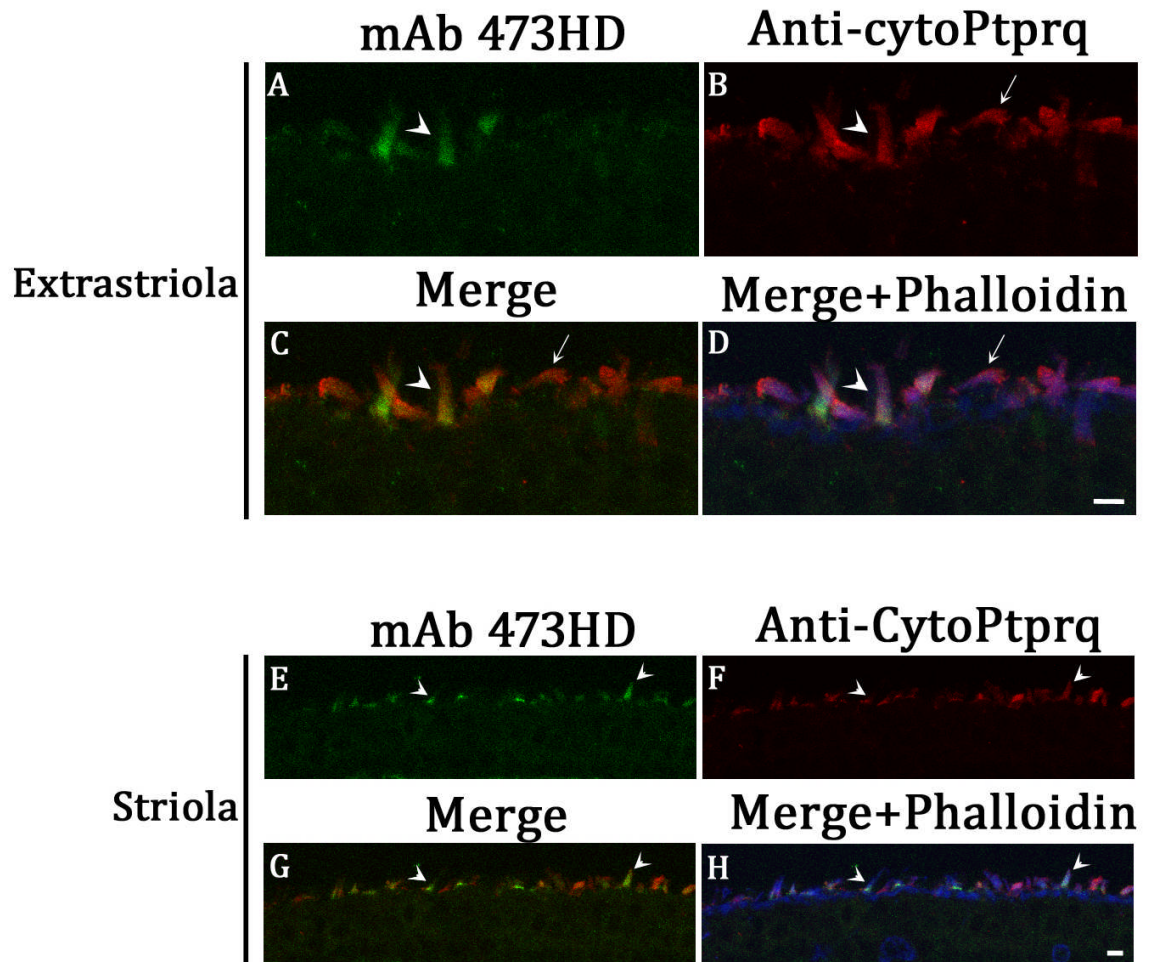
Figure 6.14: mAb 473HD and anti-cytoPtprq double labelling of mouse utricular hair bundles at P69. Green represents mAb 473HD labelling, red represents anti-cytoPtprq labelling and blue represents phalloidin counter-stain. mAb 473HD stains a subset of extrastriolar (panels A, C, D) and striolar (panels E,G,H) hair bundles, whilst anti-cytoPtprq staining is seen in all hair bundles (panels B-D and F-H) at this age. The arrowhead in panels A-D point to an extrastriolar hair bundle that stains with both antibodies and the small arrows in panels B-D point to a hair bundle that is only labelled with anti-cytoPtprq. The arrowheads in panels E-H point to the striolar hair bundles that label with both antibodies. Scale bar 5 μm.
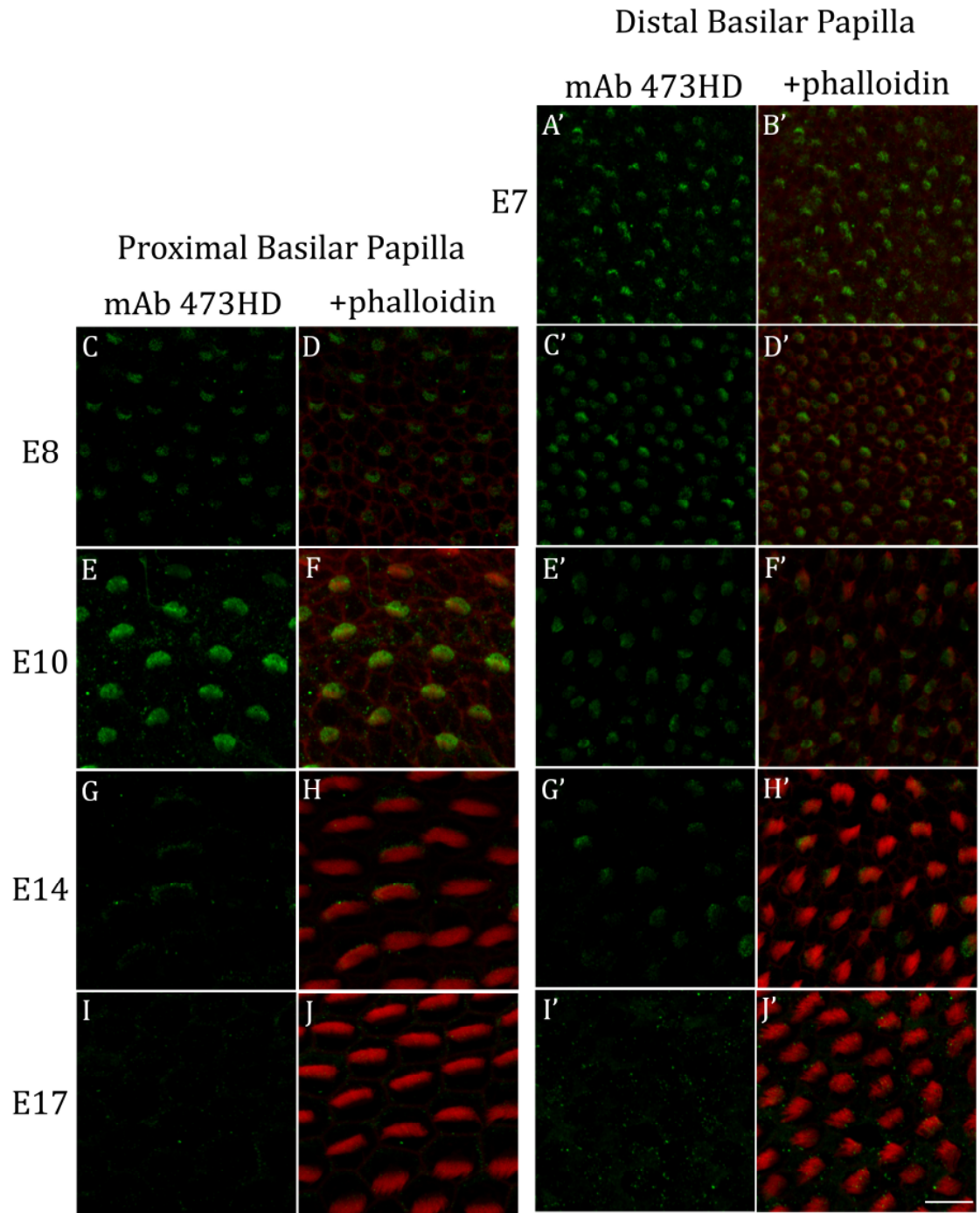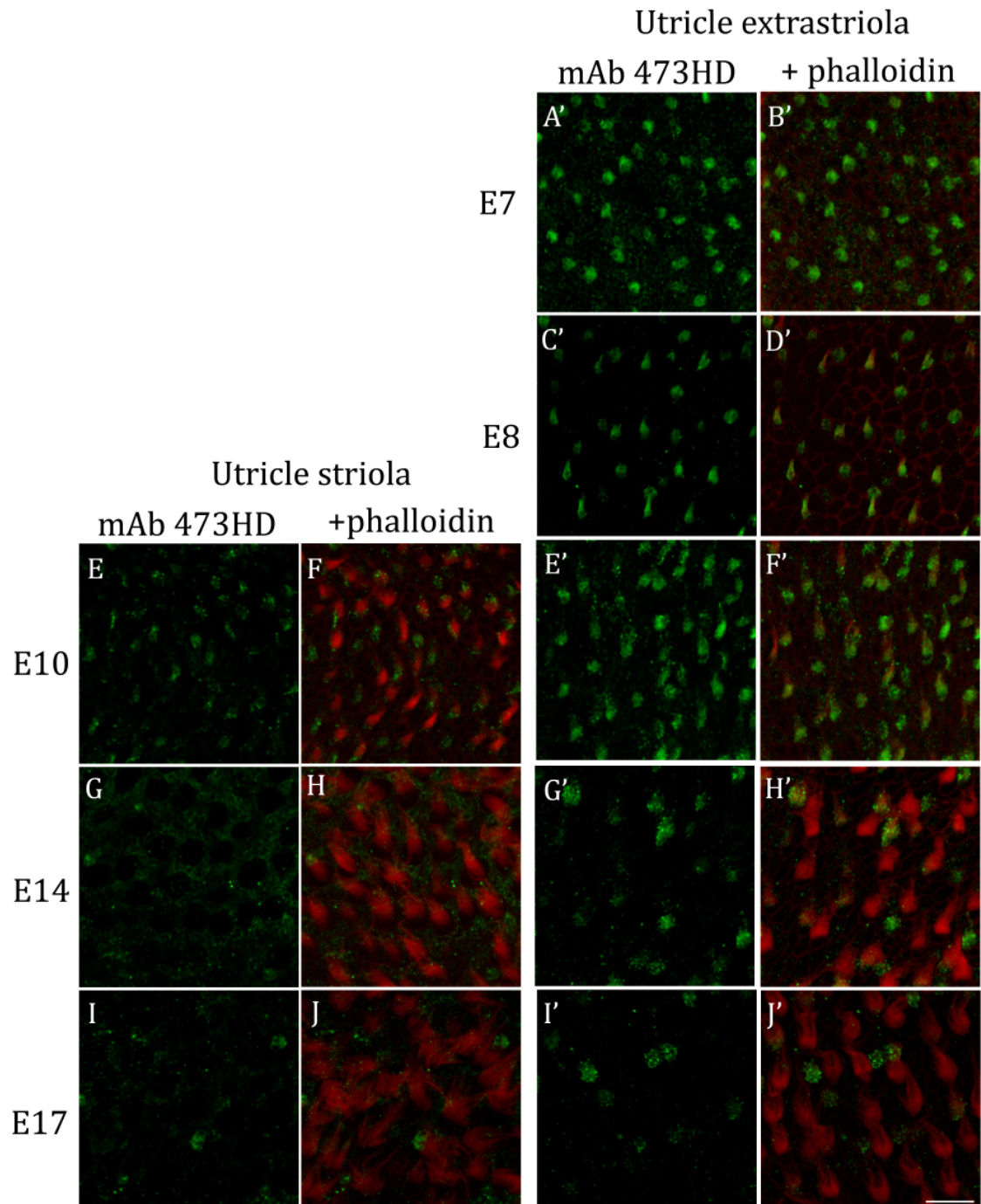
Figure 6.15: Temporal expression of the DSD-1 epitope in embryonic chick basilar papilla. Green represents mAb 473HD staining and red represents phalloidin counter-stain. Staining with the mAb is seen at E7 at the distal end (panel A') and in the proximal end by E8 (panel C). DSD-1 epitope expression peaks between E8 (panels C and C') and E10 (panels E and E'). By E14, few hair bundles label with the mAb in either region of the papilla (panels G and G'). By E17, the DSD-1 epitope expression reduces to near undetectable levels (panels I and I'). 10 μm scale bar.
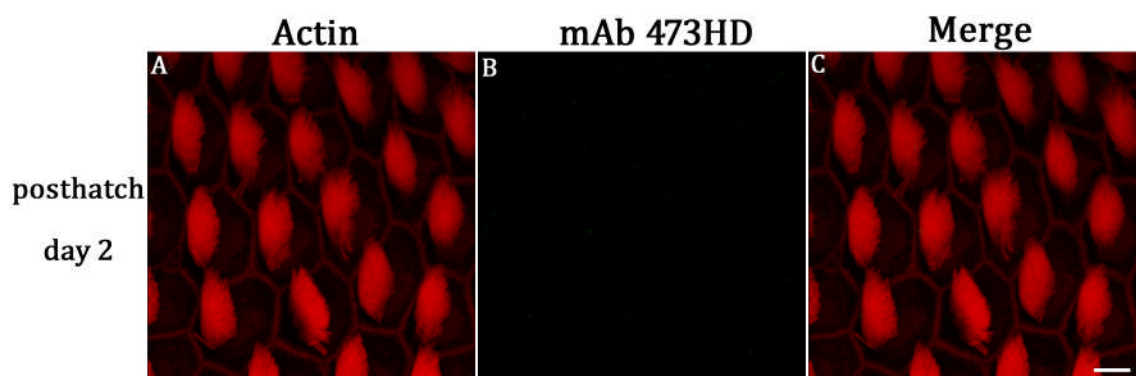
Figure 6.16: mAb 473 HD does not stain hair bundles in the basilar papilla of posthatch day 2 chick (panel B). Red represents phalloidin counter-stain. Scale bar 5 μm.

Figure 6.17: Temporal expression of the DSD-1 epitope in the embryonic chick utricle. Green represents mAb 473HD labelling and red represents phalloidin counter-stain. Staining with mAb 473HD is always more prominent in the extrastriolar (panels A'-J') hair bundles than the striolar ones (panels E-J). The DSD-1 epitope is present in nearly all hair bundles by E7 (panel A') and the expression peaks at E10 (panels E and E'). The DSD-1 epitope expression continues until E14 by which time very few hair bundles stain with the mAb (panels G and G'). At this stage staining of the apical surfaces of supporting cells in the striolar region becomes evident (panel G). At E17, the mAb still labels some hair bundles (panels I and I'). Scale bar 10 μm.
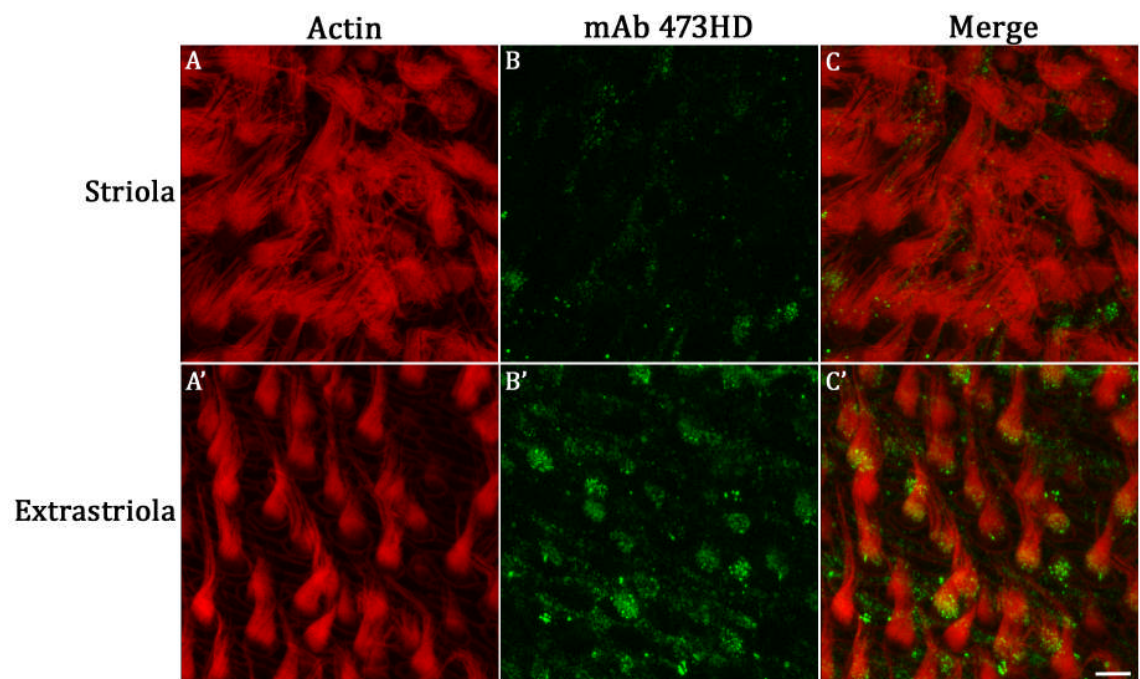
Figure 6.18: mAb 473HD labelling of posthatch day 2 chick utricles. Red represents phalloidin counter stain and green represents mAb 473HD labelling. Panel B shows mAb 473HD labelling in the striolar hair bundles and B' reveals extrastriolar hair bundles labelled with the mAb. Scale bar 5 μm.
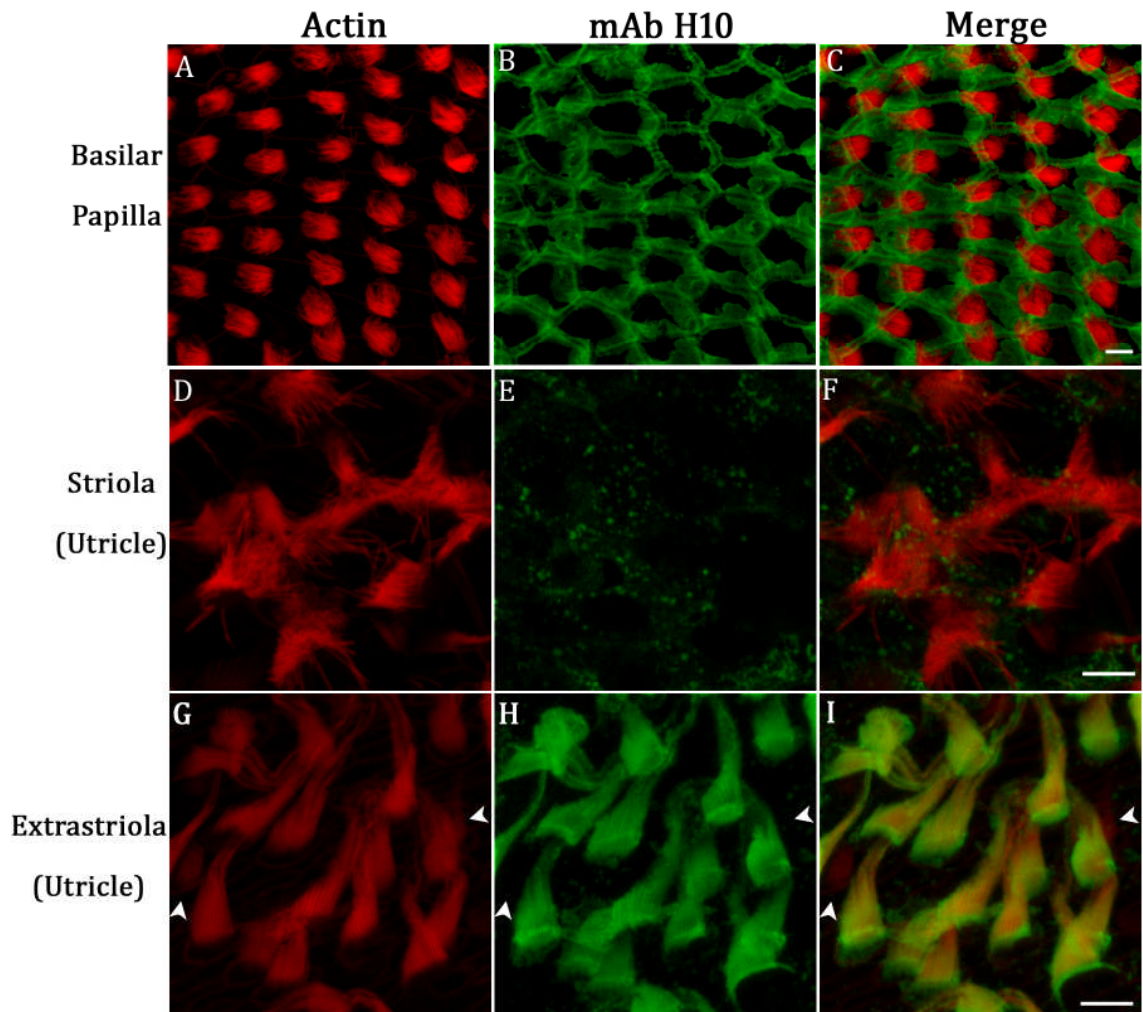
Figure 6.19: mAb H10 labelling of hair bundles in the early posthatch chick inner ear. Red represents phalloidin counter stain and green represents mAb H10 labelling. The mAb does not stain hair bundles in the basilar papilla (panel B) or the striolar hair bundles (panel E) but stains extrastriolar hair bundles (panel H) in the utricle. The mAb does not stain immature hair bundles (arrows in panels G, H and I point to the same hair bundles and the arrows in panel H show the lack of mAb H10 staining of immature hair bundles). In addition to hair bundles, mAb H10 also stains the apical surfaces of supporting cells in the basilar papilla and the striola (panels B and E). 5 μm scale bars.
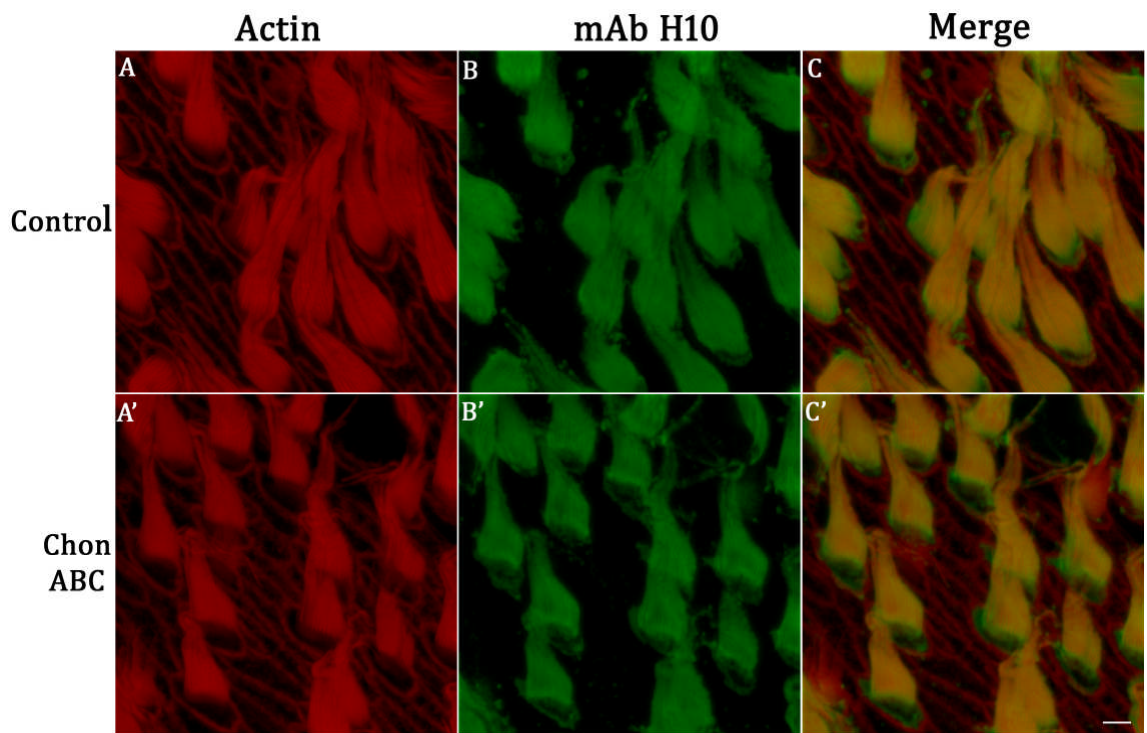
Figure 6.20: mAb H10 labelling of hair bundles following chondroitinase ABC treatment of early posthatch chick utricles. Red represents phalloidin counter-stain and green represents mAb H10 labelling. Hair bundle staining of mAb H10 is not lost after chondroitinase ABC treatment (panel B') and appears similar to that seen in control chick utricles (panel B). Scale bar 5 μm.
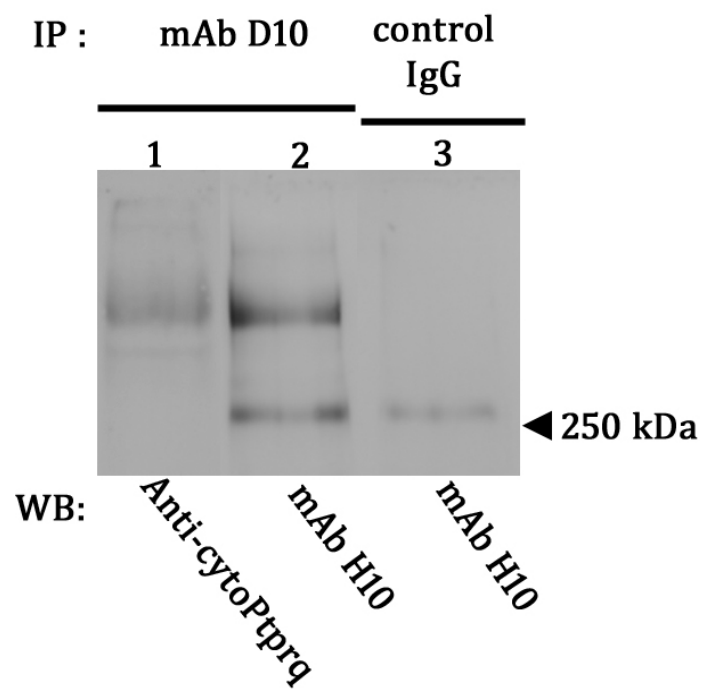
Figure 6.21: Results of immunoprecipitation of chick Ptprq from utricular lysates using mAb D10 and a control IgG. Blots 1 and 2 represent immunoprecipitation using mAb D10. Blot 3 represents immunoprecipitation using a control IgG. Blot 1 was probed with anti-cytoPtprq, while blots 2 and 3 were probed with mAb H10. Blot 2 shows that mAb H10 recognises Ptprq.
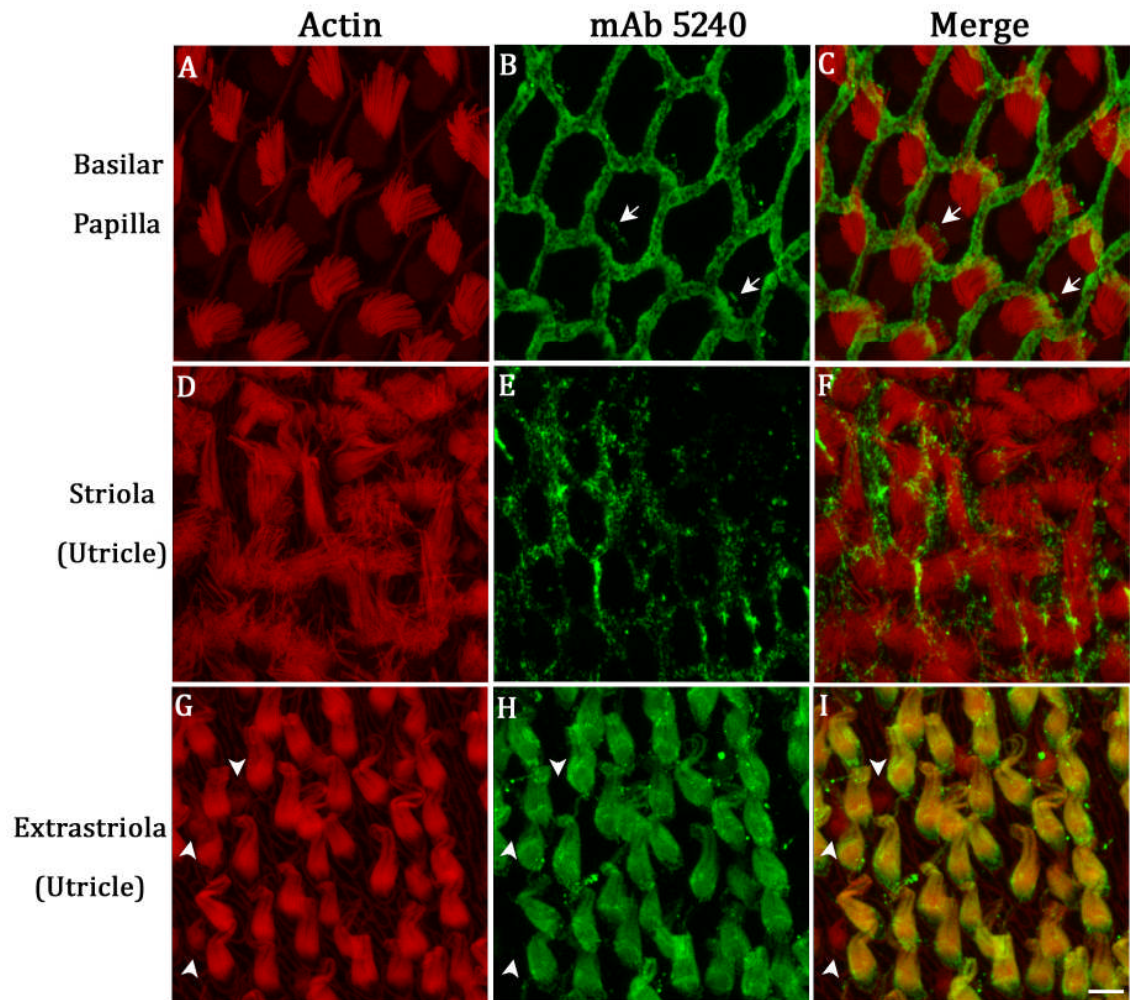
Figure 6.22: mAb 5240 staining of hair bundles in the early posthatch chick inner ear. Red represents phalloidin counter-stain and green represents mAb 5240 labelling. The mAb does not stain hair bundles in the basilar papilla (panel B) or the striola (panel E) but stains extrastriolar hair bundles (panel H) in the utricle. The arrows in panel B and C show the labelling of stereocilia tips with mAb 5240 in the basilar papilla. The mAb does not stain immature hair bundles (arrowheads in panels G, H and I point to the same hair bundles and the arrowhead in panel H show the lack of mAb 5240 staining of immature hair bundles). In addition, mAb 5240 also stains the apical surfaces of supporting cells in the basilar papilla (panel B) and the striola (panel E). Scale bar 5 μm.
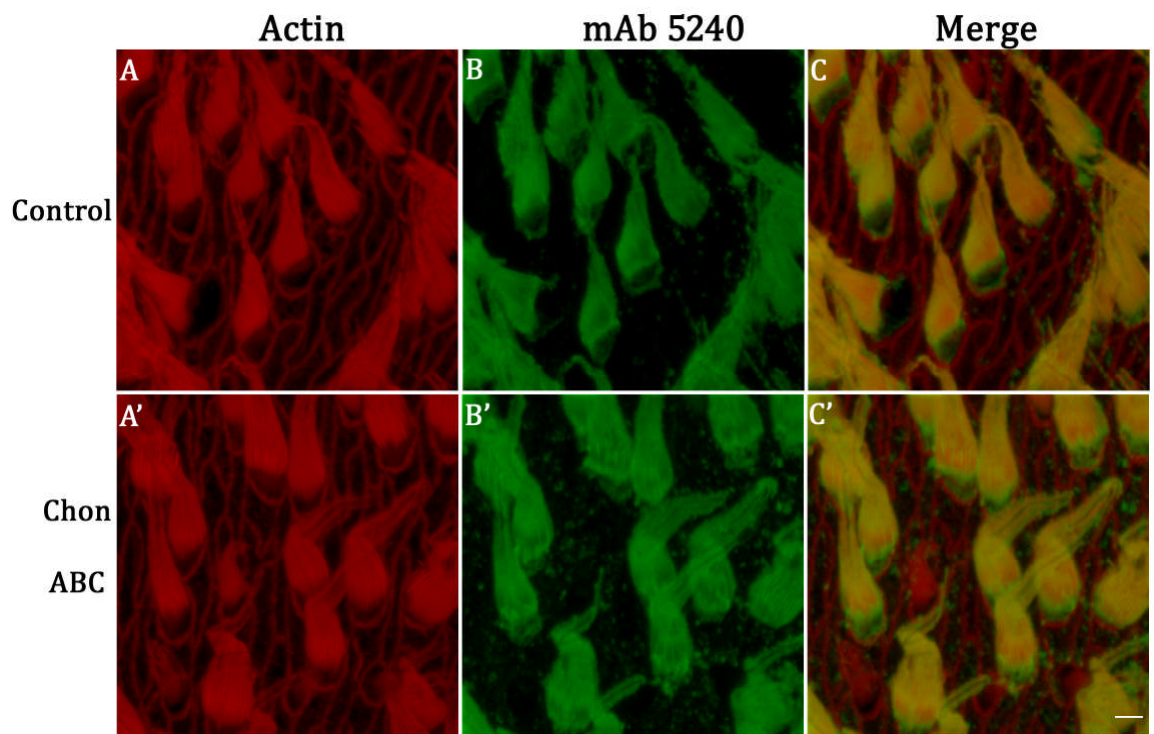
Figure 6.23: mAb 5240 staining of hair bundles on chondroitinase ABC treatment. Red represents phalloidin counter-stain and green represents mAb 5240 labelling. Hair bundle staining with mAb 5240 is seen in control samples (panel B) and chondroitinase ABC treated samples (panel B'). Scale bar 5 μm.
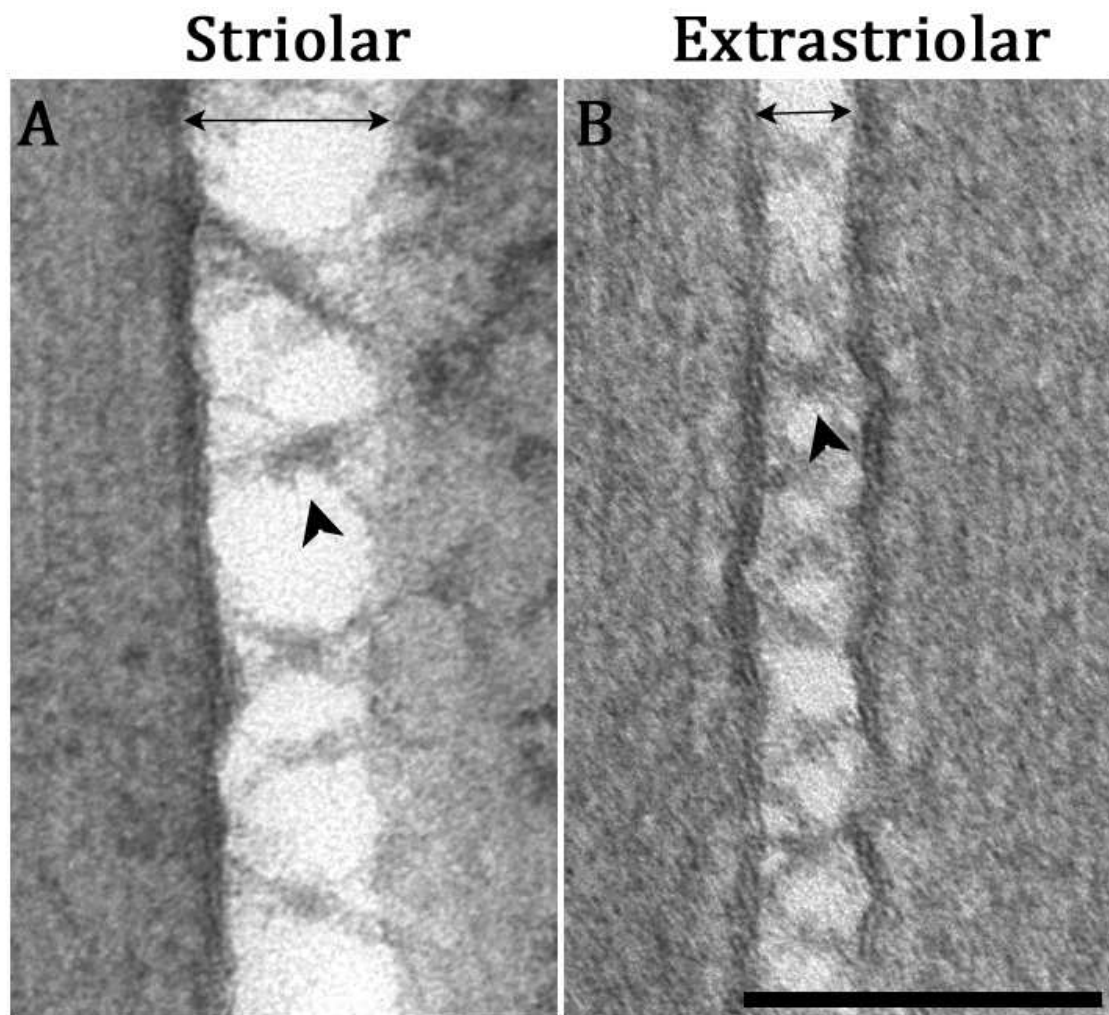
Figure 6.24: Comparison of shaft connectors in striolar and extrastriolar hair bundles. Arrowheads show the dense particles associated with shaft connectors that are seen between stereocilia in both striolar (panel A) and extrastriolar (panel B) hair bundles. However, the shaft connectors are longer in striolar hair bundles than in extrastriolar hair bundles (double arrowheads in panels A and B). 200 nm scale bar.
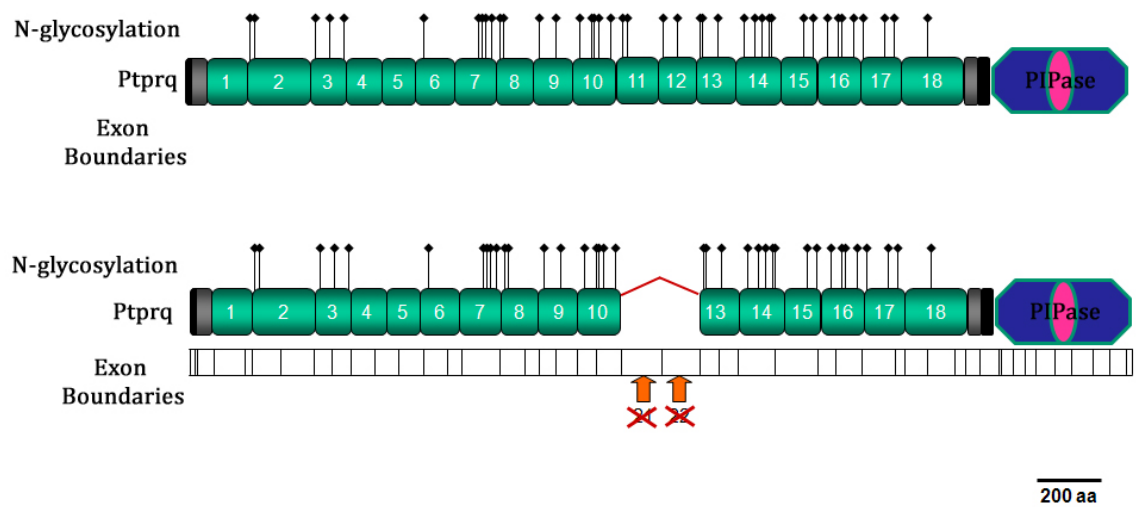
Figure 6.25: The above diagram represents the full-length isoform of Ptprq (top) and an extracellular splice variant (bottom) in which the 11th and 12th FNIII repeats are skipped. Thus, the latter splice variant loses the Ser and Thr residues that occur in the missing FNIII repeats and could therefore lack any GAG chains that may be attached to any of these residues.
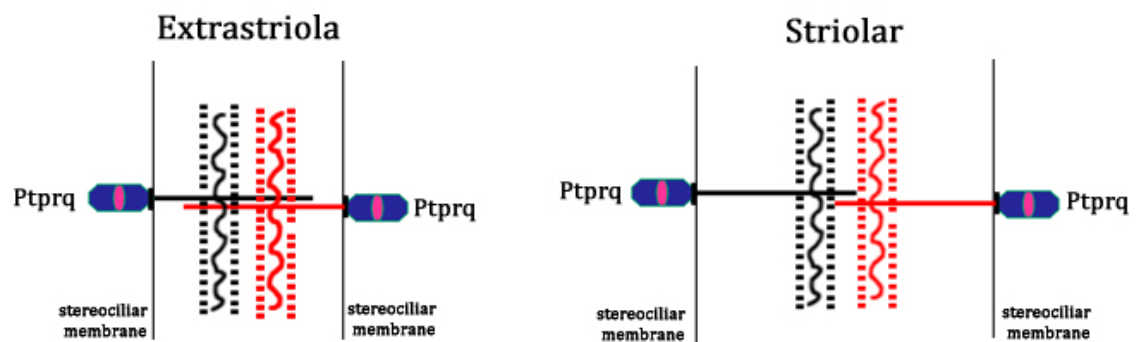
Figure 6.26: Model to explain the differential appearance of shaft connectors in the extrastriolar and striolar regions of the maculae in chick. The GAG chains on the ectodomains of opposing Ptprq molecules are shown in black and red. Ptprq isoforms with GAG chains closer to the stereociliar membrane (picture on the left) results in shorter connectors as the repulsive forces between opposing GAG chains act at shorter distances between adjacent stereocilia. The striolar hair bundles may have Ptprq isoforms with GAG chains at the ends of the molecules, which may result in longer connectors as shown on the right.